2015

Synergistic Properties-Driven Synthesis of Aluminides, Antiomonides, and Bioceramics

Pilanda Watkins-Curry
Louisiana State University and Agricultural and Mechanical College

SYNERGISTIC PROPERTIES-DRIVEN SYNTHESIS OF ALUMINIDES, ANTIMONIDES, AND BIOCERAMICS

A Dissertation

Submitted to the Graduate Faculty of the
Louisiana State University and
Agricultural and Mechanical College
in partial fulfillment of the
requirements for the degree of
Doctor of Philosophy

in

The Department of Chemistry

by
Pilanda Watkins-Curry
B.S., Spelman College, 2011
August 2015

To my loving husband Russell and my daughter Kennedy. This is definitely for you.

Acknowledgements

It is with great pleasure to be writing my dissertation, a cumulative of works that has consumed me the past four years, but I would not have been given this opportunity without the following people.

First, I would like to thank my advisor Prof. Julia Chan for being a mentor who has pushed me to maximize my growth as a student scientifically and critically in my writing. I also appreciate her allowing me to attend several workshops and conferences for student and career development including the "Neutron Powder Diffraction Workshop" at Oak Ridge National Laboratory, the Gordon Research Conference in Solid State Chemistry, and for trusting me to conduct research at the University of Houston and presenting an invited talk in their "Inorganic Chemistry Seminar Series". Her leadership and guidance has been an experience that I will never forget.

Second, I would like to thank my committee members, Profs. George Stanley and Daniel Hayes. Both of you have been active members early in my development as a graduate student. Although our interaction drifted when I moved to Dallas, TX, both of you have been extremely helpful and have always answered the call when needed. I would also like to thank Prof. Rendy Kartika for filling in on such short notice.

This dissertation would not have been possible without awesome collaborators, including Prof. John F. DiTusa, Prof. Shane Stadler and his student Tapas Samanta, Prof. David P. Young, Prof. James Analytis, Prof. Danieli Rodrigues and her students Anna, Jonathan, and Sathya, Prof. Daniel Hayes and his student Cong Chen, Prof. Paul Maggard and his students Nacole King and Jonathan Boltersdorf, Prof. Amy Walker and her student Jenny Hedlund, and Dr. Julia Bykova. To the crystallographers that taught me all I know about structure refinement and played a

pivotal role in my understanding of crystallography, Drs. Frank Fronczek and Gregory McCandless.

I would also like to acknowledge the past and current group members of the “Channites”, whom I became acquainted with in short periods of time. Each one of you have been helpful in answering my questions and reminding me about how much I knew, thought I knew, and did not know including, Dr. Melissa Menard, Dr. Adam Phelan, Dr. Devin Schmitt, Dr. Michael Kangas, Dr. Bradford Fulfer, Dr. Larico J. Treadwell, Luis Reyes, Iain Oswald, Dr. Roy McDougald (postdoc), Yixin Ren, Katie Benavides, and the newest member Kyle Pujol. It would be a disservice if I did not thank the undergraduates whom I had a pleasure working with which has led to a couple of publications, including Jacob D. McAlpin, Joseph V. Burnett, and Judy Chan.

I especially appreciate my undergraduate mentor, Prof. Leyte Winfield, thank you for believing in my potential and always being a phone call away. Also, thank you for allowing me to give a seminar on my current research at Spelman College. It was enlightening to see so many students interested in my projects as well as my graduate experience. I hope that I was able to encourage them to pursue graduate studies in the sciences.

To my family, thank you for being my number one supporters. Thank you to my Mom and Dad for always believing in me and standing by my decisions. Also, thank you for being great role-models for me and my sisters. Candice and Mercedes thank you for being the best sisters in the world and allowing me to be the N.E.R.D. (Nubian Elegance that is Rare and Devine) that I am. Also, thank you to my husband for allowing me to pursue my dreams and always being by my side throughout this process. To my daughter Kennedy, this is definitely for you sweetie. You have taught me so much in so little time. One thing I have learned from you is to not sweat the small stuff. Last, but definitely not least (Matthew 20:16), I thank God, who has

been a very present help in the time of need (Psalm 46:1) both emotionally and spiritually throughout this process.

Table of Contents

Abstract

The synthesis, characterization, and properties of selected intermetallics and ceramic materials are presented in this dissertation. In our quest to grow single crystal intermetallics from the metal flux technique, new strategies were employed to avoid thermodynamically stable phases and to ensure sample homogeneity of the crystalline product for structure elucidation and accurate measurements of their magnetic and electrical properties. The relationship between the complex crystal structures and magnetic properties are reported for $LnCo_2Al_8$ (Ln = La-Nd, Sm, Yb), $CeCo_{2-x}Mn_xAl_8$ ($0 < x < 1$), and $Pr_2Fe_{4-x}Co_xSb_5$ ($1 \leq x < 3$). The discovery of magnetic frustration in $LnCo_2Al_8$ (Ln = Ce, Nd) and complex magnetic ordering coupled with large positive magnetoresistance of up to 150% and 60% at 200 K with relatively low field of H = 1 T in $Pr_2Fe_{4-x}Co_xSb_5$ ($x \approx 2$ and 2.5) is also reported.

The demand of new inorganic solid materials as scaffolds for the engineering of bone tissue has led to the synthesis of calcium magnesium silicates such as, diopside ($CaMgSi_2O_6$), akermanite ($Ca_2MgSi_2O_7$), monticellite ($CaMgSiO_4$), and merwinite ($Ca_3Mg(SiO_4)_2$)) for studying dimensionality and mechanical properties. This dissertation highlights the synergism of solid state chemistry at the interface of condensed matter physics and biological engineering. The discovery of compounds with tunable magnetic, electrical, and mechanical properties will be described herein.

Chapter 1. Introduction

"Synergy is the creation of a whole that is greater than the sum of its parts."- Ray French

1.1 Solid State and Materials Chemistry

Solid state and materials chemistry are interdisciplinary fields that bridge with condensed matter physics, crystallography, materials science, and tissue engineering. Solid state chemistry is propelled by technological advances that will hopefully lead to societal benefits. Technological pursuits are motivated by the properties discovered in materials, which thereby leads to the engineering of new materials with enhanced properties. Thus, targeting and strategically synthesizing materials with desired properties leads to the discovery of families of compounds with unique and often tailorable properties. In this dissertation, I will discuss the synthesis and characterization of several solid state materials, including intermetallic compounds and ceramics. Desirable physical, mechanical, and/or biological properties for future technological developments, and hopes to further their fundamental understanding as well as their concomitant application, has motivated the syntheses of these materials.

1.2 Motivation for Rare Earth Ternary Intermetallics

Intermetallics is a class of materials composed of more than one metallic element and exhibit long range structural order. As shown in Table 1, several technological applications are based on the properties of intermetallic compounds. Rare earth intermetallics are of interest because of their intriguing crystal structures and their reported exotic magnetic and electrical properties.[1] For the past decade, our group has focused on the crystal growth of ternary intermetallics of Ln-M-X (Ln = lanthanide, M = transition metals, and X = main group element).[2] Materials discovered exhibit magnetic frustration,[1] spin glass,[3, 4] and thermoelectric behavior.[5, 6] Our properties-driven approach is strategically conducted through the single crystal

growth of materials via the molten metal flux technique. Thus, after a single crystal is grown, its structure is elucidated, and the properties are measured allowing the direct correlation of structure and physical properties.

Table 1. Examples of technological applications based on physical properties of intermetallics as adapted from ref. seven.[7]

Physical Properties	Application	Material
Magnetic Ordering	Hard and soft magnets	$Nd_2Fe_{14}B$
Magnetoresistance	Read Heads	$La_{0.67}Ca_{0.33}MnO_3$
Magnetocaloric Effect	Cryogenerators	$Gd_5(Si_xGe_{1-x})_6$
Peltier Effect	Refrigeration	Bi_2Te_3
Semiconductivity	Electronic Devices	GaAs, InAs, InSb
Superconductivity	Charge Transport	Nd_3Sn, Nb-Ti solid solutions

1.3. Crystal Growth

Traditional solid state growth techniques, such as hydrothermal synthesis, arc melting, floating zone methods, and the self-flux method have been used for the growth of intermetallics. The molten metal flux growth method is the desired method for the growth of single crystals , due to the kinetic control and high purity growth of the single crystal products while avoiding congruently melting phases that are thermodynamically stable.[8] New strategies for high purity crystal growth suitable for physical property measurements are aimed by changing reaction ratios, temperature profiles, and the use of an inert flux. Further details regarding the optimization of single crystal growth are discussed in Chapters 2 and 3. Standard solid state characterization methods are used to determine the structure of the materials. Details will be presented in each chapter, and when suitable, magnetic, and electrical properties will be presented.

1.4 Physical Properties

In this dissertation, unusual forms of magnetic ordering, magnetic frustration, and large positive magnetoresistance are discovered. Experimental details and results of the properties for each compound presented are discussed in the pertinent sections within each chapter. Standard references for magnetic and electrical properties include "Magnetism in Condensed Matter"[9], "Fundamental of Magnetism and Magnetic Measurements",[10] and "Introduction to Solid State Physics".[11] Brief descriptions of geometrical frustration and magnetoresistance are presented.

1.4.1 Geometrical Frustration

A.P. Ramirez defines frustration as "the inability of a system to find a unique ground state".[12] Frustration is caused by competing interactions due to site disorder or lattice structure, specifically in triangular lattices.[13] In a two-dimensional triangular lattice system with antiferromagnetic nearest neighbor interactions, there exist two adjacent spins aligned antiparallel. To minimize energy, this results in the third spin aligning ferromagnetically (geometrical frustration). These frustrated spin states can propagate to neighboring triangles in systems with extended structures and emergence of novel magnetic phases can occur. Frustration is empirically derived from temperature-dependent magnetic susceptibility using the following equation, $f = |\theta| / T_{N/c}$, where θ represents the Curie Weiss temperature, and T_N or T_c is the antiferromagnetic or ferromagnetic ordering temperature, respectively.[14] Strong geometrically frustrated materials obtain values of $f > 7$. Classical examples are oxides of the pyrochlore, kagome, and fcc antiferromagnetic lattices.[14, 15] Intermetallic systems usually display frustration values of $f < 3$. However, two examples of strong geometrically frustrated intermetallics are CePdAl (ZrNiAl-structure type) and $Ce_5Ni_2Si_3$ (Ce_2NiSi-structure type).[16, 17]

1.4.2 Magnetoresistance

Magnetoresistance is defined as the change in a material's electrical resistivity as a function of an applied magnetic field, where ρ_H is the resistivity in an applied magnetic field *H*, and ρ_0 is the resistivity at zero field, as shown in the equation below. [18]

$$MR = \frac{\rho_H - \rho_0}{\rho_0} \times 100\%$$

In 1856, William Thomson first discovered the magnetoresistance effect when he observed a 0.2% increase in the resistance of Fe by applying a magnetic field longitudinally and a decrease in the magnetoresistance of 0.4% when a field was applied transversely, known as anisotropic magnetoresistance (AMR).[19] Since then, magnetoresistance materials have found application in the field of spintronics, as read heads and magnetic sensors for magnetic recording devices as listed in Table 1. This application is based upon the giant magnetoresistance (GMR) effect first observed in the Fe/Cr multilayer, resulting from spin-dependent scattering.[20] Colossal magnetoresistance (CMR) has also been discovered in the manganese-based perovskites via the double-exchange mechanism.[21] Another Mn-containing compound that exhibits large negative magnetoresistance up to -36% at 5 T and 92 K is the Zintl phase, $Eu_{14}MnSb_{11}$, which occurs near its ferromagnetic ordering temperature at 100 K.[22] Small positive magnetoresistance is typically seen in metallic systems, but magnetoresistances over 10,000% is found in high-mobility semiconductors like the transition-metal chalcogenides. For example, large positive magnetoresistance of up to 453, 200% at 4.5 K and ~15 T was recently shown in the layered, non-magnetic WTe_2.[23] Our group has also reported large positive magnetoresistance above 100% at fields above 5 T at relatively low temperatures in the metallic Ce_2PdGa_{10},[24] $LnNi_{1-x}Sb_2$ (Ln = Y, Dy, Ho),[25] $La(Cu_{(0.2)}Ni_{(0.8)})_ySb_2$, [26] La_2NiGa_{12},[27] $Pr(Cu,Ga)_{12.85}$,[28] and Ln_4MGa_{12} (Ln = Dy-Er, M = Pd, Pt) compounds.[29]

1.5 Bioceramics

Solid state materials also have application in the area of biological engineering, particularly tissue engineering. The use of inorganic solid state materials (ceramics) as scaffolds for tissue regeneration has shown promise in bone tissue engineering.[30] Biocompatible ceramics have been reported to display improved mechanical properties, including compressive strength and low fracture toughness, when compared to living bone.[31] When ceramics are used as scaffolding materials, this exceeds the commonly used methods of hip replacements (toxic) and autografts (invasive surgery) to repair bone fractures. Ceramic material, such as hydroxyapatite,[32] is commonly used to regenerate bone tissue. However, this material is extremely brittle with a short life expectancy, which limits its use for load-bearing applications. Therefore, the search for ceramic materials with improved mechanical properties, preferably compressive strengths as high as 170 MPa, to mimic living bone is paramount due to the growing elderly population. The collaborative effort of solid state/materials chemists and biological engineers is vital towards the advancement of biomaterials.

The solid state reaction method was used for the syntheses of the bioceramics discussed in Chapter 4. This is a direct reaction method that requires grinding and mixing at high temperatures up to 1300 °C to reach phase equilibria. The advantages of the conventional solid state method are obtaining product with high purity and the ability to tune the synthetic parameters to avoid impurities and metastable phases. Unfortunately, long reaction times are required; therefore, a hybrid microwave setup was also used for the production of ceramic materials. This method employs a modern microwave oven with invertor technology to homogeneously heat the sample with low frequency electromagnetic radiation using a thermal barrier (alumina foam) to reach temperatures compared to that achieved conventionally. The

microwave method has been shown to produce material fast and without undesirable phases. Further details regarding the microwave setup used are also presented in Chapter 4.

1.6 Summary of Projects

The work and discoveries previously reported in our group has been the foundation of the research presented in this dissertation. My dissertation highlights several Al–containing and Sb–containing intermetallic systems grown from the metal flux technique and their corresponding magnetic and electrical properties. Furthermore, the syntheses of calcium magnesium silicates have shown potential application as scaffolds for bone tissue regeneration. We were able to predict the mechanical properties based on dimensionality of the structure. A brief overview of each project is as follows.

Chapter 2 discusses work on the "Strategic Crystal Growth and Physical Properties of Single–Crystalline $LnCo_2Al_8$ (Ln = La–Nd, Sm, Yb) and $CeCo_{2-x}Mn_xAl_8$ ($0 < x < 1$)". In the literature, $CeCo_2Al_8$ is reported to have a localized Ce^{3+} moment while the Fe analogue, $CeFe_2Al_8$, displays a fluctuating valence $Ce^{3+/4+}$.[33] To further study the relationship between the lanthanide and transition metal sublattice, we incorporated Mn in $CeCo_2Al_8$ and studied the effects of substitution on the structure and magnetic properties. The substitution studies on $CeCo_2Al_8$ led us to study other lanthanide containing members that adopt the $CaCo_2Al_8$–structure type,[34] $LnCo_2Al_8$ (Ln = La–Nd, Sm, Yb). $PrCo_2Al_8$ displays a step-wise metamagnetic transitions, while $CeCo_2Al_8$ and $NdCo_2Al_8$ exhibit magnetic frustration.

"Complex Magnetic Ordering and Large Positive Magnetoresistance in $Pr_2Fe_{4-x}Co_xSb_5$ ($1 \leq x < 3$)" is discussed in Chapter 3. Motivated by the discovery of spin glass behavior in the $Ln_2Fe_4Sb_5$ (Ln = La–Nd, Sm)[3] series, we investigated the structure, magnetic, and electrical properties of Co substituted $Pr_2Fe_4Sb_5$ and also studied the effect on the structure, magnetic, and

electrical properties. To grow single crystals suitable for physical property measurements, we adapted the synthetic method previously reported for the $Ln_2Fe_4Sb_5$ (Ln = La-Nd, Sm) series using an inert Bi flux. Details of the structure, characterization, magnetic and electrical properties are presented in Chapter 3.

Chapter 4 discusses the "Synthesis and Characterization of Calcium Magnesium Silicates via Solid–State and Microwave Methods as Scaffolds for Bone Tissue Engineering". The increasing need of scaffolding materials and the known properties of calcium magnesium silicates, we compared the mechanical properties to the dimensionality of several structurally related calcium magnesium silicates. Our group previously reported on the biocompatibility (in vitro), compressive strength, and degradation rate of akermanite:polycaprolactone (PCL) composite scaffolds and found that the akermanite:PCL scaffolds were biocompatible and together with the mechanical properties tested showed potential use in tissue engineering applications.[35] Motivated by this work, we synthesized diopside ($CaMgSi_2O_6$), akermanite ($Ca_2MgSi_2O_7$), monticellite ($CaMgSiO_4$), and merwinite ($Ca_3MgSi_3O_8$) via the solid state reaction technique and characterized them via powder X-ray diffraction. These materials were later studied as ceramic scaffolds and ceramic/polymer composite scaffolds, and their mechanical and biological properties were evaluated. The greatest advantage of synthesizing silicates via ceramic methods is the ease of preparation of materials in high purity and quantity, but extensively long reaction times are often required. Therefore, $Sr_2MgSi_2O_7$ was synthesized with a hybrid microwave-assisted method to compare sample quality to oxides produced with conventional ceramic methods. Further details and future work are provided in Chapter 4.

1.7 References

(1) Schmitt, D. C.; Drake, B. L.; McCandless, G. T.; Chan, J. Y., Targeted Crystal Growth of Rare Earth Intermetallics with Synergistic Magnetic and Electrical Properties: Structural Complexity to Simplicity. *Acc. Chem. Res.* **2015,** *48*, 612-618.

(2) Phelan, W. A.; Menard, M. C.; Kangas, M. J.; McCandless, G. T.; Drake, B. L.; Chan, J. Y., Adventures in Crystal Growth: Synthesis and Characterization of Single Crystals of Complex Intermetallic Compounds. *Chem. Mater.* **2012,** *24*, 409-420.

(3) Phelan, W. A.; Nguyen, G. V.; Wang, J. K.; McCandless, G. T.; Morosan, E.; DiTusa, J. F.; Chan, J. Y., Discovery of Spin Glass Behavior in $Ln_2Fe_4Sb_5$ (Ln = La-Nd and Sm). *Inorg. Chem.* **2012,** *51*, 11412-11421.

(4) Schmitt, D. C.; Prestigiacomo, J. C.; Adams, P. W.; Young, D. P.; Stadler, S.; Chan, J. Y., Field-Pulse Memory in a Spin-Glass. *Appl. Phys. Lett.* **2013,** *103*, 082403/1-082403/4.

(5) Schmitt, D. C.; Haldolaarachchige, N.; Xiong, Y.; Young, D. P.; Jin, R.; Chan, J. Y., Probing the Lower Limit of Lattice Thermal Conductivity in an Ordered Extended Solid: $Gd_{117}Co_{56}Sn_{112}$, a Phonon Glass-Electron Crystal System. *J. Am. Chem. Soc.* **2012,** *134*, 5965-5973.

(6) Schmitt, D. C.; Haldolaarachchige, N.; Prestigiacomo, J.; Karki, A.; Young, D. P.; Stadler, S.; Jin, R.; Chan, J. Y., Structural Complexity Meets Transport and Magnetic Anisotropy in Single Crystalline $Ln_{30}Ru_4Sn_{31}$ (Ln = Gd, Dy). *J. Am. Chem. Soc.* **2013,** *135*, 2748-2758.

(7) Maria L. Fornasini, F. M. a. M. P., *Intermetallic Compounds: Principle and Practice.* . ed.; John Wiley & Sons, Ltd.,: 2002; Vol. *3*, p 1033.

(8) Canfield, P.; Fisk, Z., Growth of Single Crystals from Metallic Fluxes. *Philos. Mag. B* **1992,** *65*, 1117-1123.

(9) Blundell, S., *Magnetism in Condensed Matter*. ed.; Oxford University Press: 2001; p 272

(10) McElfresh, M., Fundamentals of Magnetism and Magnetic Measurements. **1994**.

(11) Kittel, C., *Introduction to Solid State Physics*. ed.; John Wiley & Sons: New York, 2005.

(12) Ramirez, A. P., Geometric Frustration: Magic moments. *Nature* **2003,** *421*, 483.

(13) Anderson, P. W., Ordering and Antiferromagnetism in Ferrites. *Phys. Rev.* **1956,** *102*, 1008-13.

(14) Ramirez, A. P., Strongly Geometrically Frustrated Magnets. *Annu. Rev. Mater. Sci.* **1994,** *24*, 453-80.

(15) Greedan, J. E., Geometrically Frustrated Magnetic Materials. *J. Mater. Chem.* **2001,** *11*, 37-53.

(16) Doenni, A.; Ehlers, G.; Maletta, H.; Fischer, P.; Kitazawa, H.; Zolliker, M., Geometrically Frustrated Magnetic Structures of the Heavy-Fermion Compound CePdAl Studied by Powder Neutron Diffraction. *J. Phys.: Condens. Matter* **1996,** *8*, 11213-11229.

(17) Ryu, D. H.; Jung, M. H.; Kwon, Y. S., Magnetic Ordering in Frustrated $Ce_5Ni_2Si_3$. *Physica B. (Amsterdam, Neth.)* **2005,** *359-361*, 305-307.

(18) Blundell, S., *Magnetism in Condensed Matter*. ed.; Oxford University Press: Oxford, U.K.: 2001; p 184.

(19) Thomson, W., On the Electro-Dynamic Qualities of Metals:--Effects of Magnetization on the Electric Conductivity of Nickel and of Iron. *Pro. Roy. Soc. of London* **1856,** *8*, 546-550.

(20) Baibich, M. N.; Broto, J. M.; Fert, A.; Nguyen Van Dau, F.; Petroff, F.; Eitenne, P.; Creuzet, G.; Friederich, A.; Chazelas, J., Giant Magnetoresistance of (001)Iron/(001)Chromium Magnetic Superlattices. *Phys. Rev. Lett.* **1988,** *61*, 2472-5.

(21) Zener, C., Interaction Between the d-Shells in the Transition Metals. II. Ferromagnetic Compounds of Manganese with Perovskite Structure. *Phys. Rev.* **1951,** *82*, 403-5.

(22) Chan, J. Y.; Kauzlarich, S. M.; Klavins, P.; Shelton, R. N.; Webb, D. J., Colossal Magnetoresistance in the Transition-Metal Zintl Compound $Eu_{14}MnSb_{11}$. *Chem. Mater.* **1997,** *9*, 3132-3135.

(23) Ali, M. N.; Flynn, S.; Gibson, Q. D.; Schoop, L. M.; Haldolaarachchige, N.; Cava, R. J.; Xiong, J.; Liang, T.; Hirschberger, M.; Ong, N. P.; Tao, J., Large, Non-Saturating Magnetoresistance in WTe_2. *Nature* **2014,** *514*, 205-8.

(24) Millican, J. N.; Macaluso, R. T.; Young, D. P.; Moldovan, M.; Chan, J. Y., Synthesis, Structure, and Physical Properties of Ce_2PdGa_{10}. *J. Solid State Chem.* **2004,** *177*, 4695-4700.

(25) Thomas, E. L.; Moldovan, M.; Young, D. P.; Chan, J. Y., Synthesis, Structure, and Magneto-transport of $LnNi_{1-x}Sb_2$ (Ln = Y, Gd-Er). *Chem. Mater.* **2005,** *17*, 5810-5816.

(26) Gautreaux, D. P.; Parent, M.; Karki, A. B.; Young, D. P.; Chan, J. Y., Investigation of the Effect of Ni Substitution on the Physical Properties of $Ce(Cu_{(1-x)}Ni_{(x)})_{(y)}Sb_{(2)}$. *J. Phys. Condens. Matter* **2009,** *21*, 056006.

(27) Cho, J. Y.; Millican, J. N.; Capan, C.; Sokolov, D. A.; Moldovan, M.; Karki, A. B.; Young, D. P.; Aronson, M. C.; Chan, J. Y., Crystal Growth, Structure, and Physical Properties of Ln_2MGa_{12} (Ln = La, Ce; M = Ni, Cu). *Chem. Mater.* **2008,** *20*, 6116-6123.

(28) Cho, J. Y.; Thomas, E. L.; Nambu, Y.; Capan, C.; Karki, A. B.; Young, D. P.; Kuga, K.; Nakatsuji, S.; Chan, J. Y., Crystal Growth, Structure, and Physical Properties of $Ln(Cu,Ga)_{13-x}$ (Ln = La-Nd, Eu; $x \approx 0.2$). *Chem. Mater.* **2009,** *21*, 3072-3078.

(29) Cho, J. Y.; Moldovan, M.; Young, D. P.; Chan, J. Y., Crystal Growth and Magnetic Properties of Ln_4MGa_{12} (Ln = Dy-Er; M = Pd, Pt). *J. Phys.: Condens. Matter* **2007,** *19*, 266224/1-266224/11.

(30) Hench, L. L.; Splinter, R. J.; Allen, W.; Greenlee, T., Bonding mechanisms at the interface of ceramic prosthetic materials. *J. Biomed. Mater. Res.* **2004,** *5*, 117-141.

(31) Hench, L. L., Bioceramics: from Concept to Clinic. *Am. Ceram. Soc. Bull.* **1993,** *72*, 93-8.

(32) Kay, M. I.; Young, R. A.; Posner, A. S., Crystal Structure of Hydroxyapatite. *Nature (London, U. K.)* **1964,** *204*, 1050-2.

(33) Ghosh, S.; Strydom, A. M., Strongly Correlated Electron Behaviour in CeT_2Al_8 (T = Fe, Co). *Acta Phys. Polym., A* **2012,** *121*, 1082-1084.

(34) Czech, E.; Cordier, G.; Schaefer, H., Study of Calcium-Cobalt-Aluminum ($CaCo_2Al_8$). *J. Less Common Met.* **1983,** *95*, 205-11.

(35) Zanetti, A. S.; McCandless, G. T.; Chan, J. Y.; Gimble, J. M.; Hayes, D. J., In Vitro Human Adipose-Derived Stromal/Stem Cells Osteogenesis in Akermanite: Poly-ε-caprolactone Scaffolds. *J. Biomater. Appl.* **2014,** *28*, 998-1007, 10.

Chapter 2. Strategic Crystal Growth and Physical Properties of Single-Crystalline $LnCo_2Al_8$ (Ln = La–Nd, Sm, Yb)[*] and $CeCo_{2-x}Mn_xAl_8$ ($0 < x < 1$) [**]

2.1. Introduction

Motivated to understand the relationships between the crystal structure and predominant magnetic interactions in extended solids, our group and others have explored ternary/pseudoternary rare earth Ln-M-X intermetallics, where Ln = lanthanide, M = transition metal, and X = Group 13–15 elements.[1, 2] For example, synthesis and crystal growth of ternary compounds $CePdGa_6$ and Ce_2PdGa_{12} allowed the study of magnetic ordering mechanisms in similar, but slightly different crystal structures.[3, 4] $CePdGa_6$ consists of face-sharing $CeGa_{8/4}$ rectangular prisms and edge-sharing $PdGa_{8/2}$ rectangular prisms that are separated by one layer of Ga atoms. Ce_2PdGa_{12} consists of $PdGa_{8/2}$ rectangular prismatic layers with Ce atoms residing in Ga cavities with two Ga layers separating the Ce and Pd atoms. With the addition of Ga–layers, the ordering temperature increases from T_N = 5 K to 11 K because of the enhanced coupling of *f*-moments to conduction electrons, highlighting the influence of carriers on the magnetic properties of intermetallic phases.[3, 5]

We have systematically grown and characterized single crystals of several pseudo-ternary phases that adopt the $NaZn_{13}$- and $ThMn_{12}$-structure types which show unusual magnetic and electrical properties.[7, 8] For example, $Ln(Cu, Ga)_{13-x}$ (Ln = La-Nd, Eu) ($NaZn_{13}$-structure type) can be prepared with early lanthanides up to Nd.[9] The Eu analogue also forms, given the larger cationic radii and the divalent state of Eu. Surprisingly, the Pr–analogue exhibits a large positive

[*]Reprinted with permission from Watkins-Curry, P.; Burnett, J. V.; Samanta, T.; Young, D. P.; Stadler, S.; Chan, J. Y., Strategic Crystal Growth and Physical Properties of Single-Crystalline $LnCo_2Al_8$ (Ln = La-Nd, Sm, Yb). *Cryst. Growth Des.* **2015**, 10.1021/acs.cgd.5b00417. Copyright 2015 American Chemical Society

[**]Reprinted in part with permission from Treadwell, L. J.; Watkins-Curry, P.; McAlpin, J. D.; Rebar, D. J.; Hebert, J. K.; Di Tusa, J. F.; Chan, J. Y., Investigation of Mn, Fe, and Ni Incorporation in $CeCo_2Al_8$. *Inorg. Chem.* **2015,** *54*, 963-968.Copyright 2014 American Chemical Society

magnetoresistance up to 154% at 2 K with an application of magnetic field and a large electronic contribution to the heat capacity, $C_p = \gamma T + \beta T^3$, with $\gamma \approx 100$ mJ / mol-K^2. The Al and heavy Ga analogues, however, adopt the $ThMn_{12}$-structure type.[10, 11] When Ga is substituted with Al, the Sommerfeld coefficient increases to $\gamma \approx 356$ mJ / mol-K^2 in $Pr(Cu, Al, Ga)_{13-x}$ ($x \approx 0.1$).[10] Single crystals of $Ln(Cu, Al)_{12}$ (Ln ≈ Y–Pr, Sm) can also be grown with early lanthanides, and the Ce–, Pr–, and Nd–analogues have Sommerfeld coefficients of 390, 80, and 120 mJ / mol-K^2, respectively.[11]

With our interest in highly correlated systems, we sought out to grow single crystals of CeM_2Al_8 (M = Fe, Co).[12] The oxidation state of Ce in CeM_2Al_8 (M = Fe, Co) is highly dependent on the transition metal. Ce is trivalent in $CeCo_2Al_8$, while Ce is valence fluctuating in $CeFe_2Al_8$.[12] Because the oxidation state of Ce in CeM_2Al_8 (M = Fe, Co) is dependent on the transition metal, we investigated the incorporation of Mn, Fe, and Ni in $CeCo_2Al_8$, where we observed Ce fluctuating valence in $CeCo_{2-x}Fe_xAl_8$ ($x \approx 1.00$), as we moved closer to the end-member of $CeFe_2Al_8$.[13] To grow larger single crystals necessary for physical property measurements, we set out to determine the best conditions for synthesis of $LnCo_2Al_8$ (Ln = La-Nd, Yb) and $CeCo_{2-x}Mn_xAl_8$ ($0 \leq x < 1$). With the exception of $PrCo_2Al_8$, compounds of $LnCo_2Al_8$ (Ln = La-Nd, Sm, Yb) with any physical properties reported have been that of polycrystalline material.[12, 14-18] Herein, we report the crystal growth, structure, magnetization, and electrical resistivity of $LnCo_2Al_8$ (Ln = La–Nd, Sm, Yb). We also report the magnetic properties of $CeCo_{2-x}Mn_xAl_8$ ($0 < x < 1$). Details of the structure and optimization of synthesis parameters will be discussed.[6]

2.2 Experimental Section

2.2.1. Synthesis

Single crystals of $LnCo_2Al_8$ (Ln = La–Nd, Sm, Yb) and $CeCo_{2-x}Mn_xAl_8$ ($0 < x < 1$) were grown using the self-flux growth method, a technique that employs a main group element, which

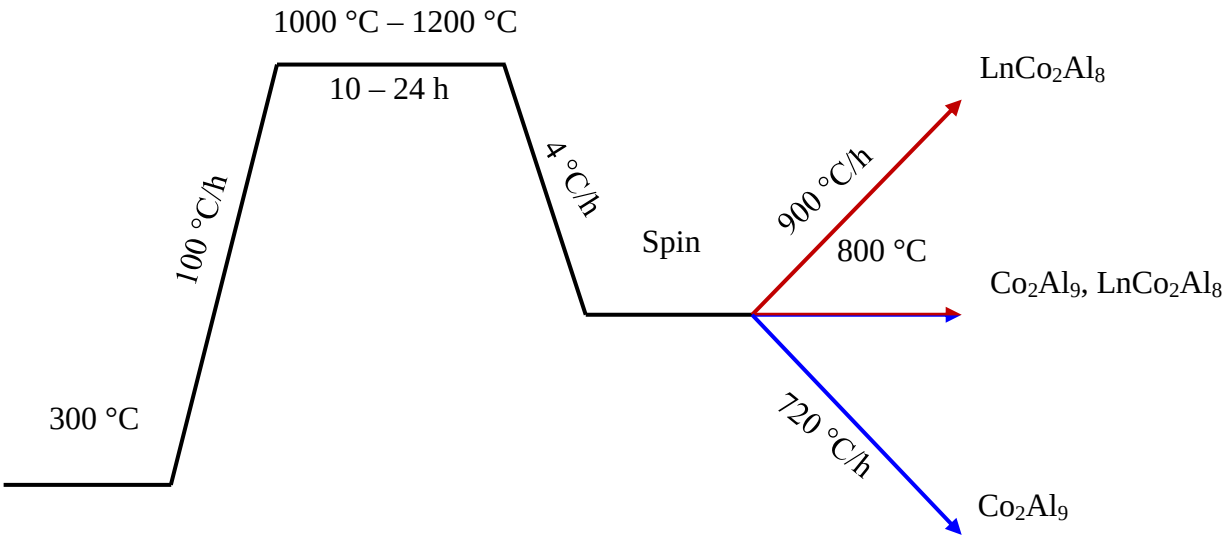

Figure 2.1. Temperature profile for the growth of $LnCo_2Al_8$ (Ln = La–Nd, Sm, Yb).[6]

typically has a lower melting point than the transition metal or lanthanide constituents, thereby leading to the growth of high quality materials.[19, 20] For the growth of $LnCo_2Al_8$ (Ln = La–Nd, Sm, Yb), the following elements, La (rod, 99.9%), Ce (rod, 99.9%), Pr (rod, 99.9%), Nd (rod, 99.9%), Sm (rod, 99.9%), Yb (ingots, 99.99%), Co (powder, 99.99%), and Al (shots, 99.99%) were used as received. Also, for the growth of $CeCo_{2-x}Mn_xAl_8$ ($0 < x < 1$), Ce (rod, 99.9%), Co (powder, 99.9%), M (Mn, 99.9%), and Al (shots, 99.9%) were used as received. The elements Ln:Co:Al in ratio of 1:2:20 were placed into an alumina crucible with a second crucible capping the first. The crucibles were sealed in an evacuated (50–70 mTorr) fused-silica tube and backfilled with ~ 0.3 atm of Ar gas. The reactions were placed in a furnace and heat treated with the parameters highlighted in Figure 2.1. For the Ce analogue, the ampule was heated to 1100 °C for 10 h at a rate of 100 °C/h, followed by cooling to 720 °C at a rate of 4 °C/h, and the excess Al flux was removed via centrifugation, yielding single crystals of Co_2Al_9.[21] In an attempt to avoid the Co_2Al_9 impurity, the subsequent reaction was

annealed at 1200 °C for 24 h at a rate of 100 °C/h, and cooled to 900 °C at a rate of 4 °C/h which yielded single crystals of $CeCo_2Al_8$. With respect to the lower melting points of La, Yb, and Pr, as well as the relatively higher vapor pressure of Yb, the growths of $LnCo_2Al_8$ (Ln = La, Pr, Yb) were annealed to 1000 °C and dwelled for 24 h, followed by slow cooling to 800 °C at a rate of 4 °C/h. For the La analogue, a polycrystalline mixture of $LaCo_2Al_8$ (~50%) and Co_2Al_9 (~50%) was obtained. In the Pr analogue, the growths resulted in $PrCo_2Al_8$ (~60%) and binaries such as $PrAl_4$/β-Pr_3Al_{11} (~20%) and Co_2Al_9 (~20%). The Yb reaction yielded $YbCo_2Al_8$ (~50%) and Co_2Al_9 (~50%). To achieve higher yields (>90%), the growths of $LnCo_2Al_8$ (La, Pr, Yb) were heated to 1200 °C for 24 h and slow cooled to 900 °C. Similarly, Nd and Sm analogues were grown up to 1200 °C and slow cooled to 900 °C, resulting in crystals up to 3.4 mm and 8 mm in length for Nd and Sm, respectively. To synthesize $CeCo_{2-x}Mn_xAl_8$ ($0 < x < 1$), the reaction ratios provided in Table 2.1 were used. The reactions were heated using the aforementioned synthesis profile. In our quest to synthesize $LnCo_2Al_8$ (Ln = La–Nd, Sm, Yb) and $CeCo_{2-x}Mn_xAl_8$ ($0 \leq x < 1$), we discovered that it was necessary to remove the sample above 900 °C to avoid the formation of Co_2Al_9. This was apparent by evaluating the Co-Al phase diagram, where Co_2Al_9 is stable below 900 °C. We found that removing the samples at a temperature lower than 900 °C consistently yielded Co_2Al_9 in such an Al-rich environment.

Table 2.1. Composition of $CeCo_{2-x}M_xAl_8$ (M = Mn, Fe, Ni)[13]

	Mn		
Nominal (x)	0.33	0.67	1.00
XRD (x)	0.22(5)	0.45(3)	0.70(4)
EDS (x)	0.29(3)	0.43(1)	0.71(2)

2.2.2 Elemental Analysis

Elemental analysis was conducted via electron dispersive spectroscopy (EDS) using a Zeiss – LEO Model 1530 variable pressure field effect scanning electron microscope equipped with an EDAX detector at an accelerating voltage of 20 kV. Spectra were integrated for 60 s, and the results from five spots were averaged and normalized to the Ln to determine the atomic percentage of each element. The compositions of $LnCo_2Al_8$ (Ln = La-Nd, Sm, Yb) $La_{1.00(2)}Co_{1.89(4)}Al_{7.88(5)}$, $Ce_{1.00(7)}Co_{1.82(11)}Al_{10.02(24)}$, $Pr_{1.00(3)}Co_{2.01(8)}Al_{7.28(11)}$, $Nd_{1.00(3)}Co_{1.87(6)}Al_{10.73(8)}$, $Sm_{1.00(2)}Co_{1.77(7)}Al_{9.27(9)}$, and $Yb_{1.00(3)}Co_{1.84(7)}Al_{11.96(8)}$.[6] The compositions of $CeCo_{2-x}Mn_xAl_8$ ($0 < x < 1$) are the following $Ce_{1.00(6)}Co_{1.47(5)}Mn_{0.29(3)}Al_{7.58(13)}$,$Ce_{1.00(10)}Co_{1.50(5)}Mn_{0.43(1)}Al_{7.97(19)}$, and $Ce_{1.00(10)}Co_{1.28(3)}Mn_{0.71(2)}Al_{7.97(9)}$.[13]

2.2.3. Powder X-ray Diffraction

Phase identification and sample homogeneity were determined by X-ray diffraction. Data were collected using a Bruker D8 Advance powder X-ray diffractometer operating at 40 kV and 30 mA with CuK_α (1.54060 Å) radiation and a LYNXEYE XE detector along 2θ from 10 – 80° with a step size of 0.01°.[6]

2.2.4. Single Crystal X-ray Diffraction

Fragments of $LnCo_2Al_8$ (Ln = La-Nd, Sm, Yb) and $CeCo_{2-x}Mn_xAl_8$ ($0 < x < 1$) single crystals were cut to appropriate sizes and mounted on a glass fiber with epoxy. The fibers containing $LnCo_2Al_8$ (Ln = La–Nd, Sm, Yb) crystals were mounted on a Bruker D8 Quest Kappa single-crystal X-ray diffractometer equipped with an IμS microfocus source (λ = 0.71073 Å) operating at 50 kV and 1 mA, a HELIOS optics monochromator, and a CMOS detector. The fibers containing $CeCo_{2-x}Mn_xAl_8$ ($0 < x < 1$) single crystals were mounted on a Nonius Kappa CCD X-ray diffractometer equipped with a Mo Kα radiation source at room temperature. The crystal structures of $LnCo_2Al_8$

were solved using direct methods in SHELXS2013,[22] and all atomic sites were refined anisotropically using SHELXL2014.[23] A starting model of $CeCo_{2-x}Mn_xAl_8$ ($0 < x < 1$)was obtained using SIR92[24] and refined with SHELXL97.[25] Multiple data collections and single crystal refinements were conducted on several crystals within the same batch of material to confirm the sample homogeneity. The crystallographic refinement details of $LnCo_2Al_8$ (Ln = La–Nd, Sm, Yb) and $CeCo_{2-x}Mn_xAl_8$ ($0 < x < 1$) are provided in Table 2.2 and 2.3. The atomic coordinates, occupancies, and anisotropic displacement parameters of $LaCo_2Al_8$ are provided in Table 2, and selected interatomic distances are provided in Table 2.4. The crystallographic data for $LnCo_2Al_8$ (Ln = La-Nd, Sm, Yb) is provided in Tables A1.1 and A1.2 in the Supporting Information (SI). In the refinement of $CeCo_{2-x}Mn_xAl_8$ ($0 < x < 1$), the dopant (M) was only modeled on the Co1 and Co2 sites. Structural models of $CeCo_{2-x}Mn_xAl_8$ ($0 < x < 1$) were refined with the atomic positions of $CeCo_2Al_8$. The atomic displacement parameter (ADP) of the Co1 site was anomalously larger than Co2 ADP. Therefore, the dopant (M) was modeled on the Co1 site and subsequently on the Co2 site. The dopant M in all refined models favored the Co1 position over the Co2 site. The Mn concentration from the structural refinement of $CeCo_{2-x}Mn_xAl_8$ ($0 < x < 1$) are provided in Table 2.1. The atomic coordinates, occupancies, and anisotropic displacement parameters are provided in Table A1.3, and selected interatomic distances are provided in Table A1.4.

2.2.5. Physical Properties

Magnetic measurements for $LnCo_2Al_8$ (Ln = La–Nd, Sm, Yb) were performed using a Quantum Design Magnetic Property Measurement System (MPMS). Direct current magnetic susceptibility was measured under zero field cooled (ZFC) conditions from 3 to 300 K under an applied magnetic field of 0.1 T. Field dependent magnetization data were collected at 2 K with applied magnetic fields up to 7 T. Electrical resistivity was measured using a Quantum Design

Table 2.2. Crystallographic Parameters of $LnCo_2Al_8$ (Ln = La–Nd, Sm, Yb)[6]

Compound	$LaCo_2Al_8$	$CeCo_2Al_8$	$PrCo_2Al_8$	$NdCo_2Al_8$	$SmCo_2Al_8$	$YbCo_2Al_8$
a (Å)	12.5143(4)	12.4720(1)	12.4602(4)	12.444(4)	12.4159(6)	12.4110(10)
b (Å)	14.4007(5)	14.3870(2)	14.3743(5)	14.362(5)	14.3366(7)	14.426(4)
c (Å)	4.0339(1)	4.0220(3)	4.0101(1)	4.0098(14)	3.9831(2)	3.962(4)
V (Å^3)	726.97(4)	721.69(5)	718.24(4)	716.6(4)	709.00(1)	709.4(7)
Z	4	4	4	4	4	4
cryst dimens (mm^3)	0.02 x 0.02 x 0.04	0.02 x 0.02 x 0.03	0.02 x 0.02 x 0.03	0.02 x 0.03 x 0.04	0.02 x 0.02 x 0.03	0.02 x 0.02 x 0.03
temperature (K)	293(2)	293(2)	298(2)	296(2)	300(2)	293(2)
θ range (deg)	2.16 – 30.54	2.89 – 31.01	2.83 – 30.54	2.84 – 28.87	2.84-41.26	3.27-31.02
μ (mm^{-1})	11.143	11.613	6.057	12.588	13.682	18.581
measd reflns	7272	2190	13872	2393	17919	1984
indep reflns	1251	1296	1248	942	1227	1248
R_{int}	0.0307	0.0243	0.0261	0.0357	0.0684	0.0304
$\Delta\rho_{max}$ (e/Å^{-3})	0.948	1.233	0.568	1.275	1.796	1.869
$\Delta\rho_{min}$ (e/Å^{-3})	–1.117	–2.013	–0.776	–1.469	–1.669	–1.223
extinction coeff	0.0073(3)	0.0048(2)	0.00066(10)	0.0166(6)	0.0038(4)	0.0065(3)
GOF	1.232	1.179	1.020	1.146	1.081	1.031
R_1 (F)[a]	0.0161	0.0255	0.0135	0.0243	0.0310	0.0281
wR_2[b]	0.0365	0.0560	0.0290	0.0619	0.0766	0.0610

[a] $R_1 = \Sigma||F_o| - |F_c||/\Sigma|F_o|$. [b] $wR_2 = [\Sigma [w(F_o^2 - F_c^2)^2]/\Sigma [w(F_o^2)^2]]^{1/2}$.

Table 2.3. Crystallographic Parameters of $CeCo_{2-x}Mn_xAl_8$ ($0 < x < 1$)[13]

Compound	$CeCo_{1.78(5)}Mn_{0.22(5)}Al_8$	$CeCo_{1.55(3)}Mn_{0.45(3)}Al_8$	$CeCo_{1.30(4)}Mn_{0.70(4)}Al_8$
Crystal System	Orthorhombic	Orthorhombic	Orthorhombic
Space Group	*Pbam*	*Pbam*	*Pbam*
a (Å)	12.484(5)	12.4950(1)	12.499(3)
*b (*Å)	14.392(4)	14.407(1)	14.410(3)
c (Å)	4.026(3)	4.032(1)	4.034 (3)
V (Å^3)	723.5(6)	725.8(2)	726.6(5)
Z	4	4	4
Crystal dimensions (mm^3)	0.02 x 0.02 x 0.03	0.03 x 0.03 x 0.05	0.05 x 0.06 x 0.08
Temperature (K)	293(2)	293(2)	293(2)
θ range (º)	2.20 – 31.00	2.83 – 31.00	2.83 – 30.99
μ (mm^{-1})	11.463	11.301	11.158
Measured Reflections	2197	2227	2231
Independent Reflections	1298	1300	1303
Reflections with I>2σ(I)	970	1005	1054
R_{int}	0.0433	0.0350	0.0278
h	-17 to 18	-17 to 18	-17 to 18
k	-20 to 20	-20 to 20	-20 to 20
l	-5 to 5	-5 to 5	-5 to 5
Reflections	2197/72	2227/72	2231/72
$\Delta\rho_{max}$ (e Å^{-3})	1.541	2.466	2.465
$\Delta\rho_{min}$ (e Å^{-3})	-1.249	-1.137	-1.121
Extinction coefficient	0.0033(3)	0.0030(2)	0.0019(2)
GOF	1.047	1.040	1.091
R_1 (F)[a]	0.0349	0.0276	0.0263
wR_2[b]	0.0756	0.0581	0.0562

[a] $R_1 = \Sigma||F_o| - |F_c||/\Sigma|F_o|$. [b] $wR_2 = [\Sigma [w(F_o^2 - F_c^2)^2]/\Sigma [w(F_o^2)^2]]^{1/2}$.

Table 2.4. Atomic Positions of $LaCo_2Al_8$[6]

site	point symmetry	*x*	*y*	*z*	occ.	U_{eq} (Å^2)[a]
La	*m*	0.34040(2)	0.31815(2)	0	1	0.00717(6)
Co1	*m*	0.03474(2)	0.40574(2)	0	1	0.00599(7)
Co2	*m*	0.15151(2)	0.09650 (2)	0	1	0.00475(7)
Al1	*m*	0.02668(5)	0.13171(4)	½	1	0.00660(12)
Al2	*m*	0.15893(4)	0.38011(5)	½	1	0.00699(13)
Al3	*m*	0.23637(5)	0.17142(4)	½	1	0.00756(12)
Al4	*m*	0.33117(5)	0.49174(4)	½	1	0.00737(12)
Al5	*m*	0.45306(5)	0.17875(4)	½	1	0.00694(12)
Al6	*m*	0.09566(4)	0.25293(3)	0	1	0.00703(12)
Al7	*m*	0.34009(4)	0.04441(5)	0	1	0.00937(14)
Al8	2/*m*	0	½	½	1	0.00677(16)
Al9	2/*m*	0	0	0	1	0.00707(15)

[a] U_{eq} is defined as one-third of the trace of the orthogonalized U_{ij} tensor

Table 2.5. Selected Interatomic Distances of $LaCo_2Al_8$ (Å)[6]

		$LaCo_2Al_8$
La		
	Al1 × 2	3.1660(5)
	Al2 × 2	3.1657(5)
	Al3 × 2	3.1981(5)
	Al4 × 2	3.2142(5)
	Al5 × 2	3.1757(5)
	Al6 × 2	3.2035(6)
	Al9 × 1	3.29347(13)
Co1		
	Al2 × 2	2.5728(4)
	Al5 × 2	2.5677(4)
	Al6 × 1	2.3228(6)
	Al7 × 2	2.5380(7)
	Al8 × 2	2.46979(15)
	Co1 × 1	2.8509(5)
Co2		
	Al1 × 2	2.6011(4)
	Al3 × 2	2.5219(4)
	Al4 × 2	2.5280(4)
	Al6 × 1	2.3586(6)
	Al7 × 1	2.4764(6)
	Al9 × 1	2.3508(3)

Physical Property Measurement System (PPMS) from 3 to 300 K using the standard four-probe method at 0.1–0.3 mA with a frequency of 17 Hz.

2.3. Results and Discussion

2.3.1. Structure of $LnCo_2Al_8$ (Ln = La-Nd, Sm, Yb) and $CeCo_{2-x}Mn_xAl_8$ (0 < x < 1)

$LnCo_2Al_8$ (Ln = La-Nd, Sm, Yb) and $CeCo_{2-x}Mn_xAl_8$ (0 < x < 1) adopt the $CaCo_2Al_8$-structure type and has been reported for Al, Ga, and In-analogues and the structure is shown in Figure 2.2[12, 14-18, 26-30] For clarity, $LaCo_2Al_8$ will be discussed as a general structural model for the $LnCo_2Al_8$ (Ln = La-Nd, Sm, Yb) series and $CeCo_{2-x}Mn_xAl_8$ ($0 \leq x < 1$), followed by trends observed as a function of the Ln and increasing Mn concentration (x). The La atoms in $LaCo_2Al_8$ are surrounded by 13 Al atoms forming a distorted tri-capped pentagonal prism. The La atom is located in the channels of the surrounding Co environment and face-share via Al(1), Al(5) , Al(2), and Al(6)

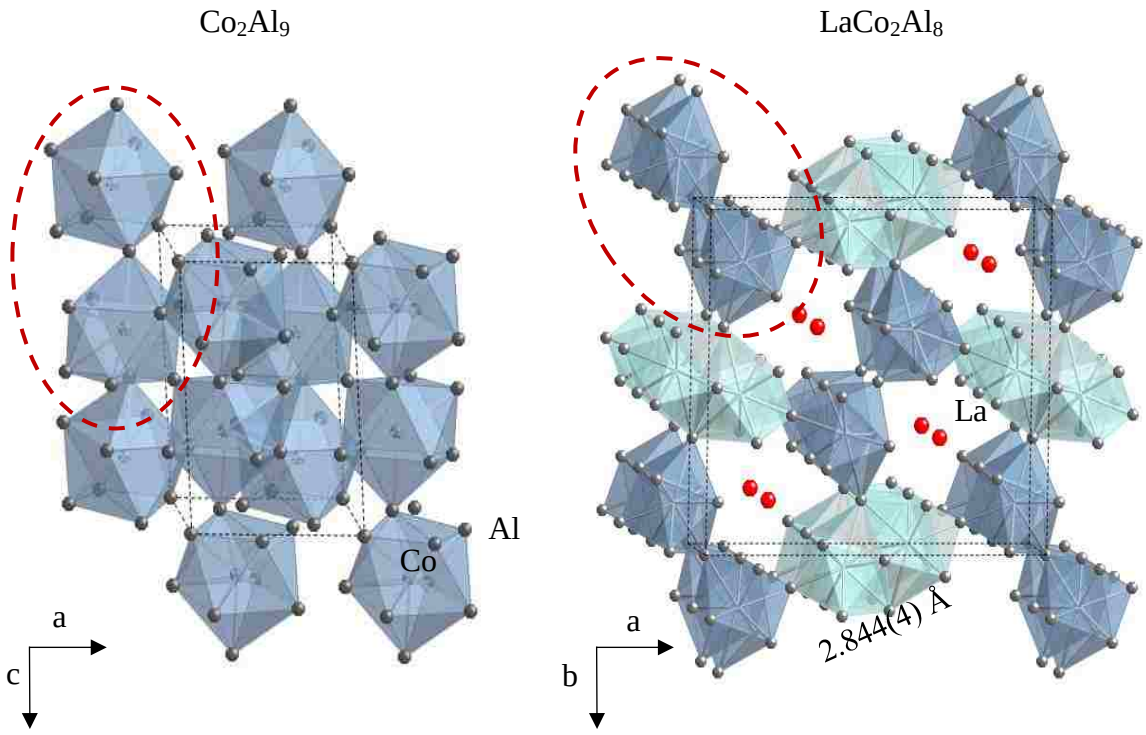

Figure 2.2. Crystal structure of Co_2Al_9 and $LaCo_2Al_8$.[6]

atoms and corner-share with one another via Al(9) forming bowtie arrangements. Except for La-Al(6) (3.354(5) Å), the La-Al distances (3.166(5) – 3.354(5) Å) are shorter than the sum of the metallic radii of La (1.88 Å) and Al (1.43 Å), yet still correspond well with the distances observed in $LaCoAl_4$.[31, 32] The transition metal sub-lattice of $LaCo_2Al_8$ is similar to Co_2Al_9.[21, 33] Both structure types consist of Co surrounded by nine atoms. The Co atoms in $LaCo_2Al_8$ form tri-capped trigonal prisms surrounded by aluminum atoms with Co-Al interatomic distances ranging from 2.3288(6) to 2.5728(4) Å, which are slightly shorter than the sum of the metallic radii for Co (1.25 Å) and Al (1.43 Å), but are similar to the distances of Co_2Al_9 and the ternary $U_2Co_6Al_{19}$, which suggests covalent bonding.[21, 32-34] Hence, the Co-Al interatomic distances in $LaCo_2Al_8$ (Ln= La-Nd, Sm, Yb) are that of strong bonding interactions. In addition, the second Co polyhedron consisting of two $Co(1)Al_8$ monocapped distorted square prisms is face-sharing in $LaCo_2Al_8$ with Co-Co dimers with an interatomic distance of 2.844(4) Å, which suggests weak bonding interactions due to the metallic radius of Co (1.25 Å).[32] The Co atoms in the binary Co_2Al_9 form monocapped distorted square antiprisms with distances ranging from ~2.38 Å to 2.48 Å, with the apical Co-Al distance of 2.54(1) Å. We also observe a subtle increase in the Al-Al contacts of the Co polyhedra in $LnCo_2Al_8$ (~ 2.8-3.016 Å) to the Co_2Al_9 framework (~ 2.488-2.766 Å). Since both Co atoms in Co_2Al_9 and $LnCo_2Al_8$ are surrounded by nine atoms, we believe that the stability of the $CaCo_2Al_8$ structure type is due to incorporation of a lanthanide or electropositive atom into Co_2Al_9 when prepared in an Al-rich environment.

A plot of the unit cell volume ($Å^3$) and *c*-axis (Å) lattice constant as a function of Ln^{3+} radii is shown in Figure 2.3. The volume decreases as a function of rare earth, consistent with the lanthanide contraction, except for $YbCo_2Al_8$. The volume of $YbCo_2Al_8$ (709.4(6) $Å^3$) and $SmCo_2Al_8$ (709.0(7) $Å^3$) are comparable, which indicates the divalent oxidation state of the Sm

and Yb–analogues. In all compounds, the Ln-Ln contacts, corresponding to the *c* axis lattice parameter for each analogue, and Co(1)-Co(1) dimer dimensions systematically decrease as a function of Ln. A plot of the volume as a function of increasing Mn concentration (x) is shown in Figure 2.4. For Mn–doped compounds, there is a steady increase in the volume, which is consistent with Mn substituting for Co, causing an expansion of the crystal lattice.

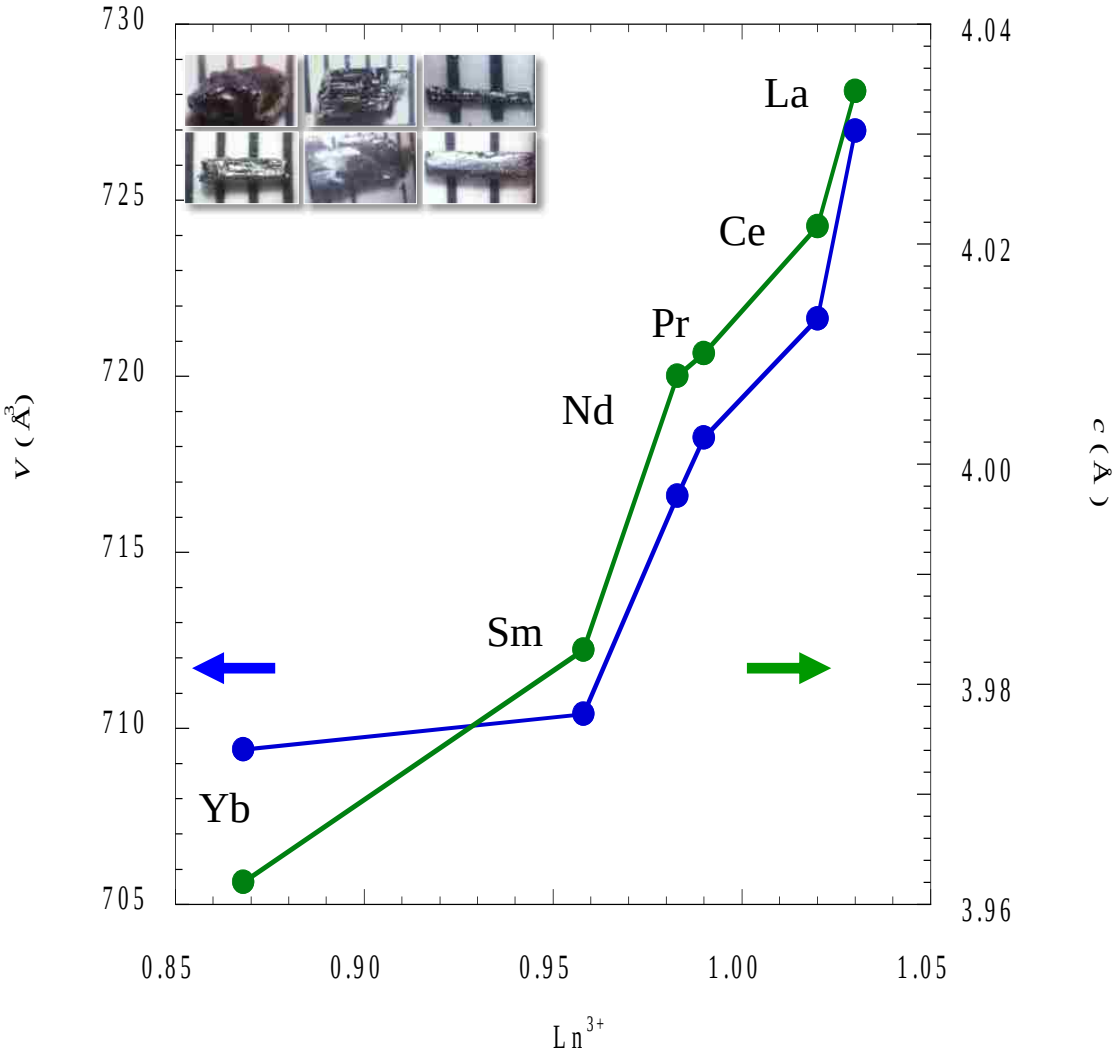

Figure 2.3. Plot of volume (blue) and *c*-axis (green) as a function of Ln^{3+} ionic radii. Inset: Single crystal aggregates of $LnCo_2Al_8$.[6]

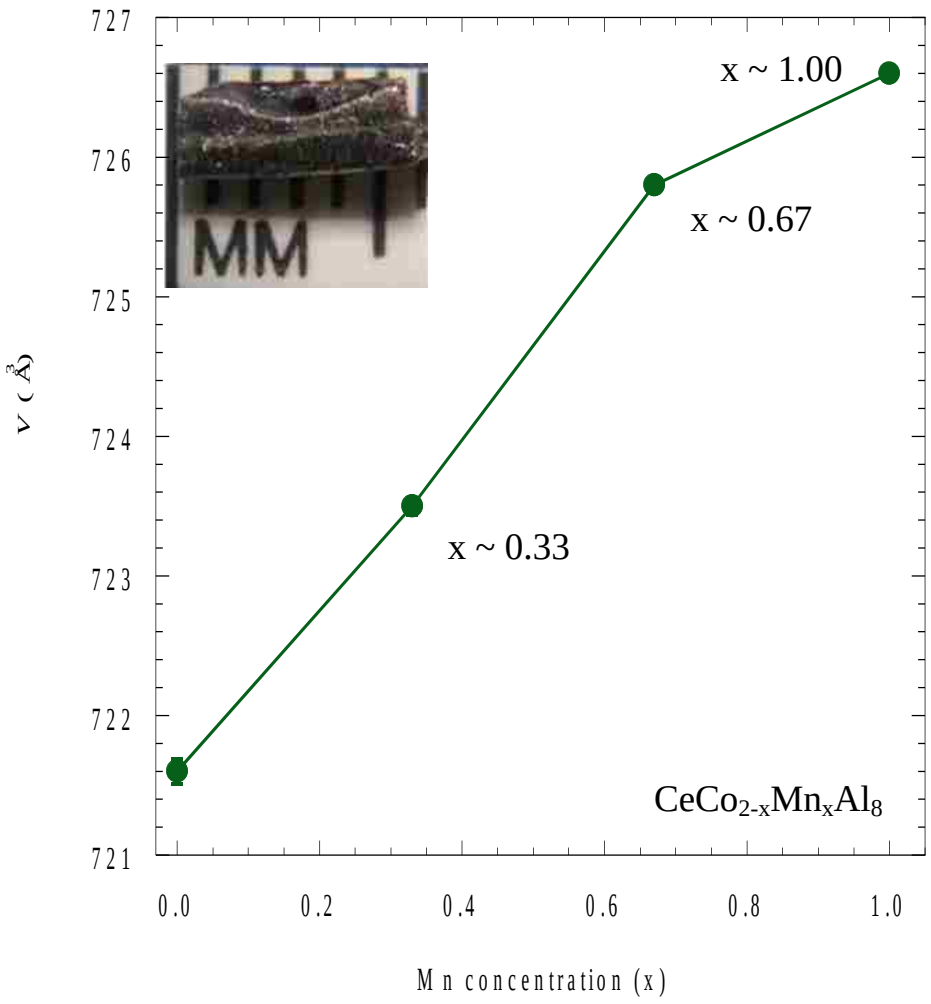

Figure 2.4. Volume (green) as a function of Mn concentration (x). Inset: Single crystal aggregate of $CeCo_{2-x}Mn_xAl_8$.[13]

2.3.2 Physical Properties

Figure 2.5 shows the field-dependent magnetization of $LnCo_2Al_8$ (Ln = Ce, Nd) at 2 K in applied fields up to 7 T. The magnetization increases as a function of applied field for the Ce and Nd analogues. Figure 2.6 shows the field-dependent magnetization of $PrCo_2Al_8$ from 2 to 20 K. At 20 K, $PrCo_2Al_8$ is linear as a function of field and upon cooling down to 2 K, a step-wise metamagnetic transition is observed at H_c = 0.09 T. The observed saturation moment is 3.15 μ_B, which is close to

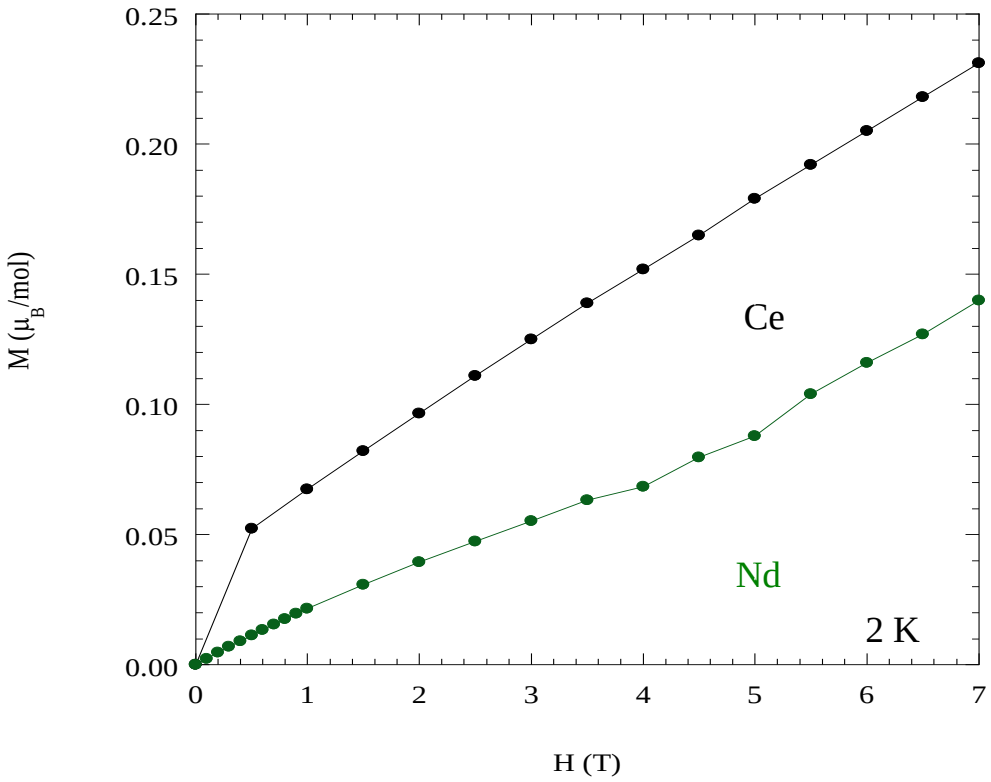

Figure 2.5. Field-dependent magnetization of $LnCo_2Al_9$ (Ln = Ce, Nd) at 2 K.[6]

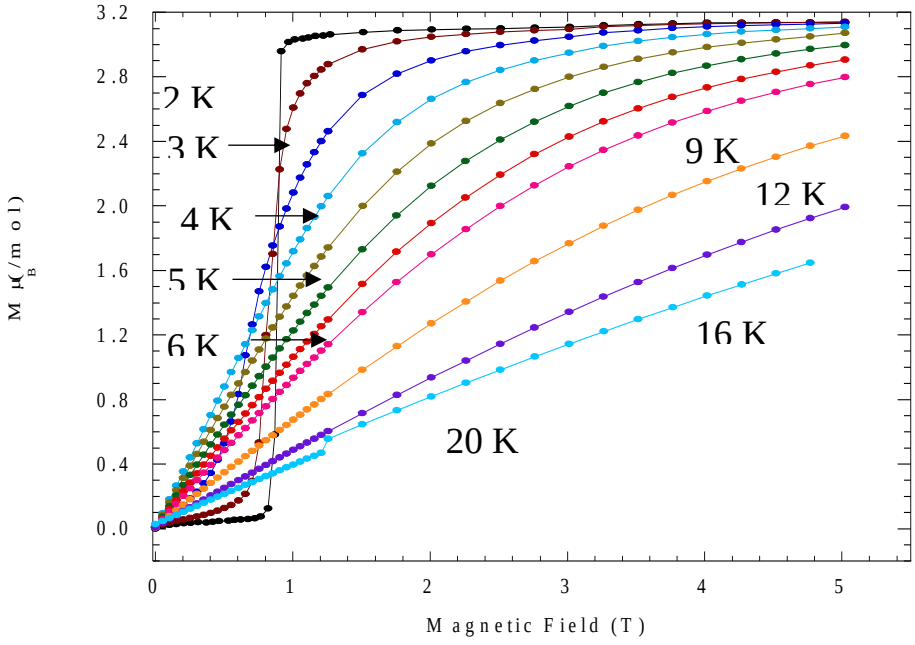

Figure 2.6. Field-dependent magnetization of $PrCo_2Al_8$ from 2 to 20 K.[6]

the calculated value of 3.2 μ_B for Pr^{3+}. The field-dependent magnetization of $CeCo_{2-x}Mn_xAl_8$ ($0 < x < 1$)at 2 K and 300 K in applied fields up to 7 T are shown in Figure 2.7[a] and 2.7[b], respectively. At 300 K, the field dependent magnetization is linear with field of 7 T. At 2 K, the magnetization of $CeCo_{2-x}Mn_xAl_8$ ($0 < x < 1$) displays a small hysteresis at low field. Above 1 T, the magnetization is linear in field up to 7 T, typical of paramagnetic behavior. The high-field magnetization shows a small systematic increase with Mn doping, consistent with a small magnetic moment likely associated with the transition-metal site in addition to the Ce^{3+} moment found in $CeCo_2Al_8$.

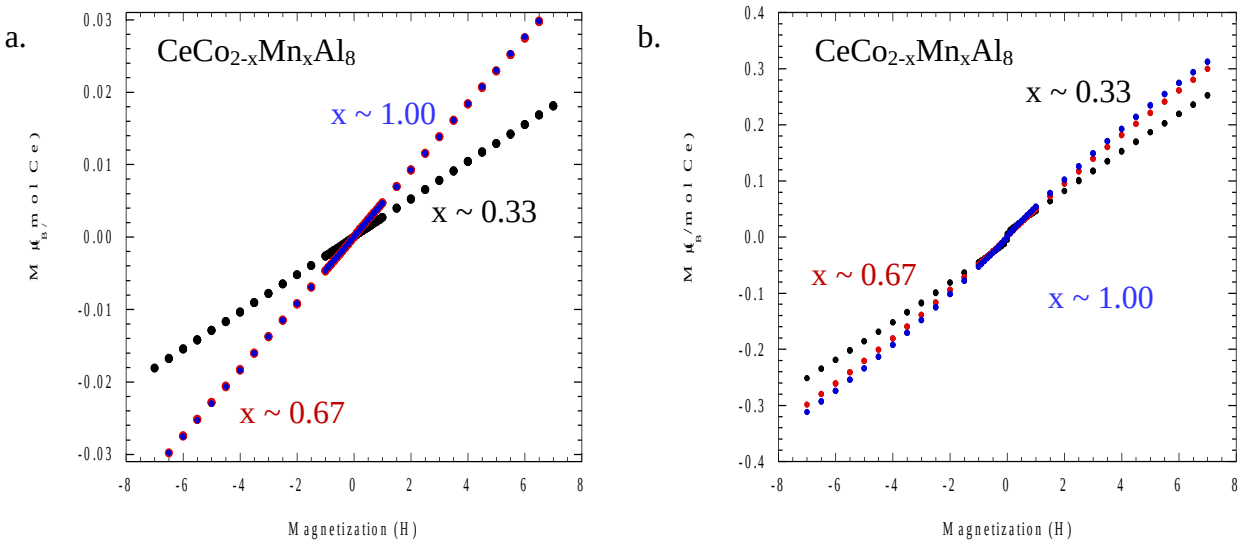

Figure 2.7. Field-dependent magnetization of $CeCo_{2-x}Mn_xAl_8$ ($0 < x < 1$) at 300 K [a] and 2 K [b].[13]

The magnetic properties are summarized in Table 2.6. Figure 2.8 shows the temperature-dependent magnetic susceptibility of $LnCo_2Al_8$ (Ln = Ce, Nd) single crystals measured with an applied field of 0.1 T. The magnetic susceptibility for $LnCo_2Al_8$ (Ln = Ce, Pr, Nd) was fitted to a Curie-Weiss equation, $\chi(T) = C / (T - \theta)$, where C represents the Curie constant, and θ is the Weiss temperature.. In contrast to polycrystalline $CeCo_2Al_8$, single-crystal $CeCo_2Al_8$ is paramagnetic down to 20 K with a small kink in the magnetization at 4.2 K due to spin reorientation.

Table 2.6. Magnetic Properties of $LnCo_2Al_8$ (Ln = Ce–Nd)[6]

compound	T_N (K)	fit range (K)	θ (K)	μ_{calc} (μ_B)	μ_{eff} (μ_B)
$CeCo_2Al_8$	-	30-200	-60(1)	2.54 Ce^{3+}	2.27(1)
$PrCo_2Al_8$	5.6 K	50-200	3(1)	3.58 Pr^{3+}	4.40(6)
$NdCo_2Al_8$	8.7 K	50-200	-123(3)	3.62 Nd^{3+}	3.46(5)

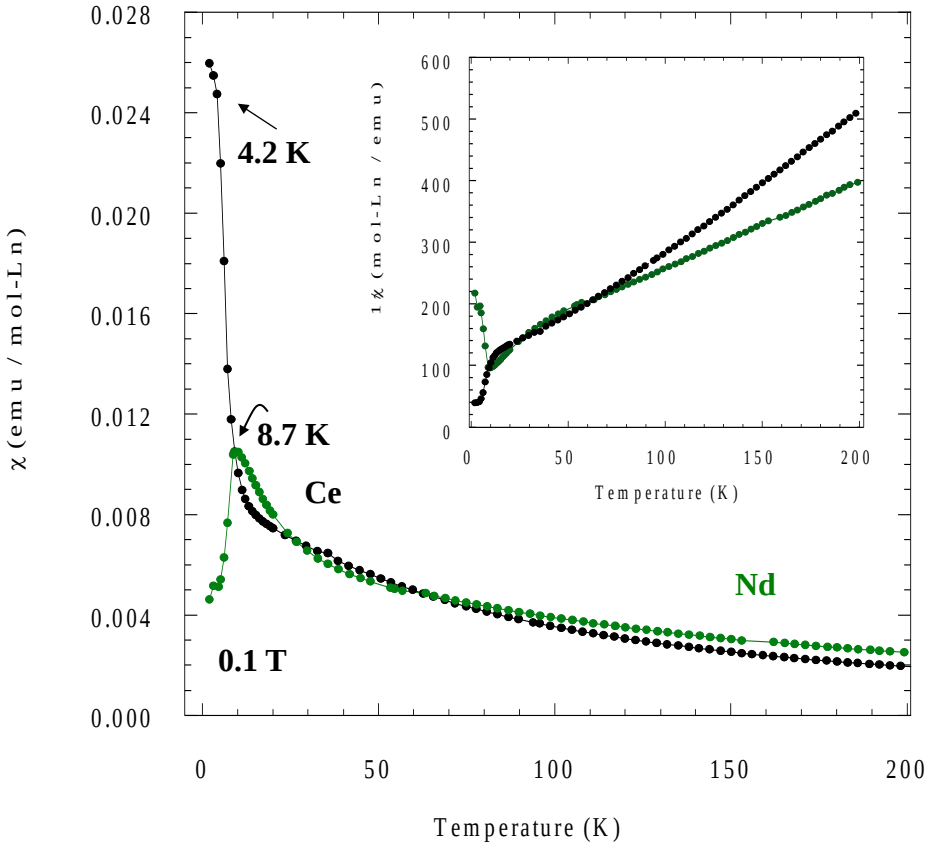

Figure 2.8. Magnetic susceptibility and inverse susceptibility (inset) of $LnCo_2Al_8$ (Ln = Ce, Nd).[6]

In addition, the magnetic moment and the Weiss temperature of the single-crystalline $CeCo_2Al_8$ (2.27(1) μ_B and -60(1) K) is lower than the magnetic moment of the polycrystalline sample (2.45(2) μ_B and -137(1) K). $PrCo_2Al_8$ (Figure 2.9) and $NdCo_2Al_8$ order antiferromagnetically at 5.6 and 8.7 K, respectively. The large Weiss temperatures of θ = -60 K and -123 K for $CeCo_2Al_8$ and $NdCo_2Al_8$ suggests antiferromagnetic interactions with strong frustration. The increase in the average

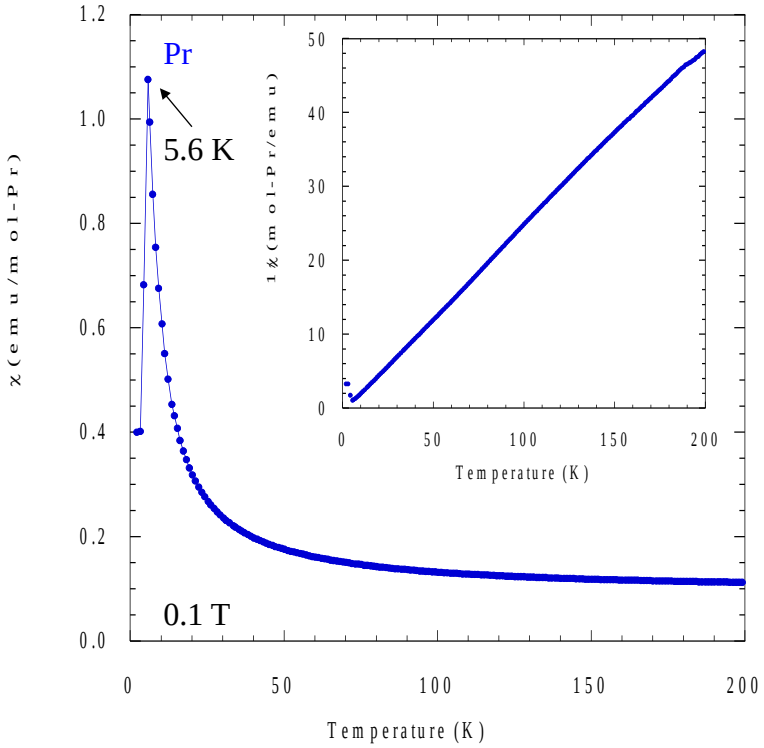

Figure 2.9. Magnetic susceptibility and inverse susceptibility (inset) of $PrCo_2Al_8$.[6]

strength of magnetic interactions in the Nd-analogue is a result of the decreasing Ln-Ln nearest neighbor distances for Nd. The frustration value $f = |\theta| / T_N$ of 14 for $NdCo_2Al_8$ indicates magnetic frustration. The magnetic susceptibility for $SmCo_2Al_8$ shows temperature independent paramagnetism down to 3 K, indicating the divalent nature of Sm^{2+}. $YbCo_2Al_8$ is nonmagnetic down to 3 K, indicative of Yb in the 2+ oxidation state. This is consistent with the isostructural analogue $YbCo_2Ga_8$,[27] but different from the mixed-valent $YbNi_{2-x}Fe_xAl_8$, where $\mu_{eff} = 2.19\ \mu_B$.[29] $LaCo_2Al_8$ is temperature independent paramagnetic with Co atoms not carrying a magnetic moment.

Figure 2.10 shows the temperature-dependent susceptibility of $CeCo_{2-x}Mn_xAl_8$ ($0 < x < 1$) measured with an applied field 0f 0.1 T. The susceptibility of $CeCo_{2-x}Mn_xAl_8$ ($0 \leq x < 1$) displays a Curie-Weiss behavior at temperatures above 70 K. At temperatures below 10 K, all are magnetically ordered and can be determined from the maximum in $d\chi/dt$, as shown in the inset of Figure 2.11. The

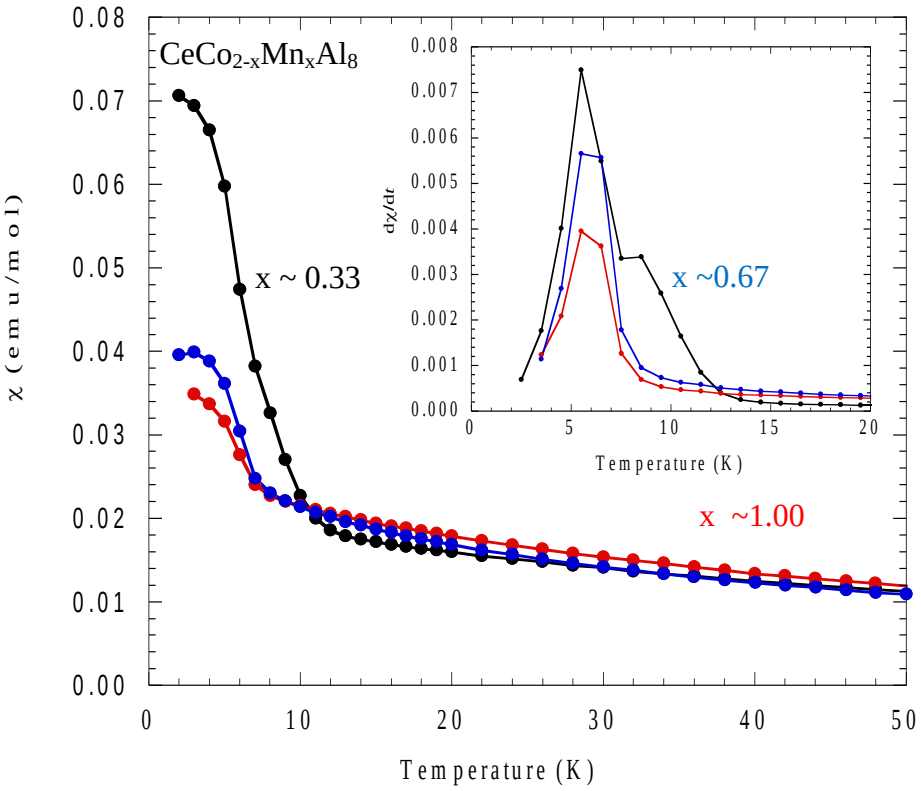

Figure 2.10. Temperature-dependent magnetization of $CeCo_{2-x}Mn_xAl_8$ ($0 < x < 1$). The inset shows the $d\chi/dt$ of $CeCo_{2-x}Mn_xAl_8$ ($0 < x < 1$).[13]

transition temperatures are confirmed with ac susceptibility, as provided in Figure A1.1. The magnetic susceptibility of $CeCo_{2-x}Mn_xAl_8$ ($0 \leq x < 1$) can be fit with a Curie–Weiss relationship. The effective moments of $CeCo_{2-x}Mn_xAl_8$ ($0 \leq x < 1$) are 2.71(4), 2.73(5), and 2.81(3) μ_B/mol–Ce with Weiss constants of -38.5(3), -37.7(3), and -30.27(5) for $x \approx 0.33$, 0.67, and 1.00, respectively.

The temperature dependent electrical resistivity of single crystalline $LnCo_2Al_8$ (Ln = La–Nd, Sm, Yb) are shown in Figure 2.11. All compounds are metallic with residual resistivity ratio (RRR) values of 3.8, 20.6, 9.6, 6.0, 1.9, and 1.8 for La, Ce, Pr, Nd, Sm, and Yb analogues, respectively. The electrical resistivity of single crystalline $CeCo_2Al_8$ decreases as a function of decreasing temperature followed by change in slope below 50 K, similar to polycrystalline $CeCo_2Al_8$, where a broadening at ~45 K is observed.[12] The electrical resistivity of $NdCo_2Al_8$, as shown in the inset of Figure 8,

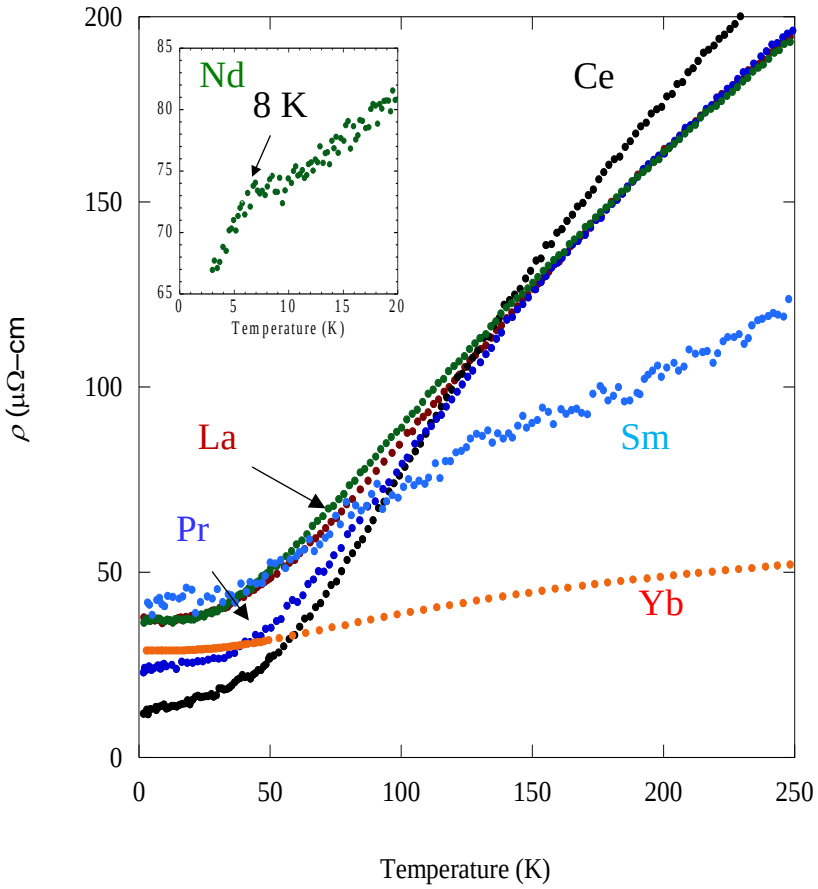

Figure 2.11. Temperature dependence of the electrical resistivity for the series $LnCo_2Al_8$. The inset shows the low temperature resistivity of the Nd analogue.[6]

decreases as a function of decreasing temperature followed by a slight curvature observed near 10 K close to the ordering temperature of T_N = 8.6 K.

2.4 Conclusions

We report the successful growths of single crystalline $LnCo_2Al_8$ (Ln = La–Nd, Sm, Yb) and $CeCo_{2-x}Mn_xAl_8$ ($0 \leq x < 1$) and present the structure, magnetization, and electrical resistivity. The unit cell volumes of $LnCo_2Al_8$ (Ln = La-Nd, Sm, Yb) decrease as a function of rare earth, consistent with the lanthanide contraction, except for the Yb-analogue, where Yb is divalent. Additionally, the volumes of $CeCo_{2-x}Mn_xAl_8$ ($0 \leq x < 1$) systematically increase as a function of increasing Mn concentration (x). $LaCo_2Al_8$, $SmCo_2Al_8$, and $YbCo_2Al_8$ are non-magnetic, and the effective moments

of $LnCo_2Al_8$ (Ce, Pr, Nd) are solely due to the trivalent rare earths. Additionally, all of the $LnCo_2Al_8$ compounds are metallic. The volumes of $CeCo_{2-x}Mn_xAl_8$ ($0 \leq x < 1$) systematically increase as a function of increasing Mn concentration (x). Also, the effective moments determined from fitting the Curie–Weiss relation $\chi(T)$ of $CeCo_{2-x}Mn_xAl_8$ ($0 \leq x < 1$) are consistent with a magnetic moment for a free Ce^{3+} ion (2.54 μ_B). Our structural and magnetic data confirm that the 4*f* electronic state of Ce is not affected by Mn substitution.[13]

Determining the optimal synthesis temperature profile is vital in obtaining phase pure $LnCo_2Al_8$ (Ln = La–Nd, Sm, Yb) and $CeCo_{2-x}Mn_xAl_8$ ($0 \leq x < 1$) and avoiding Co_2Al_9. We find that the successful growth of $LnCo_2Al_8$ (Ln = La–Nd, Sm, Yb) and $CeCo_{2-x}Mn_xAl_8$ ($0 \leq x < 1$) is dependent on the spin temperature. Removing the sample above the temperature where the related binary is formed allows sufficient diffusion for the desired ternary compounds. Employing other metal flux strategies, like eutectic flux growth, could also be successful. Two examples are the crystal growth of $Ln_{117}Ni_{53-y}Sn_{112-z}$ and Ln_2Co_2SiC (Ln = Pr, Nd) where the eutectic flux method was employed to avoid rare-earth impurities in such a rare-earth rich environment.[35, 36] Interestingly, the structure of Co_2Al_9 essentially provides the transition metal sub-lattice framework of $LnCo_2Al_8$ (Ln = La-Nd, Sm, Yb), making this a way to understand the structure of binary phases (smaller subunits) towards the growth of ternary phases (complex structures) via guest atom incorporation.[37] This is not unlike the rare-earth filled skutterudite compounds, where large voids in the $CoSb_3$ structural framework can accommodate the rare earth atoms. This leads to large thermal atomic displacement parameters and a suppression of the material's lattice thermal conductivity – a desirable quality for enhanced thermoelectric performance.[38-40] One avenue of future work would be to compare the thermal conduction properties of Co_2Al_9 to the rare earth filled compounds. Electronic structure calculations could certainly improve our understanding of the role Co_2Al_9 plays in the formation of

the ternary compounds $LnCo_2Al_8$ (Ln = La–Nd, Sm, Yb). This structural study can also provide vital information to explain the formation limits of the $CaCo_2Al_8$-structure type, behavior of the various members of this series, and eventually guide the discovery of new materials with novel or enhanced properties.[6]

2.5 References

(1) Phelan, W. A.; Menard, M. C.; Kangas, M. J.; McCandless, G. T.; Drake, B. L.; Chan, J. Y., Adventures in Crystal Growth: Synthesis and Characterization of Single Crystals of Complex Intermetallic Compounds. *Chem. Mater.* **2012,** *24*, 409-420.

(2) Schmitt, D. C.; Drake, B. L.; McCandless, G. T.; Chan, J. Y., Targeted Crystal Growth of Rare Earth Intermetallics with Synergistic Magnetic and Electrical Properties: Structural Complexity to Simplicity. *Acc. Chem. Res.* **2015,** *48*, 612-618.

(3) Macaluso, R. T.; Millican, J. N.; Nakatsuji, S.; Lee, H.-O.; Carter, B.; Moreno, N. O.; Fisk, Z.; Chan, J. Y., A Comparison of the Structure and Localized Magnetism in Ce_2PdGa_{12} with the Heavy Fermion $CePdGa_6$. *J. Solid State Chem.* **2005,** *178*, 3547-3553.

(4) Macaluso, R. T.; Nakatsuji, S.; Lee, H.; Fisk, Z.; Moldovan, M.; Young, D. P.; Chan, J. Y., Synthesis, Structure, and Magnetism of a New Heavy-Fermion Antiferromagnet, $CePdGa_6$. *J. Solid State Chem.* **2003,** *174*, 296-301.

(5) Fisk, Z.; Hess, D. W.; Pethick, C. J.; Pines, D.; Smith, J. L.; Thompson, J. D.; Willis, J. O., Heavy-Electron Metals: New Highly Correlated States of Matter. *Science* **1988,** 239, 33-42.

(6) Watkins-Curry, P.; Burnett, J. V.; Samanta, T.; Young, D. P.; Stadler, S.; Chan, J. Y., Strategic Crystal Growth and Physical Properties of Single-Crystalline $LnCo_2Al_8$ (Ln = La-Nd, Sm, Yb). *Cryst. Growth Des.* **2015,** *15*, 3293-3298.

(7) Ketelaar, J. A. A., The Crystal Structure of Alloys of Zinc with the Alkali and Alkaline Earth Metals and of Cadmium with Potassium. *J. Chem. Phys.* **1937,** *5*, 668.

(8) De Mooij, D. B.; Buschow, K. H. J., Some Novel Ternary Thorium-Manganese ($ThMn_{12}$)-Type Compounds. *J. Less-Common Met.* **1988,** *136*, 207-15.

(9) Cho, J. Y.; Thomas, E. L.; Nambu, Y.; Capan, C.; Karki, A. B.; Young, D. P.; Kuga, K.; Nakatsuji, S.; Chan, J. Y., Crystal Growth, Structure, and Physical Properties of $Ln(Cu,Ga)_{13-x}$ (Ln = La-Nd, Eu; $x \approx 0.2$). *Chem. Mater.* **2009,** *21*, 3072-3078.

(10) Phelan, W. A.; Kangas, M. J.; McCandless, G. T.; Drake, B. L.; Haldolaarachchige, N.; Zhao, L. L.; Wang, J. K.; Wang, X. P.; Young, D. P.; Morosan, E.; Hoffmann, C.; Chan, J.

Y., Synthesis, Structure, and Physical Properties of $Ln(Cu,Al,Ga)_{13-x}$ (Ln = La-Pr, and Eu) and $Eu(Cu,Al)_{13-x}$. *Inorg. Chem.* **2012,** *51*, 10193-10202.

(11) Drake, B. L.; Capan, C.; Cho, J. Y.; Nambu, Y.; Kuga, K.; Xiong, Y. M.; Karki, A. B.; Nakatsuji, S.; Adams, P. W.; Young, D. P.; Chan, J. Y., Crystal growth, Structure, and Physical Properties of $Ln(Cu, Al)_{12}$ (Ln = Y, Ce, Pr, Sm, and Yb) and $Ln(Cu, Ga)_{12}$ (Ln = Y, Gd-Er, and Yb). *J. Phys.: Condens. Matter* **2010,** *22*, 066001/1-066001/14.

(12) Ghosh, S.; Strydom, A. M., Strongly Correlated Electron Behaviour in CeT_2Al_8 (T = Fe, Co). *Acta Phys. Polym., A* **2012,** *121*, 1082-1084.

(13) Treadwell, L. J.; Watkins-Curry, P.; McAlpin, J. D.; Rebar, D. J.; Hebert, J. K.; Di Tusa, J. F.; Chan, J. Y., Investigation of Mn, Fe, and Ni Incorporation in $CeCo_2Al_8$. *Inorg. Chem.* **2015,** *54*, 963-968.

(14) Tougait, O.; Kaczorowski, D.; Noel, H., $PrCo_2Al_8$ and $Pr_2Co_6Al_{19}$: Crystal Structure and Electronic Properties. *J. Solid State Chem.* **2005,** *178*, 3639-3647.

(15) He, W.; Zhong, H.; Liu, H.; Zhang, J.; Zeng, L., Crystal Structure and Electrical Resistivity of $NdCo_2Al_8$. *J. Alloys Compd.* **2009,** *467*, 6-9.

(16) Manyako, M. B.; Tanson, T. I.; Bodak, O. I.; Cerny, R.; Yvon, K., Crystal Structure of Ytterbium Cobalt Aluminum, $YbCo_2Al_8$. *Z. Kristallogr.* **1996,** *211*, 216.

(17) Rykhal, R. M.; Zarechnyuk, O. S.; Protasov, V. S., Isothermal Sections of Ternary (Praseodymium, Samarium)-Cobalt-Aluminum systems at 873 K at Rare-Earth Concentrations of 0-0.333 Atomic Parts. *Dopov. Akad. Nauk Ukr. RSR, Ser. A: Fiz.-Mater. Tekh. Nauki* **1985**, 72-4.

(18) Zhang, Y.-z.; He, W.; Huang, J.-l.; Zhang, J.-l.; Fu, Y.-c., Crystal Structure and Rietveld Refinement of $LaCo_2Al_8$. *Guangxi Daxue Xuebao, Ziran Kexueban* **2011,** *36*, 344-347.

(19) Canfield, P. C.; Fisk, Z., Growth of Single Crystals from Metallic Fluxes. *Philos. Mag. B* **1992,** *65*, 1117-23.

(20) Kanatzidis, M. G.; Pöttgen, R.; Jeitschko, W., The Metal Flux: a Preparative Tool for the Exploration of Intermetallic Compounds. *Angew. Chem. Int. Ed.* **2005,** *44*, 6996-7023.

(21) Bostroem, M.; Rosner, H.; Prots, Y.; Burkhardt, U.; Grin, Y., The Co_2Al_9 Structure Type Revisited. *Z. Anorg. Allg. Chem.* **2005,** *631*, 534-541.

(22) Sheldrick, G., *SHELX-2013-Programs for Crystal Structure Analysis: i. Structure Determination (SHELXS) and ii. Refinement (SHELXL-2013), University of Gottingen, Germany* **2013**.

(23) Sheldrick, G. M., *Acta Crystallogr., Sect. A* **2015,** *71*, 3-8.

(24) SIR92, A., program for crystal structure solution: A. Altomare, G. Cascarano, C. Giacovazzo, A. Guagliardi. *J. Appl. Crystallogr* **1993,** 26, 343.

(25) Sheldrick, G. M., SHELXL97: GM Sheldrick. *Acta Crystallogr., A* **2008,** 64, 112-122.

(26) Czech, E.; Cordier, G.; Schaefer, H., Study of Calcium-Cobalt-Aluminum ($CaCo_2Al_8$). *J. Less Common Met.* **1983,** *95*, 205-11.

(27) Fritsch, V.; Bobev, S.; Moreno, N. O.; Fisk, Z.; Thompson, J. D.; Sarrao, J. L., Antiferromagnetic Order in $EuRh_2(Ga,In)_8$. *Phys. Rev. B: Condens. Matter* **2004,** *70*, 052410/1-052410/4.

(28) Kolenda, M.; Koterlin, M.; Hofmann, M.; Penc, B.; Szytuła, A.; Zygmunt, A.; Żukrowski, J., Low Temperature Neutron Diffraction Study of the $CeFe_2Al_8$ Compound. *J Alloys Compd* **2001,** *327*, 21-26.

(29) Wu, X.; Francisco, M.; Rak, Z.; Bakas, T.; Mahanti, S. D.; Kanatzidis, M. G., Synthesis, Magnetism and Electronic Structure of $YbNi_{2-x}Fe_xAl_8$ (x = 0.91) Isolated from Al Flux. *J. Solid State Chem.* **2008,** *181*, 3269-3277.

(30) Zarechnyuk, O. S., X-ray Diffraction Study of Cerium-Cobalt-Aluminum Ternary System Alloys in the Range of 0-33.3 Atomic % Cerium. *Dopov. Akad. Nauk Ukr. RSR, Ser. A: Fiz.-Mater. Tekh. Nauki* **1980**, 84.

(31) Rykhal, R. M.; Zarechnyuk, O. S.; Yarmolyuk, Y. P., Crystal Structure of Compounds Lanthanum-Cobalt-Aluminum ($LaCoAl_4$), Cerium-Cobalt-Aluminum ($CeCoAl_4$), and Praseodymium-Cobalt-Aluminum ($PrCoAl_4$). *Dopov. Akad. Nauk Ukr. RSR, Ser. A: Fiz.-Mater. Tekh. Nauki* **1977**, 265-8.

(32) Pauling, L., Atomic Radii and Interatomic Distances in Metals. *J. Am. Chem. Soc.* **1947,** *69*, 542-553.

(33) Douglas, A. M. B.; Raynor, G. V.; Waldron, M. B., Structure of Co_2Al_9. *Nature (London, U. K.)* **1948,** 162, 565-6.

(34) Tougait, O.; Stepien-Damm, J.; Zaremba, V.; Noel, H.; Troc, R., Synthesis, Crystal Structure and Magnetic Properties of $U_2Co_6Al_{19}$. *J. Solid State Chem.* **2003,** *174*, 152-158.

(35) Reyes, L. E.; McDougald, R. N.; McCandless, G. T.; Khan, M.; Young, D. P.; Chan, J. Y., Eutectoid Flux Growth and Physical Properties of Single Crystal $Ln_{117}Ni_{54-y}Sn_{112-z}$ (Ln = Gd-Dy). *Cryst. Growth Des.* **2015,** *15*, 295-304.

(36) Zhou, S.; Mishra, T.; Wang, M.; Shatruk, M.; Cao, H.; Latturner, S. E., Synthesis, Crystal Structure, and Magnetic Properties of Novel Intermetallic Compounds R_2Co_2SiC (R = Pr, Nd). *Inorg. Chem.* **2014,** *53*, 6141-6148.

(37) Fulfer, B. W.; McAlpin, J. D.; Engelkemier, J.; McCandless, G. T.; Prestigiacomo, J.; Stadler, S.; Fredrickson, D. C.; Chan, J. Y., Filling in the Holes: Structural and Magnetic Properties of the Chemical Pressure Stabilized $LnMn_xGa_3$ (Ln = Ho-Tm; x < 0.15). *Chem. Mater.* **2014,** *26*, 1170-1179.

(38) Lu, P.-X.; Wu, F.; Han, H.-L.; Wang, Q.; Shen, Z.-G.; Hu, X., Thermoelectric Properties of Rare Earths Filled $CoSb_3$ Based Nanostructure Skutterudite. *J. Alloys Compd.* **2010,** *505*, 255-258.

(39) Lu, P.-X.; Shen, Z.-G.; Hu, X., A Comparison Study on the Electronic Structure of the Thermoelectric Materials $CoSb_3$ and $LaFe_3CoSb_{12}$. *Phys. B (Amsterdam, Neth.)* **2010,** *405*, 1740-1744.

(40) Park, K.-H.; Seo, W.-S.; Shin, D.-K.; Kim, I.-H., Thermoelectric Properties of Yb-filled $CoSb_3$ Skutterudites. *J. Korean Phys. Soc.* **2014,** *65*, 491-495.

Chapter 3. Complex Magnetic Ordering and Large Positive Magnetoresistance in $Pr_2Fe_{4-x}Co_xSb_5$ ($1 < x < 3$)

3.1 Introduction

Rare earth intermetallics with Group 15 elements have garnered interest because of their rich structural chemistry[1-3] and potential to exhibit superconductivity,[4, 5] complex magnetic ordering,[6-12] colossal magnetoresistance,[13-18] and spin glass behavior.[12, 19-21] For instance, the filled skutterudites, $LnRu_4Sb_{12}$ (Ln = La, Pr)[4] and $PrOs_4Sb_{12}$,[5] display superconductivity at T_c = 1 K, 3.2 K, and 1.85 K, respectively, and $La_{13}Ga_8Sb_{21}$ also displays a superconducting transition at T_c = 2.4 K.[22] Eu_3InP_3,[9] a Zintl phase, displays complex magnetic ordering with two antiferromagnetic transitions at T_N = 10.4 K and 14 K. Colossal magnetoresistance (CMR) has also been observed in the Zintl phases $Eu_{14}MnSb_{11}$[13] and $EuIn_2As_2$.[23] $Eu_{14}MnSb_{11}$ shows large negative magnetoresistance up to -36% at 5 T and 100 K near its ferromagnetic ordering temperature at 100 K, while $EuIn_2As_2$ exhibits colossal magnetoresistance up to -143% at 16 T close to its ordering temperature at 16 K.

Materials which display magnetic frustration are also of interest because of the emergence of novel magnetic phases upon cooling, such as spin glass.[24] In two-dimensional systems, the triangular lattice is the ideal candidate to study geometric frustration as this can lead to spin-disordered states.[25-27] Magnetic frustration can be achieved by suppressing magnetic order by substitution of a nonmagnetic Al^{3+} in the MAl_2S_4 (M = Mn^{2+}, Fe^{2+}, and Co^{2+}), thereby resulting in a candidate for a two-dimensional Heisenberg spin glass system.[28] $Ln_2Fe_4Sb_5$ (Ln = La–Nd, Sm), which consists of two Fe sites that form nearly equilateral triangular units, have been shown to exhibit magnetically frustrated spin glass behavior.[19] Inspired by the emergence of spin glass in $Ln_2Fe_4Sb_5$ (Ln = La–Nd, Sm) and the valence instability of Pr^{3+}, we sought out to study the effects of Co doping on the magnetic and electrical properties of $Pr_2Fe_4Sb_5$. Herein, we

report the synthesis, structure, magnetism, electrical resistivity, and magnetoresistance of single-crystalline $Pr_2Fe_{4-x}Co_xSb_5$ ($1 < x < 3$).

3.2 Experimental

3.2.1 Synthesis

We chose to grow single crystals of $Pr_2Fe_{4-x}Co_xSb_5$ ($1 < x < 3$) via an inert Bi flux as adapted from the successful growths of $Ln_2Fe_4Sb_5$ (Ln = La–Nd, Sm).[19] Pr (rod, 99.9%), Fe (powder, 99.9%), Co (powder, 99.9%), Sb (ingots, 99.9%), and Bi (granules, 99.9%) were used as received. For each reaction, the elements were placed in an alumina crucible, capped with a second crucible, and then sealed in an evacuated fused silica tube filled with ~ 0.3 atm Ar. The sealed tube was then placed in a furnace. The reaction ampule was heated to 1200 °C for 24 h at a rate of 100 °C/h and slow cooled to 875 °C at a rate of 5 °C/h. The reaction was removed at a higher temperature than the reported parent $Ln_2Fe_4Sb_5$ analogues to avoid competing binaries $CoSb_2$ and $CoSb_3$.[19] The excess Bi flux was removed via centrifugation and single crystals obtained were etched in dilute 0.1 M HCl. The syntheses yielded plate-like single crystals of $Pr_2Fe_{4-x}Co_xSb_5$ ($1 < x < 3$). Attempts were made to synthesize crystals that adopt the $La_2Fe_4Sb_5$–structure type with Co concentrations of $x > 3$, but single crystals of the $ZrCuSi_2$ – structure type[29, 30] $PrCo_{1-x}Fe_xSb_2$ were stabilized. We also attempted to make the Co analogue of $Pr_2Fe_4Sb_5$, but this also led to the growth of $PrCo_{1-x}Sb_2$.

3.2.2 Structure Determination

Phase identification and sample homogeneity was determined by powder X-ray diffraction. Data was collected using a Bruker D8 Advance powder X-ray diffractometer operating at 40 kV and 30 mA with CuKα (1.54060 Å) radiation and a LYNXEYE XE detector. Data were collected from 10 - 80° with a step size of 0.01°. Single crystals of $Pr_2Fe_{4-x}Co_xSb_5$ (1

< x < 3) were cut to appropriate sizes and mounted on a glass fiber with epoxy. The fibers were mounted on a Bruker D8 Quest Kappa single-crystal X-ray diffractometer equipped with an IμS microfocus source (λ = 0.71073 Å) operating at 50 kV and 1 mA, a HELIOS optics monochromator, and a CMOS detector. The collected data was corrected for absorption correction using the default Bruker program SADABS (multi-scan method). A starting model of $Pr_2Fe_{4-x}Co_xSb_5$ (1 < x < 3) was obtained using SHELXS2013[31] and all atomic sites were refined anisotropically using SHELXL2014.[32] The final models of $Pr_2Fe_{4-x}Co_xSb_5$ (1 < x < 3) were generated from the atomic coordinates of the parent $Pr_2Fe_4Sb_5$. The atomic coordinates, occupancies, anisotropic displacement parameters, and crystallographic refinement details are provided in Tables 2 and 3. Selected interatomic distances and angles are provided in Table 4. The structures of $Pr_2Fe_{4-x}Co_xSb_5$ (1 < x < 3) was refined by starting with the atomic coordinates of the parent $Pr_2Fe_4Sb_5$. $Pr_2Fe_{4-x}Co_xSb_5$ consists of one Pr site, two M (M = Fe, Co) sites, and three Sb sites. The transition metal sites consists of a fully occupied M1 site and a partially occupied M2 site that is mixed occupied with M1 and M2, resulting in a M2′ site. For the refinement of $Pr_2Fe_{4-x}Co_xSb_5$ (1 < x < 3), Co was modeled on the partially occupied M2 site. As the Co concentration increases in $Pr_2Fe_{4-x}Co_xSb_5$ (x ~ 3), either Fe or Co can occupy the fully occupied M1 site and the partially occupied M2 site with comparable R_1 and wR_2 parameters. Therefore, the concentration obtained from the SEM/EDX results were incorporated into the single crystal refinements of $Pr_2Fe_{4-x}Co_xSb_5$ (1 < x < 3).

3.2.3 Characterization

Elemental analysis of $Pr_2Fe_{4-x}Co_xSb_5$ (1 < x < 3) single crystals was conducted via electron dispersive spectroscopy (EDS) using a Zeiss – LEO Model 1530 variable pressure field effect scanning electron microscope equipped with an EDAX detector at an accelerating voltage

of 20 kV. Spectra were integrated for 60 seconds and the results from at least 5 spots were averaged and normalized to Ln to determine the atomic percentage of each element. The normalized results are $Pr_{2.00(4)}Fe_{3.24(5)}Co_{0.89(2)}Sb_{4.94(3)}$, $Pr_{2.00(5)}Fe_{2.17(7)}Co_{1.95(4)}Sb_{4.70(9)}$, $Pr_{2.00(6)}Fe_{1.53(4)}Co_{2.27(1)}Sb_{4.46(6)}$, and $Pr_{1.86(3)}Fe_{0.28(2)}Co_{1.98(4)}Sb_{5.70(3)}$. X-ray photoelectron spectra (XPS) of ground single crystals of $Pr_2Fe_{4-x}Co_xSb_5$ (x ~ 2.5) were also measured using a PHI Versa Probe II Scanning XPS Microprobe (Physical Electronic Inc., Chanhassen, MN) equipped with an Al Kα X-ray source (E = 1486.7 eV). The XPS results show a presence of Pr^{3+}, Fe^{3+}, $Co^{2+/3+}$, and Sb^{3+} from the absorption peaks at the expected binding energies.[33]

3.2.4 Physical Properties

Magnetic measurements were collected using a Quantum Design Magnetic Property Measurement System (MPMS). Direct current magnetic susceptibility were measured under zero field cooled (ZFC) and field cooled (FC) conditions from 3 to 300 K under an applied magnetic field of 0.1 T. Field dependent magnetization data were collected at 3 K with applied magnetic fields up to 8 T. The mass of individual single crystals were too small for magnetic measurements, therefore magnetic measurements were conducted on multiple single crystals. Temperature-dependent electrical resistivity was measured on individual single crystals (~1 mm in length) using a Quantum Design Physical Property Measurement System (PPMS) in dc mode from 3 to 300 K at 0 T, 0.01 T, 0.1 T, and 1 T using the four-probe method with Pt leads and Ag epoxy at 0.01 – 5.00 mA.

Table 3.1 Crystallographic Parameters of $Pr_2Fe_{4-x}Co_xSb_5$ ($1 < x < 3$)

compound	$Pr_2Fe_{3.13}Co_{0.87}Sb_5$	$Pr_2Fe_{2.18}Co_{1.92}Sb_{4.97}$	$Pr_2Fe_{1.51}Co_{2.39}Sb_{4.97}$	$Pr_2Fe_{0.87}Co_{3.28}Sb_{4.94}$
a (Å)	4.3081(1)	4.299(5)	4.298(3)	4.2973(1)
c (Å)	25.7504(8)	25.711(5)	25.732(3)	25.7164(9)
V (Å^3)	477.92(9)	475.2(11)	475.3(4)	474.9(2)
Z	2	2	2	2
cryst dimens (mm^3)	0.03 x 0.04 x 0.04	0.03 x 0.05 x 0.05	0.02 x 0.02 x 0.03	0.03x 0.03 x 0.04
temperature (K)	293(2)	296(2)	296(2)	296(2)
θ range (º)	3.2 – 55.5	3.2 – 30.5	3.17 – 30.39	3.2 – 62.7
μ (mm^{-1})	29.871	30.263	30.340	30.499
measd reflns	20029	1867	13872	4787
indep reflns	978	270	1248	1135
R_{int}	0.050	0.047	0.0261	0.054
h	-9 to 9	-4 to 6	-8 to 8	-10 to 10
k	-9 to 9	-4 to 6	-8 to 8	-8 to 5
l	-50 to 58	-33 to 36	-50 to 46	-63 to 64
reflns/parameters	978/21	270/20	210/19	1135/20
$\Delta\rho_{max}$ (e / Å^{-3})	7.071	2.644	7.411	13.984
$\Delta\rho_{min}$ (e / Å^{-3})	-3.493	-2.108	-4.958	-7.727
extinction coeff	0.0060(9)	0.0011(3)	0.0009(9)	0.0037(5)
GOF	1.168	1.209	1.215	1.159
R_1 (F)[a]	0.040	0.034	0.0893	0.043
wR_2[b]	0.086	0.090	0.2302	0.115

[a] $R_1 = \Sigma||F_o| - |F_c||/\Sigma|F_o|$. [b] $wR_2 = [\Sigma[w(F_o^2 - F_c^2)^2]/\Sigma\,[w(F_o^2)^2]]^{1/2}$.

Table 3.2. Atomic Positions of $Pr_2Fe_{4-x}Co_xSb_5$ ($1 < x < 3$)

Atom	Wyckoff site	Point symmetry	*x*	*y*	*z*	occ.	[a]U_{eq} (Å^2)
$Pr_2Fe_{4-x}Co_xSb_5$ (x ~ 1)							
Pr	4*e*	4*mm*	0	0	0.34795(2)	1	0.00767(8)
M1	2*a*	4/*mmm*	0	0	0	1	0.0102(2)
M2	8*g*	*mm*	0	½	0.44812(5)	0.56	0.0218(3)
M2′	8*g*	*mm*	0	½	0.44812(5)	0.22	0.0218(3)
Sb1	4*d*	$\bar{4}$*m*2	0	½	¼	1	0.00661(7)
Sb2	2*b*	4/*mmm*	0	0	0.11019(5)	1	0.00772(8)
Sb3	8*j*	4/*mmm*	0	0.067(2)	½	0.12(2)	0.0016(3)
Sb3′	4*e*	4*mm*	0	0	0.4863(4)	0.25(4)	0.028(2)
$Pr_2Fe_{4-x}Co_xSb_5$ (x ~ 2)							
Pr	4*e*	4*mm*	0	0	0.34844(4)	1	0.0057(3)
M1	2*a*	4/*mmm*	0	0	0	1	0.0057(13)
M2	8*g*	*mm*	0	½	0.44730(10)	0.31	0.0118(6)
M2′	8*g*	*mm*	0	½	0.44730(10)	0.48	0.0118(6)
Sb1	4*d*	$\bar{4}$*m*2	0	½	¼	1	0.0032(3)
Sb2	4*e*	4/*mmm*	0	0	0.11018(5)	1	0.0059(3)
Sb3	4*e*	4*mm*	0	0	0.4935(6)	0.481(8)	0.024(3)
$Pr_2Fe_{4-x}Co_xSb_5$ (x ~ 2.5)							
Pr	4*e*	4*mm*	0	0	0.34879(4)	1	0.0076(12)
M1	2*a*	4/*mmm*	0	0	0	1	0.0052(2)
M2	8*g*	*mm*	0	½	0.4469(1)	0.89(3)	0.0081(6)
Sb1	4*d*	$\bar{4}$*m*2	0	½	¼	1	0.0046(4)
Sb2	4*e*	4/*mmm*	0	0	0.11024(5)	1	0.0081(4)
Sb3	4*e*	4*mm*	0	0	0.4947(9)	0.461(8)	0.018(3)
$Pr_2Fe_{4-x}Co_xSb_5$ (x ~ 3)							
Pr	4*e*	4*mm*	0	0	0.34890(2)	1	0.00595(7)
M1	2*a*	4/*mmm*	0	0	0	0.87(1)	0.0046(3)
M2	8*g*	*mm*	0	½	0.44665(4)	0.82(8)	0.0099(2)
Sb1	4*d*	$\bar{4}$*m*2	0	½	¼	1	0.00521(7)
Sb2	4*e*	4/*mmm*	0	0	0.11027(2)	1	0.00628(8)
Sb3	2*b*	4/*mmm*	0	0	½	0.942(9)	0.0241(4)

[a] U_{eq} is defined as one-third of the trace of the orthogonalized U_{ij} tensor.

Table 3.4. Selected Interatomic Distances (Å) and Angles (°) of $Pr_2Fe_{4-x}Co_xSb_5$ ($1 < x < 3$)

	$Pr_2Fe_{4-x}Co_xSb_5$ (x ~ 1)	$Pr_2Fe_{4-x}Co_xSb_5$ (x ~ 2)	$Pr_2Fe_{4-x}Co_xSb_5$ (x ~ 2.5)	$Pr_2Fe_{4-x}Co_xSb_5$ (x ~ 3)
		Distance (Å)		
Pr-Sb1 (x4)	3.33168(4)	3.321(2)	3.329(9)	3.3295(3)
Pr-Sb2 (x4)	3.2314(3)	3.221(3)	3.217(2)	3.2150(2)
M1-M2 (x8)	2.5349(2)	2.541(3)	2.547(4)	2.5494(6)
M2-M2 (x1)	2.673(3)	2.710(5)	2.734(5)	2.744(2)
M2-Sb2 (x2)	2.625(9)	2.608 (3)	2.603(2)	2.5998(7)
M2-Sb3 (x2)	2.5349(7)	2.541(3)	2.547(2)	2.5494(2)
Sb1-Sb1	3.0463(7)	3.040(4)	3.0391(11)	3.0387(7)
		Angle (deg)		
M2-M1-M1	63.63(5)	64.45(12)	64.92(10)	65.12(4)
M1- M2- M2	58.19(3)	57.77(6)	57.54(5)	57.44(2)
Sb1-Sb1-Sb1	90.0	90.0	90.0	90.0

3.3 Results and Discussion

3.3.1 Structure of $Pr_2Fe_{4-x}Co_xSb_5$ ($1 < x < 3$)

$Pr_2Fe_{4-x}Co_xSb_5$ ($1 < x < 3$) adopts the $La_2Fe_4Sb_5$ – structure type (tetragonal, *I4/mmm*) and was first reported by P. Woll.[34] For clarity, the crystal structure of $Pr_2Fe_{4-x}Co_xSb_5$ (x ~ 1) will be described first, followed by a comparison to the other Co concentrations (x). The crystal structure of $Pr_2Fe_{4-x}Co_xSb_5$ (x ~ 1) is shown in Figure 3.1, and consists of Pr atoms that are surrounded by four Sb1 and four Sb2 atoms that form square antiprisms with the Sb1 atoms and forming square nets at the base, as shown in Figure 3.2a. similar to the Pr atoms in $Pr_2Fe_4Sb_5$,[19] $PrFeSb_3$,[35] $PrCo_{1-x}Sb_2$,[36] and $PrSb_2$.[37] Additionally, the Sb1 atoms are arranged in square nets which are common subunits found in Sb-containing materials. The Pr–Sb interatomic distances range from 3.2314(3) – 3.33168(4) Å, and these distances systematically decrease as a function of increasing Co concentration (x).

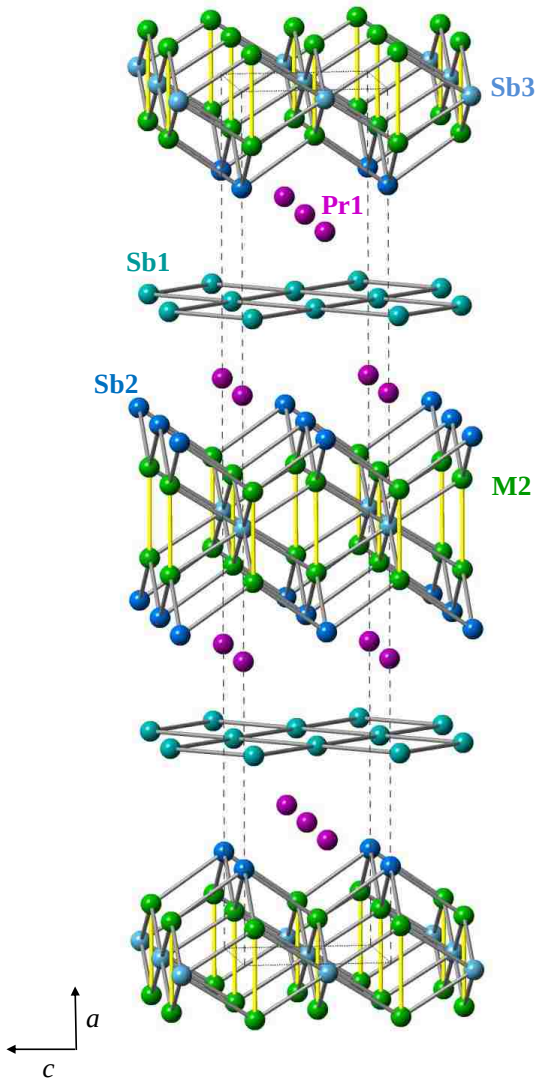

Figure 3.1 Crystal structure of $Pr_2Fe_{4-x}Co_xSb_5$ (x ~ 1).

Figure 3.2[b–d] shows the transition metal (M = Fe, Co) sublattice, which consists of a M1 site composed of Fe atoms and a mixed M2/M2′ site composed of Fe and Co atoms, respectively. The transition metal sublattice can be described in two parts (M2/M2′-Sb and M1-M2/M2′ environment), which are shown in Figure 3.2[b-c] with selected distances provided in Table 3.4. The M1 (Fe) atoms are coordinated to eight M2/M2′ atoms that are occupationally disordered (Figure 3.2[c]), and the M2/M2′ atoms are surrounded by two Sb2 and two Sb3 atoms

in a tetrahedral environment (Figure 3.2[b]). As a function of increasing Co concentration (x), the M2/M2′–Sb3 distances systematically increase, which are in the range of 2.53(7) – 2.55(2) Å. The M2/M2′–Sb3 distances are also longer than the Fe2–Sb3 distances observed for the $Ln_2Fe_4Sb_5$ (Ln = La–Nd, Sm), which are in the range of 2.24(4) – 2.36(2) Å. The shorter Fe2–Sb3 distances observed for $Ln_2Fe_4Sb_5$ (Ln = La–Nd, Sm) are attributed to the occupational disorder of the Fe2 site which has an average occupancy of 0.75. The occupational disorder of the mixed M2/M2′ site has occupancies in the range of 0.78-0.82. Therefore, as a function of increasing Co concentration (x), the mixed M2/M2′ site becomes closer to a fully occupied M2 site. The static positional disorder of the Sb3 position also leads to shorter Fe2–Sb3 interatomic distances in the $Ln_2Fe_4Sb_5$ (Ln = La–Nd, Sm) end members, consistent with an elongation of the Fe2 anisotropic displacement parameters pointing in the direction of the Sb3 positions.

Figure 3.2[c] shows the M2/M2′–M1 contacts of the transition metal sublattice of $Pr_2Fe_{4-x}Co_xSb_5$ (x ~ 1), which forms nearly equilateral triangles comprised of M1 (Fe) atoms bonded to two M2/M2′ (Fe/Co) atoms at a distance of 2.535(7) Å and a M2/M2′- M2/M2′ distance of 2.672(2) Å. The M2/M2′- M2/M2′ distance is also longer than the Fe2-Fe2 distance (2.600(5) Å) of $Pr_2Fe_4Sb_5$. The transition metal angles also change with increasing Co concentration (x). In $Pr_2Fe_4Sb_5$, the Fe2-Fe1-Fe2 angle is 63.18(13)°, and the Fe1-Fe2-Fe2 angles are 59.15(5)°. Upon Co substitution, the M2-M1-M2 angle is 63.63(5)°, while the M1-M2-M2 angles are 58.19(3)°. With the addition of Co, the M2-M1-M2 angle becomes more obtuse, coupled with the longer M2/M2′- M2/M2′ distances (Table 3.4).

Similar to $Ln_2Fe_4Sb_5$ (Ln = La-Nd, Sm), there are some differences in the static positional disorder in $Pr_2Fe_{4-x}Co_xSb_5$ ($1 < x < 3$). The Sb3 position for x ~ 1 member is positionally disordered around a mirror plane (8*j*). To account for the residual electron density in proximity to

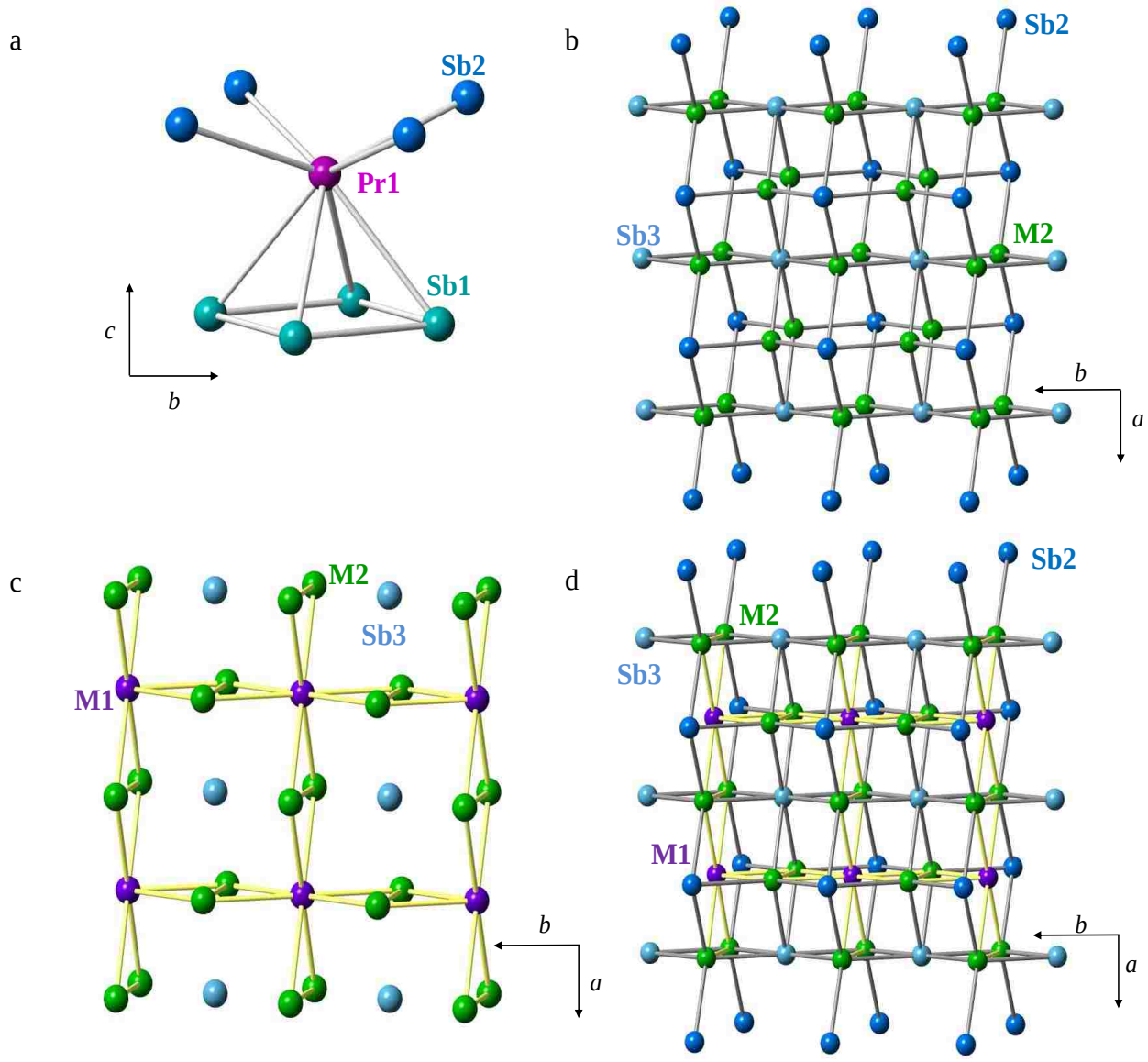

Figure 3.2. Structural subunits of $Pr_2Fe_{4-x}Co_xSb_5$ (x ~ 1).

the Sb3 position (0.43 Å), there is an Sb3′ site which is positionally disordered around a 4-fold of symmetry (4*e*). Among the $Pr_2Fe_{4-x}Co_xSb_5$ (1 < x < 3) compounds, the Sb3/Sb3′ positions for x ~ 1 represents the most positionally disordered to the least disordered Sb3 position for x ~ 3.

A plot of the *c* lattice parameters and volumes are provided in Figure 3.3. The volume decreases as a function of increasing Co concentration (x). The *c* lattice parameter initially decreases, but increases when x ~ 2.5 and decreases when x ~ 3.0. It is possible that the trend

along this direction indicates a change in the oxidation state of Fe^{2+} to Fe^{3+} and/or Co^{2+} to Co^{3+} with higher concentrations of Co (x) as evident by our XPS results.

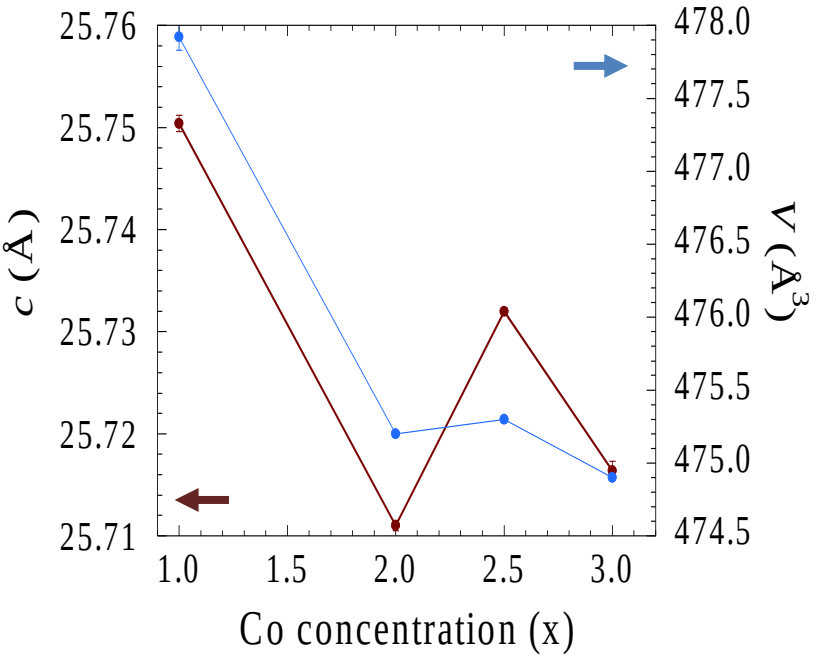

Figure 3.3. Plot of *c* lattice parameters and *V* as a function of increasing Co concentration (x).

3.3.2 Magnetic and Electrical Properties

3.3.2.1 $Pr_2Fe_{4-x}Co_xSb_5$ (x ~ 1). The field-dependent magnetization of $Pr_2Fe_{4-x}Co_xSb_5$ (x ~ 1) at 3 K and 50 K at applied fields of up to 7 T is shown in Figure 3.4[a]. The field-dependent magnetization at 50 K steadily increases with field and reaches a magnetization of 3.7 μ_B at 7 K. At 3 K, the magnetization is hysteretic below 3.5 T before converging to 6.3 μ_B at 7 T. The temperature-dependent magnetic susceptibility of $Pr_2Fe_{4-x}Co_xSb_5$ (x ~ 1) at 0.1 T is shown in Figure 3.4[b]. The magnetic susceptibility increases as a function of decreasing temperature and then a spin reorientation occurs at $T_1 \approx 15$ K, followed by a bifurcation of the zero-field (ZFC) and field-cooled (FC) susceptibility at low temperatures. Above 100 K, the magnetic susceptibility data was fit to a Curie–Weiss equation, $\chi(T) = C/(T-\theta)$, where C represents the Curie constant and θ is the Weiss temperature in the paramagnetic region. A positive Weiss

temperature of θ = 31.7(2) K suggests ferromagnetic interactions. The effective moment of 11.49(4) μ_B corresponds to two independent Pr^{3+} (3.58 μ_B / mol) and four spin-only Fe^{2+} (5.15 μ_B/mol) moments were calculated by using the equation below. The spin-only moment calculated is slightly higher than the calculated spin-only value for Fe^{2+} (4.90 μ_B), due to spin-orbital coupling of the Fe^{2+} ions.

$$\mu_{total} = \mu_{eff}^2\ 2*(Pr^{3+}) + \mu_{eff}^2\ 4*(Fe^{2+})$$

$$11.492\ \mu_B/\text{mol} - \text{f.u.} = 2*\ (3.58)^2\ \mu_B + 4*\ (Fe^{2+})^2\ \mu_B$$

$$\mu_{eff}^2\ (Fe^{2+}) = \sqrt{\frac{(11.492)^2 - (3.58)^2 * 2}{4}}$$

$$\mu_{eff}^2\ (Fe^{2+}) = 5.15\ \mu_B$$

As shown in Figure 3.4[c], the temperature-dependent electrical resistivity of $Pr_2Fe_{4-x}Co_xSb_5$ (x ~ 1) shows a linear dependence at high temperatures (above 150 K). A shoulder is then observed between 50 K and 150 K, followed by a curvature near the magnetic transition at T ~ 15 K, due to spin disorder scattering.

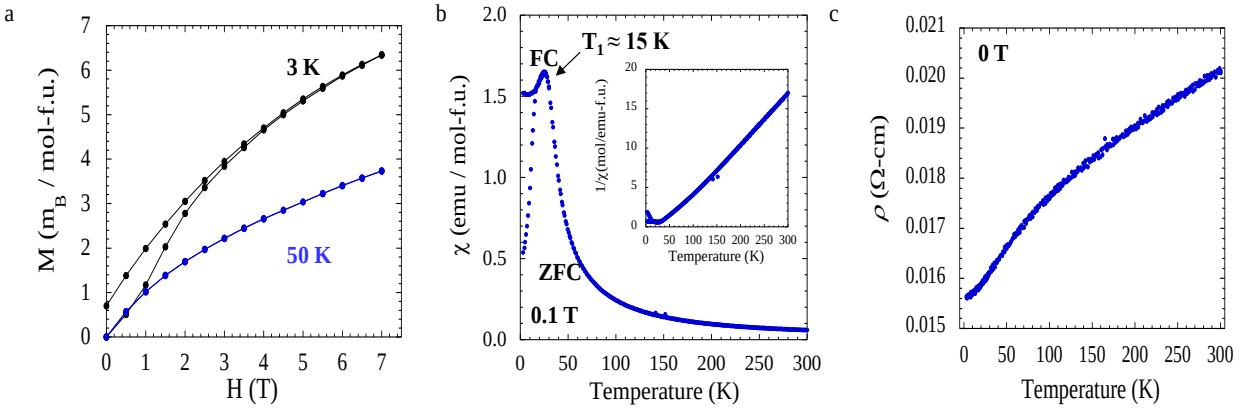

Figure 3.4. Magnetization and electrical resistivity of $Pr_2Fe_{4-x}Co_xSb_5$ (x ~ 1). [a] Field-dependent magnetization at 3 K and 50 K. [b] Temperature-dependent magnetization at 0.1 T with inverse susceptibility in inset. [c] Temperature-dependent electrical resistivity at 0 T.

3.3.2.2 $Pr_2Fe_{4-x}Co_xSb_5$ (x ~ 2). Figure 3.5[a] shows the field-dependent magnetization of $Pr_2Fe_{4-x}Co_xSb_5$ (x ~ 2). The magnetization at 50 K increases until ~ 1 T and starts to saturate at 0.7 μ_B with field up to 7 T. At 3 K, a step-wise increase in magnetization is observed at 0.5 T, followed by change in slope indicating a metamagnetic transition at H_c = 0.5 T. A sharp increase in magnetization is also observed up to 2 T before a steady increase with field. As shown in 3.5[b], the magnetic susceptibility increases with decreasing temperature. Below 180 K, susceptibility increases until a downturn at $T_1 \approx 80$ K is observed, indicating spin reorientation. The magnetic susceptibility then abruptly decreases down to $T_2 \approx 45$ K, where the ZFC and FC susceptibility diverges. The temperature dependent electrical resistivity of $Pr_2Fe_{4-x}Co_xSb_5$ (x ~ 2.0) at 0, 0.1, 0.01, and 1 T is shown in Figure 3.5[c]. At 0 T, the resistivity increases with decreasing temperature, until a change in slope is observed near ~ 250 K. Below 250 K, resistivity gradually decreases again with decreasing temperature. At 0.01 T, the resistivity increases as a function of decreasing temperature, followed by change in slope near 150 K, where a maximum is observed near the large change in slope of the magnetic susceptibility also at ~ 150 K. Below 150 K, resistivity decreases upon cooling, and this is common for a metallic

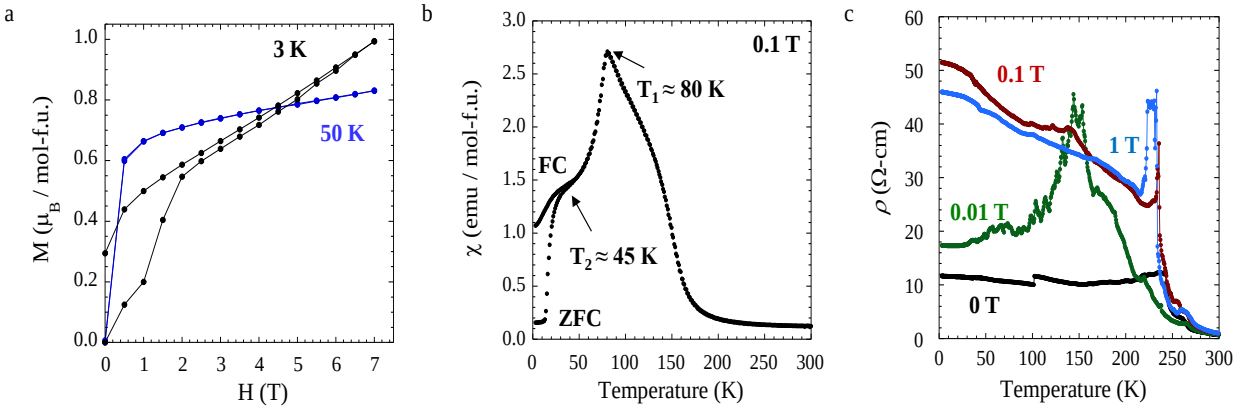

Figure 3.5. Magnetization and electrical resistivity of $Pr_2Fe_{4-x}Co_xSb_5$ (x ~ 2). [a] Field-dependent magnetization at 3 K and 50 K. [b] Temperature-dependent magnetization at 0.1 T. [c.] Temperature-dependent electrical resistivity at 0 T, 0.01 T, 0.1 T, 1 T.

system. At 0.1 T and 1 T, the resistivity begins to increase as it is cooled and rises to a maximum near 230 K. Below 230 K, the resistivity increases again with decreasing temperature.

3.3.2.3 $Pr_2Fe_{4-x}Co_xSb_5$ (x ~ 2.5). Figure 3.6[a] displays the field-dependent magnetization of $Pr_2Fe_{4-x}Co_xSb_5$ (x ~ 2.5) at 3 K and 50 K up to applied magnetic fields of 7 T, which show hysteretic behavior with no saturation with applied fields of 7 T. The temperature-dependent magnetic susceptibility at 0.001 T, 0.01 T, 0.1 T, and 1 T are shown in Figure 3.6[b]. At 0.001 T, the magnetic susceptibility of the ZFC and FC curves immediately diverge near 250 K, and then susceptibility increases followed by a change in slope near $T_1 \approx 200$ K. Below 180 K, there is a large deviation between the ZFC and FC as the susceptibility increases and then decreases at $T_2 \approx 50$ K. The magnetic transitions for the x ~ 2.5 at 0.001 T are also shown in the temperature-dependent susceptibility at 0.01 T, with divergence between the ZFC and FC data. At 0.1 T, there is no divergence of the ZFC and FC data of the susceptibility. At 1T, it is clear the $T_1 \approx 200$ K transition is suppressed at such high field, indicating the susceptibility of this material is highly field-dependent. Based on our single crystal X-ray diffraction data at 100, 200, and 290 K, no structural anomalies were found. Figure 3.6[c] shows the temperature-dependent

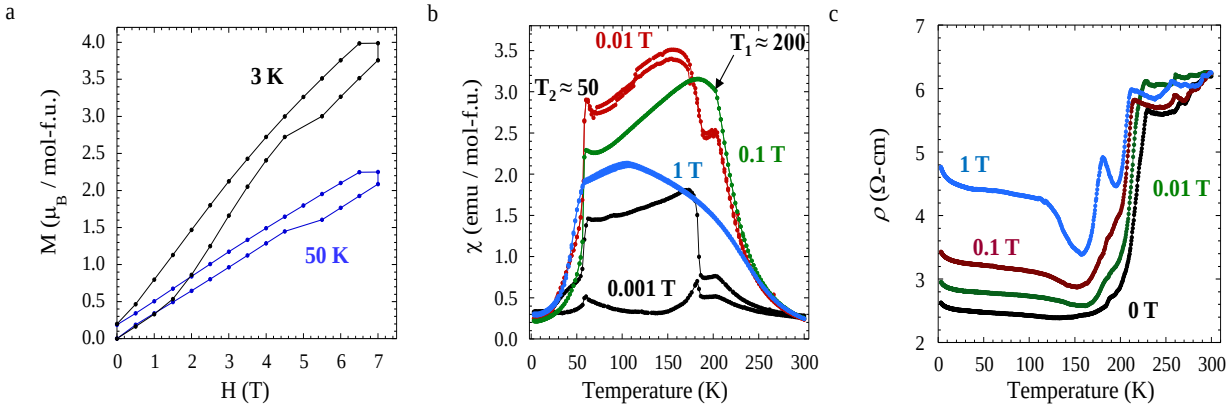

Figure 3.6. Magnetization and electrical resistivity of $Pr_2Fe_{4-x}Co_xSb_5$ (x ~ 2.5). [a] Field-dependent magnetization at 3 K and 50 K. [b] Temperature-dependent magnetization at 0.001 T, 0.01 T, 0.1 T, and 1 T. [c] Temperature-dependent electrical resistivity at 0 T, 0.01 T, 0.1 T, and 1 T.

electrical resistivity of $Pr_2Fe_{4-x}Co_xSb_5$ (x ~ 2.5) at 0 T, 0.01 T, 0.1 T, and 1 T. Above 150 K the changes in slope in the resistivity at all fields coincide with the magnetic transitions and are likely due to spin disorder scattering. Below 150 K, the resistivity gradually increases with increasing temperature.

3.3.2.4 $Pr_2Fe_{4-x}Co_xSb_5$ (x ~ 3). The field-dependent magnetization of $Pr_2Fe_{4-x}Co_xSb_5$ (x ~ 3) at 3 K and 50 K up to applied magnetic fields of 7 T is shown in Figure 3.7[a]. At 50 K, the magnetization is linear with increasing magnetic field and expected for a paramagnetic material. At 3 K and low field, magnetization is linear and then saturates up to 5.7 μ_B at 7 T, which is in agreement of close to two saturation moments of Pr^{3+} moments (3.2 μ_B / mol Pr). The magnetic susceptibility is shown in Figure 3.7[b], and is paramagnetic down to 3 K. The susceptibility data was fit to the Curie-Weiss equation and yielded an effective magnetic moment of 1.81(3) μ_B and Weiss temperature of θ = 3.36(3) K. The effective moment (μ_{eff}) is also considerably lower than the theoretical value of two independent Pr^{3+}, which suggests shielding of the 4*f* local moments by the conduction electrons (Kondo screening). The Weiss temperature (θ = 3.36(3) K) is also

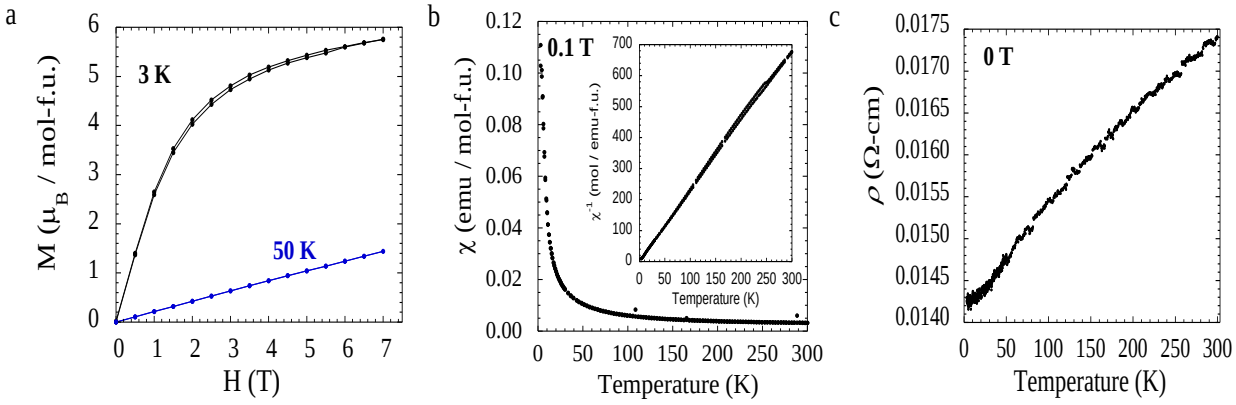

Figure 3.7. Magnetization and electrical resistivity of $Pr_2Fe_{4-x}Co_xSb_5$ (x ~ 3). [a] Field-dependent magnetization at 3 K and 50 K. [b] Temperature-dependent magnetization at 0.1 T with inverse susceptibility in inset. [c] Temperature-dependent electrical resistivity.

lower than the Weiss temperature (θ = 31.7(2) K) calculated in $Pr_2Fe_{4-x}Co_xSb_5$ (x ~ 1.0), indicating a suppression of the ferromagnetic interactions with higher concentrations of Co.

Figure 3.7[c] shows the temperature-dependent electrical resistivity. The electrical resistivity decreases with decreasing temperature also indicating its metallic nature.

3.3.3 Magnetoresistance

Figure 3.8[a] and 3.8[b] shows magnetoresistance (MR (%) = $[(\rho_H - \rho)/\rho] \times 100$ %) as a function of field of single crystalline $Pr_2Fe_{4-x}Co_xSb_5$ (x ~ 2 and 2.5) at 3 K, 50 K, 100 K, and 300 K. For x ~ 2 (Figure 3.8[a]), large positive MR of up to 350% at 50 K (near the corresponding magnetic transition, T ≈ 45 K) and 0.1 T is shown and saturates with increasing field up to 1 T. It is also evident in $Pr_2Fe_{4-x}Co_xSb_5$ (x ~ 2.5), that a large positive magnetoresistance of 40% is observed at 50 K with relatively low field of 0.1 T (Figure 3.8[b]). The parent $Ln_2Fe_4Sb_5$ (Ln = La-Nd, Sm) compounds show small positive magnetoresistances of up to 3.5% at 150 K with applied fields up to 6 T, which is typically shown in metallic systems. Our group has reported large positive magnetoresistance in several Ga and Sb-containing intermetallics, including

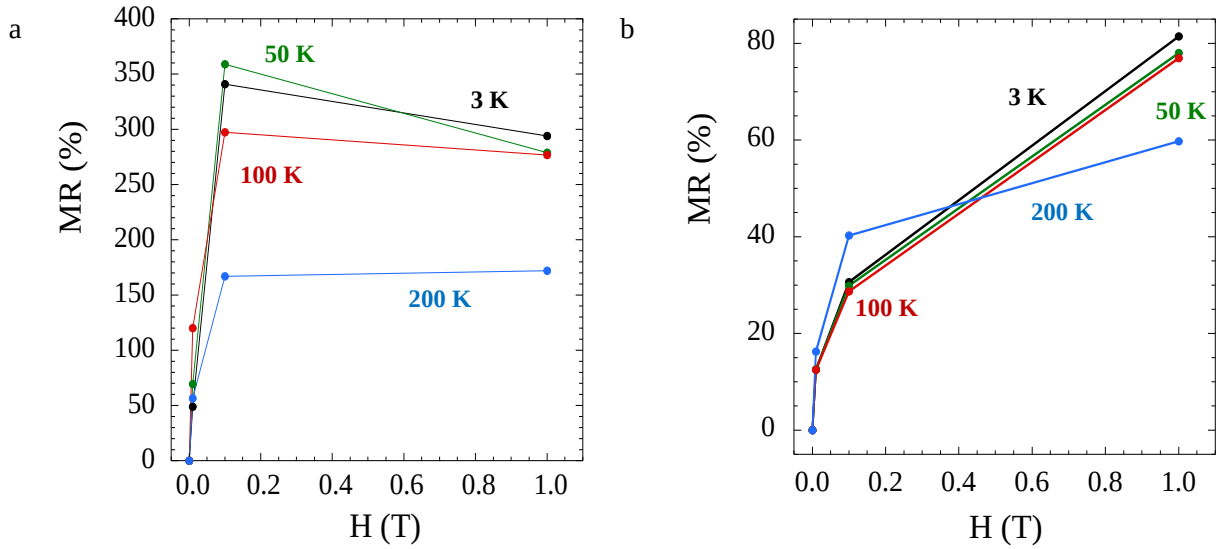

Figure 8. Magnetoresistance (%) as a function of field (T) of $Pr_2Fe_{4-x}Co_xSb_5$ (x ~ 2) [a] and $Pr_2Fe_{4-x}Co_xSb_5$ (x ~ 2) [b].

Ce_2PdGa_{10} (300 % at 2 K and 9 T),[38] $LnNi_{1-x}Sb_2$ (Ln = Y, Dy, Ho;145%, 100%, and 160% at 3 K and 9 T, respectively),[17] La_2NiGa_{12} (216% at 3 K and 9 T),[39] and Ln_4PtGa_{12} (Ln = Dy, Ho, Er; 50%, 220%, and 900% at 3 K and 9 T, respectively)[40]. It is possible that the origin of the large magnetoresistance effect in $Pr_2Fe_{4-x}Co_xSb_5$ (x ~ 2.0 and 2.5) is that of both magnetic frustration and site disorder as this has been observed in the manganites[41] and ruthenates.[42] However, the origin is still unknown and further investigation is warranted.

3.4. Conclusion

We have successfully grown single crystals of $Pr_2Fe_{4-x}Co_xSb_5$ ($1 < x < 3$) using an inert Bi flux. $Pr_2Fe_{4-x}Co_xSb_5$ ($1 < x < 3$) is isostructural to $Ln_2Fe_4Sb_5$ (Ln = La-Nd, Sm).[19] $Pr_2Fe_{4-x}Co_xSb_5$ ($1 < x < 3$) is composed of a network of Fe/Co atoms that are tetrahedrally coordinated with Sb atoms interpenetrating a triangular lattice of transition metals (M = Fe, Co) with nearest neighbor interactions of ~ 2.6 Å, potential for geometrical frustration. The occupationally and positionally disordered M2 and Sb3 sites vary as a function of increasing Co concentration (x). Site disorder and crystallographic defects have been previously shown to influence magnetic and electrical properties including magnetic frustration[28], thermoelectric behavior,[12] and electrical characteristics leading to superconductivity.[43] The site disorder and the presence of two magnetic sublattices have also led to intriguing magnetic and transport properties. It appears that changing composition can lead to highly sensitive change in electrical properties and influence magnetic fluctuations. In our quest to study the effects of Co substitution in $Pr_2Fe_4Sb_5$, we discovered complex magnetic ordering and large positive magnetoresistance of up to 160% and 40% at H = 0.01 T at T = 200 K. A summary of the magnetic and magneto-transport properties of $Pr_2Fe_{4-x}Co_xSb_5$ ($1 < x < 3$) is shown in Table 3.5 (below). $Pr_2Fe_{4-x}Co_xSb_5$ (x ~ 1 and x ~ 3) obeys a Curie–Weiss law consistent with localized magnetic moments and also displays negligible

magnetoresistance. The susceptibility data of $Pr_2Fe_{4-x}Co_xSb_5$ (x ~ 2 and x ~ 2.5) cannot be fit to the Curie–Weiss law and the system may be itinerant. They also exhibit large positive magnetoresistance at fields below 1 T. As a function of increasing Co concentration (x), the electrons become localized to itinerant. Coupled with the geometrical frustration and the structural motifs such as triangular Fe subunits and Pr capping $^2_\infty$[Sb] square nets, we believe these might be the ingredients for the observation of large positive magnetoresistance at relatively low fields. Several antimonide-based intermetallics containing Sb-square nets also display large positive magnetoresistance. Large non-saturating MR is shown in the highly anisotropic layered, $LnSb_2$ (Ln = La–Nd, Sm) with $LaSb_2$ exhibiting a 100-fold linear increase.[44, 45] This structural motif is also commonly found in the $LnMSb_3$ and $LnMSb_2$ (Ln = La-Nd, Gd; M = Cr, Fe, Cu, Ni)[35, 46-53] which also consists of M atoms octahedrally coordinated with Sb atoms $^2_\infty$[MSb_6] that are separated by layers of Ln atoms in square antiprismatic coordination environments. The magnetic and transport properties reported for this series of compounds ranges from itinerant magnetism to large positive magnetoresistance. For example, itinerant ferromagnetism was observed in $LaCrSb_3$ with a mixed-valent state of Cr^{3+} and Cr^{4+}.[46] $LnFeSb_3$ (Ln = Pr, Nd, Gd) exhibits large positive MR of up to 160%, 70%, and 30%, respectively with applied magnetic fields of 9 T with no magnetic contribution from the Fe atoms.[35] The magnetoresistance of $Ce(Cu_{1-x}Ni_x)_ySb_2$ (x = 0.25 and 0.37) rapidly increases up to ~ 1 T before saturating to ~ 80% with magnetic field up to 9 T, while the x = 0.46 composition displays linear MR of up to 90% at 9 T. Additionally, the La-analogue displays magnetoresistance of up to 300 % at 3 K and 9 T.[47] Density of states calculations of $LnCoSb_3$ (Ln = La–Nd, Sm) reveal that the Sb atoms in the Co/Sb layer have been shown to be more delocalized than that of the Sb square nets.[46] This presents a strong competition between the localized and itinerant spins in these

materials, which is also evident in $Pr_2Fe_{4-x}Co_xSb_5$ ($1 < x < 3$). Thus, a combination of competing localized and itinerant magnetic spin states coupled with two or more magnetic sublattices in systems with site disorder and a structural motif, such as the Sb square nets, may facilitate enhanced transport properties, specifically large positive magnetoresistance. Although we propose a mechanism for large positive magnetoresistance, the origin presented herein is an ongoing investigation. The layered nature of these materials also warrants the investigation of the anisotropic magnetic and transport properties. Unfortunately, larger single crystals are necessary to measure transverse magnetoresistance. We are currently optimizing our synthetic parameters to grow larger single crystals suitable for anisotropic property measurements. We are also pursuing other nonmagnetic lanthanides to further study the effects of Co doping on the magnetization and electrical resistivity behavior.

We design and present a system with characteristics that lead to large magnetoresistance. We will continue to optimize crystal growth conditions and study intermetallic compounds with structural disorder or selecting compounds with geometric units that would not satisfy pairwise interactions. While correlation and not causation, we have shown that by substituting Fe for Co to change the otherwise localized magnetic ordering to itinerant ordering leads to the discovery of magnetoresistance with magnetic ordering to itinerant ordering leads to the discovery of magnetoresistance with magnetic transitions above 200 K at relatively low fields. This concept has been introduced in Chapters 7-9 of Models of Itinerant Ordering in Crystals.[54] Therefore, we suggest pursuing intermetallics with the characteristics presented herein to discover new materials with properties useful for technological applications.

Table 3.5. Magnetic Properties of $Pr_2Fe_{4-x}Co_xSb_5$ ($1 < x < 3$)

x	T_1 (K)	T_2 (K)	fit range (K)	θ (K)	μ_{eff} $(\mu_B)^*$	μ_{sat} $(\mu_B)^*$ at 3 K	μ_{sat} $(\mu_B)^*$ at 50 K	MR (%) at 200K (0.1 T)	MR (%) at 50 K (0.1 T)
1	15	—	100-300	31.7(2)	11.49(4)	6.3	3.7	0.026	0.139
2	80	50	—	—	—	—	0.83	150	350
2.5	200	50	—	—	—	—	—	40	30
3	—	—	100-300	3.36(3)	1.81(3)	5.7	—	0.3	0.5

*Magnetic moments are presented per formula unit

3.5 References

(1) Mills, A. M.; Lam, R.; Ferguson, M. J.; Deakin, L.; Mar, A., Chains, Planes, and Antimonides. *Coord. Chem. Rev.* **2002,** *233-234*, 207-222.

(2) Phelan, W. A.; Menard, M. C.; Kangas, M. J.; McCandless, G. T.; Drake, B. L.; Chan, J. Y., Adventures in Crystal Growth: Synthesis and Characterization of Single Crystals of Complex Intermetallic Compounds. *Chem. Mater.* **2012,** *24*, 409-420.

(3) Schmitt, D. C.; Drake, B. L.; McCandless, G. T.; Chan, J. Y., Targeted Crystal Growth of Rare Earth Intermetallics with Synergistic Magnetic and Electrical Properties: Structural Complexity to Simplicity. *Acc. Chem. Res.* **2015,** *48*, 612-618.

(4) Takeda, N.; Ishikawa, M., Superconducting and Magnetic Properties of Filled Skutterudite Compounds $RERu_4Sb_{12}$ (RE=La, Ce, Pr, Nd and Eu). *J. Phys. Soc. Jpn.* **2000,** *69*, 868-873.

(5) Maple, M. B.; Frederick, N. A.; Ho, P. C.; Yuhasz, W. M.; Yanagisawa, T., Unconventional Superconductivity and Heavy Fermion Behavior in $PrOs_4Sb_{12}$. *J. Supercond. Novel Magn.* **2006,** *19*, 299-315.

(6) Tien, C.; Luo, L., Complex Magnetic Ordering in Nd_2CuSi_3. *Solid State Commun.* **1998,** *107*, 295-299.

(7) Zaharko, O.; Keller, L.; Ritter, C., Magnetic Ordering in $Ce_3Cu_4Sn_4$ and $Ce_3Cu_4Ge_4$. *J. Magn. Magn. Mater.* **2002,** *253*, 130-139.

(8) Jiang, J.; Payne, A. C.; Kauzlarich, S. M., New Magnetic Zintl Phases in Eu-In-P System. *Mater. Res. Soc. Symp. Proc.* **2005,** *848*, 89-93.

(9) Jiang, J.; Payne, A. C.; Olmstead, M. M.; Lee, H.-o.; Klavins, P.; Fisk, Z.; Kauzlarich, S. M.; Hermann, R. P.; Grandjean, F.; Long, G. J., Complex Magnetic Ordering in Eu_3InP_3: A New Rare Earth Metal Zintl Compound. *Inorg. Chem.* **2005,** *44*, 2189-2197.

(10) Goforth, A. M.; Hope, H.; Condron, C. L.; Kauzlarich, S. M.; Jensen, N.; Klavins, P.; MaQuilon, S.; Fisk, Z., Magnetism and Negative Magnetoresistance of Two Magnetically Ordering, Rare-Earth-Containing Zintl Phases with a New Structure Type: $EuGa_2Pn_2$ (Pn = P, As). *Chem. Mater.* **2009,** *21*, 4480-4489.

(11) Nasir, N.; Grytsiv, A.; Rogl, P.; Kaczorowski, D.; Effenberger, H. S., The System Nd-Fe-Sb: Phase Equilibria, Crystal Structures and Physical Properties. *Intermetallics* **2010,** *18*, 2361-2376.

(12) Schmitt, D. C.; Haldolaarachchige, N.; Prestigiacomo, J.; Karki, A.; Young, D. P.; Stadler, S.; Jin, R.; Chan, J. Y., Structural Complexity Meets Transport and Magnetic Anisotropy in Single Crystalline $Ln_{30}Ru_4Sn_{31}$ (Ln = Gd, Dy). *J. Am. Chem. Soc.* **2013,** *135*, 2748-2758.

(13) Chan, J. Y.; Kauzlarich, S. M.; Klavins, P.; Shelton, R. N.; Webb, D. J., Colossal Magnetoresistance in the Transition-Metal Zintl Compound $Eu_{14}MnSb_{11}$. *Chem. Mater.* **1997,** *9*, 3132-3135.

(14) Chan, J. Y.; Kauzlarich, S. M.; Klavins, P.; Shelton, R. N.; Webb, D. J., Colossal Negative Magnetoresistance in an Antiferromagnet. *Phys. Rev. B: Condens. Matter Mater. Phys.* **1998,** *57*, R8103-R8106.

(15) Chan, J. Y.; Kauzlarich, S. M.; Klavins, P.; Liu, J. Z.; Shelton, R. N.; Webb, D. J., Synthesis, Magnetic Properties, and Colossal Magnetoresistance of $Eu_{13.97}Gd_{0.03}MnSb_{11}$. *Phys. Rev. B: Condens. Matter Mater. Phys.* **2000,** *61*, 459-463.

(16) Kim, H.; Chan, J. Y.; Olmstead, M. M.; Klavins, P.; Webb, D. J.; Kauzlarich, S. M., Magnetism and Colossal Magnetoresistance of the Pseudo-Ternary Rare-Earth Transition-Metal Compounds, $Eu_{14-x}Ca_xMnSb_{11}$ ($x < 3$). *Chem. Mater.* **2002,** *14*, 206-216.

(17) Thomas, E. L.; Moldovan, M.; Young, D. P.; Chan, J. Y., Synthesis, Structure, and Magneto-Transport of $LnNi_{1-x}Sb_2$ (Ln = Y, Gd-Er). *Chem. Mater.* **2005,** *17*, 5810-5816.

(18) Jiang, J.; Kauzlarich, S. M., Colossal Magnetoresistance in a Rare Earth Zintl Compound with a New Structure Type: $EuIn_2P_2$. *Chem. Mater.* **2006,** *18*, 435-441.

(19) Phelan, W. A.; Nguyen, G. V.; Wang, J. K.; McCandless, G. T.; Morosan, E.; DiTusa, J. F.; Chan, J. Y., Discovery of Spin Glass Behavior in $Ln_2Fe_4Sb_5$ (Ln = La-Nd and Sm). *Inorg. Chem.* **2012,** *51*, 11412-11421.

(20) Schmitt, D. C.; Prestigiacomo, J. C.; Adams, P. W.; Young, D. P.; Stadler, S.; Chan, J. Y., Field-Pulse Memory in a Spin-glass. *Appl. Phys. Lett.* **2013,** *103*, 082403/1-082403/4.

(21) Liu, J.; Mudryk, Y.; Zou, J. D.; Pecharsky, V. K.; Gschneidner, K. A., Jr., Antiferromagnetic Cluster Spin-Glass Behavior in $Pr_{117}Co_{54.5}Sn_{115.2}$ - A Compound with a Giant Unit Cell. *J. Alloys Compd.* **2014,** 600, 101-106.

(22) Mills, A. M.; Deakin, L.; Mar, A., Electronic Structures and Properties of $RE_{12}Ga_4Sb_{23}$ (RE = La-Nd, Sm) and Superconducting $La_{13}Ga_8Sb_{21}$. *Chem. Mater.* **2001,** *13*, 1778-1788.

(23) Goforth, A. M.; Klavins, P.; Fettinger, J. C.; Kauzlarich, S. M., Magnetic Properties and Negative Colossal Magnetoresistance of the Rare Earth Zintl phase $EuIn_2As_2$. *Inorg. Chem.* **2008,** *47*, 11048-11056.

(24) Toulouse, G., Theory of the Frustration Effect in Spin Glasses: I. *Commun. Phys.* **1977,** *2*, 115-119.

(25) Anderson, P. W., Ordering and Antiferromagnetism in Ferrites. *Phys. Rev.* **1956,** *102*, 1008-13.

(26) Nakatsuji, S.; Nambu, Y.; Tonomura, H.; Sakai, O.; Jonas, S.; Broholm, C.; Tsunetsugu, H.; Qiu, Y.; Maeno, Y., Spin Disorder on a Triangular Lattice. *Science (Washington, DC, U. S.)* **2005,** *309*, 1697-1700.

(27) Greedan, J. E., Geometrically Frustrated Magnetic Materials. *J. Mater. Chem.* **2001,** *11*, 37-53.

(28) Menard, M. C.; Ishii, R.; Higo, T.; Nishibori, E.; Sawa, H.; Nakatsuji, S.; Chan, J. Y., High-Resolution Synchrotron Studies and Magnetic Properties of Frustrated Antiferromagnets MAl_2S_4 ($M = Mn^{2+}$, Fe^{2+}, Co^{2+}). *Chem. Mater.* **2011,** *23*, 3086-3094.

(29) Andrukhiv, L.; Lysenko, L., Structure of the Compounds $HfCuSi_2$, $HfCuGe_2$, $ZrCuSi_2$ and $ZrCuGe_2$. *Dop. Akad. Nauk Ukrain. RSR* **1975**, 645-648.

(30) Leithe-Jasper, A.; Rogl, P., The Crystal Structure of $NdFe_{1-x}Sb_2$ and isotypic compounds $RE(Fe,Co)_{1-x}Sb_2$, RE = La, Ce, Pr, Sm and Gd. *J. Alloys Compd.* **1994,** *204*, 13-16.

(31) Sheldrick, G., *SHELX-2013-Programs for Crystal Structure Analysis: i. Structure Determination (SHELXS) and ii. Refinement (SHELXL-2013), University of Gottingen, Germany* **2013**.

(32) Sheldrick, G. M., *Acta Crystallogr., Sect. A* **2015,** *71*, 3-8.

(33) Wagner, C.; Naumkin, A.; Kraut-Vass, A.; Allison, J.; Powell, C.; Rumble Jr, J., NIST X-ray Photoelectron Spectroscopy Database, version 4.1, National Institute of Standards and Technology. *srdata. nist. gov/xps S*.

(34) Woll, P., Ph.D. Dissertation, Technischen Hochschule Darmstadt. **1987**.

(35) Phelan, W. A.; Nguyen, G. V.; Karki, A. B.; Young, D. P.; Chan, J. Y., Synthesis, Structure, Magnetic and Transport Properties of $LnFeSb_3$ (Ln = Pr, Nd, Sm, Gd, and Tb) - Tuning of Anisotropic Long-Range Magnetic Order as a Function of Ln. *Dalton Trans.* **2010,** *39*, 6403-6409.

(36) Chykhrij, S. I.; Smetana, V. B., Phase Relations in the Pr-Fe-Sb and Pr-Co-Sb Systems. *Inorg. Mater.* **2006,** *42*, 503-507.

(37) Abdusalyamova, M. N.; Rakhmatov, O. I.; Fasleva, N. D.; Chuiko, A. G., The Phase Diagram of the Praseodymium-Antimony System. *J. Less-Common Met.* **1988,** *141*, L23-L26.

(38) Millican, J. N.; Macaluso, R. T.; Young, D. P.; Moldovan, M.; Chan, J. Y., Synthesis, Structure, and Physical Properties of Ce_2PdGa_{10}. *J. Solid State Chem.* **2004,** *177*, 4695-4700.

(39) Cho, J. Y.; Millican, J. N.; Capan, C.; Sokolov, D. A.; Moldovan, M.; Karki, A. B.; Young, D. P.; Aronson, M. C.; Chan, J. Y., Crystal Growth, Structure, and Physical Properties of Ln_2MGa_{12} (Ln = La, Ce; M = Ni, Cu). *Chem. Mater.* **2008,** *20*, 6116-6123.

(40) Cho, J. Y.; Moldovan, M.; Young, D. P.; Chan, J. Y., Crystal Growth and Magnetic Properties of Ln_4MGa_{12} (Ln = Dy-Er; M = Pd, Pt). *J. Phys.: Condens. Matter* **2007,** *19*, 266224/1-266224/11.

(41) Yamamoto, A.; Oda, K., The Relation of the Magnetoresistance and Magnetic Frustration Among Ferromagnetic Clusters in $La(Mn_{1-x}Ni_x)O_{3+\delta}$. *Rev. Adv. Mater. Sci.* **2003,** *5*, 343-347.

(42) Mamchik, A.; Chen, I. W., Large Magnetoresistance in Magnetically Frustrated Ruthenates. *Appl. Phys. Lett.* **2003,** *82*, 613-615.

(43) Rai, B. K.; Oswald, I. W. H.; Wang, J. K.; McCandless, G. T.; Chan, J. Y.; Morosan, E., Superconductivity in Single Crystals of Lu_3T4Ge_{13-x} (T = Co, Rh, Os) and Y_3T4Ge_{13-x} (T = Ir, Rh, Os). *Chem. Mater.* **2015,** *27*, 2488-2494.

(44) Bud'ko, S. L.; Canfield, P. C.; Mielke, C. H.; Lacerda, A. H., Anisotropic Magnetic Properties of Light Rare-Earth Diantimonides. *Phys. Rev. B: Condens. Matter Mater. Phys.* **1998,** *57*, 13624-13638.

(45) Young, D. P.; Goodrich, R. G.; DiTusa, J. F.; Guo, S.; Adams, P. W.; Chan, J. Y.; Hall, D., High Magnetic Field Sensor Using $LaSb_2$. *Appl. Phys. Lett.* **2003,** *82*, 3713-3715.

(46) Raju, N. P.; Greedan, J. E.; Ferguson, M. J.; Mar, A., $LaCrSb_3$: A New Itinerant Electron Ferromagnet with a Layered Structure. *Chem. Mater.* **1998,** *10*, 3630-3635.

(47) Gautreaux, D. P.; Parent, M.; Karki, A. B.; Young, D. P.; Chan, J. Y., Investigation of the Effect of Ni Substitution on the Physical Properties of $Ce(Cu_{1-x}Ni_x)_ySb_2$. *J. Phys.: Condens. Matter* **2009,** *21*, 056006/1-056006/7.

(48) Gautreaux, D. P.; Parent, M.; Moldovan, M.; Young, D. P.; Chan, J. Y., Magnetization and Transport Properties of α-$CeNi_{0.78}Co_{0.22}Sb_3$. *Phys. B* **2008,** *403*, 1005-1006.

(49) Gautreaux, D. P.; Capan, C.; DiTusa, J. F.; Young, D. P.; Chan, J. Y., Synthesis, Structure and Physical Properties of $LnNi(Sn,Sb)_3$ (Ln = Pr, Nd, Sm, Gd, Tb). *J. Solid State Chem.* **2008,** *181*, 1977-1982.

(50) Thomas, E. L.; Gautreaux, D. P.; Lee, H.-O.; Fisk, Z.; Chan, J. Y., Discovery of β-$LnNiSb_3$ (Ln = La, Ce): Crystal Growth, Structure, and Magnetic and Transport Behavior. *Inorg. Chem.* **2007,** *46*, 3010-3016.

(51) Deakin, L.; Mar, A., Magnetic Properties and Magnetoresistance of $GdCrSb_3$. *Chem. Mater.* **2003,** *15*, 3343-3346.

(52) Hartjes, K.; Jeitschko, W.; Brylak, M., Magnetic Properties of the Rare-Earth Transition Metal Antimonides $LnVSb_3$ and $LnCrSb_3$ (Ln = La-Nd, Sm). *J. Magn. Magn. Mater.* **1997,** *173*, 109-116.

(53) Brylak, M.; Jeitschko, W., Ternary antimonides $LnTSb_3$ with Ln = La-Nd, Sm and T = V, Cr. *Z. Naturforsch., B: Chem. Sci.* **1995,** *50*, 899-904.

(54) Górski, G., *Models of Itinerant Ordering in Crystals*. ed.; Elsevier Science: 2010; p 115-224.

Chapter 4. Synthesis and Characterization of Calcium Magnesium Silicates via Solid-State and Microwave Methods as Scaffolds for Bone Tissue Engineering*

4.1 Introduction

Advances in biomaterials, specifically at the interface of bioengineering and materials science have given rise to the interesting field of tissue engineering.[1-3] Tissue engineering focuses on providing methods and strategies to treat and repair musculoskeletal problems from fractures to bone diseases.[4, 5] Bone tissue defects are slowly becoming addressed through regenerative medicine by the use of biocompatible and biodegradable polymer/ceramic scaffolding composites that mimic the bone extracellular matrix.[3, 7] Biomaterial scaffolds are influential in bone tissue regeneration by providing a highly dimensional structure for cellular functions, such as proliferation and differentiation.[8] However, mechanical and functional requirements are necessary for tissue regeneration to occur, such as controlled degradation. Thus, a functional scaffold must contain characteristic properties to facilitate bone regrowth, including interconnected porosity (cell transport),[9, 10] biocompatibility (low cytotoxicity),[11, 12] bioactivity (release of bioactive ions and form chemical bonds with surrounding tissue),[12] osteoconductivity/osteoinductivity (bone formation),[13] and mechanical strength (withstand load-bearing parts).[14-16] Developing new materials that meet these requirements would significantly enhance the lifetime of an implant while also minimizing side effects.

Hydroxyapatite (HA), $Ca_{10}(PO_4)_6(OH)_2$, and β-tricalcium phosphate (β-TCP), $Ca_3(PO_4)_2$, are two commonly known bioceramic scaffolding materials that display improved bioactive properties through apatite formation in bone implant materials because they bond to living bone.[17-19] This is achieved by the formation of apatite nuclei that grow spontaneously from the

* Reproduced in part with permission from Chen, C.; Watkins-Curry, P.; Smoak, M.; Hogan, K.; Deese, S.; McCandless, G. T.; Chan, J. Y.; Hayes, D. J., ACS Biomater. Sci. Eng. 2015, *1*, 94-102. Copyright 2015 American Chemical Society. DOI: 10.1021/ab500011x

consumption of calcium and phosphate ions from the surrounding body fluid. Although these compounds are biocompatible and osteogenic, their use is limited to small non–load bearing parts due to their poor mechanical properties.[20] Therefore, a strong interest in discovering alternative ceramic scaffolding materials with superior mechanical properties to withstand heavy loads while retaining biocompatibility is imperative.[21] Recently silicate-based ceramic compounds have been studied as potential scaffolding material. For example, akermanite ($Ca_2MgSi_2O_7$), a calcium magnesium silicate, has shown to stimulate cells caused by ionic products from akermanite scaffold dissolution.[22] More recently, phase pure akermanite synthesized by the solid-state reaction method was used to produce scaffolds for human adipose-derived stem cells.[23] Additionally, silicate-based ceramics like diopside have shown to exhibit apatite like formation at the interface of diopside and newly grown bone with a fracture toughness of 3.5 MPa $m^{1/2}$ and a Young's modulus of 170 GPa compared to that of hydroxyapatite (1.1 MPa $m^{1/2}$ and 47 GPa).[24-26] The low cytotoxicity of Si-based ceramic materials as well as their improved mechanical properties has motivated us to further our study of akermanite and other related compounds for tissue regeneration.

Since the scaffold architecture plays an important role in the functionality of the scaffold, particularly its mechanical strength, we seek to consider highly dimensional oxides and study how dimensionality affects the mechanical properties. Although structurally similar, the crystal structures presented are shown in the order of structural dimensionality as shown in Figure 4.1. To further improve the mechanical properties, we also incorporated polycaprolactone (PCL), $(C_6H_{10}O_2)_n$, a biocompatible synthetic polymer, to fabricate a ceramic-polymer composite, and studied the mechanical strength with respect to each ceramic phase.

Herein, this study is focused on the synthetic preparation and X-ray characterization of calcium magnesium silicate–based bioceramics (i.e. diopside ($CaMgSi_2O_6$), akermanite ($Ca_2MgSi_2O_7$), monticellite ($CaMgSiO_4$), and merwinite ($Ca_3Mg(SiO_4)_2$) as well as strontium analogues of akermanite ($Sr_2MgSi_2O_7$) as scaffolding material for bone tissue regeneration purposes with potentially improved osteoinductive and conductive properties. The Ca-based ceramics are also incorporated into composite PCL:ceramic scaffolds to test for mechanical strength and biocompatibility.

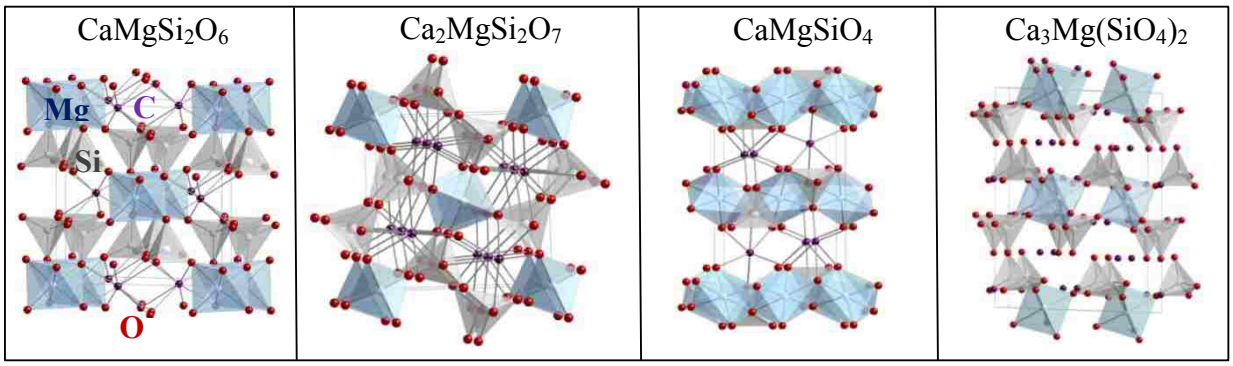

Figure 1. Crystal structures of diopside ($CaMgSi_2O_6$), akermanite ($Ca_2MgSi_2O_7$), monticellite ($CaMgSi_2O_4$), and merwinite ($Ca_3Mg(SiO_4)_2$). Purple spheres are Ca, red spheres are O, grey and blue polyhedra are Si and Mg, respectively.[6]

4.2 Experimental

4.2.1 Conventional Synthesis of Diopside ($CaMgSi_2O_6$), Akermanite ($Ca_2MgSi_2O_7$), Monticellite ($CaMgSiO_4$), and Merwinite ($Ca_3Mg(SiO_4)_2$)[6]

Diopside ($CaMgSi_2O_6$), akermanite ($Ca_2MgSi_2O_7$), monticellite ($CaMgSiO_4$), and merwinite ($Ca_3Mg(SiO_4)_2$) were synthesized by conventional ceramic methods with $CaCO_3$ (-325 mesh, 99.95%), $MgCO_3$ (98.95%), and SiO_2 (99.999%-Si). All reagents were stoichiometrically weighed, mixed, and grounded in an agate mortar and pestle (~20 min), and powders were pressed into ~1 cm pellets and annealed in alumina boats. After an initial calcination at 950 °C at a rate of 100 °C/h for 48 h, multiple heat treatments were carried out up to 1300 °C at a rate of

100 °C with intermediate grinding and re-pelletizing until reaching phase equilibrium. Monticellite ($CaMgSiO_4$) was obtained with heat treatments up to 1100 °C.[6]

4.2.2 Conventional and Microwave Synthesis of $Sr_2MgSi_2O_7$

Sr^{2+} has previously shown to have a strong affinity to bone and stimulate bone formation in vitro by ionic exchange of Ca^{2+}.[27] To improve the mechanical properties of ceramic materials, we have also prepared the Sr-analogue of akermanite. $Sr_2MgSi_2O_7$ was first prepared using the conventional ceramic method. Stoichiometric amounts of $SrCO_3$ (99.99%), $MgCO_3$ (98.95%), and SiO_2 (99.999%-Si) were ground in an agate mortar and pestle and pelletized into pellets (~ 1 cm in height), placed into an alumina boat, and then heat treated. Achieving phase-pure materials by solid state methods requires long reaction times and typically takes one month to reach phase equilibrium and requires re-grinding and re-pelletizing between heat treatments. Another common method, for example sol-gel has been used to synthesize ceramic materials, but it can be difficult to synthesize material with high purity.[28] Microwave assisted solid state methods have been used to produce a variety of materials including intermetallics,[29] oxides,[30, 31] superconductors,[32] thermoelectric materials,[29, 33, 34] and ceramics.[35] Several advantages from employing microwave assisted techniques over conventional methods include direct heating, higher purity, and shorter reaction times.[36-38] Recently, a Eu-doped $Ca_2MgSi_2O_7$ was prepared using a microwave-assisted method with reaction times as low as 45 min.[36] Microwave assisted preparation has also been a successful method to prepare $Sr_2MgSi_2O_7$.[36] For our experiments, ceramics can be prepared by using a domestic microwave oven (Panasonic NN-SN66713, 1200 W operating at 2.45 GHz). A similar hybrid setup consisting of a larger outer crucible was filled with a mixture of granular and powder activated carbon. A smaller alumina crucible is used to house the ground powder material (~ 0.5 g), and then the crucible is placed in the center of the

large crucible to surround the sample with an appreciable amount of activated carbon. The outer crucible is then topped with an alumina disc. This hybrid setup is then placed in well insulated alumina foam, which acts as a thermal barrier.[39] The alumina house is then placed off-center of the microwave cavity for homogeneous distribution of the electromagnetic radiation. The materials were heated in a two-stage process where 20% of the reaction time operated at a power level of 960 W, and 80% of the reaction time operated at a power level of 360 W. A schematic of the microwave setup is shown in Figure 4.2.

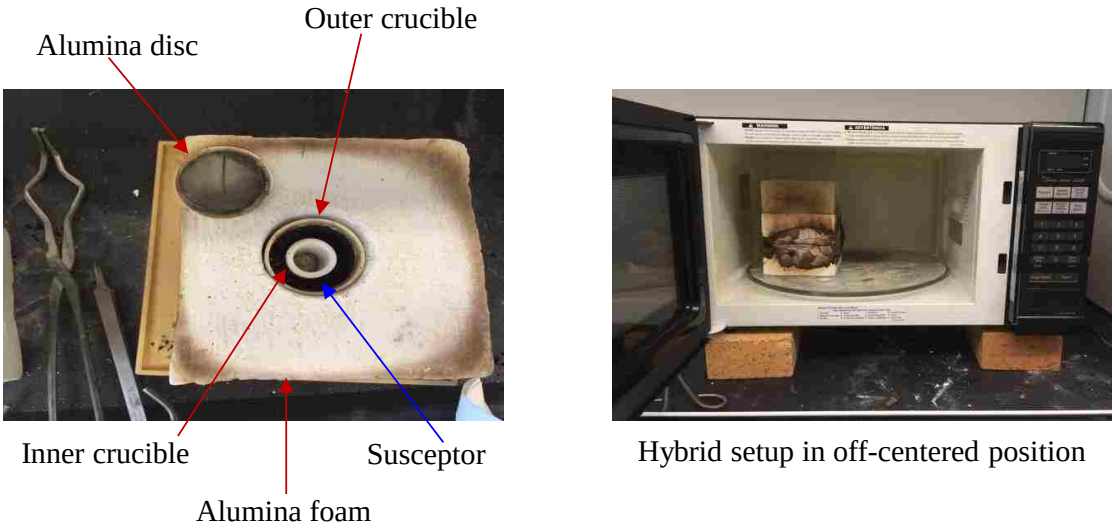

Figure 4.2. Hybrid microwave system. Left: Reaction materials housed in alumina hybrid system. Right: Hybrid system placed in off-centered position to ensure homogeneity of electromagnetic radiation in microwave cavity.

4.2.3 Characterization of Ceramics by Powder X-ray Diffraction

The as-synthesized diopside ($CaMgSi_2O_6$), akermanite ($Ca_2MgSi_2O_7$ and $Sr_2MgSi_2O_7$), monticellite ($CaMgSiO_4$), and merwinite ($Ca_3Mg(SiO_4)_2$) were characterized by powder X-ray diffraction using a Bruker D8 Advance X-ray diffractometer operating at 40 kV and 30 mA with a Cu Kα radiation source with a LYNXEYE XE detector. X-ray diffraction data were collected using Bragg Brentano geometry from 2θ of 10° to 80° using a step size of 0.02 at a rate of 1s per

step. Phase purity of samples was compared with calculated powder diffraction patterns.[40-43] Topas 4.2 was used to generate a model of X-ray data of diopside ($CaMgSi_2O_6$), akermanite ($Ca_2MgSi_2O_7$), monticellite ($CaMgSiO_4$), and merwinite ($Ca_3Mg(SiO_4)_2$), as provided in Table 4.1.[8] The unit cell refinements of $Sr_2MgSi_2O_7$ prepared through conventional and microwave methods are provided in Table 4.2.[6]

Table 4.1. Unit Cell Parameters of Diopside ($CaMgSi_2O_6$), Akermanite ($Ca_2MgSi_2O_7$), Monticellite ($CaMgSiO_4$), and Merwinite ($Ca_3Mg(SiO_4)_2$)[6]

Unit Cell Parameters				
Compound	$CaMgSi_2O_6$	$Ca_2MgSi_2O_7$	$CaMgSiO_4$	$Ca_3Mg(SiO_4)_2$
System	monoclinic	tetragonal	orthorhombic	monoclinic
Space Group	*C2/c*	$P\bar{4}2_1m$	*Pbnm*	$P2_1/c$
a (Å)	9.748(5)	7.909(4)	4.798(2)	13.175(7)
b (Å)	8.926(4)	-	11.041(4)	5.269(2)
c (Å)	5.251(2)	5.046(3)	6.356(2)	9.301(4)
β (°)	105.89 (3)	-	-	92.01(4)
V (Å^3)	439.5(4)	316.2(4)	336.7(2)	645.3(5)

Table 4.2. Unit Cell Parameters of Sr-akermanite ($Sr_2MgSi_2O_7$) Prepared by Convention and Microwave Method

Unit Cell Parameters			
Compound	$Sr_2MgSi_2O_7$*	$Sr_2MgSi_2O_7$	$Sr_2MgSi_2O_7$
Preparation	Convention	Convention	Microwave
Space Group	$P\bar{4}2_1m$	$P\bar{4}2_1m$	$P\bar{4}2_1m$
a (Å)	7.9957(10)	8.0259(12)	8.0168(17)
c (Å)	5.1521(9)	6.3411(10)	5.1671(12)
V (Å^3)	329.54(8)	408.46(14)	332.09(15)

*cell dimensions as obtained from Kimata, M. *Z. Kristallogr.* **1983,** *163*, 295-304[44]

4.3 Results and Discussion

4.3.1 Phase Identification (Conventional and Microwave)

The diffraction patterns of all Ca-based ceramic materials are shown in Figure 4.3. The X-ray powder diffraction patterns of diopside ($CaMgSi_2O_6$), akermanite ($Ca_2MgSi_2O_7$), monticellite ($CaMgSiO_4$), and merwinite ($Ca_3Mg(SiO_4)_2$). The major reflections indicate the targeted phase in all ceramic compounds, but a minor SiO_2 impurity is also detected in diopside ($CaMgSi_2O_6$), akermanite ($Ca_2MgSi_2O_7$), and monticellite ($CaMgSiO_4$). The X-ray diffraction of $CaMg(SiO_4)$ resulted in a two phase refinement of monticellite (95.9%) and merwinite (4.10%). Multiple subsequent heat treatments up to 1100 °C led to the formation of phase–pure merwinite.[6] The X-ray powder diffraction patterns of $Sr_2MgSi_2O_7$ prepared using conventional and microwave methods are shown in Figure 4.4. To achieve a phase–pure $Sr_2MgSi_2O_7$ conventionally, multiple heat treatments at 1300 °C were required similar to that of $Ca_2MgSi_2O_7$.

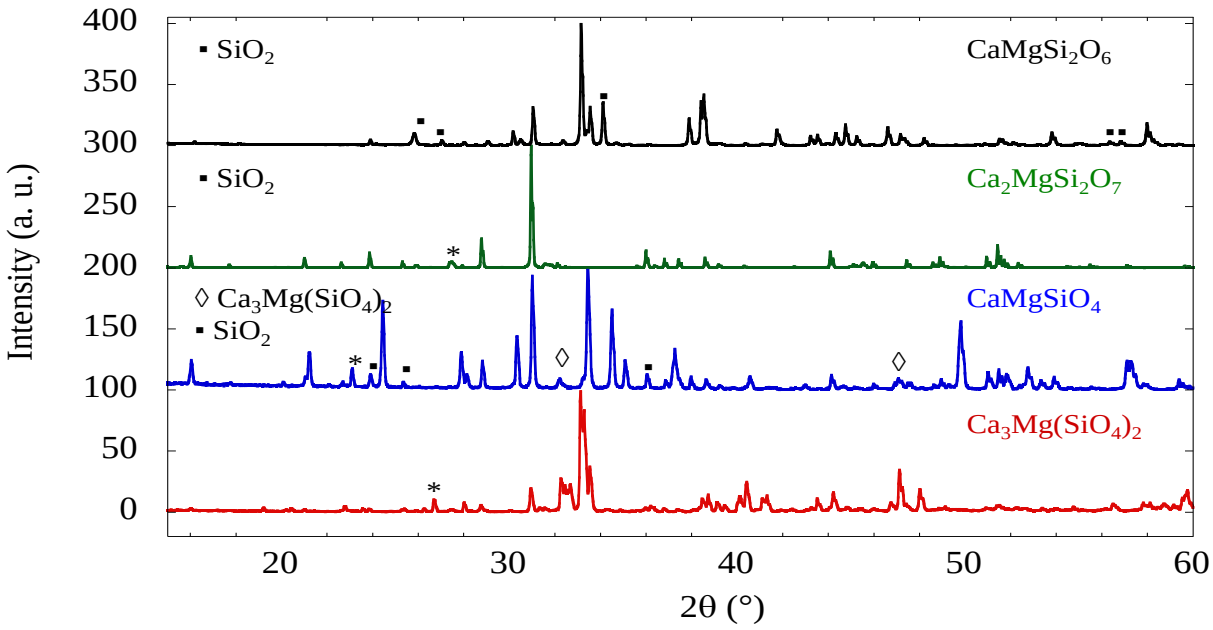

Figure 4.3. Powder X-ray diffraction patterns of $CaMgSi_2O_6$ (black), $Ca_2MgSi_2O_7$ (green), $CaMgSi_2O_4$ (blue), and $Ca_3Mg(SiO_4)_2$ (red). * represents unidentified reflections.

For the microwave prepared $Sr_2MgSi_2O_7$, several attempts were made to achieve phase formation. The $Sr_2MgSi_2O_7$ phase can be produced with a power setting of 960 W for 8 min, followed by a lower power setting of 360 W for 25 min; however, with minor impurities of $Sr_3MgSi_2O_8$. To obtain phase pure $Sr_2MgSi_2O_7$, a power setting of 960 W for 8 min, followed by a power setting of 360 W for 30 min is required. As shown in Figure 4.4, the powder X-ray diffraction patterns of $Sr_2MgSi_2O_7$ by convention and microwave methods are identical, demonstrating that the microwave prepared methods can produce material with high purity with faster reaction times.

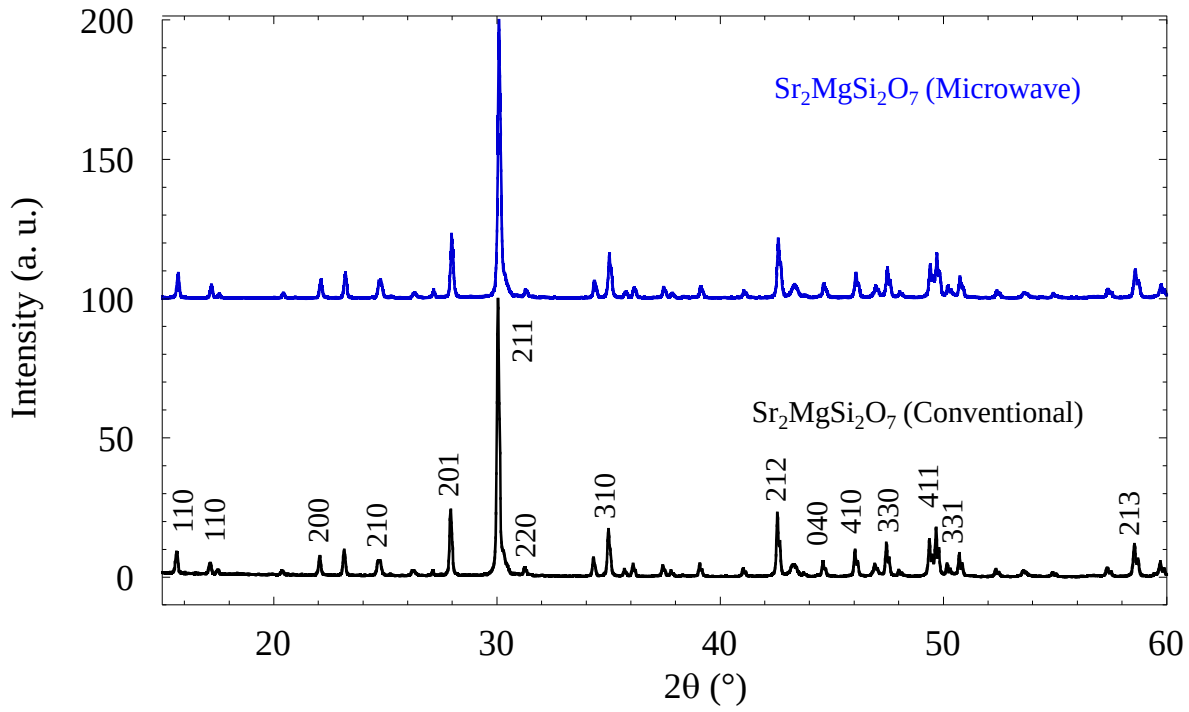

Figure 4.4. Powder X-ray diffraction patterns of akermanite ($Sr_2MgSi_2O_7$) prepared by convention and microwave methods.

4.3.2 Ceramic and PCL:Ceramic Scaffold Characterization and *In Vitro* Experiments

Figure 4.4 shows the diffraction patterns of $Sr_2MgSi_2O_7$ prepared by convention and microwave methods. The ceramics ($CaMgSi_2O_6$, $Ca_2MgSi_2O_7$, $CaMgSiO_4$, $Ca_3Mg(SiO_4)_2$) herein

are used as ceramic scaffolds and polycaprolactone/ceramic (PCL:ceramic) composite scaffolds. Full details on the fabrication of ceramic and PCL:ceramic scaffolds are provided in the previously reported work.[6] The scaffolds were tested for the following: micro-Ct and porosity, compressive strength, and biocompatibility. The porosity and average pore size of the ceramics are comparable with pore sizes in the range of 0.838 – 0.844 nm. For the pure ceramic scaffolds, diopside exhibited the highest mechanical strength (0.28 MPa), followed by akermanite (0.14 MPa), and monticellite (0.03 MPa). Merwinite degraded during scaffold formation, and as a result no compressive strength was obtained. When the ceramics are incorporated as a composite material (PCL:ceramic), the 75:25 ratio reached the highest compressive strength. A similar trend is observed with the pure ceramic scaffolds, where the diopside:polymer ceramic scaffold obtains the highest compressive strength (0.3 MPa). The viability of the pure ceramic and composite scaffolds on hASCs (human adiposed–derived stem cells) also shows improved results to the control. Diopside and akermanite composite scaffolds showed to support the highest level of relative metabolic activity.[6]

4.4 Conclusions and Future Work

Ca-based and Sr-based silicates were synthesized by conventional and microwave methods for their use as ceramic and polymer/ceramic composite scaffolds for bone tissue engineering. Microwave synthetic methods proved to produce phase pure $Sr_2MgSi_2O_7$ with shorter reaction times (~45 min) compared to the solid state reaction technique (~406 h.). The Ca-based silicates were used as scaffolding material and compressive strength, micro-Ct, and cytotoxicity was studied. Diopside, the most three-dimensional among the silicates selected for our study, showed the highest compressive strength compared to akermanite, monticellite, and merwinite, as well as the diopside:polymer composite scaffold.[6] This shows that the crystal

structure plays an influential role in scaffold architecture and design. Future work will focus on fabricating other Sr-based silicates as scaffolding material and comparing the porosity, mechanical stability, and bioactivity results to the Ca-based silicates.

4.5 References

(1) Lanza, R.; Langer, R.; Vacanti, J. P., *Principles of Tissue Engineering*. ed.; Academic press: 2011.

(2) Langer, R.; Vacanti, J. P., Tissue Engineering. *Science* **1993,** *260*, 920-6.

(3) Langer, R.; Tirrell, D. A., Designing Materials for Biology and Medicine. *Nature* **2004,** *428*, 487-492.

(4) Bianco, P.; Robey, P. G., Stem Cells in Tissue Engineering. *Nature* **2001**, 118-121.

(5) Ducheyne, P.; Mauck, R. L.; Smith, D. H., Biomaterials in the Repair of Sports Injuries. *Nat. Mater.* **2012,** *11*, 652-654.

(6) Chen, C.; Watkins-Curry, P.; Smoak, M.; Hogan, K.; Deese, S.; McCandless, G. T.; Chan, J. Y.; Hayes, D. J., Targeting Calcium Magnesium Silicates for Polycaprolactone/Ceramic Composite Scaffolds. *ACS Biomater. Sci. Eng.* **2015,** *1*, 94-102.

(7) Amini, A. R.; Laurencin, C. T.; Nukavarapu, S. P., Bone Tissue Engineering: Recent Advances and Challenges. *Crit. Rev. Biomed. Eng.* **2012,** *40*, 363-408.

(8) Stevens, B.; Yang, Y.; Mohandas, A.; Stucker, B.; Nguyen, K. T., A Review of Materials, Fabrication Methods, and Strategies Used to Enhance Bone Regeneration in Engineered Bone Tissues. *J. Biomed. Mater. Res., Part B* **2008,** *85B*, 573-582.

(9) Hollister, S. J., Porous Scaffold Design for Tissue Engineering. *Nat. Mater.* **2005,** *4*, 518-524.

(10) Hulbert, S. F.; Young, F. A.; Mathews, R. S.; Klawitter, J. J.; Talbert, C. D.; Stelling, F. H., Potential of Ceramic Materials as Permanently Implantable Skeletal Prostheses. *J. Biomed. Mater. Res.* **1970,** *4*, 433-56.

(11) Hench, L. L.; Splinter, R. J.; Allen, W.; Greenlee, T., Bonding Mechanisms at the Interface of Ceramic Prosthetic Materials. *J. Biomed. Mater. Res.* **2004,** *5*, 117-141.

(12) Cao, W.; Hench, L. L., Bioactive Materials. *Ceram. Int.* **1996,** *22*, 493-507.

(13) Vaccaro, A. R., The Role of the Osteoconductive Scaffold in Synthetic Bone Graft. *Orthopedics* **2002,** *25*, s571-8.

(14) Wagoner Johnson, A. J.; Herschler, B. A., A Review of the Mechanical Behavior of CaP and CaP/Polymer Composites for Applications in Bone Replacement and Repair. *Acta Biomater.* **2011,** *7*, 16-30.

(15) Billstrom, G. H.; Blom, A. W.; Larsson, S.; Beswick, A. D., Application of Scaffolds for Bone Regeneration Strategies: Current Trends and Future Directions. *Injury* **2013,** *44* S28-33.

(16) Hench, L. L., Bioceramics: from Concept to Clinic. *Am. Ceram. Soc. Bull.* **1993,** *72*, 93-8.

(17) Merolli, A.; Tranquilli, L. P.; Guidi, P. L.; Gabbi, C., Comparison in In-Vivo Response Between Bioactive Glass and a Non-Bioactive Glass. *J. Mater. Sci.: Mater. Med.* **2000,** *11*, 219-222.

(18) Miao, X.; Tan, D. M.; Li, J.; Xiao, Y.; Crawford, R., Mechanical and Biological Properties of Hydroxyapatite/Tricalcium Phosphate Scaffolds Coated with Poly(lactic-co-glycolic acid). *Acta Biomater.* **2008,** *4*, 638-645.

(19) Bose, S.; Roy, M.; Bandyopadhyay, A., Recent Advances in Bone Tissue Engineering Scaffolds. *Trends Biotechnol.* **2012,** *30*, (*10*), 546-554.

(20) Kim, H.-W.; Lee, S.-Y.; Bae, C.-J.; Noh, Y.-J.; Kim, H.-E.; Kim, H.-M.; Ko, J. S., Porous ZrO_2 Bone Scaffold Coated with Hydroxyapatite with Fluorapatite Intermediate Layer. *Biomaterials* **2003,** *24*, 3277-3284.

(21) Danzer, R.; Lube, T.; Supancic, P.; Damani, R., Fracture of Ceramics. *Adv. Eng. Mater.* **2008,** *10*, 275-298.

(22) Wu, C.; Chang, J., A Novel Akermanite Bioceramic: Preparation and Characteristics. *J. Biomater. Appl.* **2006,** 21, 119-129.

(23) Zanetti, A. S.; McCandless, G. T.; Chan, J. Y.; Gimble, J. M.; Hayes, D. J., In Vitro Human Adipose-Derived Stromal/Stem Cells Osteogenesis in Akermanite: Poly-ε-caprolactone Scaffolds. *J. Biomater. Appl.* **2014,** *28*, 998-1007, 10.

(24) Reidy, C., Comparative Sintering of Zirconia and Hydroxyapatite-Zirconia Composites. **2010**.

(25) Nonami, T.; Tsutsumi, S., Study of Diopside Ceramics for Biomaterials. *J. Mater. Sci.: Mater. Med.* **1999,** *10*, 475-479.

(26) Iwata, N. Y.; Lee, G.-H.; Tsunakawa, S.; Tokuoka, Y.; Kawashima, N., Preparation of Diopside with Apatite-Forming Ability by Sol-Gel Process Using Metal Alkoxide and Metal Salts. *Colloids Surf., B* **2004,** *33*, 1-6.

(27) Canalis, E.; Hott, M.; Deloffre, P.; Tsouderos, Y.; Marie, P. J., The Divalent Strontium Salt S12911 Enhances Bone Cell Replication and Bone Formation In Vitro. *Bone* **1996,** *18*, 517-23.

(28) McCandless, G. T. Chemical Crystallography at the Interface of Physics, Chemistry, and Engineering: Structure Determination of Highly Correlated Extended Solids, Main Group Compounds, Coordination Complexes, and Bioceramics. Dissertation, Louisiana State University, 2012.

(29) Birkel, C. S.; Zeier, W. G.; Douglas, J. E.; Lettiere, B. R.; Mills, C. E.; Seward, G.; Birkel, A.; Snedaker, M. L.; Zhang, Y.; Snyder, G. J.; Pollock, T. M.; Seshadri, R.; Stucky, G. D., Rapid Microwave Preparation of Thermoelectric TiNiSn and TiCoSb Half-Heusler Compounds. *Chem. Mater.* **2012,** *24*, 2558-2565.

(30) Boykin, J. R.; Smith, L. J., Rapid Microwave-Assisted Grafting of Layered Perovskites with n-Alcohols. *Inorg. Chem.* **2015,** *54*, 4177-4179.

(31) Birkel, A.; Denault, K. A.; George, N. C.; Doll, C. E.; Hery, B.; Mikhailovsky, A. A.; Birkel, C. S.; Hong, B.-C.; Seshadri, R., Rapid Microwave Preparation of Highly Efficient Ce^{3+}-Substituted Garnet Phosphors for Solid State White Lighting. *Chem. Mater.* **2012,** *24*, 1198-1204.

(32) Baghurst, D. R.; Chippindale, A. M.; Mingos, D. M. P., Microwave Syntheses for Superconducting Ceramics. *Nature* **1988,** *332*, 311.

(33) Birkel, C. S.; Douglas, J. E.; Lettiere, B. R.; Seward, G.; Verma, N.; Zhang, Y.; Pollock, T. M.; Seshadri, R.; Stucky, G. D., Improving the Thermoelectric Properties of Half-Heusler TiNiSn Through Inclusion of a Second Full-Heusler Phase: Microwave Preparation and Spark Plasma Sintering of $TiNi_{1+x}Sn$. *Phys. Chem. Chem. Phys.* **2013,** *15*, 6990-6997.

(34) Biswas, K.; Muir, S.; Subramanian, M. A., Rapid Microwave Synthesis of Indium Filled Skutterudites: An Energy Efficient Route to High Performance Thermoelectric Materials. *Mater. Res. Bull.* **2011,** *46*, 2288-2290.

(35) Katz, J. D., Microwave Sintering of Ceramics. *Annu. Rev. Mater. Sci.* **1992,** *22*, 153-70.

(36) Birkel, A.; Darago, L. E.; Morrison, A.; Lory, L.; George, N. C.; Mikhailovsky, A. A.; Birkel, C. S.; Seshadri, R., Microwave Assisted Preparation of Eu^{2+}-Doped Åkermanite $Ca_2MgSi_2O_7$. *Solid State Sci.* **2012,** *14*, 739-745.

(37) Roy, R.; Komarneni, S.; Yang, L. J., Controlled Microwave Heating and Melting of Gels. *J. Am. Ceram. Soc.* **1985,** *68*, 392-5.

(38) Baghurst, D. R.; Mingos, D. M. P., Application of Microwave Heating Techniques for the Synthesis of Solid State Inorganic Compounds. *J. Chem. Soc., Chem. Commun.* **1988**, 829-30.

(39) Harabi, A.; Karboua, N.; Achour, S., Effect of Thickness and Orientation of Alumina Fibrous Thermal Insulation on Microwave Heating in a Modified Domestic 2.45 GHz Multi-Mode Cavity. *Int. J. Appl. Ceram. Technol.* **2012,** *9*, 124-132.

(40) Clark, J. R.; Appleman, D. E.; Papike, J., Crystal-Chemical Characterization of Clinopyroxenes Based on Eight New Structure Refinements. *Mineral. Soc. Am.* **1969,** *2*, 31-50.

(41) Kuz'micheva, G.; Zharikov, E.; Denisov, A., X-ray Structural Study of Synthetic Gehlenites $Ca_2Al(AlSi)O_7$ and Akermanites $Ca_2MgSi_2O_7$ Doped with Chromium Ions. *Russ. J. Inorg. Chem.* **1995,** *40*, 1368-1374.

(42) Moore, P.; Araki, T., Atomic Arrangement of Merwinite, $Ca_3Mg(SiO_4)_2$, an Unusual Dense-Packed Structure of Geophysical Interest. *Am. Mineral.* **1972,** *57*, 1355-1374.

(43) Subbotin, K.; Iskhakova, L.; Zharikov, E.; Lavrishchev, S., Investigation of the Crystallization Features, Atomic Structure, and Microstructure of Chromium-Doped Monticellite. *Crystallogr. Rep.* **2008,** *53*, 1107-1111.

(44) Kimata, M., The Structural Properties of Synthetic Strontium Akermanite, $Sr_2MgSi_2O_7$. *Z. Kristallogr.* **1983,** *163*, 295-304.

Chapter 5. Conclusions and Closing Remarks

5.1 Conclusions

The primary focus of this dissertation is to present the syntheses, structures, and properties of several rare earth intermetallics and bioceramic materials. The targeted compounds were synthesized for the fundamental discovery of new properties for potential application. In Chapters 2-4, I present the challenges that arise in the synthesis of intermetallic and ceramic materials, and the strategies to produce desired phases without impurities. Once the desired crystalline product is obtained, and the structures are elucidated, the ultimate reward is found in the resulting measured properties.

An Al-flux was employed for the growth of $LnCo_2Al_8$ (Ln = La–Nd, Sm, Yb) and $CeCo_{2-x}Mn_xAl_8$ ($0 < x < 1$). Because these crystals were grown in such an Al-rich environment, the growth of Co_2Al_9, an unwanted binary, was also obtained when the reactions were removed below 900 °C. Stabilizing crystalline product of the $CaCo_2Al_8$-structure type[2] without the related Co_2Al_9 phase, requires the reaction to be removed at 900 °C (above the temperature where the binary is formed). Expectedly, Co_2Al_9[3] consists of Co atoms that form tri-capped trigonal prismatic environments with Al atoms similar to the Co environments of the $CaCo_2Al_8$-structure type. Therefore, it is concluded that the growths of single crystalline $LnCo_2Al_8$ (Ln = La–Nd, Sm, Yb) and $CeCo_{2-x}Mn_xAl_8$ ($0 < x < 1$) are stabilized by the incorporation of an electropositive or larger element like a rare earth in the Co_2Al_9 structure. This strategy could hopefully lead to the discovery of novel ternary intermetallics from the crystal structures of related binaries. I also find it imperative to focus on the homogeneous product of single crystals for measurement of magnetic and electrical properties. The high quality single crystal $CeCo_2Al_8$, with a RRR of ~ 20, shows metallic behavior with a change in slope near ~ 50 K in the temperature dependent electrical resistivity. This behavior is slightly different from the polycrystalline $CeCo_2Al_8$,[4] with

a RRR of ~ 2, where a weak temperature dependence is observed at high temperatures followed by broadening in the resistivity at ~ 45 K, which was attributed to Kondo-like scattering of the conduction electrons with the 4*f* local moments. This comparison is an example of the benefit of measuring properties of single crystals to determine intrinsic properties to establish structure-property relationships. $CeCo_2Al_8$ and $NdCo_2Al_8$ are both magnetically frustrated with f ~ 60, and 14 K, respectively. The Pr analogue exhibits a field-induced metamagnetic transition indicating its sensitivity with applied magnetic fields, a likely candidate to study for magnetoresistance effects. This is also groundwork for future substitution and doping studies. It has previously shown that the valence instability of Ce^{3+} is not dependent on the size of the transition metal in our substitution studies of Mn, Fe, and Ni in $CeCo_2Al_8$.[5] Together, with the changes in the magnetic properties observed in $LnCo_2Al_8$ (Ln = La–Nd, Sm, Yb) demonstrates the itinerant electron system in rare earth intermetallics.

Single crystals of $Pr_2Fe_{4-x}Co_xSb_5$ ($1 \leq x < 3$) were grown using an inert Bi flux. To avoid competing binary phases, $CoSb_2$ and $CoSb_3$, the reactions were removed at 875 °C. From the magnetization and electrical resistivity measurements, complex magnetic ordering and large positive magnetoresistance of up to 150% and 60% at 200 K at relatively low magnetic field (H = 1 T) was discovered in the successfully doped $Pr_2Fe_{4-x}Co_xSb_5$ (x ~ 2 and 2.5) compounds, respectively. It is suggested that the unusual magnetic effects have emerged from geometrical frustration of the transition metal sublattice composed of a triangular lattice of nearest neighboring distances of ~ 2.6 Å, when Co is substituted for Fe. Thus, it is proposed that geometrically frustrated materials with three-dimensional magnetic subunits with close nearest neighbor interactions and potential site disorder could exhibit several magnetic phenomena, including multiple magnetic transitions, and in highly field dependent systems, large positive

magnetoresistance effects for the design of spintronic devices, such as read heads and magnetic sensors. This has been shown in several oxide materials, but would be the first discovery in an intermetallic system.[6] Yet, the mechanism of the origin of magnetoresistance in these materials is still an ongoing investigation.

The synthesis and characterization of several related ceramic materials (diopside, akermanite, monticellite, and merwinite) were also presented. The mechanical properties of the targeted calcium magnesium silicates were predicted based on the dimensionality of the structure and the arrangement of the structural subunits. Phase pure ceramic material was synthesized using the solid state reaction technique, which is useful for the preparation of equilibrated ceramics, such as diopside ($CaMgSi_2O_6$), akermanite ($Ca_2MgSi_2O_7$), monticellite ($CaMgSiO_4$), and merwinite ($Ca_3Mg(SiO_4)_2$). Our findings show that the most three-dimensional structure will lead to improved compressive strengths. For example, the diopside scaffolds, which is the most three-dimensional among the four silicates (Figure 4.1), exhibits the highest compressive strength of 0.28 MPa. Additionally, the ceramic:PCL (25:75) composite scaffolds made with diopside also obtain compressive strengths of 0.3 MPa. While the least dimensional among the four silicates, merwinite, obtains the lowest compressive strength of 0.15 MPa when prepared as ceramic:PCL composite scaffolds. This study illustrates the influence of the crystal structure in the fabrication of ceramic and ceramic:PCL composite scaffolds. It is also a design for predicting the mechanical properties of ceramics and their potential use as scaffolds for regeneration of bone tissue. Future work will be devoted to comparing the Ca-based silicates to the Sr-based silicates, also mentioned herein, and their viability as ceramic and ceramic/polymer composite scaffolds in stromal medium. So far, the biocompatibility and mechanical properties of these materials have shown promise.

5.2 Closing Remarks

According to a word cloud (Figure 5.1) created by *Nature Chemistry* of the common words from the title of published papers of 2014 is "*synthesis*".[1] In fact for the past 30 years, *synthesis* has been the number one most used word in chemistry publications. Therefore in my opinion, research in chemistry is still governed by the ability to create material in its purest form and evaluate their use for scientific advancements and technological developments. It was *synthesis* that sparked my first interest in scientific research, and I am confident that *synthesis* will continue to be a driving force toward my future scientific endeavors.

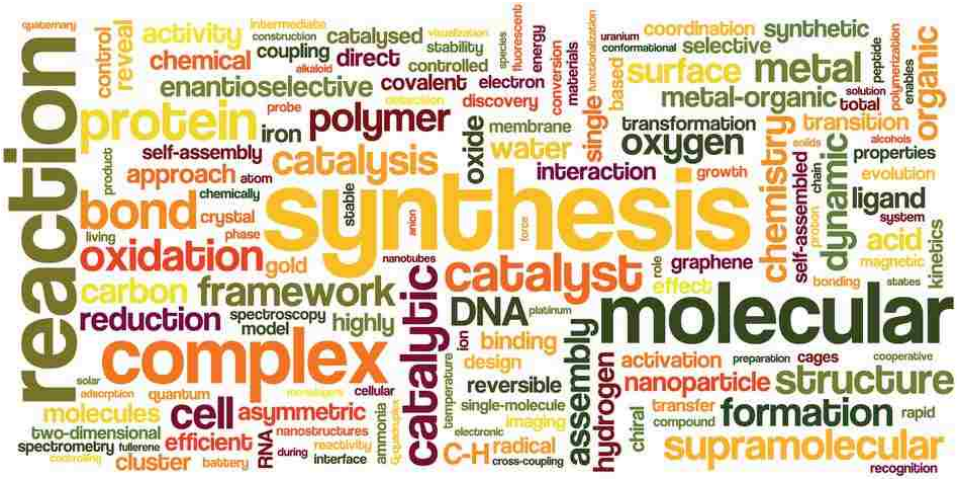

Figure 5.1 Common words from the titles of published papers in *Nature Chemistry*.[1]

5.3. References

(1) Anon, Take Five. *Nat. Chem.* **2014,** *6*, 255-257.

(2) Czech, E.; Cordier, G.; Schaefer, H., Study of Calcium-Cobalt-Aluminum ($CaCo_2Al_8$). *J. Less Common Met.* **1983,** *95*, 205-11.

(3) Bostroem, M.; Rosner, H.; Prots, Y.; Burkhardt, U.; Grin, Y., The Co_2Al_9 Structure Type Revisited. *Z. Anorg. Allg. Chem.* **2005,** *631*, 534-541.

(4) Ghosh, S.; Strydom, A. M., Strongly Correlated Electron Behaviour in CeT_2Al_8 (T = Fe, Co). *Acta Phys. Polym., A* **2012,** *121*, 1082-1084.

(5) Treadwell, L. J.; Watkins-Curry, P.; McAlpin, J. D.; Rebar, D. J.; Hebert, J. K.; Di Tusa, J. F.; Chan, J. Y., Investigation of Mn, Fe, and Ni Incorporation in $CeCo_2Al_8$. *Inorg. Chem.* **2015,** *54*, 963-968.

(6) Yamamoto, A.; Oda, K., The Relation of the Magnetoresistance and Magnetic Frustration Among Ferromagnetic Clusters in $La(Mn_{1-x}Ni_x)O_{3+\delta}$. *Rev. Adv. Mater. Sci.* **2003,** *5*, 343-347.

Appendix A1. Supporting Information for Chapter 1: Strategic Crystal Growth and Physical Properties of Single-Crystalline $LnCo_2Al_8$ (Ln = La–Nd, Sm, Yb) and $CeCo_{2-x}Mn_xAl_8$ (0 < x < 1)

Table A1. Atomic Positions for $LnCo_2Al_8$ (Ln = La–Nd, Sm, Yb)

site	point symmetry	x	y	z	Occ.	$^aU_{eq}$ (Å^2)
$LaCo_2Al_8$						
La	*m*	0.34040(2)	0.31815(2)	0	1	0.00717(6)
Co1	*m*	0.03474(2)	0.40574(2)	0	1	0.00599(7)
Co2	*m*	0.15151(2)	0.09650 (2)	0	1	0.00475(7)
Al1	*m*	0.02668(5)	0.13171(4)	½	1	0.00660(12)
Al2	*m*	0.15893(4)	0.38011(5)	½	1	0.00699(13)
Al3	*m*	0.23637(5)	0.17142(4)	½	1	0.00756(12)
Al4	*m*	0.33117(5)	0.49174(4)	½	1	0.00737(12)
Al5	*m*	0.45306(5)	0.17875(4)	½	1	0.00694(12)
Al6	*m*	0.09566(4)	0.25293(3)	0	1	0.00703(12)
Al7	*m*	0.34009(4)	0.04441(5)	0	1	0.00937(14)
Al8	2/*m*	0	½	½	1	0.00677(16)
Al9	2/*m*	0	0	0	1	0.00707(15)
$CeCo_2Al_8$						
Ce	*m*	0.34038(2)	0.31839(2)	0	1	0.00852(9)
Co1	*m*	0.03488(5)	0.40562(4)	0	1	0.00708(13)
Co2	*m*	0.15166(5)	0.09648(4)	0	1	0.00580(13)
Al1	*m*	0.02558(11)	0.13180(9)	½	1	0.0076(3)
Al2	*m*	0.15953(10)	0.37925(9)	½	1	0.0077(3)
Al3	*m*	0.23624(11)	0.17249(9)	½	1	0.0079(3)
Al4	*m*	0.33140(11)	0.49140(9)	½	1	0.0082(3)
Al5	*m*	0.45285(11)	0.17947(9)	½	1	0.0071(3)
Al6	*m*	0.09585(10)	0.25276(8)	0	1	0.0080(3)
Al7	*m*	0.33933(10)	0.04452(9)	0	1	0.0098(3)
Al8	2/*m*	0	½	½	1	0.0078(4)
Al9	2/*m*	0	0	0	1	0.0084(4)
$PrCo_2Al_8$						
Pr	*m*	0.34050(2)	0.31843(2)	0	1	0.00731(5)
Co1	*m*	0.03472(2)	0.40578(2)	0	1	0.00689(7)
Co2	*m*	0.15167(2)	0.09649(2)	0	1	0.00439(7)
Al1	*m*	0.02542(5)	0.13203(5)	½	1	0.00613(13)
Al2	*m*	0.15998(5)	0.37911(5)	½	1	0.00654(13)
Al3	*m*	0.23635(5)	0.17269(5)	½	1	0.00679(14)
Al4	*m*	0.33155(5)	0.49120(5)	½	1	0.00672(13)
Al5	*m*	0.45265(5)	0.17979(5)	½	1	0.00640(13)
Al6	*m*	0.09601(5)	0.25317(5)	0	1	0.00696(14)
Al7	*m*	0.33998(5)	0.04459(5)	0	1	0.00890(15)
Al8	2/*m*	0	½	½	1	0.00630(18)
Al9	2/*m*	0	0	0	1	0.00660(19)
$NdCo_2Al_8$						
Nd	*m*	0.34054(2)	0.31846(2)	0	1	0.00851(14)
Co1	*m*	0.03478(5)	0.40578(4)	0	1	0.00768(17)
Co2	*m*	0.15184(5)	0.09640(4)	0	1	0.00502(18)
Al1	*m*	0.02491(11)	0.13194(9)	½	1	0.0068(3)
Al2	*m*	0.16040(10)	0.37898(11)	½	1	0.0072(3)
Al3	*m*	0.23634(12)	0.17310(10)	½	1	0.0076(3)

Al4	*m*	0.33159(11)	0.49108(10)	½	1	0.0073(3)
Al5	*m*	0.45256(12)	0.18008(9)	½	1	0.0069(3)
Al6	*m*	0.09607(10)	0.25308(8)	0	1	0.0078(3)
Al7	*m*	0.34002(10)	0.04459(11)	0	1	0.0084(3)
Al8	2/*m*	0	½	½	1	0.0073(4)
Al9	2/*m*	0	0	0	1	0.0078(4)
$SmCo_2Al_8$						
Sm	*m*	0.34072(2)	0.31860(2)	0	1	0.00633(11)
Co1	*m*	0.03465(5)	0.40587(3)	0	1	0.00451(14)
Co2	*m*	0.15186(4)	0.09645(4)	0	1	0.00278(14)
Al1	*m*	0.02488(11)	0.13203(8)	½	1	0.0043(2)
Al2	*m*	0.16078(9)	0.37873(9)	½	1	0.0046(3)
Al3	*m*	0.23627(11)	0.17348(8)	½	1	0.0052(2)
Al4	*m*	0.33187(10)	0.49076(9)	½	1	0.0051(2)
Al5	*m*	0.45251(12)	0.18034(7)	½	1	0.0049(2)
Al6	*m*	0.09658(9)	0.25308(7)	0	1	0.0049(2)
Al7	*m*	0.33983(9)	0.04444(10)	0	1	0.0075(3)
Al8	2/*m*	0	½	½	1	0.0056(3)
Al9	2/*m*	0	0	0	1	0.0044(2)
$YbCo_2Al_8$						
Yb	*m*	0.34148(2)	0.31888(2)	0	1	0.01108(11)
Co1	*m*	0.03450(7)	0.40728(6)	0	1	0.00910(19)
Co2	*m*	0.15000(6)	0.09813(6)	0	1	0.00662(18)
Al1	*m*	0.02413(16)	0.13297(12)	½	1	0.0085(4)
Al2	*m*	0.16199(15)	0.37962(13)	½	1	0.0095(4)
Al3	*m*	0.23628(15)	0.17463(12)	½	1	0.0091(4)
Al4	*m*	0.33205(16)	0.49160(13)	½	1	0.0095(4)
Al5	*m*	0.45164(15)	0.18063(12)	½	1	0.0088(4)
Al6	*m*	0.09630(15)	0.25460(12)	0	1	0.0102(4)
Al7	*m*	0.33806(15)	0.04514(14)	0	1	0.0112(4)
Al8	2/*m*	0	½	½	1	0.0082(5)
Al9	2/*m*	0	0	0	1	0.0099(5)

[a] U_{eq} is defined as one-third of the trace of the orthogonalized U_{ij} tensor.

Table A2. Selected Interatomic Distances for $LnCo_2Al_8$ (Ln= La-Nd, Sm, Yb) (Å)

	$LaCo_2Al_8$	$CeCo_2Al_8$	$PrCo_2Al_8$	$NdCo_2Al_8$	$SmCo_2Al_8$	$YbCo_2Al_8$
Ln						
Al1 x 2	3.1660(5)	3.1452(10)	3.1363(5)	3.1290(13)	3.1137(10)	3.0896(19)
Al2 x 2	3.1657(5)	3.1461(10)	3.1370(5)	3.1305(13)	3.1145(9)	3.1072(18)
Al3 x 2	3.1981(5)	3.1840(10)	3.1770(5)	3.1715(13)	3.1586(9)	3.1559(18)
Al4 x 2	3.2142(5)	3.2018(10)	3.1937(6)	3.1904(14)	3.1734(10)	3.1853(19)
Al5 x 2	3.1757(5)	3.1633(10)	3.1535(5)	3.1484(12)	3.1340(9)	3.1259(18)
Al6 x 2	3.2035(6)	3.1927(13)	3.1877(7)	3.1837(17)	3.1735(12)	3.1811(19)
Al9 x 1	3.29347(13)	3.2848(2)	3.28042(15)	3.2765(8)	3.2671(2)	3.2707(6)
Co1						
Al2 x 2	2.5728(4)	2.5700(9)	2.5696(4)	2.5713(11)	2.5633(8)	2.5665(19)
Al5 x 2	2.5677(4)	2.5669(9)	2.5649(5)	2.5665(11)	2.5562(8)	2.5672(19)
Al6 x 1	2.3228(6)	2.3537(13)	2.3228(7)	2.3219(15)	2.3481(11)	2.3322(19)
Al7 x 2	2.5380(7)	2.5350(14)	2.5336(8)	2.5262(16)	2.4500(14)	2.533(2)
Al8 x 2	2.46979(15)	2.4652(3)	2.45798(19)	2.4572(7)	2.4439(3)	2.4283(15)
Co1 x 1	2.8509(5)	2.8517(11)	2.8436(6)	2.8415(15)	2.8329(10)	2.8089(17)
Co2						
Al1 x 2	2.6011(4)	2.6029(9)	2.5992(5)	2.6029(12)	2.5907(9)	2.5725(19)
Al3 x 2	2.5219(4)	2.5205(9)	2.5166(5)	2.5177(11)	2.5069(8)	2.5077(19)
Al4 x 2	2.5280(4)	2.5248(9)	2.5209(5)	2.5198(12)	2.5106(8)	2.5171(19)
Al6 x 1	2.3586(6)	2.3537(13)	2.3565(7)	2.3548(16)	2.3481(11)	2.354(2)
Al7 x 1	2.4764(6)	2.4643(14)	2.4620(7)	2.4572(16)	2.4500(14)	2.456(2)
Al9 x 1	2.3508(3)	2.3461(5)	2.3442(3)	2.3424(8)	2.3382(5)	2.3388(8)

Table A3. Atomic Positions of $CeCo_{2-x}M_xAl_8$ (M = Mn, Fe, Ni; $0 \leq x < 1$)

	Site	Symmetry	x	y	z	Occupancy	$^aU_{eq}$ (Å^2)
$CeCo_2Al_8$							
	Ce1	*m*	0.34038(2)	0.31841(2)	0	1	0.00837(11)
	Co1	*m*	0.03488(6)	0.40566(5)	0	1	0.00693(16)
	Co2	*m*	0.15166(5)	0.09643(5)	0	1	0.00565(15)
	Al1	*m*	0.09584(12)	0.25276(10)	0	1	0.0078(3)
	Al2	*m*	0.33993(12)	0.04446(11)	0	1	0.0097(3)
	Al3	*m*	0.15953(12)	0.37939(11)	1/2	1	0.0075(3)
	Al4	*m*	0.45285(13)	0.17938(10)	1/2	1	0.0070(3)
	Al5	*m*	0.23625(13)	0.17238(10)	1/2	1	0.0077(3)
	Al6	*m*	0.33139(13)	0.49140(11)	1/2	1	0.0080(3)
	Al7	*m*	0.02559(13)	0.13168(11)	1/2	1	0.0075(3)
	Al8	2/*m*	0	1/2	1/2	1	0.0076(4)
	Al9	2/*m*	0	0	0	1	0.0082(4)
$CeCo_{1.78(5)}Mn_{0.22(5)}Al_8$							
	Ce1	*m*	0.34062(3)	0.31845(3)	0	1	0.01166(14)
	Co1	*m*	0.03471(8)	0.40582(6)	0	0.81(5)	0.0094(10)
	Mn1	*m*	0.03471(8)	0.40582(6)	0	0.19(5)	0.0094(10)
	Co2	*m*	0.34858(8)	0.59656(6)	0	0.97(5)	0.0091(10)
	Mn2	*m*	0.34858(8)	0.59556(6)	0	0.03(5)	0.0091(10)
	Al1	*m*	0.02529(19)	0.13175(15)	0	1	0.0108(4)
	Al2	*m*	0.15952(19)	0.37937(15)	0	1	0.0108(4)
	Al3	*m*	0.23608(19)	0.17253(15)	1/2	1	0.0113(4)
	Al4	*m*	0.3310(2)	0.49133(14)	1/2	1	0.0108(4)
	Al5	*m*	0.45225(18)	0.17956(14)	1/2	1	0.0101(4)
	Al6	*m*	0.09588(18)	0.25306(15)	1/2	1	0.0110(4)
	Al7	*m*	0.33939(19)	0.04448(15)	1/2	1	0.0118(4)
	Al8	2/*m*	0	1/2	1/2	1	0.0107(6)
	Al9	2/*m*	0	0	0	1	0.0125(6)
$CeCo_{1.55(3)}Mn_{0.45(3)}Al_8$							
	Ce1	*m*	0.34076(2)	0.318443(19)	0	1	0.01078(10)
	Co1	*m*	0.03436(5)	0.40638(5)	0	0.68(3)	0.0091(2)
	Mn1	*m*	0.03436(5)	0.40638(5)	0	0.32(3)	0.0091(2)
	Co2	*m*	0.15115(5)	0.09683(5)	0	0.87(3)	0.0078(2)
	Mn1	*m*	0.15115(5)	0.09683(5)	0	0.13(3)	0.0078(2)
	Al1	*m*	0.02560(12)	0.13195(11)	0	1	0.0098(3)
	Al2	*m*	0.15979(12)	0.37890(11)	0	1	0.0103(3)
	Al3	*m*	0.23578(12)	0.17277(11)	1/2	1	0.0106(3)
	Al4	*m*	0.33183(12)	0.49160(10)	1/2	1	0.0104(3)
	Al5	*m*	0.45268(12)	0.17976(11)	1/2	1	0.0100(3)
	Al6	*m*	0.09564(12)	0.25300(11)	1/2	1	0.0104(3)
	Al7	*m*	0.33903(11)	0.04467(11)	1/2	1	0.0116(3)
	Al8	2/*m*	0	1/2	1/2	1	0.0095(4)
	Al9	2/*m*	0	0	0	1	0.0098(5)
$CeCo_{1.30(4)}Mn_{0.70(4)}Al_8$							
	Ce1	*m*	0.34069(2)	0.318403(18)	0	1	0.01090(10)
	Co1	*m*	0.03426(5)	0.40701(4)	0	0.48(3)	0.0091(2)
	Mn1	*m*	0.03426(5)	0.40701(4)		0.52(3)	0.0091(2)
	Co2	*m*	0.15077(5)	0.09698(4)	0	0.83(3)	0.0079(2)
	Mn2	*m*	0.15077(5)	0.09698(4)		0.17(3)	0.0079(2)
	Al1	*m*	0.02544(12)	0.13168(10)	0	1	0.0102(3)
	Al2	*m*	0.15965(11)	0.37890(10)	0	1	0.0098(3)

Al3	*m*	0.23536(12)	0.17282(10)	1/2	1	0.0110(3)
Al4	*m*	0.33181(12)	0.49169(10)	1/2	1	0.0105(3)
Al5	*m*	0.45247(11)	0.18000(9)	1/2	1	0.0103(3)
Al6	*m*	0.09526(11)	0.25321(9)	1/2	1	0.0107(3)
Al7	*m*	0.33812(11)	0.04485(10)	1/2	1	0.0119(3)
Al8	2/*m*	0	1/2	1/2	1	0.0105(4)
Al9	2/*m*	0	0	0	1	0.0104(4)

[a] U_{eq} is defined as one-third of the trace of the orthogonalized U_{ij} tensor.

Table A5. Selected Interatomic Distances of $CeCo_{2-x}Fe_xAl_8$ ($0 \leq x < 1$)

	$CeCo_2Al_8$	$CeCo_{1.78(5)}Mn_{0.22(5)}Al_8$	$CeCo_{1.55(3)}Mn_{0.45(3)}Al_8$	$CeCo_{1.30(4)}Mn_{0.70(4)}Al_8$
Ce				
Al1 x 2	3.1457(16)	3.144(2)	3.1479(12)	3.1493(14)
Al2 x 2	3.1467(14)	3.152(2)	3.1521(12)	3.1541(14)
Al3 x 2	3.1851(15)	3.188(2)	3.1921(12)	3.1941(14)
Al4 x 2	3.2017(16)	3.203(2))	3.2094(12)	3.2118(14)
Al5 x 2	3.1643(15)	3.1609(19)	3.1641(12)	3.1620(14)
M1				
Al2 x 2	2.5698(14)	2.574(2)	2.5841(10)	2.5863(14)
Al5 x 2	2.5667(14)	2.5734(19)	2.5780(11)	2.5856(14)
Al6 x 1	2.3275(16)	2.327(2)	2.3386(16)	2.3437(15)
Al7 x 2	2.5349(17)	2.540(2)	2.5440(16)	2.5476(16)
Al8 x 2	2.4649(17)	2.4654(14)	2.4633(6)	2.4591(11)
M1 x 1	2.8505(13)	2.846(2)	2.8311(14)	2.8134(14)
M2				
Al1 x 2	2.6026(15)	2.606(2)	2.6041(11)	2.6024(14)
Al3 x 2	2.5201(14)	2.5230(19)	2.5258(11)	2.5259(14)
Al4 x 2	2.5243(14)	2.5288(19)	2.5313(11)	2.5334(14)
Al6 x 1	2.3543(16)	2.357(2)	2.3545(17)	2.3558(15)
Al7 x 1	2.4643(17)	2.463(3)	2.4649(16)	2.4592(16)
Al9 x 1	2.3457(7)	2.3462(12)	2.3480(6)	2.3462(7)

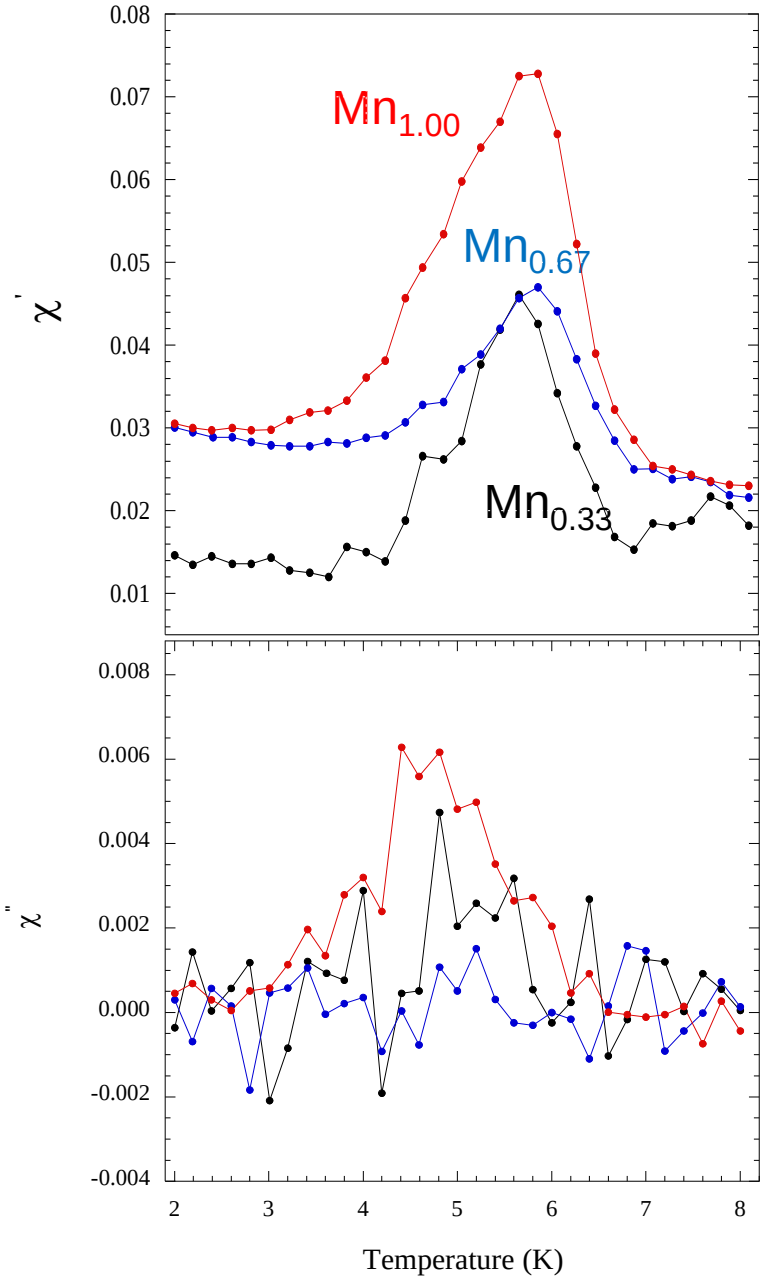

Figure A1.1 Temperature-dependent AC susceptibility of $CeCo_{2-x}Mn_xAl_8$ ($0 < x < 1$)

Appendix A2. Crystallographic Information Files (CIFs)

A2.1 $Pr_2Fe_{4-x}Co_xSb_5$ (x ~ 1)

data_shelx

_audit_update_record

;

2015-07-10 # Formatted by publCIF

_audit_creation_method 'SHELXL-2014/7'

_shelx_SHELXL_version_number '2014/7'

_chemical_name_systematic ?

_chemical_name_common ?

_chemical_melting_point ?

_chemical_formula_moiety 'Co Fe3 Pr2 Sb5'

_chemical_formula_sum

'Co Fe3 Pr2 Sb5'

_chemical_formula_weight 1117.05

loop_

_atom_type_symbol

_atom_type_description

_atom_type_scat_dispersion_real

_atom_type_scat_dispersion_imag

_atom_type_scat_source

'Fe' 'Fe' 0.3463 0.8444

'International Tables Vol C Tables 4.2.6.8 and 6.1.1.4'

'Co' 'Co' 0.3494 0.9721

'International Tables Vol C Tables 4.2.6.8 and 6.1.1.4'

'Sb' 'Sb' -0.5866 1.5461

'International Tables Vol C Tables 4.2.6.8 and 6.1.1.4'

'Pr' 'Pr' -0.2180 2.8214

'International Tables Vol C Tables 4.2.6.8 and 6.1.1.4'

_space_group_crystal_system tetragonal

_space_group_IT_number 139

_space_group_name_H-M_alt 'I 4/m m m'

_space_group_name_Hall '-I 4 2'

_shelx_space_group_comment

The symmetry employed for this shelxl refinement is uniquely defined

by the following loop, which should always be used as a source of

symmetry information in preference to the above space-group names.

They are only intended as comments.

loop_

_space_group_symop_operation_xyz

'x, y, z'

-x, -y, z'

'-y, x, z'

'y, -x, z'

'-x, y, -z'

'x, -y, -z'

'y, x, -z'

'-y, -x, -z'

'x+1/2, y+1/2, z+1/2'

'-x+1/2, -y+1/2, z+1/2'

'-y+1/2, x+1/2, z+1/2'

'y+1/2, -x+1/2, z+1/2'

'-x+1/2, y+1/2, -z+1/2'

'x+1/2, -y+1/2, -z+1/2'

'y+1/2, x+1/2, -z+1/2'

'-y+1/2, -x+1/2, -z+1/2'

'-x, -y, -z'

'x, y, -z'

'y, -x, -z'

'-y, x, -z'

'x, -y, z'

'-x, y, z'

'-y, -x, z'

'y, x, z'

'-x+1/2, -y+1/2, -z+1/2'

'x+1/2, y+1/2, -z+1/2'

'y+1/2, -x+1/2, -z+1/2'

'-y+1/2, x+1/2, -z+1/2'

'x+1/2, -y+1/2, z+1/2'

'-x+1/2, y+1/2, z+1/2'

'-y+1/2, -x+1/2, z+1/2'

'y+1/2, x+1/2, z+1/2'

_cell_length_a
4.30810(10)

_cell_length_b
4.30810(10)

_cell_length_c
25.7504(8)

_cell_angle_alpha
90

_cell_angle_beta
90

_cell_angle_gamma
90

_cell_volume
477.92(3)

_cell_formula_units_Z
2

_cell_measurement_tempe
rature 298(2)

_cell_measurement_reflns
_used ?

_cell_measurement_theta_
min ?

_cell_measurement_theta_
max ?

_exptl_crystal_description
plate

_exptl_crystal_colour
black

_exptl_crystal_density_me
as ?

_exptl_crystal_density_me
thod ?

_exptl_crystal_density_diff
rn 7.762

_exptl_crystal_F_000
956

_exptl_transmission_factor
_min ?

_exptl_transmission_factor
_max ?

_exptl_crystal_size_max
0.04

_exptl_crystal_size_mid
0.04

_exptl_crystal_size_min
0.03

_exptl_absorpt_coefficient
_mu 29.871

_shelx_estimated_absorpt_
T_min ?

_shelx_estimated_absorpt_
T_max ?

_exptl_absorpt_correction_
type multi-scan

_exptl_absorpt_correction_
T_min 0.240

_exptl_absorpt_correction_
T_max 0.403

_exptl_absorpt_process_de
tails SADABS(2014)

_exptl_absorpt_special_det
ails ?

_diffrn_ambient_temperatu
re 298(2)

_diffrn_radiation_wavelen
gth 0.71073

_diffrn_radiation_type
MoK\a

_diffrn_source
'I\mS microfocus tube'

_diffrn_measurement_devi
ce_type 'Bruker Kappa
D8 Quest CMOS'

_diffrn_measurement_method '\f and \w scans'

_diffrn_detector_area_resol_mean ?

_diffrn_reflns_number 20029

_diffrn_reflns_av_unetI/netI 0.0218

_diffrn_reflns_av_R_equivalents 0.0496

_diffrn_reflns_limit_h_min -9

_diffrn_reflns_limit_h_max 9

_diffrn_reflns_limit_k_min -9

_diffrn_reflns_limit_k_max 9

_diffrn_reflns_limit_l_min -50

_diffrn_reflns_limit_l_max 58

_diffrn_reflns_theta_min 3.164

_diffrn_reflns_theta_max 55.495

_diffrn_reflns_theta_full 25.242

_diffrn_measured_fraction_theta_max 0.979

_diffrn_measured_fraction_theta_full 0.977

_diffrn_reflns_Laue_measured_fraction_max 0.979

_diffrn_reflns_Laue_measured_fraction_full 0.977

_diffrn_reflns_point_group_measured_fraction_max 0.979

_diffrn_reflns_point_group_measured_fraction_full 0.977

_reflns_number_total 978

_reflns_number_gt 866

_reflns_threshold_expression 'I > 2\s(I)'

_reflns_Friedel_coverage 0.000

_reflns_Friedel_fraction_max .

_reflns_Friedel_fraction_full .

_reflns_special_details

;

Reflections were merged by SHELXL according to the crystal

class for the calculation of statistics and refinement.

_reflns_Friedel_fraction is defined as the number of unique

Friedel pairs measured divided by the number that would be

possible theoretically, ignoring centric projections and

systematic absences.

;

_computing_data_collection 'Bruker APEX2'

_computing_cell_refinement 'Bruker SAINT'

_computing_data_reduction 'Bruker SAINT'

_computing_structure_solution 'SHELXS Direct Methods (Sheldrick, 2013)'

_computing_structure_refinement 'SHELXL-2014/7 (Sheldrick, 2014)'

_computing_molecular_graphics CrystalMaker

_computing_publication_material 'publCIF (Westrip, 2014)'

_refine_special_details ?

_refine_ls_structure_factor_coef Fsqd

_refine_ls_matrix_type full

_refine_ls_weighting_scheme calc

_refine_ls_weighting_details

'w=1/[\s^2^(Fo^2^)+(0.0231P)^2^+12.2419P] where P=(Fo^2^+2Fc^2^)/3'

_atom_sites_solution_primary ?

_atom_sites_solution_secondary ?

_atom_sites_solution_hydrogens .

_refine_ls_hydrogen_treatment undef

_refine_ls_extinction_method 'SHELXL-2014/7 (Sheldrick 2014'

_refine_ls_extinction_coef 0.0060(3)

_refine_ls_extinction_expression

'Fc^*^=kFc[1+0.001xFc^2^\l^3^/sin(2\q)]^-1/4^'

_refine_ls_number_reflns 978

_refine_ls_number_parameters 25

_refine_ls_number_restraints 0

_refine_ls_R_factor_all 0.0425

_refine_ls_R_factor_gt 0.0345

_refine_ls_wR_factor_ref 0.0770

_refine_ls_wR_factor_gt 0.0747

_refine_ls_goodness_of_fit_ref 1.199

_refine_ls_restrained_S_all 1.199

_refine_ls_shift/su_max 0.000

_refine_ls_shift/su_mean 0.000

loop_

_atom_site_label

_atom_site_type_symbol

_atom_site_fract_x

_atom_site_fract_y

_atom_site_fract_z

_atom_site_U_iso_or_equiv

_atom_site_adp_type

_atom_site_occupancy

_atom_site_site_symmetry_order

_atom_site_calc_flag

_atom_site_refinement_flags_posn

_atom_site_refinement_flags_adp

_atom_site_refinement_flags_occupancy

_atom_site_disorder_assembly

_atom_site_disorder_group

Pr1 Pr 0.0000 0.0000 0.34795(2) 0.00768(7) Uani 1 8 d S T P . .

Fe1 Fe 0.0000 0.0000 0.0000 0.0102(2) Uani 1 16 d S T P . .

Fe2 Fe 0.0000 0.5000 0.44812(5) 0.0218(3) Uani 0.56 4 d S T P . .

Co1 Co 0.0000 0.5000 0.44812(5) 0.0218(3) Uani 0.224 4 d S T P . .

Sb1 Sb 0.0000 0.5000 0.2500 0.00661(7) Uani 1 8 d S T P . .

Sb2 Sb 0.0000 0.0000 0.11019(2) 0.00773(8) Uani 1 8 d S T P . .

Sb3 Sb 0.0000 0.067(2) 0.5000 0.015(3) Uani 0.118(18) 4 d S T P . .

Sb3' Sb 0.0000 0.0000 0.4863(7) 0.028(2) Uani 0.25(4) 8 d S T P . .

loop_

_atom_site_aniso_label

_atom_site_aniso_U_11

_atom_site_aniso_U_22

_atom_site_aniso_U_33

_atom_site_aniso_U_23

_atom_site_aniso_U_13

_atom_site_aniso_U_12

Pr1 0.00693(8) 0.00693(8) 0.00917(12) 0.000 0.000 0.000

Fe1 0.0112(3) 0.0112(3) 0.0081(4) 0.000 0.000 0.000

Fe2 0.0084(4) 0.0467(9) 0.0104(3) 0.000 0.0000.000

Co1 0.0084(4) 0.0467(9) 0.0104(3) 0.000 0.000 0.000

treatment of cell esds is used for estimating esds involving l.s. planes.

;

loop_

_geom_bond_atom_site_label_1

_geom_bond_atom_site_label_2

_geom_bond_distance

_geom_bond_site_symmetry_2

_geom_bond_publ_flag

Pr1 Sb2 3.2314(2) 25 ?

Pr1 Sb2 3.2314(2) 25_445 ?

Sb1 0.00641(9) 0.00641(9) 0.00701(12) 0.000 0.000 0.000

Sb2 0.00676(9) 0.00676(9) 0.00966(14) 0.000 0.000 0.000

Sb3 0.0109(15) 0.0176(19) 0.018(6) 0.000 0.000 0.000

Sb3' 0.034(3) 0.034(3) 0.016(3) 0.000 0.000 0.000

_geom_special_details

;

Pr1 Sb2 3.2314(2) 25_455 ?

Pr1 Sb2 3.2314(2) 25_545 ?

Pr1 Sb1 3.3169(3) 25_455 ?

Pr1 Sb1 3.3169(3) 1_545 ?

Pr1 Sb1 3.3169(3) . ?

Pr1 Sb1 3.3169(3) 25 ?

Pr1 Fe2 3.3606(10) . ?

Pr1 Fe2 3.3606(10) 3_655 ?

Pr1 Co1 3.3606(10) 3_655 ?

Fe1 Co1 2.5347(6) 27_455 ?

Fe1 Co1 2.5347(6) 11_544 ?

Fe1 Fe2 2.5347(6) 9_444 ?

All esds (except the esd in the dihedral angle between two l.s. planes)

are estimated using the full covariance matrix. The cell esds are taken

into account individually in the estimation of esds in distances, angles

and torsion angles; correlations between esds in cell parameters are only

used when they are defined by crystal symmetry. An approximate (isotropic

Fe1 Co1 2.5347(6) 25 ?

Fe1 Co1 2.5347(6) 9_444 ?

Fe1 Fe2 2.5347(6) 25 ?

Fe1 Fe2 2.5347(6) 11_544 ?

Fe1 Fe2 2.5347(6) 27_455 ?

Fe1 Co1 2.5347(6) 27_445 ?

Fe1 Fe2 2.5347(6) 27_445 ?

Fe1 Fe2 2.5347(6) 11_554 ?

Fe1 Co1 2.5347(6) 9_544 ?

Fe2 Sb3 2.296(8) 17_566 ?

Fe2 Sb3 2.296(8) . ?

Fe2 Sb3' 2.368(8) 1_565 ?

Fe2 Sb3' 2.368(8) . ?

Fe2 Fe1 2.5347(6) 9 ?

Fe2 Fe1 2.5347(6) 9_455 ?

Fe2 Sb3 2.5509(13) 19_566 ?

Fe2 Sb3 2.5509(13) 3_565 ?

Fe2 Sb3 2.5509(13) 3 ?

Fe2 Sb3 2.5509(13) 19_556 ?

Fe2 Sb2 2.6257(7) 25_455 ?

Fe2 Sb2 2.6257(7) 25 ?

Sb1 Sb1 3.04629(7) 25_565 ?

Sb1 Sb1 3.04629(7) 25_455 ?

Sb1 Sb1 3.04629(7) 25_465 ?

Sb1 Sb1 3.04629(7) 25 ?

Sb1 Pr1 3.3168(3) 25_455 ?

Sb1 Pr1 3.3168(3) 1_565 ?

Sb1 Pr1 3.3168(3) 25 ?

Sb2 Co1 2.6257(7) 27_445 ?

Sb2 Co1 2.6257(7) 25_455 ?

Sb2 Fe2 2.6257(7) 27_445 ?

Sb2 Fe2 2.6257(7) 25_455 ?

Sb2 Co1 2.6257(7) 27_455 ?

Sb2 Co1 2.6257(7) 25 ?

Sb2 Fe2 2.6257(7) 27_455 ?

Sb2 Fe2 2.6257(7) 25 ?

Sb2 Pr1 3.2314(2) 25 ?

Sb2 Pr1 3.2314(2) 25_445 ?

Sb2 Pr1 3.2314(2) 25_455 ?

Sb3 Sb3 0.406(13) 3 ?

Sb3 Sb3 0.406(13) 19_556 ?

Sb3 Sb3' 0.455(10) 17_556 ?

Sb3 Sb3 0.574(19) 17_556 ?

Sb3 Co1 2.296(8) 17_566 ?

Sb3 Fe2 2.296(8) 17_566 ?

Sb3 Fe2 2.5509(12) 3 ?

Sb3 Co1 2.5509(12) 3 ?

Sb3 Co1 2.5509(13) 19_556 ?

Sb3 Fe2 2.5509(13) 19_556 ?

Sb3' Sb3 0.455(10) 19_556 ?

Sb3' Sb3 0.455(10) 3 ?

Sb3' Sb3 0.455(10) 17_556 ?

Sb3' Sb3' 0.71(4) 17_556 ?

Sb3' Co1 2.368(8) 3 ?

Sb3' Co1 2.368(8) 1_545 ?

Sb3' Fe2 2.368(8) 3 ?

Sb3' Fe2 2.368(8) 1_545 ?

Sb3' Co1 2.368(8) 3_655 ?

Sb3' Fe2 2.368(8) 3_655 ?

loop_

_geom_angle_atom_site_label_1

_geom_angle_atom_site_label_2

_geom_angle_atom_site_label_3

_geom_angle

_geom_angle_site_symmetry_1

_geom_angle_site_symmetry_3

_geom_angle_publ_flag

Sb2 Pr1 Sb2 141.02(2) 25 25_445 ?

Sb2 Pr1 Sb2 83.609(7) 25 25_455 ?

Sb2 Pr1 Sb2 83.609(7) 25_445 25_455 ?

Sb2 Pr1 Sb2 83.609(7) 25 25_545 ?

Sb2 Pr1 Sb2 83.609(7) 25_445 25_545 ?

Sb2 Pr1 Sb2 141.02(2) 25_455 25_545 ?

Sb2 Pr1 Sb1 133.361(9) 25 25_455 ?

Sb2 Pr1 Sb1 79.676(8) 25_445 25_455 ?

Sb2 Pr1 Sb1 79.676(8) 25_455 25_455 ?

Sb2 Pr1 Sb1 133.361(9) 25_545 25_455 ?

Sb2 Pr1 Sb1 133.361(9) 25 1_545 ?

Sb2 Pr1 Sb1 79.676(8) 25_445 1_545 ?

Sb2 Pr1 Sb1 133.361(9) 25_455 1_545 ?

Sb2 Pr1 Sb1 79.676(8) 25_545 1_545 ?

Sb1 Pr1 Sb1 54.673(6) 25_455 1_545 ?

Sb2 Pr1 Sb1 79.676(8) 25 . ?

Sb2 Pr1 Sb1 133.361(9) 25_445 . ?

Sb2 Pr1 Sb1 79.676(8) 25_455 . ?

Sb2 Pr1 Sb1 133.361(9) 25_545 . ?

Sb1 Pr1 Sb1 54.673(6) 25_455 . ?

Sb1 Pr1 Sb1 80.997(9) 1_545 . ?

Sb2 Pr1 Sb1 79.676(8) 25 25 ?

Sb2 Pr1 Sb1 133.361(9) 25_445 25 ?

Sb2 Pr1 Sb1 133.361(9) 25_455 25 ?

Sb2 Pr1 Sb1 79.676(8) 25_545 25 ?

Sb1 Pr1 Sb1 80.997(9) 25_455 25 ?

Sb1 Pr1 Sb1 54.673(6) 1_545 25 ?

Sb1 Pr1 Sb1 54.673(6) . 25 ?

Sb2 Pr1 Fe2 46.894(9) 25 . ?

Sb2 Pr1 Fe2 99.857(15) 25_445 . ?

Sb2 Pr1 Fe2 46.894(9) 25_455 . ?

Sb2 Pr1 Fe2 99.857(15) 25_545 . ?

Sb1 Pr1 Fe2 125.709(8) 25_455 . ?

Sb1 Pr1 Fe2 179.366(16) 1_545 . ?

Sb1 Pr1 Fe2 99.637(13) . . ?

Sb1 Pr1 Fe2 125.709(8) 25 . ?

Sb2 Pr1 Fe2 46.894(9) 25 3_655 ?

Sb2 Pr1 Fe2 99.857(15) 25_445 3_655 ?

Sb2 Pr1 Fe2 99.857(15) 25_455 3_655 ?

Sb2 Pr1 Fe2 46.894(9) 25_545 3_655 ?

Sb1 Pr1 Fe2 179.366(16) 25_455 3_655 ?

Sb1 Pr1 Fe2 125.709(8) 1_545 3_655 ?

Sb1 Pr1 Fe2 125.709(8) . 3_655 ?

Sb1 Pr1 Fe2 99.637(13) 25 3_655 ?

Fe2 Pr1 Fe2 53.903(17) . 3_655 ?

Sb2 Pr1 Co1 46.894(9) 25 3_655 ?

Sb2 Pr1 Co1 99.857(15) 25_445 3_655 ?

Sb2 Pr1 Co1 99.857(15) 25_455 3_655 ?

Sb2 Pr1 Co1 46.894(9) 25_545 3_655 ?

Sb1 Pr1 Co1 179.366(16) 25_455 3_655 ?

Sb1 Pr1 Co1 125.709(8) 1_545 3_655 ?

Sb1 Pr1 Co1 125.709(8) . 3_655 ?

Sb1 Pr1 Co1 99.637(13) 25 3_655 ?

Fe2 Pr1 Co1 53.9 . 3_655 ?

Fe2 Pr1 Co1 0.00(3) 3_655 3_655 ?

Co1 Fe1 Co1 180.00(5) 27_455 11_544 ?

Co1 Fe1 Fe2 106.1 27_455 9_444 ?

Co1 Fe1 Fe2 73.9 11_544 9_444 ?

Co1 Fe1 Co1 73.87(2) 27_455 25 ?

Co1 Fe1 Co1 106.13(2) 11_544 25 ?

Fe2 Fe1 Co1 180.00(5) 9_444 25 ?

Co1 Fe1 Co1 106.13(2) 27_455 9_444 ?

Co1 Fe1 Co1 73.87(2) 11_544 9_444 ?

Fe2 Fe1 Co1 0.00(5) 9_444 9_444 ?

Co1 Fe1 Co1 180.00(5) 25 9_444 ?

Co1 Fe1 Fe2 73.9 27_455 25 ?

Co1 Fe1 Fe2 106.1 11_544 25 ?

Fe2 Fe1 Fe2 180.00(5) 9_444 25 ?

Co1 Fe1 Fe2 0.0 25 25 ?

Co1 Fe1 Fe2 180.0 9_444 25 ?

Co1 Fe1 Fe2 180.0 27_455 11_544 ?

Co1 Fe1 Fe2 0.0 11_544 11_544 ?

Fe2 Fe1 Fe2 73.87(2) 9_444 11_544 ?

Co1 Fe1 Fe2 106.1 25 11_544 ?

Co1 Fe1 Fe2 73.9 9_444 11_544 ?

Fe2 Fe1 Fe2 106.13(2) 25 11_544 ?

Co1 Fe1 Fe2 0.0 27_455 27_455 ?

Co1 Fe1 Fe2 180.0 11_544 27_455 ?

Fe2 Fe1 Fe2 106.13(2) 9_444 27_455 ?

Co1 Fe1 Fe2 73.9 25 27_455 ?

Co1 Fe1 Fe2 106.1 9_444 27_455 ?

Fe2 Fe1 Fe2 73.87(2) 25 27_455 ?

Fe2 Fe1 Fe2 180.00(5) 11_544 27_455 ?

Co1 Fe1 Co1 116.39(5) 27_455 27_445 ?

Co1 Fe1 Co1 63.61(5) 11_544 27_445 ?

Fe2 Fe1 Co1 106.13(2) 9_444 27_445 ?

Co1 Fe1 Co1 73.87(2) 25 27_445 ?

Co1 Fe1 Co1 106.13(2) 9_444 27_445 ?

Fe2 Fe1 Co1 73.87(2) 25 27_445 ?

Fe2 Fe1 Co1 63.61(5) 11_544 27_445 ?

Fe2 Fe1 Co1 116.39(5) 27_455 27_445 ?

Co1 Fe1 Fe2 116.4 27_455 27_445 ?

Co1 Fe1 Fe2 63.6 11_544 27_445 ?

Fe2 Fe1 Fe2 106.13(2) 9_444 27_445 ?

Co1 Fe1 Fe2 73.9 25 27_445 ?

Co1 Fe1 Fe2 106.1 9_444 27_445 ?

Fe2 Fe1 Fe2 73.87(2) 25 27_445 ?

Fe2 Fe1 Fe2 63.61(5) 11_544 27_445 ?

Fe2 Fe1 Fe2 116.39(5) 27_455 27_445 ?

Co1 Fe1 Fe2 0.0 27_445 27_445 ?

Co1 Fe1 Fe2 63.6 27_455 11_554 ?

Co1 Fe1 Fe2 116.4 11_544 11_554 ?

Fe2 Fe1 Fe2 73.87(2) 9_444 11_554 ?

Co1 Fe1 Fe2 106.1 25 11_554 ?

Co1 Fe1 Fe2 73.9 9_444 11_554 ?

Fe2 Fe1 Fe2 106.13(2) 25 11_554 ?

Fe2 Fe1 Fe2 116.39(5) 11_544 11_554 ?

Fe2 Fe1 Fe2 63.61(5) 27_455 11_554 ?

Co1 Fe1 Fe2 180.0 27_445 11_554 ?

Fe2 Fe1 Fe2 180.00(5) 27_445 11_554 ?

Co1 Fe1 Co1 106.13(2) 27_455 9_544 ?

Co1 Fe1 Co1 73.87(2) 11_544 9_544 ?

Fe2 Fe1 Co1 116.39(5) 9_444 9_544 ?

Co1 Fe1 Co1 63.61(5) 25 9_544 ?

Co1 Fe1 Co1 116.39(5) 9_444 9_544 ?

Fe2 Fe1 Co1 63.61(5) 25 9_544 ?

Fe2 Fe1 Co1 73.87(2) 11_544 9_544 ?

Fe2 Fe1 Co1 106.13(2) 27_455 9_544 ?

Co1 Fe1 Co1 106.13(2) 27_445 9_544 ?

Fe2 Fe1 Co1 106.13(2) 27_445 9_544 ?

Fe2 Fe1 Co1 73.87(2) 11_554 9_544 ?

Sb3 Fe2 Sb3 108.8(3) 17_566 . ?

Sb3 Fe2 Sb3' 11.1(3) 17_566 1_565 ?

Sb3 Fe2 Sb3' 119.9(6) . 1_565 ?

Sb3 Fe2 Sb3' 119.9(6) 17_566 . ?

Sb3 Fe2 Sb3' 11.1(3) . . ?

Sb3' Fe2 Sb3' 130.9(8) 1_565 . ?

Sb3 Fe2 Fe1 72.14(7) 17_566 9 ?

Sb3 Fe2 Fe1 72.14(7) . 9 ?

Sb3' Fe2 Fe1 77.4(2) 1_565 9 ?

Sb3' Fe2 Fe1 77.4(2) . 9 ?

Sb3 Fe2 Fe1 72.14(7) 17_566 9_455 ?

Sb3 Fe2 Fe1 72.14(7) . 9_455 ?

Sb3' Fe2 Fe1 77.4(2) 1_565 9_455 ?

Sb3' Fe2 Fe1 77.4(2) . 9_455 ?

Fe1 Fe2 Fe1 116.39(5) 9 9_455 ?

Sb3 Fe2 Sb3 7.5(3) 17_566 19_566 ?

Sb3 Fe2 Sb3 112.45(16) . 19_566 ?

Sb3' Fe2 Sb3 9.7(2) 1_565 19_566 ?

Sb3' Fe2 Sb3 123.4(4) . 19_566 ?

Fe1 Fe2 Sb3 68.18(19) 9 19_566 ?

Fe1 Fe2 Sb3 79.61(19) 9_455 19_566 ?

Sb3 Fe2 Sb3 7.5(3) 17_566 3_565 ?

Sb3 Fe2 Sb3 112.45(16) . 3_565 ?

Sb3' Fe2 Sb3 9.7(2) 1_565 3_565 ?

Sb3' Fe2 Sb3 123.4(4) . 3_565 ?

Fe1 Fe2 Sb3 79.61(19) 9 3_565 ?

Fe1 Fe2 Sb3 68.18(19) 9_455 3_565 ?

Sb3 Fe2 Sb3 12.9(4) 19_566 3_565 ?

Sb3 Fe2 Sb3 112.45(16) 17_566 3 ?

Sb3 Fe2 Sb3 7.5(3) . 3 ?

Sb3' Fe2 Sb3 123.4(4) 1_565 3 ?

Sb3' Fe2 Sb3 9.7(2) . 3 ?

Fe1 Fe2 Sb3 79.61(19) 9 3 ?

Fe1 Fe2 Sb3 68.18(19) 9_455 3 ?

Sb3 Fe2 Sb3 116.84(5) 19_566 3 ?

Sb3 Fe2 Sb3 115.22(9) 3_565 3 ?

Sb3 Fe2 Sb3 112.45(16) 17_566 19_556 ?

Sb3 Fe2 Sb3 7.5(3) . 19_556 ?

Sb3' Fe2 Sb3 123.4(4) 1_565 19_556 ?

Sb3' Fe2 Sb3 9.7(2) . 19_556 ?

Fe1 Fe2 Sb3 68.18(19) 9 19_556 ?

Fe1 Fe2 Sb3 79.61(19) 9_455 19_556 ?

Sb3 Fe2 Sb3 115.22(9) 19_566 19_556 ?

Sb3 Fe2 Sb3 116.84(5) 3_565 19_556 ?

Sb3 Fe2 Sb3 12.9(4) 3 19_556 ?

Sb3 Fe2 Sb2 109.44(7) 17_566 25_455 ?

Sb3 Fe2 Sb2 109.44(7) . 25_455 ?

Sb3' Fe2 Sb2 103.7(2) 1_565 25_455 ?

Sb3' Fe2 Sb2 103.7(2) . 25_455 ?

Fe1 Fe2 Sb2 176.93(5) 9 25_455 ?

Fe1 Fe2 Sb2 66.683(9) 9_455 25_455 ?

Sb3 Fe2 Sb2 113.07(18) 19_566 25_455 ?

Sb3 Fe2 Sb2 101.95(18) 3_565 25_455 ?

Sb3 Fe2 Sb2 101.95(18) 3 25_455 ?

Sb3 Fe2 Sb2 113.07(18) 19_556 25_455 ?

Sb3 Fe2 Sb2 109.44(7) 17_566 25 ?

Sb3 Fe2 Sb2 109.44(7) . 25 ?

Sb3' Fe2 Sb2 103.7(2) 1_565 25 ?

Sb3' Fe2 Sb2 103.7(2) . 25 ?

Fe1 Fe2 Sb2 66.683(9) 9 25 ?

Fe1 Fe2 Sb2 176.93(5) 9_455 25 ?

Sb3 Fe2 Sb2 101.95(18) 19_566 25 ?

Sb3 Fe2 Sb2 113.07(18) 3_565 25 ?

Sb3 Fe2 Sb2 113.07(18) 3 25 ?

Sb3 Fe2 Sb2 101.95(18) 19_556 25 ?

Sb2 Fe2 Sb2 110.25(5) 25_455 25 ?

Sb1 Sb1 Sb1 180.0 25_565 25_455 ?

Sb1 Sb1 Sb1 90.0 25_565 25_465 ?

Sb1 Sb1 Sb1 90.0 25_455 25_465 ?

Sb1 Sb1 Sb1 90.0 25_565 25 ?

Sb1 Sb1 Sb1 90.0 25_455 25 ?

Sb1 Sb1 Sb1 180.0 25_465 25 ?

Sb1 Sb1 Pr1 117.337(3) 25_565 25_455 ?

Sb1 Sb1 Pr1 62.663(3) 25_455 25_455 ?

Sb1 Sb1 Pr1 62.663(3) 25_465 25_455 ?

Sb1 Sb1 Pr1 117.337(3) 25 25_455 ?

Sb1 Sb1 Pr1 62.663(3) 25_565 1_565 ?

Sb1 Sb1 Pr1 117.337(3) 25_455 1_565 ?

Sb1 Sb1 Pr1 62.663(3) 25_465 1_565 ?

Sb1 Sb1 Pr1 117.337(3) 25 1_565 ?

Pr1 Sb1 Pr1 125.327(5) 25_455 1_565 ?

Sb1 Sb1 Pr1 62.663(3) 25_565 25 ?

Sb1 Sb1 Pr1 117.337(3) 25_455 25 ?

Sb1 Sb1 Pr1 117.337(3) 25_465 25 ?

Sb1 Sb1 Pr1 62.663(3) 25 25 ?

Pr1 Sb1 Pr1 80.998(9) 25_455 25 ?

Pr1 Sb1 Pr1 125.327(6) 1_565 25 ?

Sb1 Sb1 Pr1 117.336(3) 25_565 . ?

Sb1 Sb1 Pr1 62.664(3) 25_455 . ?

Sb1 Sb1 Pr1 117.336(3) 25_465 . ?

Sb1 Sb1 Pr1 62.664(3) 25 . ?

Pr1 Sb1 Pr1 125.327(6) 25_455 . ?

Pr1 Sb1 Pr1 80.997(9) 1_565 . ?

Pr1 Sb1 Pr1 125.327(6) 25 . ?

Co1 Sb2 Co1 70.91(2) 27_445 25_455 ?

Co1 Sb2 Fe2 0.0 27_445 27_445 ?

Co1 Sb2 Fe2 70.9 25_455 27_445 ?

Co1 Sb2 Fe2 70.9 27_445 25_455 ?

Co1 Sb2 Fe2 0.0 25_455 25_455 ?

Fe2 Sb2 Fe2 70.91(2) 27_445 25_455 ?

Co1 Sb2 Co1 110.24(5) 27_445 27_455 ?

Co1 Sb2 Co1 70.91(2) 25_455 27_455 ?

Fe2 Sb2 Co1 110.24(5) 27_445 27_455 ?

Fe2 Sb2 Co1 70.91(2) 25_455 27_455 ?

Co1 Sb2 Co1 70.91(2) 27_445 25 ?

Co1 Sb2 Co1 110.24(5) 25_455 25 ?

Fe2 Sb2 Co1 70.91(2) 27_445 25 ?

Fe2 Sb2 Co1 110.24(5) 25_455 25 ?

Co1 Sb2 Co1 70.91(2) 27_455 25 ?

Co1 Sb2 Fe2 110.2 27_445 27_455 ?

Co1 Sb2 Fe2 70.9 25_455 27_455 ?

Fe2 Sb2 Fe2 110.24(5) 27_445 27_455 ?

Fe2 Sb2 Fe2 70.91(2) 25_455 27_455 ?

Co1 Sb2 Fe2 0.0 27_455 27_455 ?

Co1 Sb2 Fe2 70.9 25 27_455 ?

Co1 Sb2 Fe2 70.9 27_445 25 ?

Co1 Sb2 Fe2 110.2 25_455 25 ?

Fe2 Sb2 Fe2 70.91(2) 27_445 25 ?

Fe2 Sb2 Fe2 110.24(5) 25_455 25 ?

Co1 Sb2 Fe2 70.9 27_455 25 ?

Co1 Sb2 Fe2 0.0 25 25 ?

Fe2 Sb2 Fe2 70.91(2) 27_455 25 ?

Co1 Sb2 Fe1 55.12(2) 27_445 . ?

Co1 Sb2 Fe1 55.12(2) 25_455 . ?

Fe2 Sb2 Fe1 55.12(2) 27_445 . ?

Fe2 Sb2 Fe1 55.12(2) 25_455 . ?

Co1 Sb2 Fe1 55.12(2) 27_455 . ?

Co1 Sb2 Fe1 55.12(2) 25 . ?

Fe2 Sb2 Fe1 55.12(2) 27_455 . ?

Fe2 Sb2 Fe1 55.12(2) 25 . ?

Co1 Sb2 Pr1 137.530(7) 27_445 25 ?

Co1 Sb2 Pr1 137.530(7) 25_455 25 ?

Fe2 Sb2 Pr1 137.530(7) 27_445 25 ?

Fe2 Sb2 Pr1 137.530(7) 25_455 25 ?

Co1 Sb2 Pr1 69.140(16) 27_455 25 ?

Co1 Sb2 Pr1 69.140(16) 25 25 ?

Fe2 Sb2 Pr1 69.140(16) 27_455 25 ?

Fe2 Sb2 Pr1 69.140(16) 25 25 ?

Fe1 Sb2 Pr1 109.488(11) . 25 ?

Co1 Sb2 Pr1 69.140(16) 27_445 25_445 ?

Co1 Sb2 Pr1 69.140(16) 25_455 25_445 ?

Fe2 Sb2 Pr1 69.140(16) 27_445 25_445 ?

Fe2 Sb2 Pr1 69.140(16) 25_455 25_445 ?

Co1 Sb2 Pr1 137.530(7) 27_455 25_445 ?

Co1 Sb2 Pr1 137.530(7) 25 25_445 ?

Fe2 Sb2 Pr1 137.530(7) 27_455 25_445 ?

Fe2 Sb2 Pr1 137.530(7) 25 25_445 ?

Fe1 Sb2 Pr1 109.488(11) . 25_445 ?

Pr1 Sb2 Pr1 141.02(2) 25 25_445 ?

Co1 Sb2 Pr1 137.530(7) 27_445 25_455 ?

Co1 Sb2 Pr1 69.140(16) 25_455 25_455 ?

Fe2 Sb2 Pr1 137.530(7) 27_445 25_455 ?

Fe2 Sb2 Pr1 69.140(16) 25_455 25_455 ?

Co1 Sb2 Pr1 69.140(16) 27_455 25_455 ?

Co1 Sb2 Pr1 137.530(7) 25 25_455 ?

Fe2 Sb2 Pr1 69.140(16) 27_455 25_455 ?

Fe2 Sb2 Pr1 137.530(7) 25 25_455 ?

Fe1 Sb2 Pr1 109.488(11) . 25_455 ?

Pr1 Sb2 Pr1 83.610(7) 25 25_455 ?

Pr1 Sb2 Pr1 83.610(7) 25_445 25_455 ?

Sb3 Sb3 Sb3 90.000(16) 3 19_556 ?

Sb3 Sb3 Sb3' 63.5(15) 3 17_556 ?

Sb3 Sb3 Sb3' 63.5(15) 19_556 17_556 ?

Sb3 Sb3 Sb3 45.000(10) 3 17_556 ?

Sb3 Sb3 Sb3 45.000(6) 19_556 17_556 ?

Sb3' Sb3 Sb3 51(2) 17_556 17_556 ?

Sb3 Sb3 Co1 125.10(7) 3 17_566 ?

Sb3 Sb3 Co1 125.10(8) 19_556 17_566 ?

Sb3' Sb3 Co1 94(2) 17_556 17_566 ?

Sb3 Sb3 Co1 144.41(14) 17_556 17_566 ?

Sb3 Sb3 Fe2 125.10(7) 3 17_566 ?

Sb3 Sb3 Fe2 125.10(8) 19_556 17_566 ?

Sb3' Sb3 Fe2 94(2) 17_556 17_566 ?

Sb3 Sb3 Fe2 144.41(14) 17_556 17_566 ?

Co1 Sb3 Fe2 0.0 17_566 17_566 ?

Sb3 Sb3 Fe2 125.10(7) 3 . ?

Sb3 Sb3 Fe2 125.10(8) 19_556 . ?

Sb3' Sb3 Fe2 165(3) 17_556 . ?

Sb3 Sb3 Fe2 144.41(14) 17_556 . ?

Co1 Sb3 Fe2 71.2 17_566 . ?

Fe2 Sb3 Fe2 71.2(3) 17_566 . ?

Sb3 Sb3 Fe2 47.41(18) 3 3 ?

Sb3 Sb3 Fe2 121.16(18) 19_556 3 ?

Sb3' Sb3 Fe2 109.6(12) 17_556 3 ?

Sb3 Sb3 Fe2 83.5(2) 17_556 3 ?

Co1 Sb3 Fe2 113.3 17_566 3 ?

Fe2 Sb3 Fe2 113.3(2) 17_566 3 ?

Fe2 Sb3 Fe2 77.69(11) . 3 ?

Sb3 Sb3 Co1 47.41(18) 3 3 ?

Sb3 Sb3 Co1 121.16(18) 19_556 3 ?

Sb3' Sb3 Co1 109.6(12) 17_556 3 ?

Sb3 Sb3 Co1 83.5(2) 17_556 3 ?

Co1 Sb3 Co1 113.3(2) 17_566 3 ?

Fe2 Sb3 Co1 113.3(2) 17_566 3 ?

Fe2 Sb3 Co1 77.7 . 3 ?

Fe2 Sb3 Co1 0.00(5) 3 3 ?

Sb3 Sb3 Co1 121.16(19) 3 19_556 ?

Sb3 Sb3 Co1 47.41(19) 19_556 19_556 ?

Sb3' Sb3 Co1 61.5(5) 17_556 19_556 ?

Sb3 Sb3 Co1 83.5(2) 17_556 19_556 ?

Co1 Sb3 Co1 77.69(11) 17_566 19_556 ?

Fe2 Sb3 Co1 77.69(11) 17_566 19_556 ?

Fe2 Sb3 Co1 113.3 . 19_556 ?

Fe2 Sb3 Co1 167.1(4) 3 19_556 ?

Co1 Sb3 Co1 167.1(4) 3 19_556 ?

Sb3 Sb3 Fe2 121.16(19) 3 19_556 ?

Sb3 Sb3 Fe2 47.41(19) 19_556 19_556 ?

Sb3' Sb3 Fe2 61.5(5) 17_556 19_556 ?

Sb3 Sb3 Fe2 83.5(2) 17_556 19_556 ?

Co1 Sb3 Fe2 77.7 17_566 19_556 ?

Fe2 Sb3 Fe2 77.69(11) 17_566 19_556 ?

Fe2 Sb3 Fe2 113.3(2) . 19_556 ?

Fe2 Sb3 Fe2 167.1(4) 3 19_556 ?

Co1 Sb3 Fe2 167.1 3 19_556 ?

Co1 Sb3 Fe2 0.0 19_556 19_556 ?

Sb3 Sb3' Sb3 78(5) 19_556 3 ?

Sb3 Sb3' Sb3 53(3) 19_556 17_556 ?

Sb3 Sb3' Sb3 53(3) 3 17_556 ?

Sb3 Sb3' Sb3' 39(2) 19_556 17_556 ?

Sb3 Sb3' Sb3' 39(2) 3 17_556 ?

Sb3 Sb3' Sb3' 39(2) 17_556 17_556 ?

Sb3 Sb3' Co1 154(3) 19_556 3 ?

Sb3 Sb3' Co1 75(2) 3 3 ?

Sb3 Sb3' Co1 108.8(4) 17_556 3 ?

Sb3' Sb3' Co1 114.5(4) 17_556 3 ?

Sb3 Sb3' Co1 108.8(4) 19_556 1_545 ?

Sb3 Sb3' Co1 108.8(4) 3 1_545 ?

Sb3 Sb3' Co1 75(2) 17_556 1_545 ?

Sb3' Sb3' Co1 114.5(4) 17_556 1_545 ?

Co1 Sb3' Co1 80.1(3) 3 1_545 ?

Sb3 Sb3' Fe2 154(3) 19_556 3 ?

Sb3 Sb3' Fe2 75(2) 3 3 ?

Sb3 Sb3' Fe2 108.8(4) 17_556 3 ?

Sb3' Sb3' Fe2 114.5(4) 17_556 3 ?

Co1 Sb3' Fe2 0.0 3 3 ?

Co1 Sb3' Fe2 80.1 1_545 3 ?

Sb3 Sb3' Fe2 108.8(4) 19_556 1_545 ?

Sb3 Sb3' Fe2 108.8(4) 3 1_545 ?

Sb3 Sb3' Fe2 75(2) 17_556 1_545 ?

Sb3' Sb3' Fe2 114.5(4) 17_556 1_545 ?

Co1 Sb3' Fe2 80.1 3 1_545 ?

Co1 Sb3' Fe2 0.0 1_545 1_545 ?

Fe2 Sb3' Fe2 80.1(3) 3 1_545 ?

Sb3 Sb3' Fe2 108.8(4) 19_556 . ?

Sb3 Sb3' Fe2 108.8(4) 3 . ?

Sb3 Sb3' Fe2 154(3) 17_556 . ?

Sb3' Sb3' Fe2 114.5(4) 17_556 . ?

Co1 Sb3' Fe2 80.1 3 . ?

Co1 Sb3' Fe2 130.9 1_545 . ?

Fe2 Sb3' Fe2 80.1(3) 3 . ?

Fe2 Sb3' Fe2 130.9(8) 1_545 . ?

Sb3 Sb3' Co1 75(2) 19_556 3_655 ?

Sb3 Sb3' Co1 154(3) 3 3_655 ?

Sb3 Sb3' Co1 108.8(4) 17_556 3_655 ?

Sb3' Sb3' Co1 114.5(4) 17_556 3_655 ?

Co1 Sb3' Co1 130.9(8) 3 3_655 ?

data_shelx

_audit_update_record

;

2015-07-10 # Formatted by publCIF

;

Co1 Sb3' Co1 80.1(3) 1_545 3_655 ?

Fe2 Sb3' Co1 130.9(8) 3 3_655 ?

Fe2 Sb3' Co1 80.1(3) 1_545 3_655 ?

Fe2 Sb3' Co1 80.1 . 3_655 ?

Sb3 Sb3' Fe2 75(2) 19_556 3_655 ?

Sb3 Sb3' Fe2 154(3) 3 3_655 ?

Sb3 Sb3' Fe2 108.8(4) 17_556 3_655 ?

Sb3' Sb3' Fe2 114.5(4) 17_556 3_655 ?

Co1 Sb3' Fe2 130.9 3 3_655 ?

Co1 Sb3' Fe2 80.1 1_545 3_655 ?

Fe2 Sb3' Fe2 130.9(8) 3 3_655 ?

Fe2 Sb3' Fe2 80.1(3) 1_545 3_655 ?

_audit_creation_method 'SHELXL-2014/7'

_shelx_SHELXL_version_number '2014/7'

_chemical_name_systematic ?

_chemical_name_common ?

_chemical_melting_point ?

Fe2 Sb3' Fe2 80.1(3) . 3_655 ?

Co1 Sb3' Fe2 0.0 3_655 3_655 ?

_refine_diff_density_max 7.040

_refine_diff_density_min -3.482

_refine_diff_density_rms 0.549

–

A2.2 $Pr_2Fe_{4-x}Co_xSb_5$ (x ~ 2)

_shelx_hkl_checksum 29949

#===END

_chemical_formula_moiety 'Co2 Fe2 Pr2 Sb5'

_chemical_formula_sum

'Co2 Fe2 Pr2 Sb5'

_chemical_formula_weight 1120.13

loop_

_atom_type_symbol

_atom_type_description

_atom_type_scat_dispersion_real

_atom_type_scat_dispersion_imag

_atom_type_scat_source

'Fe' 'Fe' 0.3463 0.8444

'International Tables Vol C Tables 4.2.6.8 and 6.1.1.4'

'Co' 'Co' 0.3494 0.9721

'International Tables Vol C Tables 4.2.6.8 and 6.1.1.4'

'Sb' 'Sb' -0.5866 1.5461

'International Tables Vol C Tables 4.2.6.8 and 6.1.1.4'

'Pr' 'Pr' -0.2180 2.8214

'International Tables Vol C Tables 4.2.6.8 and 6.1.1.4'

_space_group_crystal_system tetragonal

_space_group_IT_number 139

_space_group_name_H-M_alt 'I 4/m m m'

_space_group_name_Hall '-I 4 2'

_shelx_space_group_comment

;

The symmetry employed for this shelxl refinement is uniquely defined

by the following loop, which should always be used as a source of

symmetry information in preference to the above space-group names.

They are only intended as comments.

;

loop_

_space_group_symop_operation_xyz

'x, y, z'

'-x, -y, z'

'x, -y, -z'

'-x, y, -z'

'-y, -x, -z'

'y, x, -z'

'y, -x, z'

'-y, x, z'

'x+1/2, y+1/2, z+1/2'

'-x+1/2, -y+1/2, z+1/2'

'x+1/2, -y+1/2, -z+1/2'

'-x+1/2, y+1/2, -z+1/2'

'-y+1/2, -x+1/2, -z+1/2'

'y+1/2, x+1/2, -z+1/2'

'y+1/2, -x+1/2, z+1/2'

'-y+1/2, x+1/2, z+1/2'

'-x, -y, -z'

'x, y, -z'

'-x, y, z'

'x, -y, z'

'y, x, z'

'-y, -x, z'

'-y, x, -z'

'y, -x, -z'

'-x+1/2, -y+1/2, -z+1/2'

'x+1/2, y+1/2, -z+1/2'

'-x+1/2, y+1/2, z+1/2'

'x+1/2, -y+1/2, z+1/2'

'y+1/2, x+1/2, z+1/2'

'-y+1/2, -x+1/2, z+1/2'

'-y+1/2, x+1/2, -z+1/2'

'y+1/2, -x+1/2, -z+1/2'

_cell_length_a 4.299(5)

_cell_length_b 4.299(5)

_cell_length_c 25.711(5)

_cell_angle_alpha 90.000(5)

_cell_angle_beta 90.000(5)

_cell_angle_gamma 90.000(5)

_cell_volume 475.2(11)

_cell_formula_units_Z 2

_cell_measurement_temperature 293(2)

_cell_measurement_reflns_used ?

_cell_measurement_theta_min ?

_cell_measurement_theta_max ?

_exptl_crystal_description plate

_exptl_crystal_colour black

_exptl_crystal_density_meas ?

_exptl_crystal_density_method ?

_exptl_crystal_density_diffrn 7.829

_exptl_crystal_F_000 962.3

_exptl_transmission_factor_min ?

_exptl_transmission_factor_max ?

_exptl_crystal_size_max 0.05

_exptl_crystal_size_mid 0.05

_exptl_crystal_size_min 0.03

_exptl_absorpt_coefficient_mu 30.263

_shelx_estimated_absorpt_T_min ?

_shelx_estimated_absorpt_T_max ?

_exptl_absorpt_correction_type multi-scan

_exptl_absorpt_correction_T_min 0.240

_exptl_absorpt_correction_T_max 0.403

_exptl_absorpt_process_details SADABS(2014)

_exptl_absorpt_special_details ?

_diffrn_ambient_temperature 293(2)

_diffrn_radiation_wavelength 0.71073

_diffrn_radiation_type MoK\a

_diffrn_source 'I\mS microfocus tube'

_diffrn_measurement_device_type 'Bruker Kappa D8 Quest CMOS'

_diffrn_measurement_method '\f and \w scans'

_diffrn_detector_area_resol_mean ?

_diffrn_reflns_number 1867

_diffrn_reflns_av_unetI/netI 0.0334

_diffrn_reflns_av_R_equivalents 0.0470

_diffrn_reflns_limit_h_min -4

_diffrn_reflns_limit_h_max 6

_diffrn_reflns_limit_k_min -4

_diffrn_reflns_limit_k_max 6

_diffrn_reflns_limit_l_min -33

_diffrn_reflns_limit_l_max 36

_diffrn_reflns_theta_min 3.169

_diffrn_reflns_theta_max 30.541

_diffrn_reflns_theta_full 25.242

_diffrn_measured_fraction_theta_max 0.993

_diffrn_measured_fraction_theta_full 0.994

_diffrn_reflns_Laue_measured_fraction_max 0.993

_diffrn_reflns_Laue_measured_fraction_full 0.994

_diffrn_reflns_point_group_measured_fraction_max 0.993

_diffrn_reflns_point_group_measured_fraction_full 0.994

_reflns_number_total 270

_reflns_number_gt 265

_reflns_threshold_expression 'I > 2\s(I)'

_reflns_Friedel_coverage 0.000

_reflns_Friedel_fraction_max .

_reflns_Friedel_fraction_full .

_reflns_special_details

;

Reflections were merged by SHELXL according to the crystal

class for the calculation of statistics and refinement.

_reflns_Friedel_fraction is defined as the number of unique

Friedel pairs measured divided by the number that would be

possible theoretically, ignoring centric projections and

systematic absences.

;

_computing_data_collection 'Bruker APEX2'

_computing_cell_refinement 'Bruker SAINT'

_computing_data_reduction 'Bruker SAINT'

_computing_structure_solution 'SHELXS Direct Methods (Sheldrick, 2013)'

_computing_structure_refinement 'SHELXL-2014/7 (Sheldrick, 2014)'

_computing_molecular_graphics CrystalMaker

_computing_publication_material 'publCIF (Westrip, 2014)'

_refine_special_details ?

_refine_ls_structure_factor_coef Fsqd

_refine_ls_matrix_type full

_refine_ls_weighting_scheme calc

_refine_ls_weighting_details 'w=1/[\s^2^(Fo^2^)+(0.0392P)^2^+30.5086P] where P=(Fo^2^+2Fc^2^)/3'

_atom_sites_solution_primary ?

_atom_sites_solution_secondary ?

_atom_sites_solution_hydrogens .

_refine_ls_hydrogen_treatment undef

_refine_ls_extinction_method 'SHELXL-2014/7 (Sheldrick 2014'

_refine_ls_extinction_coef 0.0011(3)

_refine_ls_extinction_expression

'Fc^*^=kFc[1+0.001xFc^2^\l^3^/sin(2\q)]^-1/4^'

_refine_ls_number_reflns 270

_refine_ls_number_parameters 20

_refine_ls_number_restraints 0

_refine_ls_R_factor_all 0.0340

_refine_ls_R_factor_gt 0.0335

_refine_ls_wR_factor_ref 0.0913

_refine_ls_wR_factor_gt 0.0909

_refine_ls_goodness_of_fit_ref 1.214

_refine_ls_restrained_S_all 1.214

_refine_ls_shift/su_max 0.001

_refine_ls_shift/su_mean 0.000

loop_

_atom_site_label

_atom_site_type_symbol

_atom_site_fract_x

_atom_site_fract_y

_atom_site_fract_z

_atom_site_U_iso_or_equiv

_atom_site_adp_type

_atom_site_occupancy

_atom_site_site_symmetry_order

_atom_site_calc_flag

_atom_site_refinement_flags_posn

_atom_site_refinement_flags_adp

_atom_site_refinement_flags_occupancy

_atom_site_disorder_assembly

_atom_site_disorder_group

Pr1 Pr 0.0000 0.0000 0.34843(4) 0.0062(3) Uani 1 8 d S T P . .

Fe1 Fe 0.0000 0.0000 0.0000 0.0080(7) Uani 1 16 d S T P . .

Fe2 Fe 0.0000 0.5000 0.44736(9) 0.0122(6) Uani 0.3075 4 d S T P . .

Co2 Co 0.0000 0.5000 0.44736(9) 0.0122(6) Uani 0.48 4 d S T P . .

Sb1 Sb 0.0000 0.5000 0.2500 0.0036(3) Uani 1 8 d S T P . .

Sb2 Sb 0.0000 0.0000 0.11018(5) 0.0064(4) Uani 1 8 d S T P . .

Sb3 Sb 0.0000 0.0000 0.4934(4) 0.024(2) Uani 0.483(7) 8 d S T P . .

loop_

_atom_site_aniso_label

_atom_site_aniso_U_11

_atom_site_aniso_U_22

_atom_site_aniso_U_33

_atom_site_aniso_U_23

_atom_site_aniso_U_13

_atom_site_aniso_U_12

Pr1 0.0047(4) 0.0047(4) 0.0092(5) 0.000 0.000 0.000

Fe1 0.0077(11) 0.0077(11) 0.0086(16) 0.000 0.000 0.000

Fe2 0.0040(10) 0.0240(14) 0.0085(10) 0.000 0.000 0.000

Co2 0.0040(10) 0.0240(14) 0.0085(10) 0.000 0.000 0.000

Sb1 0.0029(4) 0.0029(4) 0.0050(5) 0.000 0.000 0.000

Sb2 0.0048(4) 0.0048(4) 0.0095(6) 0.000 0.000 0.000

Sb3 0.0267(11) 0.0267(11) 0.018(6) 0.000 0.000 0.000

_geom_special_details

;

All esds (except the esd in the dihedral angle between two l.s. planes)

are estimated using the full covariance matrix. The cell esds are taken

into account individually in the estimation of esds in distances, angles

and torsion angles; correlations between esds in cell parameters are only

used when they are defined by crystal symmetry. An approximate (isotropic)

treatment of cell esds is used for estimating esds involving l.s. planes.

;

loop_

_geom_bond_atom_site_label_1

_geom_bond_atom_site_label_2

_geom_bond_distance

_geom_bond_site_symmetry_2

_geom_bond_publ_flag

Pr1 Sb2 3.221(3) 25 ?

Pr1 Sb2 3.221(3) 25_445 ?

Pr1 Sb2 3.221(3) 25_455 ?

Pr1 Sb2 3.221(3) 25_545 ?

Pr1 Sb1 3.3204(18) 25_455 ?

Pr1 Sb1 3.3204(18) 1_545 ?

Pr1 Sb1 3.3204(18) . ?

Pr1 Sb1 3.3204(18) 25 ?

Pr1 Fe2 3.330(3) 21 ?

Pr1 Co2 3.330(3) 21 ?

Pr1 Co2 3.330(3) 21_455 ?

Pr1 Fe2 3.330(3) 21_455 ?

Fe1 Co2 2.540(2) 29_444 ?

Fe1 Co2 2.540(2) 13 ?

Fe1 Fe2 2.540(2) 9_444 ?

Fe1 Co2 2.540(2) 25 ?

Fe1 Co2 2.540(2) 9_444 ?

Fe1 Fe2 2.540(2) 25 ?

Fe1 Fe2 2.540(2) 29_444 ?

Fe1 Fe2 2.540(2) 13 ?

Fe1 Co2 2.540(2) 29_454 ?

Fe1 Fe2 2.540(2) 29_454 ?

Fe1 Fe2 2.540(2) 13_545 ?

Fe1 Co2 2.540(2) 9_544 ?

Fe2 Sb3 2.453(6) 1_565 ?

Fe2 Sb3 2.453(6) . ?

Fe2 Fe1 2.540(2) 9 ?

Fe2 Fe1 2.540(2) 9_455 ?

Fe2 Sb2 2.609(3) 25_455 ?

Fe2 Sb2 2.609(3) 25 ?

Fe2 Sb3 2.635(7) 17_566 ?

Fe2 Sb3 2.635(7) 17_556 ?

Fe2 Co2 2.707(5) 17_566 ?

Fe2 Fe2 2.707(5) 17_566 ?

Fe2 Pr1 3.330(3) 1_565 ?

Sb1 Sb1 3.040(4) 25_565 ?

Sb1 Sb1 3.040(4) 25_455 ?

Sb1 Sb1 3.040(4) 25_465 ?

Sb1 Sb1 3.040(4) 25 ?

Sb1 Pr1 3.3205(18) 1_565 ?

Sb1 Pr1 3.3205(18) 25_455 ?

Sb1 Pr1 3.3205(18) 25 ?

Sb2 Co2 2.609(3) 13_545 ?

Sb2 Co2 2.609(3) 25_455 ?

Sb2 Fe2 2.609(3) 13_545 ?

Sb2 Fe2 2.609(3) 25_455 ?

Sb2 Co2 2.609(3) 13 ?

Sb2 Co2 2.609(3) 25 ?

Sb2 Fe2 2.609(3) 13 ?

Sb2 Fe2 2.609(3) 25 ?

Sb2 Pr1 3.221(3) 25 ?

Sb2 Pr1 3.221(3) 25_445 ?

Sb2 Pr1 3.221(3) 25_455 ?

Sb3 Sb3 0.34(2) 17_556 ?

Sb3 Co2 2.453(6) 21_455 ?

Sb3 Co2 2.453(6) 1_545 ?

Sb3 Fe2 2.453(6) 21_455 ?

Sb3 Fe2 2.453(6) 1_545 ?

Sb3 Co2 2.453(6) 21 ?

Sb3 Fe2 2.453(6) 21 ?

Sb3 Co2 2.635(7) 5_656 ?

Sb3 Fe2 2.635(7) 17_566 ?

Sb3 Co2 2.635(7) 17_566 ?

loop_

_geom_angle_atom_site_label_1

_geom_angle_atom_site_label_2

_geom_angle_atom_site_label_3

_geom_angle

_geom_angle_site_symmetry_1

_geom_angle_site_symmetry_3

_geom_angle_publ_flag

Sb2 Pr1 Sb2 141.42(7) 25 25_445 ?

Sb2 Pr1 Sb2 83.73(2) 25 25_455 ?

Sb2 Pr1 Sb2 83.73(2) 25_445 25_455 ?

Sb2 Pr1 Sb2 83.73(2) 25 25_545 ?

Sb2 Pr1 Sb2 83.73(2) 25_445 25_545 ?

Sb2 Pr1 Sb2 141.42(7) 25_455 25_545 ?

Sb2 Pr1 Sb1 133.15(2) 25 25_455 ?

Sb2 Pr1 Sb1 79.62(5) 25_445 25_455 ?

Sb2 Pr1 Sb1 79.62(5) 25_455 25_455 ?

Sb2 Pr1 Sb1 133.15(2) 25_545 25_455 ?

Sb2 Pr1 Sb1 133.15(2) 25 1_545 ?

Sb2 Pr1 Sb1 79.62(5) 25_445 1_545 ?

Sb2 Pr1 Sb1 133.15(2) 25_455 1_545 ?

Sb2 Pr1 Sb1 79.62(5) 25_545 1_545 ?

Sb1 Pr1 Sb1 54.48(4) 25_455 1_545 ?

Sb2 Pr1 Sb1 79.62(5) 25 . ?

Sb2 Pr1 Sb1 133.15(2) 25_445 . ?

Sb2 Pr1 Sb1 79.62(5) 25_455 . ?

Sb2 Pr1 Sb1 133.15(2) 25_545 . ?

Sb1 Pr1 Sb1 54.48(4) 25_455 . ?

Sb1 Pr1 Sb1 80.69(7) 1_545 . ?

Sb2 Pr1 Sb1 79.62(5) 25 25 ?

Sb2 Pr1 Sb1 133.15(2) 25_445 25 ?

Sb2 Pr1 Sb1 133.15(2) 25_455 25 ?

Sb2 Pr1 Sb1 79.62(5) 25_545 25 ?

Sb1 Pr1 Sb1 80.69(7) 25_455 25 ?

Sb1 Pr1 Sb1 54.48(4) 1_545 25 ?

Sb1 Pr1 Sb1 54.48(4) . 25 ?

Sb2 Pr1 Fe2 46.91(2) 25 21 ?

Sb2 Pr1 Fe2 100.28(6) 25_445 21 ?

Sb2 Pr1 Fe2 100.28(5) 25_455 21 ?

Sb2 Pr1 Fe2 46.91(2) 25_545 21 ?

Sb1 Pr1 Fe2 179.86(3) 25_455 21 ?

Sb1 Pr1 Fe2 125.60(4) 1_545 21 ?

Sb1 Pr1 Fe2 125.60(4) . 21 ?

Sb1 Pr1 Fe2 99.46(7) 25 21 ?

Sb2 Pr1 Co2 46.91(2) 25 21 ?

Sb2 Pr1 Co2 100.28(6) 25_445 21 ?

Sb2 Pr1 Co2 100.28(5) 25_455 21 ?

Sb2 Pr1 Co2 46.91(2) 25_545 21 ?

Sb1 Pr1 Co2 179.86(3) 25_455 21 ?

Sb1 Pr1 Co2 125.60(4) 1_545 21 ?

Sb1 Pr1 Co2 125.60(4) . 21 ?

Sb1 Pr1 Co2 99.46(7) 25 21 ?

Fe2 Pr1 Co2 0.00(5) 21 21 ?

Sb2 Pr1 Co2 100.28(5) 25 21_455 ?

Sb2 Pr1 Co2 46.91(2) 25_445 21_455 ?

Sb2 Pr1 Co2 46.91(2) 25_455 21_455 ?

Sb2 Pr1 Co2 100.28(5) 25_545 21_455 ?

Sb1 Pr1 Co2 99.46(7) 25_455 21_455 ?

Sb1 Pr1 Co2 125.60(4) 1_545 21_455 ?

Sb1 Pr1 Co2 125.60(4) . 21_455 ?

Sb1 Pr1 Co2 179.86(3) 25 21_455 ?

Fe2 Pr1 Co2 80.40(9) 21 21_455 ?

Co2 Pr1 Co2 80.40(9) 21 21_455 ?

Sb2 Pr1 Fe2 100.28(5) 25 21_455 ?

Sb2 Pr1 Fe2 46.91(2) 25_445 21_455 ?

Sb2 Pr1 Fe2 46.91(2) 25_455 21_455 ?

Sb2 Pr1 Fe2 100.28(5) 25_545 21_455 ?

Sb1 Pr1 Fe2 99.46(7) 25_455 21_455 ?

Sb1 Pr1 Fe2 125.60(4) 1_545 21_455 ?

Sb1 Pr1 Fe2 125.60(4) . 21_455 ?

Sb1 Pr1 Fe2 179.86(3) 25 21_455 ?

Fe2 Pr1 Fe2 80.40(9) 21 21_455 ?

Co2 Pr1 Fe2 80.4 21 21_455 ?

Co2 Pr1 Fe2 0.0 21_455 21_455 ?

Co2 Fe1 Co2 180.00(9) 29_444 13 ?

Co2 Fe1 Fe2 73.5 29_444 9_444 ?

Co2 Fe1 Fe2 106.5 13 9_444 ?

Co2 Fe1 Co2 106.49(5) 29_444 25 ?

Co2 Fe1 Co2 73.51(5) 13 25 ?

Fe2 Fe1 Co2 180.00(9) 9_444 25 ?

Co2 Fe1 Co2 73.51(5) 29_444 9_444 ?

Co2 Fe1 Co2 106.49(5) 13 9_444 ?

Fe2 Fe1 Co2 0.00(9) 9_444 9_444 ?

Co2 Fe1 Co2 180.00(9) 25 9_444 ?

Co2 Fe1 Fe2 106.5 29_444 25 ?

Co2 Fe1 Fe2 73.5 13 25 ?

Fe2 Fe1 Fe2 180.00(9) 9_444 25 ?

Co2 Fe1 Fe2 0.0 25 25 ?

Co2 Fe1 Fe2 180.0 9_444 25 ?

Co2 Fe1 Fe2 0.0 29_444 29_444 ?

Co2 Fe1 Fe2 180.0 13 29_444 ?

Fe2 Fe1 Fe2 73.51(5) 9_444 29_444 ?

Co2 Fe1 Fe2 106.5 25 29_444 ?

Co2 Fe1 Fe2 73.5 9_444 29_444 ?

Fe2 Fe1 Fe2 106.49(5) 25 29_444 ?

Co2 Fe1 Fe2 180.0 29_444 13 ?

Co2 Fe1 Fe2 0.0 13 13 ?

Fe2 Fe1 Fe2 106.49(5) 9_444 13 ?

Co2 Fe1 Fe2 73.5 25 13 ?

Co2 Fe1 Fe2 106.5 9_444 13 ?

Fe2 Fe1 Fe2 73.51(5) 25 13 ?

Fe2 Fe1 Fe2 180.00(9) 29_444 13 ?

Co2 Fe1 Co2 115.61(11) 29_444 29_454 ?

Co2 Fe1 Co2 64.39(11) 13 29_454 ?

Fe2 Fe1 Co2 73.51(5) 9_444 29_454 ?

Co2 Fe1 Co2 106.49(5) 25 29_454 ?

Co2 Fe1 Co2 73.51(5) 9_444 29_454 ?

Fe2 Fe1 Co2 106.49(5) 25 29_454 ?

Fe2 Fe1 Co2 115.61(11) 29_444 29_454 ?

Fe2 Fe1 Co2 64.39(11) 13 29_454 ?

Co2 Fe1 Fe2 115.6 29_444 29_454 ?

Co2 Fe1 Fe2 64.4 13 29_454 ?

Fe2 Fe1 Fe2 73.51(5) 9_444 29_454 ?

Co2 Fe1 Fe2 106.5 25 29_454 ?

Co2 Fe1 Fe2 73.5 9_444 29_454 ?

Fe2 Fe1 Fe2 106.49(5) 25 29_454 ?

Fe2 Fe1 Fe2 115.61(11) 29_444 29_454 ?

Fe2 Fe1 Fe2 64.39(11) 13 29_454 ?

Co2 Fe1 Fe2 0.0 29_454 29_454 ?

Co2 Fe1 Fe2 64.4 29_444 13_545 ?

Co2 Fe1 Fe2 115.6 13 13_545 ?

Fe2 Fe1 Fe2 106.49(5) 9_444 13_545 ?

Co2 Fe1 Fe2 73.5 25 13_545 ?

Co2 Fe1 Fe2 106.5 9_444 13_545 ?

Fe2 Fe1 Fe2 73.51(5) 25 13_545 ?

Fe2 Fe1 Fe2 64.39(11) 29_444 13_545 ?

Fe2 Fe1 Fe2 115.61(11) 13 13_545 ?

Co2 Fe1 Fe2 180.0 29_454 13_545 ?

Fe2 Fe1 Fe2 180.00(9) 29_454 13_545 ?

Co2 Fe1 Co2 73.51(5) 29_444 9_544 ?

Co2 Fe1 Co2 106.49(5) 13 9_544 ?

Fe2 Fe1 Co2 115.61(11) 9_444 9_544 ?

Co2 Fe1 Co2 64.39(11) 25 9_544 ?

Co2 Fe1 Co2 115.61(11) 9_444 9_544 ?

Fe2 Fe1 Co2 64.39(11) 25 9_544 ?

Fe2 Fe1 Co2 73.51(5) 29_444 9_544 ?

Fe2 Fe1 Co2 106.49(5) 13 9_544 ?

Co2 Fe1 Co2 73.51(5) 29_454 9_544 ?

Fe2 Fe1 Co2 73.51(5) 29_454 9_544 ?

Fe2 Fe1 Co2 106.49(5) 13_545 9_544 ?

Sb3 Fe2 Sb3 122.4(5) 1_565 . ?

Sb3 Fe2 Fe1 75.12(12) 1_565 9 ?

Sb3 Fe2 Fe1 75.12(12) . 9 ?

Sb3 Fe2 Fe1 75.12(12) 1_565 9_455 ?

Sb3 Fe2 Fe1 75.12(12) . 9_455 ?

Fe1 Fe2 Fe1 115.61(11) 9 9_455 ?

Sb3 Fe2 Sb2 105.86(12) 1_565 25_455 ?

Sb3 Fe2 Sb2 105.86(12) . 25_455 ?

Fe1 Fe2 Sb2 177.66(9) 9 25_455 ?

Fe1 Fe2 Sb2 66.74(7) 9_455 25_455 ?

Sb3 Fe2 Sb2 105.86(12) 1_565 25 ?

Sb3 Fe2 Sb2 105.86(12) . 25 ?

Fe1 Fe2 Sb2 66.74(7) 9 25 ?

Fe1 Fe2 Sb2 177.66(9) 9_455 25 ?

Sb2 Fe2 Sb2 110.92(11) 25_455 25 ?

Sb3 Fe2 Sb3 6.5(4) 1_565 17_566 ?

Sb3 Fe2 Sb3 115.84(12) . 17_566 ?

Fe1 Fe2 Sb3 72.05(10) 9 17_566 ?

Fe1 Fe2 Sb3 72.05(10) 9_455 17_566 ?

Sb2 Fe2 Sb3 109.15(10) 25_455 17_566 ?

Sb2 Fe2 Sb3 109.15(10) 25 17_566 ?

Sb3 Fe2 Sb3 115.84(12) 1_565 17_556 ?

Sb3 Fe2 Sb3 6.5(4) . 17_556 ?

Fe1 Fe2 Sb3 72.05(10) 9 17_556 ?

Fe1 Fe2 Sb3 72.05(10) 9_455 17_556 ?

Sb2 Fe2 Sb3 109.15(10) 25_455 17_556 ?

Sb2 Fe2 Sb3 109.15(10) 25 17_556 ?

Sb3 Fe2 Sb3 109.3(4) 17_566 17_556 ?

Sb3 Fe2 Co2 61.2(2) 1_565 17_566 ?

Sb3 Fe2 Co2 61.2(2) . 17_566 ?

Fe1 Fe2 Co2 57.80(6) 9 17_566 ?

Fe1 Fe2 Co2 57.80(6) 9_455 17_566 ?

Sb2 Fe2 Co2 124.54(6) 25_455 17_566 ?

Sb2 Fe2 Co2 124.54(6) 25 17_566 ?

Sb3 Fe2 Co2 54.7(2) 17_566 17_566 ?

Sb3 Fe2 Co2 54.7(2) 17_556 17_566 ?

Sb3 Fe2 Fe2 61.2(2) 1_565 17_566 ?

Sb3 Fe2 Fe2 61.2(2) . 17_566 ?

Fe1 Fe2 Fe2 57.80(6) 9 17_566 ?

Fe1 Fe2 Fe2 57.80(6) 9_455 17_566 ?

Sb2 Fe2 Fe2 124.54(6) 25_455 17_566 ?

Sb2 Fe2 Fe2 124.54(6) 25 17_566 ?

Sb3 Fe2 Fe2 54.7(2) 17_566 17_566 ?

Sb3 Fe2 Fe2 54.7(2) 17_556 17_566 ?

Co2 Fe2 Fe2 0.0 17_566 17_566 ?

Sb3 Fe2 Pr1 78.6(2) 1_565 1_565 ?

Sb3 Fe2 Pr1 159.0(2) . 1_565 ?

Fe1 Fe2 Pr1 114.01(4) 9 1_565 ?

Fe1 Fe2 Pr1 114.01(4) 9_455 1_565 ?

Sb2 Fe2 Pr1 64.34(6) 25_455 1_565 ?

Sb2 Fe2 Pr1 64.34(6) 25 1_565 ?

Sb3 Fe2 Pr1 85.1(2) 17_566 1_565 ?

Sb3 Fe2 Pr1 165.5(2) 17_556 1_565 ?

Co2 Fe2 Pr1 139.80(4) 17_566 1_565 ?

Fe2 Fe2 Pr1 139.80(4) 17_566 1_565 ?

Sb3 Fe2 Pr1 159.0(2) 1_565 . ?

Sb3 Fe2 Pr1 78.6(2) . . ?

Fe1 Fe2 Pr1 114.01(4) 9 . ?

Fe1 Fe2 Pr1 114.01(4) 9_455 . ?

Sb2 Fe2 Pr1 64.34(6) 25_455 . ?

Sb2 Fe2 Pr1 64.34(6) 25 . ?

Sb3 Fe2 Pr1 165.5(2) 17_566 . ?

Sb3 Fe2 Pr1 85.1(2) 17_556 . ?

Co2 Fe2 Pr1 139.80(4) 17_566 . ?

Fe2 Fe2 Pr1 139.80(4) 17_566 . ?

Pr1 Fe2 Pr1 80.40(9) 1_565 . ?

Sb1 Sb1 Sb1 180.0 25_565 25_455 ?

Sb1 Sb1 Sb1 90.0 25_565 25_465 ?

Sb1 Sb1 Sb1 90.0 25_455 25_465 ?

Sb1 Sb1 Sb1 90.0 25_565 25 ?

Sb1 Sb1 Sb1 90.0 25_455 25 ?

Sb1 Sb1 Sb1 180.0 25_465 25 ?

Sb1 Sb1 Pr1 117.24(2) 25_565 . ?

Sb1 Sb1 Pr1 62.76(2) 25_455 . ?

Sb1 Sb1 Pr1 117.24(2) 25_465 . ?

Sb1 Sb1 Pr1 62.76(2) 25 . ?

Sb1 Sb1 Pr1 62.76(2) 25_565 1_565 ?

Sb1 Sb1 Pr1 117.24(2) 25_455 1_565 ?

Sb1 Sb1 Pr1 62.76(2) 25_465 1_565 ?

Sb1 Sb1 Pr1 117.24(2) 25 1_565 ?

Pr1 Sb1 Pr1 80.68(7) . 1_565 ?

Sb1 Sb1 Pr1 117.24(2) 25_565 25_455 ?

Sb1 Sb1 Pr1 62.76(2) 25_455 25_455 ?

Sb1 Sb1 Pr1 62.76(2) 25_465 25_455 ?

Sb1 Sb1 Pr1 117.24(2) 25 25_455 ?

Pr1 Sb1 Pr1 125.52(4) . 25_455 ?

Pr1 Sb1 Pr1 125.52(4) 1_565 25_455 ?

Sb1 Sb1 Pr1 62.76(2) 25_565 25 ?

Sb1 Sb1 Pr1 117.24(2) 25_455 25 ?

Sb1 Sb1 Pr1 117.24(2) 25_465 25 ?

Sb1 Sb1 Pr1 62.76(2) 25 25 ?

Pr1 Sb1 Pr1 125.52(4) . 25 ?

Pr1 Sb1 Pr1 125.52(4) 1_565 25 ?

Pr1 Sb1 Pr1 80.68(7) 25_455 25 ?

Co2 Sb2 Co2 71.25(6) 13_545 25_455 ?

Co2 Sb2 Fe2 0.0 13_545 13_545 ?

Co2 Sb2 Fe2 71.3 25_455 13_545 ?

Co2 Sb2 Fe2 71.3 13_545 25_455 ?

Co2 Sb2 Fe2 0.0 25_455 25_455 ?

Fe2 Sb2 Fe2 71.25(6) 13_545 25_455 ?

Co2 Sb2 Co2 110.92(12) 13_545 13 ?

Co2 Sb2 Co2 71.25(6) 25_455 13 ?

Fe2 Sb2 Co2 110.92(12) 13_545 13 ?

Fe2 Sb2 Co2 71.25(6) 25_455 13 ?

Co2 Sb2 Co2 71.25(6) 13_545 25 ?

Co2 Sb2 Co2 110.92(12) 25_455 25 ?

Fe2 Sb2 Co2 71.25(6) 13_545 25 ?

Fe2 Sb2 Co2 110.92(12) 25_455 25 ?

Co2 Sb2 Co2 71.25(6) 13 25 ?

Co2 Sb2 Fe2 110.9 13_545 13 ?

Co2 Sb2 Fe2 71.3 25_455 13 ?

Fe2 Sb2 Fe2 110.92(12) 13_545 13 ?

Fe2 Sb2 Fe2 71.25(6) 25_455 13 ?

Co2 Sb2 Fe2 0.0 13 13 ?

Co2 Sb2 Fe2 71.3 25 13 ?

Co2 Sb2 Fe2 71.3 13_545 25 ?

Co2 Sb2 Fe2 110.9 25_455 25 ?

Fe2 Sb2 Fe2 71.25(6) 13_545 25 ?

Fe2 Sb2 Fe2 110.92(12) 25_455 25 ?

Co2 Sb2 Fe2 71.3 13 25 ?

Co2 Sb2 Fe2 0.0 25 25 ?

Fe2 Sb2 Fe2 71.25(6) 13 25 ?

Co2 Sb2 Fe1 55.46(6) 13_545 . ?

Co2 Sb2 Fe1 55.46(6) 25_455 . ?

Fe2 Sb2 Fe1 55.46(6) 13_545 . ?

Fe2 Sb2 Fe1 55.46(6) 25_455 . ?

Co2 Sb2 Fe1 55.46(6) 13 . ?

Co2 Sb2 Fe1 55.46(6) 25 . ?

Fe2 Sb2 Fe1 55.46(6) 13 . ?

Fe2 Sb2 Fe1 55.46(6) 25 . ?

Co2 Sb2 Pr1 137.483(19) 13_545 25 ?

Co2 Sb2 Pr1 137.483(19) 25_455 25 ?

Fe2 Sb2 Pr1 137.483(19) 13_545 25 ?

Fe2 Sb2 Pr1 137.483(19) 25_455 25 ?

Co2 Sb2 Pr1 68.75(5) 13 25 ?

Co2 Sb2 Pr1 68.75(5) 25 25 ?

Fe2 Sb2 Pr1 68.75(5) 13 25 ?

Fe2 Sb2 Pr1 68.75(5) 25 25 ?

Fe1 Sb2 Pr1 109.29(3) . 25 ?

Co2 Sb2 Pr1 68.75(5) 13_545 25_445 ?

Co2 Sb2 Pr1 68.75(5) 25_455 25_445 ?

Fe2 Sb2 Pr1 68.75(5) 13_545 25_445 ?

Fe2 Sb2 Pr1 68.75(5) 25_455 25_445 ?

Co2 Sb2 Pr1 137.483(19) 13 25_445 ?

Co2 Sb2 Pr1 137.483(19) 25 25_445 ?

Fe2 Sb2 Pr1 137.483(19) 13 25_445 ?

Fe2 Sb2 Pr1 137.483(19) 25 25_445 ?

Fe1 Sb2 Pr1 109.29(3) . 25_445 ?

Pr1 Sb2 Pr1 141.42(7) 25 25_445 ?

Co2 Sb2 Pr1 137.483(19) 13_545 25_455 ?

Co2 Sb2 Pr1 68.75(5) 25_455 25_455 ?

Fe2 Sb2 Pr1 137.483(19) 13_545 25_455 ?

Fe2 Sb2 Pr1 68.75(5) 25_455 25_455 ?

Co2 Sb2 Pr1 68.75(5) 13 25_455 ?

Co2 Sb2 Pr1 137.483(19) 25 25_455 ?

Fe2 Sb2 Pr1 68.75(5) 13 25_455 ?

Fe2 Sb2 Pr1 137.483(19) 25 25_455 ?

Fe1 Sb2 Pr1 109.29(3) . 25_455 ?

Pr1 Sb2 Pr1 83.73(2) 25 25_455 ?

Pr1 Sb2 Pr1 83.73(2) 25_445 25_455 ?

Sb3 Sb3 Fe2 118.8(2) 17_556 . ?

Sb3 Sb3 Co2 118.8(2) 17_556 21_455 ?

Fe2 Sb3 Co2 76.6 . 21_455 ?

Sb3 Sb3 Co2 118.8(2) 17_556 1_545 ?

Fe2 Sb3 Co2 122.4 . 1_545 ?

Co2 Sb3 Co2 76.6(2) 21_455 1_545 ?

Sb3 Sb3 Fe2 118.8(2) 17_556 21_455 ?

Fe2 Sb3 Fe2 76.6(2) . 21_455 ?

Co2 Sb3 Fe2 0.0 21_455 21_455 ?

Co2 Sb3 Fe2 76.6 1_545 21_455 ?

Sb3 Sb3 Fe2 118.8(2) 17_556 1_545 ?

Fe2 Sb3 Fe2 122.4(5) . 1_545 ?

Co2 Sb3 Fe2 76.6 21_455 1_545 ?

Co2 Sb3 Fe2 0.0 1_545 1_545 ?

Fe2 Sb3 Fe2 76.6(2) 21_455 1_545 ?

Sb3 Sb3 Co2 118.8(2) 17_556 21 ?

Fe2 Sb3 Co2 76.6 . 21 ?

Co2 Sb3 Co2 122.4(5) 21_455 21 ?

Co2 Sb3 Co2 76.6(2) 1_545 21 ?

Fe2 Sb3 Co2 122.4(5) 21_455 21 ?

Fe2 Sb3 Co2 76.6(2) 1_545 21 ?

Sb3 Sb3 Fe2 118.8(2) 17_556 21 ?

Fe2 Sb3 Fe2 76.6(2) . 21 ?

Co2 Sb3 Fe2 122.4 21_455 21 ?

Co2 Sb3 Fe2 76.6 1_545 21 ?

Fe2 Sb3 Fe2 122.4(5) 21_455 21 ?

Fe2 Sb3 Fe2 76.6(2) 1_545 21 ?

Co2 Sb3 Fe2 0.0 21 21 ?

Sb3 Sb3 Co2 54.66(19) 17_556 5_656 ?

Fe2 Sb3 Co2 106.2 . 5_656 ?

Co2 Sb3 Co2 173.5(4) 21_455 5_656 ?

Co2 Sb3 Co2 106.19(7) 1_545 5_656 ?

Fe2 Sb3 Co2 173.5(4) 21_455 5_656 ?

Fe2 Sb3 Co2 106.19(7) 1_545 5_656 ?

Co2 Sb3 Co2 64.16(12) 21 5_656 ?

Fe2 Sb3 Co2 64.16(12) 21 5_656 ?

Sb3 Sb3 Fe2 54.66(19) 17_556 17_566 ?

Fe2 Sb3 Fe2 64.16(12) . 17_566 ?

Co2 Sb3 Fe2 106.2 21_455 17_566 ?

Co2 Sb3 Fe2 173.5 1_545 17_566 ?

Fe2 Sb3 Fe2 106.19(7) 21_455 17_566 ?

Fe2 Sb3 Fe2 173.5(4) 1_545 17_566 ?

Co2 Sb3 Fe2 106.2 21 17_566 ?

Fe2 Sb3 Fe2 106.19(7) 21 17_566 ?

Co2 Sb3 Fe2 70.5 5_656 17_566 ?

Sb3 Sb3 Co2 54.66(19) 17_556 17_566 ?

Fe2 Sb3 Co2 64.2 . 17_566 ?

Co2 Sb3 Co2 106.19(7) 21_455 17_566 ?

Co2 Sb3 Co2 173.5(4) 1_545 17_566 ?

Fe2 Sb3 Co2 106.19(7) 21_455 17_566 ?

Fe2 Sb3 Co2 173.5(4) 1_545 17_566 ?

Co2 Sb3 Co2 106.19(7) 21 17_566 ?

Fe2 Sb3 Co2 106.19(7) 21 17_566 ?

Co2 Sb3 Co2 70.5(2) 5_656 17_566 ?

Fe2 Sb3 Co2 0.00(9) 17_566 17_566 ?

_refine_diff_density_max 2.730

_refine_diff_density_min
-2.069

_refine_diff_density_rms
0.473

_shelx_res_file

;

shelx.res created by
SHELXL-2014/7

TITL scd0395_JB62 in
I4/mmm

CELL 0.71073 4.299
4.299 25.711 90.000
90.000 90.000

ZERR 2 0.005
0.005 0.005 0.005
0.005 0.005

LATT 2

SYMM -X,-Y,Z

SYMM X,-Y,-Z

SYMM -X,Y,-Z

SYMM -Y,-X,-Z

SYMM Y,X,-Z

SYMM Y,-X,Z

SYMM -Y,X,Z

SFAC FE CO SB PR

UNIT 4 4 10 4

MERG 2

L.S. 4

FMAP 2

PLAN 25

ACTA

EXYZ FE2 CO2

EADP FE2 CO2

WGHT 0.039200
30.508600

EXTI 0.001076

FVAR 0.04870
0.48286

PR1 4 0.000000
0.000000 0.348432
10.12500 0.00472
0.00472 =

0.00917 0.00000
0.00000 0.00000

FE1 1 0.000000
0.000000 0.000000
10.06250 0.00771
0.00771 =

0.00865 0.00000
0.00000 0.00000

FE2 1 0.000000
0.500000 0.447361
10.07688 0.00397
0.02399 =

0.00851 0.00000
0.00000 0.00000

CO2 2 0.000000
0.500000 0.447361
10.12000 0.00397
0.02399 =

0.00851 0.00000
0.00000 0.00000

SB1 3 0.000000
0.500000 0.250000
10.12500 0.00289
0.00289 =

0.00497 0.00000
0.00000 0.00000

SB2 3 0.000000
0.000000 0.110181
10.12500 0.00481
0.00481 =

0.00954 0.00000
0.00000 0.00000

SB3 3 0.000000
0.000000 0.493354
20.12500 0.02670
0.02670 =

0.01794 0.00000
0.00000 0.00000

HKLF 4

REM scd0395_JB62 in
I4/mmm

REM R1 = 0.0335 for
265 Fo > 4sig(Fo) and
0.0340 for all 270 data

REM 20 parameters
refined using 0
restraints

END

WGHT 0.0328
31.0767

REM Highest difference peak 2.730, deepest hole -2.069, 1-sigma level 0.473

Q1 1 0.0000 0.5000 0.2630 10.25000 0.05 2.73

Q2 1 0.0000 0.2453 0.2502 10.50000 0.05 2.48

Q3 1 0.0000 0.2425 0.3489 10.50000 0.05 2.05

Q4 1 0.0000 0.0000 0.1413 10.12500 0.05 1.85

Q5 1 0.0000 0.2523 0.0000 10.25000 0.05 1.41

Q6 1 0.0000 0.4237 0.3695 10.50000 0.05 1.40

Q7 1 0.0410 0.2443 0.1122 11.00000 0.05 1.38

Q8 1 0.2529 0.0754 0.0000 10.50000 0.05 1.25

Q9 1 0.2561 0.5000 0.4485 10.50000 0.05 1.08

A2.3 $Pr_2Fe_{4-x}Co_xSb_5$ (x ~ 2.5)

data_shelx

_audit_update_record

Q10 1 0.1011 0.2398 0.5000 10.50000 0.05 0.95

Q11 1 0.0000 0.2602 0.1526 10.50000 0.05 0.93

Q12 1 0.0000 0.0000 0.4107 10.12500 0.05 0.91

Q13 1 0.2459 0.2459 0.2612 10.50000 0.05 0.88

Q14 1 0.0000 0.2200 0.5000 10.25000 0.05 0.85

Q15 1 0.0000 0.5000 0.3991 10.25000 0.05 0.85

Q16 1 0.0000 0.2395 0.4436 10.50000 0.05 0.81

Q17 1 0.3310 0.4214 0.2298 11.00000 0.05 0.72

Q18 1 0.3871 0.0000 0.3321 10.50000 0.05 0.68

Q19 1 -0.5000 0.0000 0.3400 10.25000 0.05 0.65

Q20 1 0.1143 0.2396 0.2886 11.00000 0.05 0.64

;

2015-07-10 # Formatted by publCIF

Q21 1 0.0730 0.2470 0.4494 11.00000 0.05 0.58

Q22 1 0.2615 0.3517 0.4596 11.00000 0.05 0.55

Q23 1 0.2143 0.2143 0.0344 10.50000 0.05 0.54

Q24 1 0.2357 0.2357 0.1316 10.50000 0.05 0.54

Q25 1 0.2684 0.2684 0.4309 10.50000 0.05 0.52

;

_shelx_res_checksum 19905

;

_shelx_hkl_checksum 35246

#===END

;

_audit_creation_method 'SHELXL-2014/7'

_shelx_SHELXL_version_number '2014/7'

_chemical_name_systematic ?

_chemical_name_common ?

_chemical_melting_point ?

_chemical_formula_moiety 'Co1.5 Fe2.5 Pr Sb5'

_chemical_formula_sum

'Co1.5 Fe2.5 Pr Sb5'

_chemical_formula_weight 982.30

loop_

_atom_type_symbol

_atom_type_description

_atom_type_scat_dispersion_real

_atom_type_scat_dispersion_imag

_atom_type_scat_source

'Fe' 'Fe' 0.3463 0.8444

'International Tables Vol C Tables 4.2.6.8 and 6.1.1.4'

'Co' 'Co' 0.3494 0.9721

'International Tables Vol C Tables 4.2.6.8 and 6.1.1.4'

'Sb' 'Sb' -0.5866 1.5461

'International Tables Vol C Tables 4.2.6.8 and 6.1.1.4'

'Pr' 'Pr' -0.2180 2.8214

'International Tables Vol C Tables 4.2.6.8 and 6.1.1.4'

_space_group_crystal_system tetragonal

_space_group_IT_number 139

_space_group_name_H-M_alt 'I 4/m m m'

_space_group_name_Hall '-I 4 2'

_shelx_space_group_comment

;

The symmetry employed for this shelxl refinement is uniquely defined

by the following loop, which should always be used as a source of

symmetry information in preference to the above space-group names.

They are only intended as comments.

;

loop_

_space_group_symop_operation_xyz

'x, y, z'

'-x, -y, z'

'-y, x, z'

'y, -x, z'

'-x, y, -z'

'x, -y, -z'

'y, x, -z'

'-y, -x, -z'

'x+1/2, y+1/2, z+1/2'

'-x+1/2, -y+1/2, z+1/2'

'-y+1/2, x+1/2, z+1/2'

'y+1/2, -x+1/2, z+1/2'

'-x+1/2, y+1/2, -z+1/2'

'x+1/2, -y+1/2, -z+1/2'

'y+1/2, x+1/2, -z+1/2'

'-y+1/2, -x+1/2, -z+1/2'

'-x, -y, -z'

'x, y, -z'

'y, -x, -z'

'-y, x, -z'

'x, -y, z'

'-x, y, z'

'-y, -x, z'

'y, x, z'

'-x+1/2, -y+1/2, -z+1/2'

'x+1/2, y+1/2, -z+1/2'

'y+1/2, -x+1/2, -z+1/2'

'-y+1/2, x+1/2, -z+1/2'

'x+1/2, -y+1/2, z+1/2'

'-x+1/2, y+1/2, z+1/2'

'-y+1/2, -x+1/2, z+1/2'

'y+1/2, x+1/2, z+1/2'

_cell_length_a
4.3021(3)

_cell_length_b
4.3021(3)

_cell_length_c
25.6958(19)

_cell_angle_alpha
90

_cell_angle_beta
90

_cell_angle_gamma
90

_cell_volume
475.58(8)

_cell_formula_units_Z
2

_cell_measurement_temperature 350(2)

_cell_measurement_reflns_used ?

_cell_measurement_theta_min ?

_cell_measurement_theta_max ?

_exptl_crystal_description
plate

_exptl_crystal_colour
black

_exptl_crystal_density_meas ?

_exptl_crystal_density_method ?

_exptl_crystal_density_diffrn 6.860

_exptl_crystal_F_000
962.3

_exptl_transmission_factor_min ?

_exptl_transmission_factor_max ?

_exptl_crystal_size_max
0.03

_exptl_crystal_size_mid
0.02

_exptl_crystal_size_min
0.02

_exptl_absorpt_coefficient_mu 25.451

_shelx_estimated_absorpt_T_min ?

_shelx_estimated_absorpt_T_max ?

_exptl_absorpt_correction_type multi-scan

_exptl_absorpt_correction_T_min 0.240

_exptl_absorpt_correction_T_max 0.403

_exptl_absorpt_process_details SADABS(2014)

_exptl_absorpt_special_details ?

_diffrn_ambient_temperature 350(2)

_diffrn_radiation_wavelength 0.71073

_diffrn_radiation_type
MoK\a

_diffrn_source
'I\mS microfocus tube'

_diffrn_measurement_device_type 'Bruker Kappa D8 Quest CMOS'

_diffrn_measurement_method '\f and \w scans'

_diffrn_detector_area_resol_mean ?

_diffrn_reflns_number
4292

_diffrn_reflns_av_unetI/netI 0.0374

_diffrn_reflns_av_R_equivalents 0.0520

_diffrn_reflns_limit_h_min
-8

_diffrn_reflns_limit_h_max 8

_diffrn_reflns_limit_k_min -8

_diffrn_reflns_limit_k_max 8

_diffrn_reflns_limit_l_min -50

_diffrn_reflns_limit_l_max 46

_diffrn_reflns_theta_min 3.171

_diffrn_reflns_theta_max 45.032

_diffrn_reflns_theta_full 25.242

_diffrn_measured_fraction_theta_max 0.992

_diffrn_measured_fraction_theta_full 0.988

_diffrn_reflns_Laue_measured_fraction_max 0.992

_diffrn_reflns_Laue_measured_fraction_full 0.988

_diffrn_reflns_point_group_measured_fraction_max 0.992

_diffrn_reflns_point_group_measured_fraction_full 0.988

_reflns_number_total 653

_reflns_number_gt 587

_reflns_threshold_expression 'I > 2\s(I)'

_reflns_Friedel_coverage 0.000

_reflns_Friedel_fraction_max .

_reflns_Friedel_fraction_full .

_reflns_special_details

;

Reflections were merged by SHELXL according to the crystal

class for the calculation of statistics and refinement.

_reflns_Friedel_fraction is defined as the number of unique

Friedel pairs measured divided by the number that would be

possible theoretically, ignoring centric projections and

systematic absences.

;

_computing_data_collection 'Bruker APEX2'

_computing_cell_refinement 'Bruker SAINT'

_computing_data_reduction 'Bruker SAINT'

_computing_structure_solution 'SHELXS Direct Methods (Sheldrick, 2013)'

_computing_structure_refinement 'SHELXL-2014/7 (Sheldrick, 2014)'

_computing_molecular_graphics CrystalMaker

_computing_publication_material 'publCIF (Westrip, 2014)'

_refine_special_details ?

_refine_ls_structure_factor_coef Fsqd

_refine_ls_matrix_type full

_refine_ls_weighting_scheme calc

_refine_ls_weighting_details

'w=1/[\s^2^(Fo^2^)+(0.0502P)^2^+14.3794P] where P=(Fo^2^+2Fc^2^)/3'

_atom_sites_solution_primary ?

_atom_sites_solution_secondary ?

_atom_sites_solution_hydrogens .

_refine_ls_hydrogen_treatment undef

_refine_ls_extinction_method 'SHELXL-2014/7 (Sheldrick 2014'

_refine_ls_extinction_coef 0.0031(6)

_refine_ls_extinction_expression

'Fc^*^=kFc[1+0.001xFc^2^\l^3^/sin(2\q)]^-1/4^'

_refine_ls_number_reflns 653

_refine_ls_number_parameters 21

_refine_ls_number_restraints 0

_refine_ls_R_factor_all 0.0487

_refine_ls_R_factor_gt 0.0433

_refine_ls_wR_factor_ref 0.1183

_refine_ls_wR_factor_gt 0.1158

_refine_ls_goodness_of_fit_ref 1.268

_refine_ls_restrained_S_all 1.268

_refine_ls_shift/su_max 0.000

_refine_ls_shift/su_mean 0.000

loop_

_atom_site_label

_atom_site_type_symbol

_atom_site_fract_x

_atom_site_fract_y

_atom_site_fract_z

_atom_site_U_iso_or_equiv

_atom_site_adp_type

_atom_site_occupancy

_atom_site_site_symmetry_order

_atom_site_calc_flag

_atom_site_refinement_flags_posn

_atom_site_refinement_flags_adp

_atom_site_refinement_flags_occupancy

_atom_site_disorder_assembly

_atom_site_disorder_group

Pr1 Pr 0.0000 0.0000 0.34881(2) 0.00812(15) Uani 1 8 d S T P . .

Fe1 Fe 0.0000 0.0000 0.0000 0.0049(6) Uani 0.807(17) 16 d S T P . .

Co1 Co 0.0000 0.5000 0.44676(6) 0.0111(3) Uani 0.5972 4 d S T P . .

Fe2 Fe 0.0000 0.5000 0.44676(6) 0.0111(3) Uani 0.1394 4 d S T P . .

Sb1 Sb 0.0000 0.5000 0.2500 0.00700(15) Uani 1 8 d S T P . .

Sb2 Sb 0.0000 0.0000 0.11021(3) 0.00854(17) Uani 1 8 d S T P . .

Sb3 Sb 0.0000 0.0000 0.49447(16) 0.0193(9) Uani 0.445(6) 8 d S T P . .

loop_

_atom_site_aniso_label

_atom_site_aniso_U_11

_atom_site_aniso_U_22

_atom_site_aniso_U_33

_atom_site_aniso_U_23

_atom_site_aniso_U_13

_atom_site_aniso_U_12

Pr1 0.00752(18) 0.00752(18) 0.0093(2) 0.000 0.000 0.000

Fe1 0.0053(8) 0.0053(8) 0.0040(9) 0.000 0.000 0.000

Co1 0.0060(6) 0.0206(9) 0.0068(5) 0.000 0.000 0.000

Fe2 0.0060(6) 0.0206(9) 0.0068(5) 0.000 0.000 0.000

Sb1 0.0066(2) 0.0066(2) 0.0078(2) 0.000 0.000 0.000

Sb2 0.0073(2) 0.0073(2) 0.0110(3) 0.000 0.000 0.000

Sb3 0.0222(7) 0.0222(7) 0.014(2) 0.000 0.000 0.000

_geom_special_details

;

All esds (except the esd in the dihedral angle between two l.s. planes)

are estimated using the full covariance matrix. The cell esds are taken

into account individually in the estimation of esds in distances, angles

and torsion angles; correlations between esds in cell parameters are only

used when they are defined by crystal symmetry. An approximate (isotropic)

treatment of cell esds is used for estimating esds involving l.s. planes.

;

loop_

_geom_bond_atom_site_label_1

_geom_bond_atom_site_label_2

_geom_bond_distance

_geom_bond_site_symmetry_2

_geom_bond_publ_flag

Pr1 Sb2 3.2191(4) 25 ?

Pr1 Sb2 3.2191(4) 25_445 ?

Pr1 Sb2 3.2191(4) 25_455 ?

Pr1 Sb2 3.2191(4) 25_545 ?

Pr1 Fe2 3.3108(13) 3_655 ?

Pr1 Co1 3.3108(13) 3_655 ?

Pr1 Co1 3.3107(13) 1_545 ?

Pr1 Fe2 3.3107(13) 1_545 ?

Pr1 Fe2 3.3107(13) 3 ?

Pr1 Co1 3.3107(13) 3 ?

Pr1 Co1 3.3108(13) . ?

Fe1 Fe2 2.5493(9) 27_455 ?

Fe1 Fe2 2.5493(9) 11_544 ?

Fe1 Co1 2.5493(9) 9_444 ?

Fe1 Fe2 2.5493(9) 25 ?

Fe1 Fe2 2.5493(9) 9_444 ?

Fe1 Co1 2.5493(9) 25 ?

Fe1 Co1 2.5493(9) 11_544 ?

Fe1 Co1 2.5493(9) 27_455 ?

Fe1 Fe2 2.5493(9) 27_445 ?

Fe1 Co1 2.5493(9) 27_445 ?

Fe1 Co1 2.5493(9) 11_554 ?

Fe1 Fe2 2.5493(9) 9_544 ?

Co1 Sb3 2.476(2) . ?

Co1 Sb3 2.476(2) 1_565 ?

Co1 Fe1 2.5493(9) 9 ?

Co1 Fe1 2.5493(9) 9_455 ?

Co1 Sb2 2.6019(10) 25_455 ?

Co1 Sb2 2.6019(10) 25 ?

Co1 Sb3 2.628(3) 17_566 ?

Co1 Sb3 2.628(3) 17_556 ?

Co1 Fe2 2.736(3) 17_566 ?

Co1 Co1 2.736(3) 17_566 ?

Co1 Pr1 3.3108(13) 1_565 ?

Sb1 Sb1 3.0420(2) 25_565 ?

Sb1 Sb1 3.0420(2) 25_455 ?

Sb1 Sb1 3.0420(2) 25_465 ?

Sb1 Sb1 3.0420(2) 25 ?

Sb1 Pr1 3.3276(5) 25_455 ?

Sb1 Pr1 3.3277(5) 1_565 ?

Sb1 Pr1 3.3276(5) 25 ?

Sb2 Fe2 2.6019(10) 27_445 ?

Sb2 Fe2 2.6019(10) 25_455 ?

Sb2 Co1 2.6019(10) 27_445 ?

Sb2 Co1 2.6019(10) 25_455 ?

Sb2 Fe2 2.6019(10) 27_455 ?

Sb2 Fe2 2.6019(10) 25 ?

Sb2 Co1 2.6019(10) 27_455 ?

Sb2 Co1 2.6019(10) 25 ?

Sb2 Pr1 3.2191(4) 25 ?

Sb2 Pr1 3.2191(4) 25_445 ?

Sb2 Pr1 3.2191(4) 25_455 ?

Sb3 Sb3 0.284(8) 17_556 ?

Sb3 Fe2 2.476(2) 3 ?

Sb3 Fe2 2.476(2) 1_545 ?

Sb3 Co1 2.476(2) 3 ?

Sb3 Co1 2.476(2) 1_545 ?

Sb3 Fe2 2.476(2) 3_655 ?

Sb3 Co1 2.476(2) 3_655 ?

Sb3 Fe2 2.628(3) 19_556 ?

Sb3 Fe2 2.628(3) 17_566 ?

Sb3 Co1 2.628(3) 17_566 ?

loop_

_geom_angle_atom_site_label_1

_geom_angle_atom_site_label_2

_geom_angle_atom_site_label_3

_geom_angle

_geom_angle_site_symmetry_1

_geom_angle_site_symmetry_3

_geom_angle_publ_flag

Sb2 Pr1 Sb2 141.82(4) 25 25_445 ?

Sb2 Pr1 Sb2 83.858(11) 25 25_455 ?

Sb2 Pr1 Sb2 83.858(11) 25_445 25_455 ?

Sb2 Pr1 Sb2 83.858(11) 25 25_545 ?

Sb2 Pr1 Sb2 83.858(11) 25_445 25_545 ?

Sb2 Pr1 Sb2 141.82(4) 25_455 25_545 ?

Sb2 Pr1 Fe2 46.938(14) 25 3_655 ?

Sb2 Pr1 Fe2 100.69(2) 25_445 3_655 ?

Sb2 Pr1 Fe2 100.69(2) 25_455 3_655 ?

Sb2 Pr1 Fe2 46.938(14) 25_545 3_655 ?

Sb2 Pr1 Co1 46.938(14) 25 3_655 ?

Sb2 Pr1 Co1 100.69(2) 25_445 3_655 ?

Sb2 Pr1 Co1 100.69(2) 25_455 3_655 ?

Sb2 Pr1 Co1 46.938(14) 25_545 3_655 ?

Fe2 Pr1 Co1 0.0 3_655 3_655 ?

Sb2 Pr1 Co1 100.69(2) 25 1_545 ?

Sb2 Pr1 Co1 46.938(14) 25_445 1_545 ?

Sb2 Pr1 Co1 100.69(2) 25_455 1_545 ?

Sb2 Pr1 Co1 46.938(14) 25_545 1_545 ?

Fe2 Pr1 Co1 54.7 3_655 1_545 ?

Co1 Pr1 Co1 54.70(2) 3_655 1_545 ?

Sb2 Pr1 Fe2 100.69(2) 25 1_545 ?

Sb2 Pr1 Fe2 46.938(14) 25_445 1_545 ?

Sb2 Pr1 Fe2 100.69(2) 25_455 1_545 ?

Sb2 Pr1 Fe2 46.938(14) 25_545 1_545 ?

Fe2 Pr1 Fe2 54.70(2) 3_655 1_545 ?

Co1 Pr1 Fe2 54.70(2) 3_655 1_545 ?

Co1 Pr1 Fe2 0.0 1_545 1_545 ?

Sb2 Pr1 Fe2 100.69(2) 25 3 ?

Sb2 Pr1 Fe2 46.938(14) 25_445 3 ?

Sb2 Pr1 Fe2 46.938(14) 25_455 3 ?

Sb2 Pr1 Fe2 100.69(2) 25_545 3 ?

Fe2 Pr1 Fe2 81.04(4) 3_655 3 ?

Co1 Pr1 Fe2 81.04(4) 3_655 3 ?

Co1 Pr1 Fe2 54.70(2) 1_545 3 ?

Fe2 Pr1 Fe2 54.70(2) 1_545 3 ?

Sb2 Pr1 Co1 100.69(2) 25 3 ?

Sb2 Pr1 Co1 46.938(14) 25_445 3 ?

Sb2 Pr1 Co1 46.938(14) 25_455 3 ?

Sb2 Pr1 Co1 100.69(2) 25_545 3 ?

Fe2 Pr1 Co1 81.0 3_655 3 ?

Co1 Pr1 Co1 81.04(4) 3_655 3 ?

Co1 Pr1 Co1 54.70(2) 1_545 3 ?

Fe2 Pr1 Co1 54.7 1_545 3 ?

Fe2 Pr1 Co1 0.0 3 3 ?

Sb2 Pr1 Co1 46.938(14) 25 . ?

Sb2 Pr1 Co1 100.69(2) 25_445 . ?

Sb2 Pr1 Co1 46.938(14) 25_455 . ?

Sb2 Pr1 Co1 100.69(2) 25_545 . ?

Fe2 Pr1 Co1 54.7 3_655 . ?

Co1 Pr1 Co1 54.70(2) 3_655 . ?

Co1 Pr1 Co1 81.04(4) 1_545 . ?

Fe2 Pr1 Co1 81.0 1_545 . ?

Fe2 Pr1 Co1 54.7 3 . ?

Co1 Pr1 Co1 54.70(2) 3 . ?

Fe2 Fe1 Fe2 180.00(6) 27_455 11_544 ?

Fe2 Fe1 Co1 106.7 27_455 9_444 ?

Fe2 Fe1 Co1 73.3 11_544 9_444 ?

Fe2 Fe1 Fe2 73.26(3) 27_455 25 ?

Fe2 Fe1 Fe2 106.74(3) 11_544 25 ?

Co1 Fe1 Fe2 180.00(6) 9_444 25 ?

Fe2 Fe1 Fe2 106.74(3) 27_455 9_444 ?

Fe2 Fe1 Fe2 73.26(3) 11_544 9_444 ?

Co1 Fe1 Fe2 0.00(6) 9_444 9_444 ?

Fe2 Fe1 Fe2 180.00(6) 25 9_444 ?

Fe2 Fe1 Co1 73.3 27_455 25 ?

Fe2 Fe1 Co1 106.7 11_544 25 ?

Co1 Fe1 Co1 180.00(6) 9_444 25 ?

Fe2 Fe1 Co1 0.0 25 25 ?

Fe2 Fe1 Co1 180.0 9_444 25 ?

Fe2 Fe1 Co1 180.0 27_455 11_544 ?

Fe2 Fe1 Co1 0.0 11_544 11_544 ?

Co1 Fe1 Co1 73.26(3) 9_444 11_544 ?

Fe2 Fe1 Co1 106.7 25 11_544 ?

Fe2 Fe1 Co1 73.3 9_444 11_544 ?

Co1 Fe1 Co1 106.74(3) 25 11_544 ?

Fe2 Fe1 Co1 0.0 27_455 27_455 ?

Fe2 Fe1 Co1 180.0 11_544 27_455 ?

Co1 Fe1 Co1 106.74(3) 9_444 27_455 ?

Fe2 Fe1 Co1 73.3 25 27_455 ?

Fe2 Fe1 Co1 106.7 9_444 27_455 ?

Co1 Fe1 Co1 73.26(3) 25 27_455 ?

Co1 Fe1 Co1 180.00(6) 11_544 27_455 ?

Fe2 Fe1 Fe2 115.08(6) 27_455 27_445 ?

Fe2 Fe1 Fe2 64.92(6) 11_544 27_445 ?

Co1 Fe1 Fe2 106.74(3) 9_444 27_445 ?

Fe2 Fe1 Fe2 73.26(3) 25 27_445 ?

Fe2 Fe1 Fe2 106.74(3) 9_444 27_445 ?

Co1 Fe1 Fe2 73.26(3) 25 27_445 ?

Co1 Fe1 Fe2 64.92(6) 11_544 27_445 ?

Co1 Fe1 Fe2 115.08(6) 27_455 27_445 ?

Fe2 Fe1 Co1 115.1 27_455 27_445 ?

Fe2 Fe1 Co1 64.9 11_544 27_445 ?

Co1 Fe1 Co1 106.74(3) 9_444 27_445 ?

Fe2 Fe1 Co1 73.3 25 27_445 ?

Fe2 Fe1 Co1 106.7 9_444 27_445 ?

Co1 Fe1 Co1 73.26(3) 25 27_445 ?

Co1 Fe1 Co1 64.92(6) 11_544 27_445 ?

Co1 Fe1 Co1 115.08(6) 27_455 27_445 ?

Fe2 Fe1 Co1 0.0 27_445 27_445 ?

Fe2 Fe1 Co1 64.9 27_455 11_554 ?

Fe2 Fe1 Co1 115.1 11_544 11_554 ?

Co1 Fe1 Co1 73.26(3) 9_444 11_554 ?

Fe2 Fe1 Co1 106.7 25 11_554 ?

Fe2 Fe1 Co1 73.3 9_444 11_554 ?

Co1 Fe1 Co1 106.74(3) 25 11_554 ?

Co1 Fe1 Co1 115.08(6) 11_544 11_554 ?

Co1 Fe1 Co1 64.92(6) 27_455 11_554 ?

Fe2 Fe1 Co1 180.0 27_445 11_554 ?

Co1 Fe1 Co1 180.00(6) 27_445 11_554 ?

Fe2 Fe1 Fe2 106.74(3) 27_455 9_544 ?

Fe2 Fe1 Fe2 73.26(3) 11_544 9_544 ?

Co1 Fe1 Fe2 115.08(6) 9_444 9_544 ?

Fe2 Fe1 Fe2 64.92(6) 25 9_544 ?

Fe2 Fe1 Fe2 115.08(6) 9_444 9_544 ?

Co1 Fe1 Fe2 64.92(6) 25 9_544 ?

Co1 Fe1 Fe2 73.26(3) 11_544 9_544 ?

Co1 Fe1 Fe2 106.74(3) 27_455 9_544 ?

Fe2 Fe1 Fe2 106.74(3) 27_445 9_544 ?

Co1 Fe1 Fe2 106.74(3) 27_445 9_544 ?

Co1 Fe1 Fe2 73.26(3) 11_554 9_544 ?

Sb3 Co1 Sb3 120.64(18) . 1_565 ?

Sb3 Co1 Fe1 74.59(5) . 9 ?

Sb3 Co1 Fe1 74.59(5) 1_565 9 ?

Sb3 Co1 Fe1 74.59(5) . 9_455 ?

Sb3 Co1 Fe1 74.59(5) 1_565 9_455 ?

Fe1 Co1 Fe1 115.08(6) 9 9_455 ?

Sb3 Co1 Sb2 106.18(4) . 25_455 ?

Sb3 Co1 Sb2 106.18(4) 1_565 25_455 ?

Fe1 Co1 Sb2 178.22(6) 9 25_455 ?

Fe1 Co1 Sb2 66.695(16) 9_455 25_455 ?

Sb3 Co1 Sb2 106.18(4) . 25 ?

Sb3 Co1 Sb2 106.18(4) 1_565 25 ?

Fe1 Co1 Sb2 66.695(16) 9 25 ?

Fe1 Co1 Sb2 178.22(6) 9_455 25 ?

Sb2 Co1 Sb2 111.53(6) 25_455 25 ?

Sb3 Co1 Sb3 115.25(6) . 17_566 ?

Sb3 Co1 Sb3 5.39(16) 1_565 17_566 ?

Fe1 Co1 Sb3 72.04(4) 9 17_566 ?

Fe1 Co1 Sb3 72.04(4) 9_455 17_566 ?

Sb2 Co1 Sb3 108.86(4) 25_455 17_566 ?

Sb2 Co1 Sb3 108.86(4) 25 17_566 ?

Sb3 Co1 Sb3 5.39(16) . 17_556 ?

Sb3 Co1 Sb3 115.24(6) 1_565 17_556 ?

Fe1 Co1 Sb3 72.04(4) 9 17_556 ?

Fe1 Co1 Sb3 72.04(4) 9_455 17_556 ?

Sb2 Co1 Sb3 108.86(4) 25_455 17_556 ?

Sb2 Co1 Sb3 108.86(4) 25 17_556 ?

Sb3 Co1 Sb3 109.85(16) 17_566 17_556 ?

Sb3 Co1 Fe2 60.32(9) . 17_566 ?

Sb3 Co1 Fe2 60.32(9) 1_565 17_566 ?

Fe1 Co1 Fe2 57.54(3) 9 17_566 ?

Fe1 Co1 Fe2 57.54(3) 9_455 17_566 ?

Sb2 Co1 Fe2 124.24(3) 25_455 17_566 ?

Sb2 Co1 Fe2 124.24(3) 25 17_566 ?

Sb3 Co1 Fe2 54.93(8) 17_566 17_566 ?

Sb3 Co1 Fe2 54.93(8) 17_556 17_566 ?

Sb3 Co1 Co1 60.32(9) . 17_566 ?

Sb3 Co1 Co1 60.32(9) 1_565 17_566 ?

Fe1 Co1 Co1 57.54(3) 9 17_566 ?

Fe1 Co1 Co1 57.54(3) 9_455 17_566 ?

Sb2 Co1 Co1 124.24(3) 25_455 17_566 ?

Sb2 Co1 Co1 124.24(3) 25 17_566 ?

Sb3 Co1 Co1 54.93(8) 17_566 17_566 ?

Sb3 Co1 Co1 54.93(8) 17_556 17_566 ?

Fe2 Co1 Co1 0.0 17_566 17_566 ?

Sb3 Co1 Pr1 79.16(9) . . ?

Sb3 Co1 Pr1 160.20(10) 1_565 . ?

Fe1 Co1 Pr1 114.078(15) 9 . ?

Fe1 Co1 Pr1 114.078(15) 9_455 . ?

Sb2 Co1 Pr1 64.68(3) 25_455 . ?

Sb2 Co1 Pr1 64.68(3) 25 . ?

Sb3 Co1 Pr1 165.59(9) 17_566 . ?

Sb3 Co1 Pr1 84.55(8) 17_556 . ?

Fe2 Co1 Pr1 139.480(19) 17_566 . ?

Co1 Co1 Pr1 139.480(19) 17_566 . ?

Sb3 Co1 Pr1 160.20(10) . 1_565 ?

Sb3 Co1 Pr1 79.16(9) 1_565 1_565 ?

Fe1 Co1 Pr1 114.078(15) 9 1_565 ?

Fe1 Co1 Pr1 114.078(15) 9_455 1_565 ?

Sb2 Co1 Pr1 64.68(3) 25_455 1_565 ?

Sb2 Co1 Pr1 64.68(3) 25 1_565 ?

Sb3 Co1 Pr1 84.55(8) 17_566 1_565 ?

Sb3 Co1 Pr1 165.59(9) 17_556 1_565 ?

Fe2 Co1 Pr1 139.481(19) 17_566 1_565 ?

Co1 Co1 Pr1 139.481(19) 17_566 1_565 ?

Pr1 Co1 Pr1 81.04(4) . 1_565 ?

Sb1 Sb1 Sb1 180.0 25_565 25_455 ?

Sb1 Sb1 Sb1 90.0 25_565 25_465 ?

Sb1 Sb1 Sb1 90.0 25_455 25_465 ?

Sb1 Sb1 Sb1 90.0 25_565 25 ?

Sb1 Sb1 Sb1 90.0 25_455 25 ?

Sb1 Sb1 Sb1 180.0 25_465 25 ?

Sb1 Sb1 Pr1 117.199(5) 25_565 25_455 ?

Sb1 Sb1 Pr1 62.801(5) 25_455 25_455 ?

Sb1 Sb1 Pr1 62.801(4) 25_465 25_455 ?

Sb1 Sb1 Pr1 117.199(5) 25 25_455 ?

Sb1 Sb1 Pr1 62.801(5) 25_565 1_565 ?

Sb1 Sb1 Pr1 117.199(5) 25_455 1_565 ?

Sb1 Sb1 Pr1 62.801(4) 25_465 1_565 ?

Sb1 Sb1 Pr1 117.199(4) 25 1_565 ?

Pr1 Sb1 Pr1 125.602(9) 25_455 1_565 ?

Sb1 Sb1 Pr1 62.801(4) 25_565 25 ?

Sb1 Sb1 Pr1 117.199(4) 25_455 25 ?

Sb1 Sb1 Pr1 117.199(5) 25_465 25 ?

Sb1 Sb1 Pr1 62.801(4) 25 25 ?

Pr1 Sb1 Pr1 80.544(15) 25_455 25 ?

Pr1 Sb1 Pr1 125.602(9) 1_565 25 ?

Sb1 Sb1 Pr1 117.199(4) 25_565 . ?

Sb1 Sb1 Pr1 62.801(4) 25_455 . ?

Sb1 Sb1 Pr1 117.199(4) 25_465 . ?

Sb1 Sb1 Pr1 62.801(4) 25 . ?

Pr1 Sb1 Pr1 125.602(9) 25_455 . ?

Pr1 Sb1 Pr1 80.544(15) 1_565 . ?

Pr1 Sb1 Pr1 125.602(9) 25 . ?

Fe2 Sb2 Fe2 71.55(3) 27_445 25_455 ?

Fe2 Sb2 Co1 0.0 27_445 27_445 ?

Fe2 Sb2 Co1 71.5 25_455 27_445 ?

Fe2 Sb2 Co1 71.5 27_445 25_455 ?

Fe2 Sb2 Co1 0.0 25_455 25_455 ?

Co1 Sb2 Co1 71.55(3) 27_445 25_455 ?

Fe2 Sb2 Fe2 111.53(6) 27_445 27_455 ?

Fe2 Sb2 Fe2 71.55(3) 25_455 27_455 ?

Co1 Sb2 Fe2 111.53(6) 27_445 27_455 ?

Co1 Sb2 Fe2 71.55(3) 25_455 27_455 ?

Fe2 Sb2 Fe2 71.55(3) 27_445 25 ?

Fe2 Sb2 Fe2 111.53(6) 25_455 25 ?

Co1 Sb2 Fe2 71.55(3) 27_445 25 ?

Co1 Sb2 Fe2 111.53(6) 25_455 25 ?

Fe2 Sb2 Fe2 71.55(3) 27_455 25 ?

Fe2 Sb2 Co1 111.5 27_445 27_455 ?

Fe2 Sb2 Co1 71.5 25_455 27_455 ?

Co1 Sb2 Co1 111.53(6) 27_445 27_455 ?

Co1 Sb2 Co1 71.55(3) 25_455 27_455 ?

Fe2 Sb2 Co1 0.0 27_455 27_455 ?

Fe2 Sb2 Co1 71.5 25 27_455 ?

Fe2 Sb2 Co1 71.5 27_445 25 ?

Fe2 Sb2 Co1 111.5 25_455 25 ?

Co1 Sb2 Co1 71.55(3) 27_445 25 ?

Co1 Sb2 Co1 111.53(6) 25_455 25 ?

Fe2 Sb2 Co1 71.5 27_455 25 ?

Fe2 Sb2 Co1 0.0 25 25 ?

Co1 Sb2 Co1 71.55(3) 27_455 25 ?

Fe2 Sb2 Fe1 55.76(3) 27_445 . ?

Fe2 Sb2 Fe1 55.76(3) 25_455 . ?

Co1 Sb2 Fe1 55.76(3) 27_445 . ?

Co1 Sb2 Fe1 55.76(3) 25_455 . ?

Fe2 Sb2 Fe1 55.76(3) 27_455 . ?

Fe2 Sb2 Fe1 55.76(3) 25 . ?

Co1 Sb2 Fe1 55.76(3) 27_455 . ?

Co1 Sb2 Fe1 55.76(3) 25 . ?

Fe2 Sb2 Pr1 137.430(12) 27_445 25 ?

Fe2 Sb2 Pr1 137.430(12) 25_455 25 ?

Co1 Sb2 Pr1 137.430(12) 27_445 25 ?

Co1 Sb2 Pr1 137.430(12) 25_455 25 ?

Fe2 Sb2 Pr1 68.38(2) 27_455 25 ?

Fe2 Sb2 Pr1 68.38(2) 25 25 ?

Co1 Sb2 Pr1 68.38(2) 27_455 25 ?

Co1 Sb2 Pr1 68.38(2) 25 25 ?

Fe1 Sb2 Pr1 109.093(18) . 25 ?

Fe2 Sb2 Pr1 68.38(2) 27_445 25_445 ?

Fe2 Sb2 Pr1 68.38(2) 25_455 25_445 ?

Co1 Sb2 Pr1 68.38(2) 27_445 25_445 ?

Co1 Sb2 Pr1 68.38(2) 25_455 25_445 ?

Fe2 Sb2 Pr1 137.430(12) 27_455 25_445 ?

Fe2 Sb2 Pr1 137.430(12) 25 25_445 ?

Co1 Sb2 Pr1 137.430(12) 27_455 25_445 ?

Co1 Sb2 Pr1 137.430(12) 25 25_445 ?

Fe1 Sb2 Pr1 109.093(18) . 25_445 ?

Pr1 Sb2 Pr1 141.81(4) 25 25_445 ?

Fe2 Sb2 Pr1 137.430(12) 27_445 25_455 ?

Fe2 Sb2 Pr1 68.38(2) 25_455 25_455 ?

Co1 Sb2 Pr1 137.430(12) 27_445 25_455 ?

Co1 Sb2 Pr1 68.38(2) 25_455 25_455 ?

Fe2 Sb2 Pr1 68.38(2) 27_455 25_455 ?

Fe2 Sb2 Pr1 137.430(12) 25 25_455 ?

Co1 Sb2 Pr1 68.38(2) 27_455 25_455 ?

Co1 Sb2 Pr1 137.430(12) 25 25_455 ?

Fe1 Sb2 Pr1 109.093(18) . 25_455 ?

Pr1 Sb2 Pr1 83.858(11) 25 25_455 ?

Pr1 Sb2 Pr1 83.858(11) 25_445 25_455 ?

Sb3 Sb3 Co1 119.68(9) 17_556 . ?

Sb3 Sb3 Fe2 119.68(9) 17_556 3 ?

Co1 Sb3 Fe2 75.8 . 3 ?

Sb3 Sb3 Fe2 119.68(9) 17_556 1_545 ?

Co1 Sb3 Fe2 120.6 . 1_545 ?

Fe2 Sb3 Fe2 75.81(8) 3 1_545 ?

Sb3 Sb3 Co1 119.68(9) 17_556 3 ?

Co1 Sb3 Co1 75.81(8) . 3 ?

Fe2 Sb3 Co1 0.0 3 3 ?

Fe2 Sb3 Co1 75.8 1_545 3 ?

Sb3 Sb3 Co1 119.68(9) 17_556 1_545 ?

Co1 Sb3 Co1 120.64(18) . 1_545 ?

Fe2 Sb3 Co1 75.8 3 1_545 ?

Fe2 Sb3 Co1 0.0 1_545 1_545 ?

Co1 Sb3 Co1 75.81(8) 3 1_545 ?

Sb3 Sb3 Fe2 119.68(9) 17_556 3_655 ?

Co1 Sb3 Fe2 75.8 . 3_655 ?

Fe2 Sb3 Fe2 120.64(18) 3 3_655 ?

Fe2 Sb3 Fe2 75.81(8) 1_545 3_655 ?

Co1 Sb3 Fe2 120.64(18) 3 3_655 ?

Co1 Sb3 Fe2 75.81(8) 1_545 3_655 ?

Sb3 Sb3 Co1 119.68(9) 17_556 3_655 ?

Co1 Sb3 Co1 75.81(8) . 3_655 ?

Fe2 Sb3 Co1 120.6 3 3_655 ?

Fe2 Sb3 Co1 75.8 1_545 3_655 ?

Co1 Sb3 Co1 120.64(18) 3 3_655 ?

Co1 Sb3 Co1 75.81(8) 1_545 3_655 ?

Fe2 Sb3 Co1 0.0 3_655 3_655 ?

Sb3 Sb3 Fe2 54.93(8) 17_556 19_556 ?

Co1 Sb3 Fe2 106.5 . 19_556 ?

Fe2 Sb3 Fe2 174.61(16) 3 19_556 ?

Fe2 Sb3 Fe2 106.53(3) 1_545 19_556 ?

Co1 Sb3 Fe2 174.61(16) 3 19_556 ?

Co1 Sb3 Fe2 106.53(3) 1_545 19_556 ?

Fe2 Sb3 Fe2 64.76(6) 3_655 19_556 ?

Co1 Sb3 Fe2 64.76(6) 3_655 19_556 ?

Sb3 Sb3 Fe2 54.93(8) 17_556 17_566 ?

Co1 Sb3 Fe2 64.8 . 17_566 ?

Fe2 Sb3 Fe2 106.53(3) 3 17_566 ?

Fe2 Sb3 Fe2 174.61(16) 1_545 17_566 ?

Co1 Sb3 Fe2 106.53(3) 3 17_566 ?

Co1 Sb3 Fe2 174.61(16) 1_545 17_566 ?

Fe2 Sb3 Fe2 106.53(3) 3_655 17_566 ?

Co1 Sb3 Fe2 106.53(3) 3_655 17_566 ?

Fe2 Sb3 Fe2 70.72(8) 19_556 17_566 ?

Sb3 Sb3 Co1 54.93(8) 17_556 17_566 ?

Co1 Sb3 Co1 64.76(6) . 17_566 ?

Fe2 Sb3 Co1 106.5 3 17_566 ?

Fe2 Sb3 Co1 174.6 1_545 17_566 ?

Co1 Sb3 Co1 106.53(3) 3 17_566 ?

Co1 Sb3 Co1 174.61(16) 1_545 17_566 ?

Fe2 Sb3 Co1 106.5 3_655 17_566 ?

Co1 Sb3 Co1 106.53(3) 3_655 17_566 ?

Fe2 Sb3 Co1 70.7 19_556 17_566 ?

Fe2 Sb3 Co1 0.0 17_566 17_566 ?

_refine_diff_density_max 6.146

_refine_diff_density_min -4.634

_refine_diff_density_rms 0.735

_shelx_res_file

;

shelx.res created by SHELXL-2014/7

TITL scd0491_JB65_290K in I4/mmm

CELL 0.71073 4.30210 4.30210 25.69580 90.0000 90.0000 90.0000

ZERR 2.00 0.00030 0.00030 0.00190 0.0000 0.0000 0.0000

LATT 2

SYMM -X, -Y, Z

SYMM -Y, X, Z

SYMM Y, -X, Z

SYMM -X, Y, -Z

SYMM X, -Y, -Z

SYMM Y, X, -Z

SYMM -Y, -X, -Z

SFAC FE CO SB PR

UNIT 2 6 10 2

TEMP 76.850

ACTA

L.S. 15

BOND

FMAP 2

PLAN 20

EXYZ CO1 FE2

EADP CO1 FE2

WGHT 0.050200 14.379399

EXTI 0.003137

FVAR 0.05622 0.80676 0.44484

PR1 4 0.000000 0.000000 0.348810 10.12500 0.00752 0.00752 =

0.00933 0.00000 0.00000 0.00000

FE1 1 0.000000 0.000000 0.000000 20.06250 0.00534 0.00534 =

0.00401 0.00000 0.00000 0.00000

CO1 2 0.000000 0.500000 0.446755 10.14930 0.00602 0.02059 =

0.00682 0.00000 0.00000 0.00000

FE2 1 0.000000 0.500000 0.446755 10.03486 0.00602 0.02059 =

0.00682 0.00000 0.00000 0.00000

SB1 3 0.000000 0.500000 0.250000 10.12500 0.00660 0.00660 =

0.00779 0.00000 0.00000 0.00000

SB2 3 0.000000 0.000000 0.110214 10.12500 0.00730 0.00730 =

0.01103 0.00000 0.00000 0.00000

SB3 3 0.000000 0.000000 0.494468

30.12500 0.02223 0.02223 =

0.01355 0.00000 0.00000 0.00000

HKLF 4

REM scd0491_JB65_290K in I4/mmm

REM R1 = 0.0433 for 587 Fo > 4sig(Fo) and 0.0487 for all 653 data

REM 21 parameters refined using 0 restraints

END

WGHT 0.0502 14.3006

REM Highest difference peak 6.146, deepest hole -4.634, 1-sigma level 0.735

Q1 1 0.0815 0.5000 0.2505 10.50000 0.05 6.15

Q2 1 0.0930 0.0000 0.5000 10.25000 0.05 4.25

Q3 1 0.0000 0.0000 0.3885 10.12500 0.05 4.19

Q4 1 0.0000 0.5000 0.3227 10.25000 0.05 3.56

Q5 1 0.0000 0.0000 0.1752 10.12500 0.05 3.36

Q6 1 0.0000 0.1357 0.3492 10.50000 0.05 3.28

Q7 1 0.0000 0.4263 0.4484 10.50000 0.05 2.81

Q8 1 0.0000 0.0000 0.3078 10.12500 0.05 2.71

Q9 1 0.0000 0.1387 0.1094 10.50000 0.05 2.70

Q10 1 0.0000 0.5000 0.3852 10.25000 0.05 2.47

Q11 1 0.0000 0.2191 0.2492 10.50000 0.05 2.20

Q12 1 0.0000 0.0582 0.1437 10.50000 0.05 2.02

Q13 1 0.4207 0.0000 0.1374 10.50000 0.05 1.96

Q14 1 0.0000 0.2690 0.3498 10.50000 0.05 1.92

Q15 1 0.2414 0.0000 0.0000 10.25000 0.05 1.92

Q16 1 0.0000 0.5000 0.4303 10.25000 0.05 1.84

Q17 1 0.0551 0.0000 0.4271 10.50000 0.05 1.82

Q18 1 0.4253 0.0000 0.3663 10.50000 0.05 1.72

Q19 1 0.2567 0.5000 0.4495 10.50000 0.05 1.69

Q20 1 0.0000 0.4055 0.4007 10.50000 0.05 1.64

;

_shelx_res_checksum 32316

;

_shelx_hkl_checksum 12292

#===END

A2.4 $Pr_2Fe_{4-x}Co_xSb_5$ (x ~ 3)

data_shelx

_audit_update_record

;

2015-07-10 # Formatted by publCIF

;

_audit_creation_method 'SHELXL-2014/7'

_shelx_SHELXL_version_number '2014/7'

_chemical_name_systematic ?

_chemical_name_common ?

_chemical_melting_point ?

_chemical_formula_moiety 'Co3 Fe Pr2 Sb5'

_chemical_formula_sum

'Co3 Fe Pr2 Sb5'

_chemical_formula_weight 1123.21

loop_

_atom_type_symbol

_atom_type_description

_atom_type_scat_dispersion_real

_atom_type_scat_dispersion_imag

_atom_type_scat_source

'Fe' 'Fe' 0.3463 0.8444

'International Tables Vol C Tables 4.2.6.8 and 6.1.1.4'

'Co' 'Co' 0.3494 0.9721

'International Tables Vol C Tables 4.2.6.8 and 6.1.1.4'

'Sb' 'Sb' -0.5866 1.5461

'International Tables Vol C Tables 4.2.6.8 and 6.1.1.4'

'Pr' 'Pr' -0.2180 2.8214

'International Tables Vol C Tables 4.2.6.8 and 6.1.1.4'

_space_group_crystal_system tetragonal

_space_group_IT_number 139

_space_group_name_H-M_alt 'I 4/m m m'

_space_group_name_Hall '-I 4 2'

_shelx_space_group_comment

;

The symmetry employed for this shelxl refinement is uniquely defined

by the following loop, which should always be used as a source of

symmetry information in preference to the above space-group names.

They are only intended as comments.

;

loop_

_space_group_symop_operation_xyz

'x, y, z'

'-x, -y, z'

'-y, x, z'

'y, -x, z'

'-x, y, -z'

'x, -y, -z'

'y, x, -z'

'-y, -x, -z'

'x+1/2, y+1/2, z+1/2'

'-x+1/2, -y+1/2, z+1/2'

'-y+1/2, x+1/2, z+1/2'

'y+1/2, -x+1/2, z+1/2'

'-x+1/2, y+1/2, -z+1/2'

'x+1/2, -y+1/2, -z+1/2'

'y+1/2, x+1/2, -z+1/2'

'-y+1/2, -x+1/2, -z+1/2'

'-x, -y, -z'

'x, y, -z'

'y, -x, -z'

'-y, x, -z'

'x, -y, z'

'-x, y, z'

'-y, -x, z'

'y, x, z'

'-x+1/2, -y+1/2, -z+1/2'

'x+1/2, y+1/2, -z+1/2'

'y+1/2, -x+1/2, -z+1/2'

'-y+1/2, x+1/2, -z+1/2'

'x+1/2, -y+1/2, z+1/2'

'-x+1/2, y+1/2, z+1/2'

'-y+1/2, -x+1/2, z+1/2'

'y+1/2, x+1/2, z+1/2'

_cell_length_a
4.29730(10)

_cell_length_b
4.29730(10)

_cell_length_c
25.7164(9)

_cell_angle_alpha
90

_cell_angle_beta
90

_cell_angle_gamma
90

_cell_volume
474.90(3)

_cell_formula_units_Z
2

_cell_measurement_temperature 571(2)

_cell_measurement_reflns_used ?

_cell_measurement_theta_min ?

_cell_measurement_theta_max ?

_exptl_crystal_description
plate

_exptl_crystal_colour
black

_exptl_crystal_density_meas ?

_exptl_crystal_density_method ?

_exptl_crystal_density_diffrn 7.855

_exptl_crystal_F_000
960

_exptl_transmission_factor_min ?

_exptl_transmission_factor_max ?

_exptl_crystal_size_max
0.04

_exptl_crystal_size_mid
0.03

_exptl_crystal_size_min
0.03

_exptl_absorpt_coefficient_mu 30.499

_shelx_estimated_absorpt_T_min ?

_shelx_estimated_absorpt_T_max ?

_exptl_absorpt_correction_type multi-scan

_exptl_absorpt_correction_T_min 0.240

_exptl_absorpt_correction_T_max 0.403

_exptl_absorpt_process_details SADABS(2014)

_exptl_absorpt_special_details ?

_diffrn_ambient_temperature 571(2)

_diffrn_radiation_wavelength 0.71073

_diffrn_radiation_type
MoK\a

_diffrn_source
'I\mS microfocus tube'

_diffrn_measurement_device_type 'Bruker Kappa D8 Quest CMOS'

_diffrn_measurement_method '\f and \w scans'

_diffrn_detector_area_resol_mean ?

_diffrn_reflns_number
4787

_diffrn_reflns_av_unetI/netI 0.0466

_diffrn_reflns_av_R_equivalents 0.0539

_diffrn_reflns_limit_h_min
-10

_diffrn_reflns_limit_h_max 10

_diffrn_reflns_limit_k_min -8

_diffrn_reflns_limit_k_max 5

_diffrn_reflns_limit_l_min -63

_diffrn_reflns_limit_l_max 64

_diffrn_reflns_theta_min 3.169

_diffrn_reflns_theta_max 62.684

_diffrn_reflns_theta_full 25.242

_diffrn_measured_fraction_theta_max 0.924

_diffrn_measured_fraction_theta_full 0.988

_diffrn_reflns_Laue_measured_fraction_max 0.924

_diffrn_reflns_Laue_measured_fraction_full 0.988

_diffrn_reflns_point_group_measured_fraction_max 0.924

_diffrn_reflns_point_group_measured_fraction_full 0.988

_reflns_number_total 1135

_reflns_number_gt 983

_reflns_threshold_expression 'I > 2\s(I)'

_reflns_Friedel_coverage 0.000

_reflns_Friedel_fraction_max .

_reflns_Friedel_fraction_full .

_reflns_special_details

;

Reflections were merged by SHELXL according to the crystal

class for the calculation of statistics and refinement.

_reflns_Friedel_fraction is defined as the number of unique

Friedel pairs measured divided by the number that would be

possible theoretically, ignoring centric projections and

systematic absences.

;

_computing_data_collection 'Bruker APEX2'

_computing_cell_refinement 'Bruker SAINT'

_computing_data_reduction 'Bruker SAINT'

_computing_structure_solution 'SHELXS Direct Methods (Sheldrick, 2013)'

_computing_structure_refinement 'SHELXL-2014/7 (Sheldrick, 2014)'

_computing_molecular_graphics CrystalMaker

_computing_publication_material 'publCIF (Westrip, 2014)'

_refine_special_details ?

_refine_ls_structure_factor_coef Fsqd

_refine_ls_matrix_type full

_refine_ls_weighting_scheme calc

_refine_ls_weighting_details

'w=1/[\s^2^(Fo^2^)+(0.0479P)^2^+14.2442P] where P=(Fo^2^+2Fc^2^)/3'

_atom_sites_solution_primary ?

_atom_sites_solution_secondary ?

_atom_sites_solution_hydrogens .

_refine_ls_hydrogen_treatment undef

_refine_ls_extinction_method 'SHELXL-2014/7 (Sheldrick 2014'

_refine_ls_extinction_coef 0.0037(5)

_refine_ls_extinction_expression

'Fc^*^=kFc[1+0.001xFc^2^\l^3^/sin(2\q)]^-1/4^'

_refine_ls_number_reflns 1135

_refine_ls_number_parameters 21

_refine_ls_number_restraints 0

_refine_ls_R_factor_all 0.0511

_refine_ls_R_factor_gt 0.0435

_refine_ls_wR_factor_ref 0.1187

_refine_ls_wR_factor_gt 0.1152

_refine_ls_goodness_of_fit_ref 1.159

_refine_ls_restrained_S_all 1.159

_refine_ls_shift/su_max 0.000

_refine_ls_shift/su_mean 0.000

loop_

_atom_site_label

_atom_site_type_symbol

_atom_site_fract_x

_atom_site_fract_y

_atom_site_fract_z

_atom_site_U_iso_or_equiv

_atom_site_adp_type

_atom_site_occupancy

_atom_site_site_symmetry_order

_atom_site_calc_flag

_atom_site_refinement_flags_posn

_atom_site_refinement_flags_adp

_atom_site_refinement_flags_occupancy

_atom_site_disorder_assembly

_atom_site_disorder_group

Pr1 Pr 0.0000 0.0000 0.34890(2) 0.00595(7) Uani 1 8 d S T P . .

CO1 Fe 0.0000 0.0000 0.0000 0.0046(3) Uani 0.871(13) 16 d S T P . .

Co2 Co 0.0000 0.5000 0.44665(4) 0.0099(2) Uani 0.818(8) 4 d S T P . .

Sb1 Sb 0.0000 0.5000 0.2500 0.00521(7) Uani 1 8 d S T P . .

Sb2 Sb 0.0000 0.0000 0.11027(2) 0.00628(8) Uani 1 8 d S T P . .

Sb3 Sb 0.0000 0.0000 0.5000 0.0241(4) Uani 0.942(9) 16 d S T P . .

loop_

_atom_site_aniso_label

_atom_site_aniso_U_11

_atom_site_aniso_U_22

_atom_site_aniso_U_33

_atom_site_aniso_U_23

_atom_site_aniso_U_13

_atom_site_aniso_U_12

Pr1 0.00550(9) 0.00550(9) 0.00684(12) 0.000 0.000 0.000

CO1 0.0047(4) 0.0047(4) 0.0045(5) 0.000 0.000 0.000

Co2 0.0057(3) 0.0166(5) 0.0075(3) 0.000 0.000 0.000

Sb1 0.00500(9) 0.00500(9) 0.00564(12) 0.000 0.000 0.000

Sb2 0.00514(10) 0.00514(10) 0.00856(15) 0.000 0.000 0.000

Sb3 0.0178(4) 0.0178(4) 0.0368(9) 0.000 0.000 0.000

_geom_special_details

;

All esds (except the esd in the dihedral angle between two l.s. planes)

are estimated using the full covariance matrix. The cell esds are taken

into account individually in the estimation of esds in distances, angles

and torsion angles; correlations between esds in cell parameters are only

used when they are defined by crystal symmetry. An approximate (isotropic)

treatment of cell esds is used for estimating esds involving l.s. planes.

;

loop_

_geom_bond_atom_site_label_1

_geom_bond_atom_site_label_2

_geom_bond_distance

_geom_bond_site_symmetry_2

_geom_bond_publ_flag

Pr1 Sb2 3.2150(2) 25 ?

Pr1 Sb2 3.2150(2) 25_445 ?

Pr1 Sb2 3.2150(2) 25_455 ?

Pr1 Sb2 3.2150(2) 25_545 ?

Pr1 Co2 3.3069(9) . ?

Pr1 Co2 3.3069(9) 3_655 ?

Pr1 Co2 3.3069(9) 1_545 ?

Pr1 Co2 3.3069(9) 3 ?

Pr1 Sb1 3.3295(3) 1_545 ?

Pr1 Sb1 3.3295(3) 25_455 ?

Pr1 Sb1 3.3295(3) . ?

Pr1 Sb1 3.3295(3) 25 ?

CO1 Co2 2.5493(6) 27_455 ?

CO1 Co2 2.5493(6) 11_544 ?

CO1 Co2 2.5493(6) 9_444 ?

CO1 Co2 2.5493(6) 25 ?

CO1 Co2 2.5493(6) 27_445 ?

CO1 Co2 2.5493(6) 25_455 ?

CO1 Co2 2.5493(6) 9_544 ?

CO1 Co2 2.5493(6) 11_554 ?

CO1 Sb2 2.8356(6) . ?

CO1 Sb2 2.8357(6) 17 ?

CO1 Sb3 3.03865(7) 9_554 ?

CO1 Sb3 3.03865(7) 9_444 ?

Co2 Sb3 2.5494(6) 1_565 ?

Co2 CO1 2.5494(6) 9 ?

Co2 Sb3 2.5494(6) . ?

Co2 CO1 2.5494(6) 9_455 ?

Co2 Sb2 2.5998(7) 25_455 ?

Co2 Sb2 2.5998(7) 25 ?

Co2 Co2 2.744(2) 17_566 ?

Co2 Pr1 3.3069(9) 1_565 ?

Sb1 Sb1 3.03865(7) 25_565 ?

Sb1 Sb1 3.03865(7) 25_455 ?

Sb1 Sb1 3.03865(7) 25_465 ?

Sb1 Sb1 3.03865(7) 25 ?

Sb1 Pr1 3.3295(3) 25_455 ?

Sb1 Pr1 3.3295(3) 1_565 ?

Sb1 Pr1 3.3295(3) 25 ?

Sb2 Co2 2.5998(7) 27_445 ?

Sb2 Co2 2.5998(7) 25_455 ?

Sb2 Co2 2.5998(7) 27_455 ?

Sb2 Co2 2.5998(7) 25 ?

Sb2 Pr1 3.2150(2) 25 ?

Sb2 Pr1 3.2150(2) 25_445 ?

Sb2 Pr1 3.2150(2) 25_545 ?

Sb2 Pr1 3.2150(2) 25_455 ?

Sb3 Co2 2.5493(6) 19_556 ?

Sb3 Co2 2.5493(6) 3 ?

Sb3 Co2 2.5493(6) 17_566 ?

Sb3 Co2 2.5493(6) 1_545 ?

Sb3 Co2 2.5493(6) 19_456 ?

Sb3 Co2 2.5493(6) 3_655 ?

Sb3 Co2 2.5493(6) 17_556 ?

Sb3 CO1 3.03865(7) 9 ?

Sb3 CO1 3.03865(7) 9_445 ?

Sb3 CO1 3.03865(7) 9_545 ?

Sb3 CO1 3.03865(7) 9_455 ?

loop_

_geom_angle_atom_site_label_1

_geom_angle_atom_site_label_2

_geom_angle_atom_site_label_3

_geom_angle

_geom_angle_site_symmetry_1

_geom_angle_site_symmetry_3

_geom_angle_publ_flag

Sb2 Pr1 Sb2 141.87(2) 25 25_445 ?

Sb2 Pr1 Sb2 83.876(8) 25 25_455 ?

Sb2 Pr1 Sb2 83.876(8) 25_445 25_455 ?

Sb2 Pr1 Sb2 83.876(8) 25 25_545 ?

Sb2 Pr1 Sb2 83.876(8) 25_445 25_545 ?

Sb2 Pr1 Sb2 141.87(2) 25_455 25_545 ?

Sb2 Pr1 Co2 46.959(10) 25 . ?

Sb2 Pr1 Co2 100.718(16) 25_445 . ?

Sb2 Pr1 Co2 46.959(10) 25_455 . ?

Sb2 Pr1 Co2 100.718(16) 25_545 . ?

Sb2 Pr1 Co2 46.959(10) 25 3_655 ?

Sb2 Pr1 Co2 100.718(16) 25_445 3_655 ?

Sb2 Pr1 Co2 100.718(16) 25_455 3_655 ?

Sb2 Pr1 Co2 46.959(10) 25_545 3_655 ?

Co2 Pr1 Co2 54.703(16) . 3_655 ?

Sb2 Pr1 Co2 100.718(16) 25 1_545 ?

Sb2 Pr1 Co2 46.959(10) 25_445 1_545 ?

Sb2 Pr1 Co2 100.718(16) 25_455 1_545 ?

Sb2 Pr1 Co2 46.959(10) 25_545 1_545 ?

Co2 Pr1 Co2 81.05(3) . 1_545 ?

Co2 Pr1 Co2 54.703(16) 3_655 1_545 ?

Sb2 Pr1 Co2 100.718(16) 25 3 ?

Sb2 Pr1 Co2 46.959(10) 25_445 3 ?

Sb2 Pr1 Co2 46.959(10) 25_455 3 ?

Sb2 Pr1 Co2 100.718(16) 25_545 3 ?

Co2 Pr1 Co2 54.703(16) . 3 ?

Co2 Pr1 Co2 81.05(3) 3_655 3 ?

Co2 Pr1 Co2 54.703(16) 1_545 3 ?

Sb2 Pr1 Sb1 132.906(11) 25 1_545 ?

Sb2 Pr1 Sb1 79.525(9) 25_445 1_545 ?

Sb2 Pr1 Sb1 132.906(11) 25_455 1_545 ?

Sb2 Pr1 Sb1 79.525(9) 25_545 1_545 ?

Co2 Pr1 Sb1 179.668(15) . 1_545 ?

Co2 Pr1 Sb1 125.498(8) 3_655 1_545 ?

Co2 Pr1 Sb1 99.286(13) 1_545 1_545 ?

Co2 Pr1 Sb1 125.498(8) 3 1_545 ?

Sb2 Pr1 Sb1 132.906(11) 25 25_455 ?

Sb2 Pr1 Sb1 79.525(9) 25_445 25_455 ?

Sb2 Pr1 Sb1 79.525(9) 25_455 25_455 ?

Sb2 Pr1 Sb1 132.906(11) 25_545 25_455 ?

Co2 Pr1 Sb1 125.498(8) . 25_455 ?

Co2 Pr1 Sb1 179.668(15) 3_655 25_455 ?

Co2 Pr1 Sb1 125.498(8) 1_545 25_455 ?

Co2 Pr1 Sb1 99.286(13) 3 25_455 ?

Sb1 Pr1 Sb1 54.300(6) 1_545 25_455 ?

Sb2 Pr1 Sb1 79.525(9) 25 . ?

Sb2 Pr1 Sb1 132.906(11) 25_445 . ?

Sb2 Pr1 Sb1 79.525(9) 25_455 . ?

Sb2 Pr1 Sb1 132.906(11) 25_545 . ?

Co2 Pr1 Sb1 99.286(13) . . ?

Co2 Pr1 Sb1 125.498(8) 3_655 . ?

Co2 Pr1 Sb1 179.668(15) 1_545 . ?

Co2 Pr1 Sb1 125.498(8) 3 . ?

Sb1 Pr1 Sb1 80.382(10) 1_545 . ?

Sb1 Pr1 Sb1 54.300(6) 25_455 . ?

Sb2 Pr1 Sb1 79.525(9) 25 25 ?

Sb2 Pr1 Sb1 132.906(11) 25_445 25 ?

Sb2 Pr1 Sb1 132.906(11) 25_455 25 ?

Sb2 Pr1 Sb1 79.525(9) 25_545 25 ?

Co2 Pr1 Sb1 125.498(8) . 25 ?

Co2 Pr1 Sb1 99.286(13) 3_655 25 ?

Co2 Pr1 Sb1 125.498(8) 1_545 25 ?

Co2 Pr1 Sb1 179.668(15) 3 25 ?

Sb1 Pr1 Sb1 54.300(6) 1_545 25 ?

Sb1 Pr1 Sb1 80.382(10) 25_455 25 ?

Sb1 Pr1 Sb1 54.300(6) . 25 ?

Co2 CO1 Co2 180.00(4) 27_455 11_544 ?

Co2 CO1 Co2 106.84(2) 27_455 9_444 ?

Co2 CO1 Co2 73.16(2) 11_544 9_444 ?

Co2 CO1 Co2 73.16(2) 27_455 25 ?

Co2 CO1 Co2 106.84(2) 11_544 25 ?

Co2 CO1 Co2 180.00(4) 9_444 25 ?

Co2 CO1 Co2 114.88(4) 27_455 27_445 ?

Co2 CO1 Co2 65.12(4) 11_544 27_445 ?

Co2 CO1 Co2 106.84(2) 9_444 27_445 ?

Co2 CO1 Co2 73.16(2) 25 27_445 ?

Co2 CO1 Co2 73.16(2) 27_455 25_455 ?

Co2 CO1 Co2 106.84(2) 11_544 25_455 ?

Co2 CO1 Co2 65.12(4) 9_444 25_455 ?

Co2 CO1 Co2 114.88(4) 25 25_455 ?

Co2 CO1 Co2 73.16(2) 27_445 25_455 ?

Co2 CO1 Co2 106.84(2) 27_455 9_544 ?

Co2 CO1 Co2 73.16(2) 11_544 9_544 ?

Co2 CO1 Co2 114.88(4) 9_444 9_544 ?

Co2 CO1 Co2 65.12(4) 25 9_544 ?

Co2 CO1 Co2 106.84(2) 27_445 9_544 ?

Co2 CO1 Co2 180.00(4) 25_455 9_544 ?

Co2 CO1 Co2 65.12(4) 27_455 11_554 ?

Co2 CO1 Co2 114.88(4) 11_544 11_554 ?

Co2 CO1 Co2 73.16(2) 9_444 11_554 ?

Co2 CO1 Co2 106.84(2) 25 11_554 ?

Co2 CO1 Co2 180.00(4) 27_445 11_554 ?

Co2 CO1 Co2 106.84(2) 25_455 11_554 ?

Co2 CO1 Co2 73.16(2) 9_544 11_554 ?

Co2 CO1 Sb2 57.44(2) 27_455 . ?

Co2 CO1 Sb2 122.56(2) 11_544 . ?

Co2 CO1 Sb2 122.56(2) 9_444 . ?

Co2 CO1 Sb2 57.44(2) 25 . ?

Co2 CO1 Sb2 57.44(2) 27_445 . ?

Co2 CO1 Sb2 57.44(2) 25_455 . ?

Co2 CO1 Sb2 122.56(2) 9_544 . ?

Co2 CO1 Sb2 122.56(2) 11_554 . ?

Co2 CO1 Sb2 122.56(2) 27_455 17 ?

Co2 CO1 Sb2 57.44(2) 11_544 17 ?

Co2 CO1 Sb2 57.44(2) 9_444 17 ?

Co2 CO1 Sb2 122.56(2) 25 17 ?

Co2 CO1 Sb2 122.56(2) 27_445 17 ?

Co2 CO1 Sb2 122.56(2) 25_455 17 ?

Co2 CO1 Sb2 57.44(2) 9_544 17 ?

Co2 CO1 Sb2 57.44(2) 11_554 17 ?

Sb2 CO1 Sb2 180.0 . 17 ?

Co2 CO1 Sb3 53.418(10) 27_455 9_554 ?

Co2 CO1 Sb3 126.582(10) 11_544 9_554 ?

Co2 CO1 Sb3 126.582(10) 9_444 9_554 ?

Co2 CO1 Sb3 53.418(10) 25 9_554 ?

Co2 CO1 Sb3 126.582(10) 27_445 9_554 ?

Co2 CO1 Sb3 126.582(10) 25_455 9_554 ?

Co2 CO1 Sb3 53.418(10) 9_544 9_554 ?

Co2 CO1 Sb3 53.418(10) 11_554 9_554 ?

Sb2 CO1 Sb3 90.0 . 9_554 ?

Sb2 CO1 Sb3 90.0 17 9_554 ?

Co2 CO1 Sb3 126.582(10) 27_455 9_444 ?

Co2 CO1 Sb3 53.418(10) 11_544 9_444 ?

Co2 CO1 Sb3 53.418(10) 9_444 9_444 ?

Co2 CO1 Sb3 126.582(10) 25 9_444 ?

Co2 CO1 Sb3 53.418(10) 27_445 9_444 ?

Co2 CO1 Sb3 53.418(10) 25_455 9_444 ?

Co2 CO1 Sb3 126.582(10) 9_544 9_444 ?

Co2 CO1 Sb3 126.582(10) 11_554 9_444 ?

Sb2 CO1 Sb3 90.0 . 9_444 ?

Sb2 CO1 Sb3 90.0 17 9_444 ?

Sb3 CO1 Sb3 180.0 9_554 9_444 ?

Sb3 Co2 CO1 73.16(2) 1_565 9 ?

Sb3 Co2 Sb3 114.88(4) 1_565 . ?

CO1 Co2 Sb3 73.16(2) 9 . ?

Sb3 Co2 CO1 73.16(2) 1_565 9_455 ?

CO1 Co2 CO1 114.88(4) 9 9_455 ?

Sb3 Co2 CO1 73.16(2) . 9_455 ?

Sb3 Co2 Sb2 107.637(5) 1_565 25_455 ?

CO1 Co2 Sb2 178.30(4) 9 25_455 ?

Sb3 Co2 Sb2 107.637(5) . 25_455 ?

CO1 Co2 Sb2 66.823(10) 9_455 25_455 ?

Sb3 Co2 Sb2 107.637(5) 1_565 25 ?

CO1 Co2 Sb2 66.823(11) 9 25 ?

Sb3 Co2 Sb2 107.637(5) . 25 ?

CO1 Co2 Sb2 178.30(4) 9_455 25 ?

Sb2 Co2 Sb2 111.48(4) 25_455 25 ?

Sb3 Co2 Co2 57.44(2) 1_565 17_566 ?

CO1 Co2 Co2 57.44(2) 9 17_566 ?

Sb3 Co2 Co2 57.44(2) . 17_566 ?

CO1 Co2 Co2 57.44(2) 9_455 17_566 ?

Sb2 Co2 Co2 124.26(2) 25_455 17_566 ?

Sb2 Co2 Co2 124.26(2) 25 17_566 ?

Sb3 Co2 Pr1 163.08(3) 1_565 . ?

CO1 Co2 Pr1 114.148(10) 9 . ?

Sb3 Co2 Pr1 82.037(10) . . ?

CO1 Co2 Pr1 114.148(10) 9_455 . ?

Sb2 Co2 Pr1 64.66(2) 25_455 . ?

Sb2 Co2 Pr1 64.66(2) 25 . ?

Co2 Co2 Pr1 139.477(13) 17_566 . ?

Sb3 Co2 Pr1 82.038(10) 1_565 1_565 ?

CO1 Co2 Pr1 114.149(10) 9 1_565 ?

Sb3 Co2 Pr1 163.08(3) . 1_565 ?

CO1 Co2 Pr1 114.149(10) 9_455 1_565 ?

Sb2 Co2 Pr1 64.66(2) 25_455 1_565 ?

Sb2 Co2 Pr1 64.66(2) 25 1_565 ?

Co2 Co2 Pr1 139.477(13) 17_566 1_565 ?

Pr1 Co2 Pr1 81.05(3) . 1_565 ?

Sb1 Sb1 Sb1 180.0 25_565 25_455 ?

Sb1 Sb1 Sb1 90.0 25_565 25_465 ?

Sb1 Sb1 Sb1 90.0 25_455 25_465 ?

Sb1 Sb1 Sb1 90.0 25_565 25 ?

Sb1 Sb1 Sb1 90.0 25_455 25 ?

Sb1 Sb1 Sb1 180.0 25_465 25 ?

Sb1 Sb1 Pr1 117.150(3) 25_565 25_455 ?

Sb1 Sb1 Pr1 62.850(3) 25_455 25_455 ?

Sb1 Sb1 Pr1 62.850(3) 25_465 25_455 ?

Sb1 Sb1 Pr1 117.150(3) 25 25_455 ?

Sb1 Sb1 Pr1 62.850(3) 25_565 1_565 ?

Sb1 Sb1 Pr1 117.150(3) 25_455 1_565 ?

Sb1 Sb1 Pr1 62.850(3) 25_465 1_565 ?

Sb1 Sb1 Pr1 117.150(3) 25 1_565 ?

Pr1 Sb1 Pr1 125.699(6) 25_455 1_565 ?

Sb1 Sb1 Pr1 62.850(3) 25_565 25 ?

Sb1 Sb1 Pr1 117.150(3) 25_455 25 ?

Sb1 Sb1 Pr1 117.150(3) 25_465 25 ?

Sb1 Sb1 Pr1 62.850(3) 25 25 ?

Pr1 Sb1 Pr1 80.383(10) 25_455 25 ?

Pr1 Sb1 Pr1 125.699(6) 1_565 25 ?

Sb1 Sb1 Pr1 117.150(3) 25_565 . ?

Sb1 Sb1 Pr1 62.850(3) 25_455 . ?

Sb1 Sb1 Pr1 117.150(3) 25_465 . ?

Sb1 Sb1 Pr1 62.850(3) 25 . ?

Pr1 Sb1 Pr1 125.700(6) 25_455 . ?

Pr1 Sb1 Pr1 80.383(10) 1_565 . ?

Pr1 Sb1 Pr1 125.700(6) 25 . ?

Co2 Sb2 Co2 71.52(2) 27_445 25_455 ?

Co2 Sb2 Co2 111.48(4) 27_445 27_455 ?

Co2 Sb2 Co2 71.52(2) 25_455 27_455 ?

Co2 Sb2 Co2 71.52(2) 27_445 25 ?

Co2 Sb2 Co2 111.48(4) 25_455 25 ?

Co2 Sb2 Co2 71.52(2) 27_455 25 ?

Co2 Sb2 CO1 55.74(2) 27_445 . ?

Co2 Sb2 CO1 55.74(2) 25_455 . ?

Co2 Sb2 CO1 55.74(2) 27_455 . ?

Co2 Sb2 CO1 55.74(2) 25 . ?

Co2 Sb2 Pr1 137.412(8) 27_445 25 ?

Co2 Sb2 Pr1 137.412(8) 25_455 25 ?

Co2 Sb2 Pr1 68.379(15) 27_455 25 ?

Co2 Sb2 Pr1 68.379(15) 25 25 ?

CO1 Sb2 Pr1 109.064(12) . 25 ?

Co2 Sb2 Pr1 68.379(15) 27_445 25_445 ?

Co2 Sb2 Pr1 68.379(15) 25_455 25_445 ?

Co2 Sb2 Pr1 137.412(8) 27_455 25_445 ?

Co2 Sb2 Pr1 137.412(8) 25 25_445 ?

CO1 Sb2 Pr1 109.064(12) . 25_445 ?

Pr1 Sb2 Pr1 141.87(2) 25 25_445 ?

Co2 Sb2 Pr1 68.379(15) 27_445 25_545 ?

Co2 Sb2 Pr1 137.412(8) 25_455 25_545 ?

Co2 Sb2 Pr1 137.412(8) 27_455 25_545 ?

Co2 Sb2 Pr1 68.379(15) 25 25_545 ?

CO1 Sb2 Pr1 109.064(12) . 25_545 ?

Pr1 Sb2 Pr1 83.876(8) 25 25_545 ?

Pr1 Sb2 Pr1 83.876(8) 25_445 25_545 ?

Co2 Sb2 Pr1 137.412(8) 27_445 25_455 ?

Co2 Sb2 Pr1 68.379(15) 25_455 25_455 ?

Co2 Sb2 Pr1 68.379(15) 27_455 25_455 ?

Co2 Sb2 Pr1 137.412(8) 25 25_455 ?

CO1 Sb2 Pr1 109.064(12) . 25_455 ?

Pr1 Sb2 Pr1 83.876(8) 25 25_455 ?

Pr1 Sb2 Pr1 83.876(8) 25_445 25_455 ?

Pr1 Sb2 Pr1 141.87(2) 25_545 25_455 ?

Co2 Sb3 Co2 180.0 19_556 3 ?

Co2 Sb3 Co2 73.16(2) 19_556 17_566 ?

Co2 Sb3 Co2 106.84(2) 3 17_566 ?

Co2 Sb3 Co2 106.84(2) 19_556 1_545 ?

Co2 Sb3 Co2 73.16(2) 3 1_545 ?

Co2 Sb3 Co2 180.0 17_566 1_545 ?

Co2 Sb3 Co2 114.88(4) 19_556 19_456 ?

Co2 Sb3 Co2 65.12(4) 3 19_456 ?

Co2 Sb3 Co2 73.16(2) 17_566 19_456 ?

Co2 Sb3 Co2 106.84(2) 1_545 19_456 ?

Co2 Sb3 Co2 65.12(4) 19_556 3_655 ?

Co2 Sb3 Co2 114.88(4) 3 3_655 ?

Co2 Sb3 Co2 106.84(2) 17_566 3_655 ?

Co2 Sb3 Co2 73.16(2) 1_545 3_655 ?

Co2 Sb3 Co2 180.00(4) 19_456 3_655 ?

Co2 Sb3 Co2 73.16(2) 19_556 17_556 ?

Co2 Sb3 Co2 106.84(2) 3 17_556 ?

Co2 Sb3 Co2 114.88(4) 17_566 17_556 ?

Co2 Sb3 Co2 65.12(4) 1_545 17_556 ?

Co2 Sb3 Co2 73.16(2) 19_456 17_556 ?

Co2 Sb3 Co2 106.84(2) 3_655 17_556 ?

Co2 Sb3 Co2 106.84(2) 19_556 . ?

Co2 Sb3 Co2 73.16(2) 3 . ?

Co2 Sb3 Co2 65.12(4) 17_566 . ?

Co2 Sb3 Co2 114.88(4) 1_545 . ?

Co2 Sb3 Co2 106.84(2) 19_456 . ?

Co2 Sb3 Co2 73.16(2) 3_655 . ?

Co2 Sb3 Co2 180.00(4) 17_556 . ?

Co2 Sb3 CO1 53.418(10) 19_556 9 ?

Co2 Sb3 CO1 126.582(10) 3 9 ?

Co2 Sb3 CO1 53.418(10) 17_566 9 ?

Co2 Sb3 CO1 126.582(10) 1_545 9 ?

Co2 Sb3 CO1 126.582(10) 19_456 9 ?

Co2 Sb3 CO1 53.418(10) 3_655 9 ?

Co2 Sb3 CO1 126.582(10) 17_556 9 ?

Co2 Sb3 CO1 53.419(10) . 9 ?

Co2 Sb3 CO1 126.582(10) 19_556 9_445 ?

Co2 Sb3 CO1 53.418(10) 3 9_445 ?

Co2 Sb3 CO1 126.582(10) 17_566 9_445 ?

Co2 Sb3 CO1 53.418(10) 1_545 9_445 ?

Co2 Sb3 CO1 53.418(10) 19_456 9_445 ?

Co2 Sb3 CO1 126.582(10) 3_655 9_445 ?

Co2 Sb3 CO1 53.418(10) 17_556 9_445 ?

Co2 Sb3 CO1 126.581(10) . 9_445 ?

CO1 Sb3 CO1 180.0 9 9_445 ?

Co2 Sb3 CO1 53.418(10) 19_556 9_545 ?

Co2 Sb3 CO1 126.582(10) 3 9_545 ?

Co2 Sb3 CO1 126.582(10) 17_566 9_545 ?

Co2 Sb3 CO1 53.418(10) 1_545 9_545 ?

Co2 Sb3 CO1 126.582(10) 19_456 9_545 ?

Co2 Sb3 CO1 53.418(10) 3_655 9_545 ?

Co2 Sb3 CO1 53.418(10) 17_556 9_545 ?

Co2 Sb3 CO1 126.581(10) . 9_545 ?

CO1 Sb3 CO1 90.0 9 9_545 ?

CO1 Sb3 CO1 90.0 9_445 9_545 ?

Co2 Sb3 CO1 126.582(10) 19_556 9_455 ?

Co2 Sb3 CO1 53.418(10) 3 9_455 ?

Co2 Sb3 CO1 53.418(10) 17_566 9_455 ?

Co2 Sb3 CO1 126.582(10) 1_545 9_455 ?

Co2 Sb3 CO1 53.418(10) 19_456 9_455 ?

Co2 Sb3 CO1 126.582(10) 3_655 9_455 ?

Co2 Sb3 CO1 126.582(10) 17_556 9_455 ?

Co2 Sb3 CO1 53.419(10) . 9_455 ?

CO1 Sb3 CO1 90.0 9 9_455 ?

CO1 Sb3 CO1 90.0 9_445 9_455 ?

CO1 Sb3 CO1 180.0 9_545 9_455 ?

_refine_diff_density_max 13.984

_refine_diff_density_min -7.727

_refine_diff_density_rms 0.925

_shelx_res_file

;

shelx.res created by SHELXL-2014/7

TITL pm141_PRFECOSB in I4/mmm

CELL 0.71073 4.29730 4.29730 25.71640 90.0000 90.0000 90.0000

ZERR 2.00 0.00010 0.00010 0.00090 0.0000 0.0000 0.0000

LATT 2

SYMM -X, -Y, Z

SYMM -Y, X, Z

SYMM Y, -X, Z

SYMM -X, Y, -Z

SYMM X, -Y, -Z

SYMM Y, X, -Z

SYMM -Y, -X, -Z

SFAC FE CO SB PR

UNIT 2 6 10 4

TEMP 298

L.S. 12

ACTA

BOND

FMAP 2

PLAN 20

WGHT 0.047900 14.244200

EXTI 0.003716

FVAR 0.05393 0.47091 0.87145 0.81784

PR1 4 0.000000 0.000000 0.348901 10.12500 0.00550 0.00550 =

0.00684 0.00000 0.00000 0.00000

CO1 1 0.000000 0.000000 0.000000 30.06250 0.00468 0.00468 =

0.00446 0.00000 0.00000 0.00000

CO2 2 0.000000 0.500000 0.446647 40.25000 0.00570 0.01660 =

0.00748 0.00000 0.00000 0.00000

SB1 3 0.000000 0.500000 0.250000 10.12500 0.00500 0.00500 =

0.00564 0.00000 0.00000 0.00000

SB2 3 0.000000 0.000000 0.110266 10.12500 0.00514 0.00514 =

0.00856 0.00000 0.00000 0.00000

SB3 3 0.000000 0.000000 0.500000 20.12500 0.01784 0.01784 =

0.03677 0.00000 0.00000 0.00000

HKLF 4

REM pm141_PRFECOSB in I4/mmm

REM R1 = 0.0435 for 983 Fo > 4sig(Fo) and 0.0511 for all 1135 data

REM 21 parameters refined using 0 restraints

END

WGHT 0.0474 14.4464

REM Highest difference peak 13.984, deepest hole -7.727, 1-sigma level 0.925

Q1 1 0.0000 0.0000 0.3976 10.12500 0.05 4.53

Q2 1 0.0000 0.0000 0.5646 10.12500 0.05 4.45

Q3 1 0.0000 0.5000 0.3992 10.25000 0.05 4.44

Q4 1 0.0000 0.0000 0.3067 10.12500 0.05 4.35

Q5 1 0.0000 0.4582 0.3526 10.50000 0.05 3.96

Q6 1 0.0000 0.5000 0.3158 10.25000 0.05 3.46

Q7 1 0.0000 0.0000 0.1616 10.12500 0.05 3.34

Q8 1 0.0000 0.0651 0.0924 10.50000 0.05 2.59

Q9 1 0.0000 0.0000 0.0649 10.12500 0.05 2.49

Q10 1 0.0000 0.0736 0.0543 10.50000 0.05 2.39

Q11 1 0.0000 0.0566 0.1480 10.50000 0.05 2.32

Q12 1 0.1191 0.0000 0.3184 10.50000 0.05 2.09

Q13 1 0.0000 0.5000 0.3686 10.25000 0.05 2.00

Q14 1 0.0778 0.0778 0.3336 10.50000 0.05 1.96

Q15 1 0.0000 0.4401 0.1956 10.50000 0.05 1.93

Q16 1 0.0000 0.5000 0.4855 10.25000 0.05 1.91

Q17 1 0.2646 0.2646 0.3228 10.50000 0.05 1.90

Q18 1 0.0889 0.4190 0.2945 11.00000 0.05 1.87

Q19 1 0.0776 0.0776 0.3633 10.50000 0.05 1.83

Q20 1 0.1303 0.0569 0.3001 11.00000 0.05 1.82

;

_shelx_res_checksum 3234

_shelx_hkl_checksum
10037

#===END

A2.5 Li_2IrO_3

data_analytis6fortho

_audit_update_record

;

2015-07-10 # Formatted by publCIF

;

_audit_creation_method
SHELXL-97

_chemical_name_systematic

;

?

;

_chemical_name_common
?

_chemical_melting_point
?

_chemical_formula_moiety 'Ir Li2 O3'

_chemical_formula_sum

'Ir Li2 O3'

_chemical_formula_weight
254.08

loop_

_atom_type_symbol

_atom_type_description

_atom_type_scat_dispersion_real

_atom_type_scat_dispersion_imag

_atom_type_scat_source

'Li' 'Li' -0.0003 0.0001

'International Tables Vol C Tables 4.2.6.8 and 6.1.1.4'

'O' 'O' 0.0106 0.0060

'International Tables Vol C Tables 4.2.6.8 and 6.1.1.4'

'Ir' 'Ir' -1.4442 7.9887

'International Tables Vol C Tables 4.2.6.8 and 6.1.1.4'

_symmetry_cell_setting
?

_symmetry_space_group_name_H-M ?

loop_

_symmetry_equiv_pos_as_xyz

'x, y, z'

'-x, -y, z'

'x, -y, -z+1/2'

'-x, y, -z+1/2'

'x+1/2, y+1/2, z'

'-x+1/2, -y+1/2, z'

'x+1/2, -y+1/2, -z+1/2'

'-x+1/2, y+1/2, -z+1/2'

'-x, -y, -z'

'x, y, -z'

'-x, y, z-1/2'

'x, -y, z-1/2'

'-x+1/2, -y+1/2, -z'

'x+1/2, y+1/2, -z'

'-x+1/2, y+1/2, z-1/2'

'x+1/2, -y+1/2, z-1/2'

_cell_length_a
5.9083(3)

_cell_length_b
8.4295(5)

_cell_length_c
17.8349(9)

_cell_angle_alpha
90.00

_cell_angle_beta
90.00

_cell_angle_gamma
90.00

_cell_volume
888.25(8)

_cell_formula_units_Z
8

_cell_measurement_temperature 300(2)

_cell_measurement_reflns_used ?

_cell_measurement_theta_min ?

_cell_measurement_theta_max ?

_exptl_crystal_description fragment

_exptl_crystal_colour grey

_exptl_crystal_size_max 0.06

_exptl_crystal_size_mid 0.05

_exptl_crystal_size_min 0.04

_exptl_crystal_density_meas ?

_exptl_crystal_density_diffrn 3.800

_exptl_crystal_density_method 'not measured'

_exptl_crystal_F_000 856

_exptl_absorpt_coefficient_mu 29.903

_exptl_absorpt_correction_type multi-scan

_exptl_absorpt_correction_T_min 0.2670

_exptl_absorpt_correction_T_max 0.3809

_exptl_absorpt_process_details 'HKL scalepack (Otwinski & Minor, 1997)'

_exptl_special_details

;

?

;

_diffrn_ambient_temperature 300(2)

_diffrn_radiation_wavelength 0.71073

_diffrn_radiation_type MoK\a

_diffrn_radiation_source 'fine-focus sealed tube'

_diffrn_radiation_monochromator graphite

_diffrn_measurement_device_type 'Nonius Kappa CCD'

_diffrn_measurement_method '\f and \w scans'

_diffrn_detector_area_resol_mean ?

_diffrn_standards_number ?

_diffrn_standards_interval_count ?

_diffrn_standards_interval_time ?

_diffrn_standards_decay_% ?

_diffrn_reflns_number 17039

_diffrn_reflns_av_R_equivalents 0.1192

_diffrn_reflns_av_sigmaI/netI 0.0561

_diffrn_reflns_limit_h_min -10

_diffrn_reflns_limit_h_max 10

_diffrn_reflns_limit_k_min -14

_diffrn_reflns_limit_k_max 15

_diffrn_reflns_limit_l_min -29

_diffrn_reflns_limit_l_max 32

_diffrn_reflns_theta_min 2.28

_diffrn_reflns_theta_max 40.41

_reflns_number_total 1456

_reflns_number_gt 888

_reflns_threshold_expression >2\s(I)

_computing_data_collection 'Collect (Nonius 1999)'

_computing_cell_refinement 'Denzo and Scalepack (Otwinski & Minor

1997)'

_computing_data_reduction 'Denzo and Scalepack (Otwinski & Minor 1997)'

_computing_structure_solution 'Direct Methods, SIR 97'

_computing_structure_refinement 'SHELXL-97 (Sheldrick, 2008)'

_computing_molecular_graphics 'Crystal Maker'

_computing_publication_material 'Publcif'

_refine_special_details

;

Refinement of F^2^ against ALL reflections. The weighted R-factor wR and

goodness of fit S are based on F^2^, conventional R-factors R are based

on F, with F set to zero for negative F^2^. The threshold expression of

F^2^ > 2\s(F^2^) is used only for calculating R-factors(gt) etc. and is

not relevant to the choice of reflections for refinement. R-factors based

on F^2^ are statistically about twice as large as those based on F, and R-

factors based on ALL data will be even larger.

;

_refine_ls_structure_factor_coef Fsqd

_refine_ls_matrix_type full

_refine_ls_weighting_scheme calc

_refine_ls_weighting_details

'calc w=1/[\s^2^(Fo^2^)+(0.0281P)^2^+0.0000P] where P=(Fo^2^+2Fc^2^)/3'

_atom_sites_solution_primary direct

_atom_sites_solution_secondary difmap

_atom_sites_solution_hydrogens geom

_refine_ls_hydrogen_treatment mixed

_refine_ls_extinction_method SHELXL

_refine_ls_extinction_coef 0.00000(5)

_refine_ls_extinction_expression

'Fc^*^=kFc[1+0.001xFc^2^\l^3^/sin(2\q)]^-1/4^'

_refine_ls_number_reflns 1456

_refine_ls_number_parameters 22

_refine_ls_number_restraints 0

_refine_ls_R_factor_all 0.0867

_refine_ls_R_factor_gt 0.0623

_refine_ls_wR_factor_ref 0.1203

_refine_ls_wR_factor_gt 0.1125

_refine_ls_goodness_of_fit_ref 1.651

_refine_ls_restrained_S_all 1.651

_refine_ls_shift/su_max 10.558

_refine_ls_shift/su_mean 0.481

loop_

_atom_site_label

_atom_site_type_symbol

_atom_site_fract_x

_atom_site_fract_y

_atom_site_fract_z

_atom_site_U_iso_or_equiv

_atom_site_adp_type

_atom_site_occupancy

_atom_site_symmetry_multiplicity

_atom_site_calc_flag

_atom_site_refinement_flags

_atom_site_disorder_assembly

_atom_site_disorder_group

Li1 Li 0.0000 0.5000 0.3330(19) 0.010 Uiso 1 2 d S . .

Li2 Li 0.7500 0.2500 0.2603(19) 0.010 Uiso 1 2 d S . .

Li3 Li 0.7500 0.2500 0.9341(19) 0.010 Uiso 1 2 d S . .

Li4 Li 0.5000 0.5000 0.5000 0.010 Uiso 1 4 d S . .

Li5 Li 0.5000 0.0000 0.0000 0.010 Uiso 1 4 d S . .

Ir1 Ir 0.2500 0.2500 0.08356(3) 0.00249(11) Uiso 1 2 d S . .

Ir2 Ir 0.5000 0.5000 0.16665(3) 0.00552(13) Uiso 1 2 d S . .

O1 O 0.742(3) 0.5103(9) 0.0867(6) 0.0081(13) Uiso 1 1 d . . .

O2 O 0.735(3) 0.5000 0.2500 0.010(2) Uiso 1 2 d S . .

O3 O 0.0178(19) 0.2524(18) 0.0000 0.0054(17) Uiso 1 2 d S . .

O4 O 0.4943(17) 0.2588(16) 0.1629(6) 0.0085(15) Uiso 1 1 d . . .

_geom_special_details

;

All s.u.'s (except the s.u. in the dihedral angle between two l.s. planes)

are estimated using the full covariance matrix. The cell s.u.'s are taken

into account individually in the estimation of s.u.'s in distances, angles

and torsion angles; correlations between s.u.'s in cell parameters are only

used when they are defined by crystal symmetry. An approximate (isotropic)

treatment of cell s.u.'s is used for estimating s.u.'s involving l.s. planes.

;

loop_

_geom_bond_atom_site_label_1

_geom_bond_atom_site_label_2

_geom_bond_distance

_geom_bond_site_symmetry_2

_geom_bond_publ_flag

Li1 O1 2.09(3) 4_655 ?

Li1 O1 2.09(3) 3_465 ?

Li1 O2 2.15(3) 1_455 ?

Li1 O2 2.15(3) 2_665 ?

Li1 O4 2.183(14) 8 ?

Li1 O4 2.183(14) 7_455 ?

Li1 Li2 2.88(2) 1_455 ?

Li1 Li2 2.88(2) 5_455 ?

Li1 Ir2 2.95416(18) 3_565 ?

Li1 Ir2 2.95416(18) 3_465 ?

Li1 Li1 2.96(7) 3_565 ?

Li1 Ir1 2.973(17) 3_565 ?

Li2 O4 1.99(3) 7 ?

Li2 O4 1.99(3) 4_655 ?

Li2 O2 2.117(3) 6_655 ?

Li2 O2 2.117(3) . ?

Li2 O4 2.30(3) . ?

Li2 O4 2.30(3) 6_655 ?

Li2 Ir1 2.79(3) 7 ?

Li2 Li1 2.88(2) 1_655 ?

Li2 Li1 2.88(2) 5_545 ?

Li2 Ir2 2.885(15) 3_565 ?

Li2 Ir2 2.885(15) 7 ?

Li2 Li2 2.977(8) 7_455 ?

Li3 O3 1.97(2) 1_656 ?

Li3 O3 1.97(2) 13_556 ?

Li3 O1 2.226(10) 13_656 ?

Li3 O1 2.226(10) 10_556 ?

Li3 O4 2.30(3) 10_556 ?

Li3 O4 2.30(3) 13_656 ?

Li3 Li3 2.35(7) 13_657 ?

Li3 Li5 2.829(14) 5_556 ?

Li3 Li5 2.829(14) 1_556 ?

Li3 Li4 2.829(14) 3_566 ?

Li3 Li4 2.829(14) 7_556 ?

Li3 Ir1 2.971(4) 13_556 ?

Li4 O1 2.108(13) 12_566 ?

Li4 O1 2.108(13) 11_656 ?

Li4 O1 2.108(13) 4_655 ?

Li4 O1 2.108(13) 3_565 ?

Li4 O3 2.131(15) 15_556 ?

Li4 O3 2.131(15) 7 ?

Li4 Li3 2.829(14) 3_566 ?

Li4 Li3 2.829(14) 11_655 ?

Li4 Li3 2.829(14) 7_456 ?

Li4 Li3 2.829(14) 15_655 ?

Li4 Li5 2.95415(15) 7_455 ?

Li4 Li5 2.95415(15) 7 ?

Li5 O3 2.089(15) 13 ?

Li5 O3 2.089(15) 5_545 ?

Li5 O1 2.172(13) 14_445 ?

Li5 O1 2.172(13) 13_655 ?

Li5 O1 2.172(13) 6_655 ?

Li5 O1 2.172(13) 5_445 ?

Li5 Li3 2.829(14) 5_444 ?

Li5 Li3 2.829(14) 13_656 ?

Li5 Li3 2.829(14) 1_554 ?

Li5 Li3 2.829(14) 9_656 ?

Li5 Li4 2.95415(15) 7_455 ?

Li5 Li4 2.95415(15) 7 ?

Ir1 O1 2.022(7) 2_665 ?

Ir1 O1 2.022(7) 5_445 ?

Ir1 O4 2.023(10) . ?

Ir1 O4 2.023(10) 6 ?

Ir1 O3 2.026(8) . ?

Ir1 O3 2.026(8) 13 ?

Ir1 Li2 2.79(3) 7_455 ?

Ir1 Ir2 2.9697(3) . ?

Ir1 Ir2 2.9697(3) 5_445 ?

Ir1 Li3 2.971(4) 13_556 ?

Ir1 Li3 2.971(4) 13_656 ?

Ir1 Li1 2.973(17) 3_565 ?

Ir2 O1 2.022(13) 2_665 ?

Ir2 O1 2.022(13) . ?

Ir2 O4 2.034(14) . ?

Ir2 O4 2.034(14) 2_665 ?

Ir2 O2 2.035(12) . ?

Ir2 O2 2.035(12) 2_665 ?

Ir2 Li2 2.885(15) 3_565 ?

Ir2 Li2 2.885(15) 7_455 ?

Ir2 Li1 2.95416(17) 3_565 ?

Ir2 Li1 2.9542(2) 3_665 ?

Ir2 Ir1 2.9697(3) 5 ?

O1 Ir1 2.022(7) 5 ?

O1 Li1 2.09(3) 3_665 ?

O1 Li4 2.108(13) 3_565 ?

O1 Li5 2.172(13) 5 ?

O1 Li3 2.226(10) 13_656 ?

O2 Ir2 2.035(12) 3_565 ?

O2 Li2 2.117(3) 3_565 ?

O2 Li1 2.15(3) 1_655 ?

O2 Li1 2.15(3) 3_665 ?

O3 Li3 1.97(2) 1_454 ?

O3 Li3 1.97(2) 13_556 ?

O3 Ir1 2.026(8) 13 ?

O3 Li5 2.089(15) 5_455 ?

O3 Li4 2.131(15) 7_455 ?

O4 Li2 1.99(3) 7_455 ?

O4 Li1 2.183(14) 7 ?

O4 Li3 2.30(3) 13_656 ?

loop_

_geom_angle_atom_site_label_1

_geom_angle_atom_site_label_2

_geom_angle_atom_site_label_3

_geom_angle

_geom_angle_site_symmetry_1

_geom_angle_site_symmetry_3

_geom_angle_publ_flag

O1 Li1 O1 93.6(15) 4_655 3_465 ?

O1 Li1 O2 177.6(3) 4_655 1_455 ?

O1 Li1 O2 86.7(6) 3_465 1_455 ?

O1 Li1 O2 86.7(6) 4_655 2_665 ?

O1 Li1 O2 177.6(3) 3_465 2_665 ?

O2 Li1 O2 93.2(14) 1_455 2_665 ?

O1 Li1 O4 85.7(7) 4_655 8 ?

O1 Li1 O4 91.7(7) 3_465 8 ?

O2 Li1 O4 92.0(7) 1_455 8 ?

O2 Li1 O4 90.7(7) 2_665 8 ?

O1 Li1 O4 91.7(7) 4_655 7_455 ?

O1 Li1 O4 85.7(7) 3_465 7_455 ?

O2 Li1 O4 90.7(7) 1_455 7_455 ?

O2 Li1 O4 92.0(7) 2_665 7_455 ?

O4 Li1 O4 176.1(19) 8 7_455 ?

O1 Li1 Li2 135.4(6) 4_655 1_455 ?

O1 Li1 Li2 84.5(6) 3_465 1_455 ?

O2 Li1 Li2 47.0(5) 1_455 1_455 ?

O2 Li1 Li2 93.6(11) 2_665 1_455 ?

O4 Li1 Li2 138.9(10) 8 1_455 ?

O4 Li1 Li2 43.7(5) 7_455 1_455 ?

O1 Li1 Li2 84.5(6) 4_655 5_455 ?

O1 Li1 Li2 135.4(6) 3_465 5_455 ?

O2 Li1 Li2 93.6(11) 1_455 5_455 ?

O2 Li1 Li2 47.0(5) 2_665 5_455 ?

O4 Li1 Li2 43.7(5) 8 5_455 ?

O4 Li1 Li2 138.9(10) 7_455 5_455 ?

Li2 Li1 Li2 126.5(17) 1_455 5_455 ?

O1 Li1 Ir2 43.2(3) 4_655 3_565 ?

O1 Li1 Ir2 136.6(14) 3_465 3_565 ?

O2 Li1 Ir2 136.7(13) 1_455 3_565 ?

O2 Li1 Ir2 43.6(3) 2_665 3_565 ?

O4 Li1 Ir2 89.1(3) 8 3_565 ?

O4 Li1 Ir2 90.9(3) 7_455 3_565 ?

Li2 Li1 Ir2 120.9(5) 1_455 3_565 ?

Li2 Li1 Ir2 59.2(2) 5_455 3_565 ?

O1 Li1 Ir2 136.6(14) 4_655 3_465 ?

O1 Li1 Ir2 43.2(3) 3_465 3_465 ?

O2 Li1 Ir2 43.6(3) 1_455 3_465 ?

O2 Li1 Ir2 136.7(13) 2_665 3_465 ?

O4 Li1 Ir2 90.9(3) 8 3_465 ?

O4 Li1 Ir2 89.1(3) 7_455 3_465 ?

Li2 Li1 Ir2 59.2(2) 1_455 3_465 ?

Li2 Li1 Ir2 120.9(5) 5_455 3_465 ?

Ir2 Li1 Ir2 179.7(13) 3_565 3_465 ?

O1 Li1 Li1 133.2(8) 4_655 3_565 ?

O1 Li1 Li1 133.2(8) 3_465 3_565 ?

O2 Li1 Li1 46.6(7) 1_455 3_565 ?

O2 Li1 Li1 46.6(7) 2_665 3_565 ?

O4 Li1 Li1 91.9(9) 8 3_565 ?

O4 Li1 Li1 91.9(9) 7_455 3_565 ?

Li2 Li1 Li1 63.3(8) 1_455 3_565 ?

Li2 Li1 Li1 63.3(8) 5_455 3_565 ?

Ir2 Li1 Li1 90.1(6) 3_565 3_565 ?

Ir2 Li1 Li1 90.1(6) 3_465 3_565 ?

O1 Li1 Ir1 42.8(4) 4_655 3_565 ?

O1 Li1 Ir1 92.8(10) 3_465 3_565 ?

O2 Li1 Ir1 134.8(3) 1_455 3_565 ?

O2 Li1 Ir1 89.0(2) 2_665 3_565 ?

O4 Li1 Ir1 42.9(4) 8 3_565 ?

O4 Li1 Ir1 134.4(10) 7_455 3_565 ?

Li2 Li1 Ir1 176.7(13) 1_455 3_565 ?

Li2 Li1 Ir1 56.8(6) 5_455 3_565 ?

Ir2 Li1 Ir1 60.14(19) 3_565 3_565 ?

Ir2 Li1 Ir1 119.7(6) 3_465 3_565 ?

Li1 Li1 Ir1 120.0(6) 3_565 3_565 ?

O4 Li2 O4 93.1(15) 7 4_655 ?

O4 Li2 O2 89.6(8) 7 6_655 ?

O4 Li2 O2 97.3(8) 4_655 6_655 ?

O4 Li2 O2 97.3(8) 7 . ?

O4 Li2 O2 89.6(8) 4_655 . ?

O2 Li2 O2 170.1(18) 6_655 . ?

O4 Li2 O4 174.5(13) 7 . ?

O4 Li2 O4 92.4(4) 4_655 . ?

O2 Li2 O4 89.6(9) 6_655 . ?

O2 Li2 O4 82.9(8) . . ?

O4 Li2 O4 92.4(4) 7 6_655 ?

O4 Li2 O4 174.5(13) 4_655 6_655 ?

O2 Li2 O4 82.9(8) 6_655 6_655 ?

O2 Li2 O4 89.6(9) . 6_655 ?

O4 Li2 O4 82.1(12) . 6_655 ?

O4 Li2 Ir1 46.5(7) 7 7 ?

O4 Li2 Ir1 46.5(7) 4_655 7 ?

O2 Li2 Ir1 95.0(9) 6_655 7 ?

O2 Li2 Ir1 95.0(9) . 7 ?

O4 Li2 Ir1 138.9(6) . 7 ?

O4 Li2 Ir1 138.9(6) 6_655 7 ?

O4 Li2 Li1 49.2(6) 7 1_655 ?

O4 Li2 Li1 92.0(11) 4_655 1_655 ?

O2 Li2 Li1 138.2(9) 6_655 1_655 ?

O2 Li2 Li1 48.1(6) . 1_655 ?

O4 Li2 Li1 130.7(7) . 1_655 ?

O4 Li2 Li1 91.5(6) 6_655 1_655 ?

Ir1 Li2 Li1 63.3(8) 7 1_655 ?

O4 Li2 Li1 92.0(11) 7 5_545 ?

O4 Li2 Li1 49.2(6) 4_655 5_545 ?

O2 Li2 Li1 48.1(6) 6_655 5_545 ?

O2 Li2 Li1 138.2(9) . 5_545 ?

O4 Li2 Li1 91.5(6) . 5_545 ?

O4 Li2 Li1 130.7(7) 6_655 5_545 ?

Ir1 Li2 Li1 63.3(8) 7 5_545 ?

Li1 Li2 Li1 126.5(17) 1_655 5_545 ?

O4 Li2 Ir2 95.0(10) 7 3_565 ?

O4 Li2 Ir2 44.8(5) 4_655 3_565 ?

O2 Li2 Ir2 141.9(9) 6_655 3_565 ?

O2 Li2 Ir2 44.8(4) . 3_565 ?

O4 Li2 Ir2 88.9(3) . 3_565 ?

O4 Li2 Ir2 134.4(6) 6_655 3_565 ?

Ir1 Li2 Ir2 63.1(6) 7 3_565 ?

Li1 Li2 Ir2 61.6(4) 1_655 3_565 ?

Li1 Li2 Ir2 93.9(7) 5_545 3_565 ?

O4 Li2 Ir2 44.8(5) 7 7 ?

O4 Li2 Ir2 95.0(10) 4_655 7 ?

O2 Li2 Ir2 44.8(4) 6_655 7 ?

O2 Li2 Ir2 141.9(9) . 7 ?

O4 Li2 Ir2 134.4(6) . 7 ?

O4 Li2 Ir2 88.9(3) 6_655 7 ?

Ir1 Li2 Ir2 63.1(6) 7 7 ?

Li1 Li2 Ir2 93.9(7) 1_655 7 ?

Li1 Li2 Ir2 61.6(4) 5_545 7 ?

Ir2 Li2 Ir2 126.3(12) 3_565 7 ?

O4 Li2 Li2 143(2) 7 7_455 ?

O4 Li2 Li2 50.6(7) 4_655 7_455 ?

O2 Li2 Li2 91.7(5) 6_655 7_455 ?

O2 Li2 Li2 87.1(5) . 7_455 ?

O4 Li2 Li2 41.9(8) . 7_455 ?

O4 Li2 Li2 123.9(18) 6_655 7_455 ?

Ir1 Li2 Li2 97.1(13) 7 7_455 ?

Li1 Li2 Li2 124.3(7) 1_655 7_455 ?

Li1 Li2 Li2 63.0(5) 5_545 7_455 ?

Ir2 Li2 Li2 63.1(5) 3_565 7_455 ?

Ir2 Li2 Li2 124.3(7) 7 7_455 ?

O3 Li3 O3 106.8(16) 1_656 13_556 ?

O3 Li3 O1 95.3(7) 1_656 13_656 ?

O3 Li3 O1 96.1(7) 13_556 13_656 ?

O3 Li3 O1 96.1(7) 1_656 10_556 ?

O3 Li3 O1 95.3(7) 13_556 10_556 ?

O1 Li3 O1 160.8(18) 13_656 10_556 ?

O3 Li3 O4 167.5(14) 1_656 10_556 ?

O3 Li3 O4 85.5(4) 13_556 10_556 ?

O1 Li3 O4 85.4(9) 13_656 10_556 ?

O1 Li3 O4 80.2(8) 10_556 10_556 ?

O3 Li3 O4 85.5(4) 1_656 13_656 ?

O3 Li3 O4 167.5(14) 13_556 13_656 ?

O1 Li3 O4 80.2(8) 13_656 13_656 ?

O1 Li3 O4 85.4(9) 10_556 13_656 ?

O4 Li3 O4 82.3(12) 10_556 13_656 ?

O3 Li3 Li3 53.4(8) 1_656 13_657 ?

O3 Li3 Li3 53.4(8) 13_556 13_657 ?

O1 Li3 Li3 99.6(9) 13_656 13_657 ?

O1 Li3 Li3 99.6(9) 10_556 13_657 ?

O4 Li3 Li3 138.8(6) 10_556 13_657 ?

O4 Li3 Li3 138.8(6) 13_656 13_657 ?

O3 Li3 Li5 47.6(5) 1_656 5_556 ?

O3 Li3 Li5 100.3(11) 13_556 5_556 ?

O1 Li3 Li5 142.4(7) 13_656 5_556 ?

O1 Li3 Li5 49.1(4) 10_556 5_556 ?

O4 Li3 Li5 129.2(6) 10_556 5_556 ?

O4 Li3 Li5 89.6(4) 13_656 5_556 ?

Li3 Li3 Li5 65.5(6) 13_657 5_556 ?

O3 Li3 Li5 100.3(11) 1_656 1_556 ?

O3 Li3 Li5 47.6(5) 13_556 1_556 ?

O1 Li3 Li5 49.1(4) 13_656 1_556 ?

O1 Li3 Li5 142.4(7) 10_556 1_556 ?

O4 Li3 Li5 89.6(4) 10_556 1_556 ?

O4 Li3 Li5 129.2(6) 13_656 1_556 ?

Li3 Li3 Li5 65.5(6) 13_657 1_556 ?

Li5 Li3 Li5 130.9(13) 5_556 1_556 ?

O3 Li3 Li4 99.4(10) 1_656 3_566 ?

O3 Li3 Li4 48.8(6) 13_556 3_566 ?

O1 Li3 Li4 144.5(7) 13_656 3_566 ?

O1 Li3 Li4 47.5(4) 10_556 3_566 ?

O4 Li3 Li4 86.9(3) 10_556 3_566 ?

O4 Li3 Li4 132.8(7) 13_656 3_566 ?

Li3 Li3 Li4 65.5(6) 13_657 3_566 ?

Li5 Li3 Li4 62.9(4) 5_556 3_566 ?

Li5 Li3 Li4 96.3(6) 1_556 3_566 ?

O3 Li3 Li4 48.8(6) 1_656 7_556 ?

O3 Li3 Li4 99.4(10) 13_556 7_556 ?

O1 Li3 Li4 47.5(4) 13_656 7_556 ?

O1 Li3 Li4 144.5(7) 10_556 7_556 ?

O4 Li3 Li4 132.8(7) 10_556 7_556 ?

O4 Li3 Li4 86.9(3) 13_656 7_556 ?

Li3 Li3 Li4 65.5(6) 13_657 7_556 ?

Li5 Li3 Li4 96.3(6) 5_556 7_556 ?

Li5 Li3 Li4 62.9(4) 1_556 7_556 ?

Li4 Li3 Li4 130.9(13) 3_566 7_556 ?

O3 Li3 Ir1 149.5(15) 1_656 13_556 ?

O3 Li3 Ir1 42.7(2) 13_556 13_556 ?

O1 Li3 Ir1 90.2(5) 13_656 13_556 ?

O1 Li3 Ir1 87.8(4) 10_556 13_556 ?

O4 Li3 Ir1 42.8(3) 10_556 13_556 ?

O4 Li3 Ir1 125.0(12) 13_656 13_556 ?

Li3 Li3 Ir1 96.1(7) 13_657 13_556 ?

Li5 Li3 Ir1 124.3(4) 5_556 13_556 ?

Li5 Li3 Ir1 61.63(11) 1_556 13_556 ?

Li4 Li3 Ir1 61.63(11) 3_566 13_556 ?

Li4 Li3 Ir1 124.3(4) 7_556 13_556 ?

O1 Li4 O1 85.7(7) 12_566 11_656 ?

O1 Li4 O1 180.000(3) 12_566 4_655 ?

O1 Li4 O1 94.3(7) 11_656 4_655 ?

O1 Li4 O1 94.3(7) 12_566 3_565 ?

O1 Li4 O1 180.000(2) 11_656 3_565 ?

O1 Li4 O1 85.7(7) 4_655 3_565 ?

O1 Li4 O3 94.3(3) 12_566 15_556 ?

O1 Li4 O3 85.7(3) 11_656 15_556 ?

O1 Li4 O3 85.7(3) 4_655 15_556 ?

O1 Li4 O3 94.3(3) 3_565 15_556 ?

O1 Li4 O3 85.7(3) 12_566 7 ?

O1 Li4 O3 94.3(3) 11_656 7 ?

O1 Li4 O3 94.3(3) 4_655 7 ?

O1 Li4 O3 85.7(3) 3_565 7 ?

O3 Li4 O3 180.000(3) 15_556 7 ?

O1 Li4 Li3 51.1(5) 12_566 3_566 ?

O1 Li4 Li3 91.1(6) 11_656 3_566 ?

O1 Li4 Li3 128.9(5) 4_655 3_566 ?

O1 Li4 Li3 88.9(6) 3_565 3_566 ?

O3 Li4 Li3 44.1(4) 15_556 3_566 ?

O3 Li4 Li3 135.9(4) 7 3_566 ?

O1 Li4 Li3 128.9(5) 12_566 11_655 ?

O1 Li4 Li3 88.9(6) 11_656 11_655 ?

O1 Li4 Li3 51.1(5) 4_655 11_655 ?

O1 Li4 Li3 91.1(6) 3_565 11_655 ?

O3 Li4 Li3 135.9(4) 15_556 11_655 ?

O3 Li4 Li3 44.1(4) 7 11_655 ?

Li3 Li4 Li3 180.0 3_566 11_655 ?

O1 Li4 Li3 91.1(6) 12_566 7_456 ?

O1 Li4 Li3 51.1(5) 11_656 7_456 ?

O1 Li4 Li3 88.9(6) 4_655 7_456 ?

O1 Li4 Li3 128.9(5) 3_565 7_456 ?

O3 Li4 Li3 135.9(4) 15_556 7_456 ?

O3 Li4 Li3 44.1(4) 7 7_456 ?

Li3 Li4 Li3 130.9(13) 3_566 7_456 ?

Li3 Li4 Li3 49.1(13) 11_655 7_456 ?

O1 Li4 Li3 88.9(6) 12_566 15_655 ?

O1 Li4 Li3 128.9(5) 11_656 15_655 ?

O1 Li4 Li3 91.1(6) 4_655 15_655 ?

O1 Li4 Li3 51.1(5) 3_565 15_655 ?

O3 Li4 Li3 44.1(4) 15_556 15_655 ?

O3 Li4 Li3 135.9(4) 7 15_655 ?

Li3 Li4 Li3 49.1(13) 3_566 15_655 ?

Li3 Li4 Li3 130.9(13) 11_655 15_655 ?

Li3 Li4 Li3 180.000(2) 7_456 15_655 ?

O1 Li4 Li5 132.7(4) 12_566 7_455 ?

O1 Li4 Li5 47.3(4) 11_656 7_455 ?

O1 Li4 Li5 47.3(4) 4_655 7_455 ?

O1 Li4 Li5 132.7(4) 3_565 7_455 ?

O3 Li4 Li5 87.2(3) 15_556 7_455 ?

O3 Li4 Li5 92.8(3) 7 7_455 ?

Li3 Li4 Li5 121.47(18) 3_566 7_455 ?

Li3 Li4 Li5 58.53(18) 11_655 7_455 ?

Li3 Li4 Li5 58.53(18) 7_456 7_455 ?

Li3 Li4 Li5 121.47(18) 15_655 7_455 ?

O1 Li4 Li5 47.3(4) 12_566 7 ?

O1 Li4 Li5 132.7(4) 11_656 7 ?

O1 Li4 Li5 132.7(4) 4_655 7 ?

O1 Li4 Li5 47.3(4) 3_565 7 ?

O3 Li4 Li5 92.8(3) 15_556 7 ?

O3 Li4 Li5 87.2(3) 7 7 ?

Li3 Li4 Li5 58.53(18) 3_566 7 ?

Li3 Li4 Li5 121.47(18) 11_655 7 ?

Li3 Li4 Li5 121.47(18) 7_456 7 ?

Li3 Li4 Li5 58.53(18) 15_655 7 ?

Li5 Li4 Li5 180.0 7_455 7 ?

O3 Li5 O3 180.000(1) 13 5_545 ?

O3 Li5 O1 85.7(3) 13 14_445 ?

O3 Li5 O1 94.3(3) 5_545 14_445 ?

O3 Li5 O1 94.3(3) 13 13_655 ?

O3 Li5 O1 85.7(3) 5_545 13_655 ?

O1 Li5 O1 89.3(7) 14_445 13_655 ?

O3 Li5 O1 94.3(3) 13 6_655 ?

O3 Li5 O1 85.7(3) 5_545 6_655 ?

O1 Li5 O1 180.0(6) 14_445 6_655 ?

O1 Li5 O1 90.7(7) 13_655 6_655 ?

O3 Li5 O1 85.7(3) 13 5_445 ?

O3 Li5 O1 94.3(3) 5_545 5_445 ?

O1 Li5 O1 90.7(7) 14_445 5_445 ?

O1 Li5 O1 180.0(7) 13_655 5_445 ?

O1 Li5 O1 89.3(7) 6_655 5_445 ?

O3 Li5 Li3 135.9(4) 13 5_444 ?

O3 Li5 Li3 44.1(4) 5_545 5_444 ?

O1 Li5 Li3 50.8(5) 14_445 5_444 ?

O1 Li5 Li3 92.3(6) 13_655 5_444 ?

O1 Li5 Li3 129.2(5) 6_655 5_444 ?

O1 Li5 Li3 87.7(6) 5_445 5_444 ?

O3 Li5 Li3 44.1(4) 13 13_656 ?

O3 Li5 Li3 135.9(4) 5_545 13_656 ?

O1 Li5 Li3 129.2(5) 14_445 13_656 ?

O1 Li5 Li3 87.7(6) 13_655 13_656 ?

O1 Li5 Li3 50.8(5) 6_655 13_656 ?

O1 Li5 Li3 92.3(6) 5_445 13_656 ?

Li3 Li5 Li3 180.0(13) 5_444 13_656 ?

O3 Li5 Li3 44.1(4) 13 1_554 ?

O3 Li5 Li3 135.9(4) 5_545 1_554 ?

O1 Li5 Li3 92.3(6) 14_445 1_554 ?

O1 Li5 Li3 50.8(5) 13_655 1_554 ?

O1 Li5 Li3 87.7(6) 6_655 1_554 ?

O1 Li5 Li3 129.2(5) 5_445 1_554 ?

Li3 Li5 Li3 130.9(13) 5_444 1_554 ?

Li3 Li5 Li3 49.1(13) 13_656 1_554 ?

O3 Li5 Li3 135.9(4) 13 9_656 ?

O3 Li5 Li3 44.1(4) 5_545 9_656 ?

O1 Li5 Li3 87.7(6) 14_445 9_656 ?

O1 Li5 Li3 129.2(5) 13_655 9_656 ?

O1 Li5 Li3 92.3(6) 6_655 9_656 ?

O1 Li5 Li3 50.8(5) 5_445 9_656 ?

Li3 Li5 Li3 49.1(13) 5_444 9_656 ?

Li3 Li5 Li3 130.9(13) 13_656 9_656 ?

Li3 Li5 Li3 180.0(13) 1_554 9_656 ?

O3 Li5 Li4 87.1(3) 13 7_455 ?

O3 Li5 Li4 92.9(3) 5_545 7_455 ?

O1 Li5 Li4 45.5(4) 14_445 7_455 ?

O1 Li5 Li4 134.5(4) 13_655 7_455 ?

O1 Li5 Li4 134.5(4) 6_655 7_455 ?

O1 Li5 Li4 45.5(4) 5_445 7_455 ?

Li3 Li5 Li4 58.53(18) 5_444 7_455 ?

Li3 Li5 Li4 121.47(18) 13_656 7_455 ?

Li3 Li5 Li4 121.47(18) 1_554 7_455 ?

Li3 Li5 Li4 58.53(18) 9_656 7_455 ?

O3 Li5 Li4 92.9(3) 13 7 ?

O3 Li5 Li4 87.1(3) 5_545 7 ?

O1 Li5 Li4 134.5(4) 14_445 7 ?

O1 Li5 Li4 45.5(4) 13_655 7 ?

O1 Li5 Li4 45.5(4) 6_655 7 ?

O1 Li5 Li4 134.5(4) 5_445 7 ?

Li3 Li5 Li4 121.47(18) 5_444 7 ?

Li3 Li5 Li4 58.53(18) 13_656 7 ?

Li3 Li5 Li4 58.53(18) 1_554 7 ?

Li3 Li5 Li4 121.47(18) 9_656 7 ?

Li4 Li5 Li4 180.0 7_455 7 ?

O1 Ir1 O1 176.9(6) 2_665 5_445 ?

O1 Ir1 O4 85.9(6) 2_665 . ?

O1 Ir1 O4 91.9(5) 5_445 . ?

O1 Ir1 O4 91.9(5) 2_665 6 ?

O1 Ir1 O4 85.9(6) 5_445 6 ?

O4 Ir1 O4 91.2(6) . 6 ?

O1 Ir1 O3 91.5(6) 2_665 . ?

O1 Ir1 O3 90.8(6) 5_445 . ?

O4 Ir1 O3 176.0(4) . . ?

O4 Ir1 O3 91.8(3) 6 . ?

O1 Ir1 O3 90.8(6) 2_665 13 ?

O1 Ir1 O3 91.5(6) 5_445 13 ?

O4 Ir1 O3 91.8(3) . 13 ?

O4 Ir1 O3 176.0(4) 6 13 ?

O3 Ir1 O3 85.3(5) . 13 ?

O1 Ir1 Li2 88.4(3) 2_665 7_455 ?

O1 Ir1 Li2 88.4(3) 5_445 7_455 ?

O4 Ir1 Li2 45.6(3) . 7_455 ?

O4 Ir1 Li2 45.6(3) 6 7_455 ?

O3 Ir1 Li2 137.4(2) . 7_455 ?

O3 Ir1 Li2 137.4(2) 13 7_455 ?

O1 Ir1 Ir2 42.8(4) 2_665 . ?

O1 Ir1 Ir2 135.0(4) 5_445 . ?

O4 Ir1 Ir2 43.1(4) . . ?

O4 Ir1 Ir2 91.8(3) 6 . ?

O3 Ir1 Ir2 134.2(4) . . ?

O3 Ir1 Ir2 92.2(4) 13 . ?

Li2 Ir1 Ir2 60.064(10) 7_455 . ?

O1 Ir1 Ir2 135.0(4) 2_665 5_445 ?

O1 Ir1 Ir2 42.8(4) 5_445 5_445 ?

O4 Ir1 Ir2 91.8(3) . 5_445 ?

O4 Ir1 Ir2 43.1(4) 6 5_445 ?

O3 Ir1 Ir2 92.2(4) . 5_445 ?

O3 Ir1 Ir2 134.2(4) 13 5_445 ?

Li2 Ir1 Ir2 60.064(10) 7_455 5_445 ?

Ir2 Ir1 Ir2 120.13(2) . 5_445 ?

O1 Ir1 Li3 91.5(4) 2_665 13_556 ?

O1 Ir1 Li3 88.9(4) 5_445 13_556 ?

O4 Ir1 Li3 141.6(7) . 13_556 ?

O4 Ir1 Li3 50.6(7) 6 13_556 ?

O3 Ir1 Li3 41.3(7) . 13_556 ?

O3 Ir1 Li3 126.5(7) 13 13_556 ?

Li2 Ir1 Li3 96.1(7) 7_455 13_556 ?

Ir2 Ir1 Li3 123.2(3) . 13_556 ?

Ir2 Ir1 Li3 63.8(4) 5_445 13_556 ?

O1 Ir1 Li3 88.9(4) 2_665 13_656 ?

O1 Ir1 Li3 91.5(4) 5_445 13_656 ?

O4 Ir1 Li3 50.6(7) . 13_656 ?

O4 Ir1 Li3 141.6(7) 6 13_656 ?

O3 Ir1 Li3 126.5(7) . 13_656 ?

O3 Ir1 Li3 41.3(7) 13 13_656 ?

Li2 Ir1 Li3 96.1(7) 7_455 13_656 ?

Ir2 Ir1 Li3 63.8(4) . 13_656 ?

Ir2 Ir1 Li3 123.2(3) 5_445 13_656 ?

Li3 Ir1 Li3 167.8(13) 13_556 13_656 ?

O1 Ir1 Li1 44.7(5) 2_665 3_565 ?

O1 Ir1 Li1 133.1(5) 5_445 3_565 ?

O4 Ir1 Li1 88.8(6) . 3_565 ?

O4 Ir1 Li1 47.3(5) 6 3_565 ?

O3 Ir1 Li1 91.4(6) . 3_565 ?

O3 Ir1 Li1 135.4(6) 13 3_565 ?

Li2 Ir1 Li1 60.0(6) 7_455 3_565 ?

Ir2 Ir1 Li1 59.62(18) . 3_565 ?

Ir2 Ir1 Li1 90.3(3) 5_445 3_565 ?

Li3 Ir1 Li1 63.8(5) 13_556 3_565 ?

Li3 Ir1 Li1 123.2(4) 13_656 3_565 ?

O1 Ir2 O1 90.3(8) 2_665 . ?

O1 Ir2 O4 85.5(4) 2_665 . ?

O1 Ir2 O4 91.8(4) . . ?

O1 Ir2 O4 91.8(4) 2_665 2_665 ?

O1 Ir2 O4 85.5(4) . 2_665 ?

O4 Ir2 O4 176.2(6) . 2_665 ?

O1 Ir2 O2 176.8(3) 2_665 . ?

O1 Ir2 O2 91.8(6) . . ?

O4 Ir2 O2 92.0(3) . . ?

O4 Ir2 O2 90.7(3) 2_665 . ?

O1 Ir2 O2 91.8(6) 2_665 2_665 ?

O1 Ir2 O2 176.8(3) . 2_665 ?

O4 Ir2 O2 90.7(3) . 2_665 ?

O4 Ir2 O2 92.0(3) 2_665 2_665 ?

O2 Ir2 O2 86.2(7) . 2_665 ?

O1 Ir2 Li2 135.4(4) 2_665 3_565 ?

O1 Ir2 Li2 85.7(6) . 3_565 ?

O4 Ir2 Li2 138.9(4) . 3_565 ?

O4 Ir2 Li2 43.6(5) 2_665 3_565 ?

O2 Ir2 Li2 47.2(4) . 3_565 ?

O2 Ir2 Li2 91.1(5) 2_665 3_565 ?

O1 Ir2 Li2 85.7(6) 2_665 7_455 ?

O1 Ir2 Li2 135.4(4) . 7_455 ?

O4 Ir2 Li2 43.6(5) . 7_455 ?

O4 Ir2 Li2 138.9(4) 2_665 7_455 ?

O2 Ir2 Li2 91.1(5) . 7_455 ?

O2 Ir2 Li2 47.2(4) 2_665 7_455 ?

Li2 Ir2 Li2 126.3(12) 3_565 7_455 ?

O1 Ir2 Li1 45.1(8) 2_665 3_565 ?

O1 Ir2 Li1 135.2(7) . 3_565 ?

O4 Ir2 Li1 89.1(3) . 3_565 ?

O4 Ir2 Li1 91.0(3) 2_665 3_565 ?

O2 Ir2 Li1 133.0(7) . 3_565 ?

O2 Ir2 Li1 46.8(7) 2_665 3_565 ?

Li2 Ir2 Li1 120.7(4) 3_565 3_565 ?

Li2 Ir2 Li1 59.1(4) 7_455 3_565 ?

O1 Ir2 Li1 135.2(7) 2_665 3_665 ?

O1 Ir2 Li1 45.1(8) . 3_665 ?

O4 Ir2 Li1 91.0(3) . 3_665 ?

O4 Ir2 Li1 89.1(3) 2_665 3_665 ?

O2 Ir2 Li1 46.8(7) . 3_665 ?

O2 Ir2 Li1 133.0(7) 2_665 3_665 ?

Li2 Ir2 Li1 59.1(4) 3_565 3_665 ?

Li2 Ir2 Li1 120.7(4) 7_455 3_665 ?

Li1 Ir2 Li1 179.7(13) 3_565 3_665 ?

O1 Ir2 Ir1 42.7(2) 2_665 . ?

O1 Ir2 Ir1 91.7(3) . . ?

O4 Ir2 Ir1 42.8(3) . . ?

O4 Ir2 Ir1 134.5(3) 2_665 . ?

O2 Ir2 Ir1 134.766(14) . . ?

O2 Ir2 Ir1 91.4(3) 2_665 . ?

Li2 Ir2 Ir1 176.9(6) 3_565 . ?

Li2 Ir2 Ir1 56.8(6) 7_455 . ?

Li1 Ir2 Ir1 60.2(4) 3_565 . ?

Li1 Ir2 Ir1 119.9(4) 3_665 . ?

O1 Ir2 Ir1 91.7(3) 2_665 5 ?

O1 Ir2 Ir1 42.7(2) . 5 ?

O4 Ir2 Ir1 134.5(3) . 5 ?

O4 Ir2 Ir1 42.8(3) 2_665 5 ?

O2 Ir2 Ir1 91.4(3) . 5 ?

O2 Ir2 Ir1 134.766(14) 2_665 5 ?

Li2 Ir2 Ir1 56.8(6) 3_565 5 ?

Li2 Ir2 Ir1 176.9(6) 7_455 5 ?

Li1 Ir2 Ir1 119.9(4) 3_565 5 ?

Li1 Ir2 Ir1 60.2(4) 3_665 5 ?

Ir1 Ir2 Ir1 120.13(2) . 5 ?

Ir1 O1 Ir2 94.5(4) 5 . ?

Ir1 O1 Li1 92.5(5) 5 3_665 ?

Ir2 O1 Li1 91.7(8) . 3_665 ?

Ir1 O1 Li4 92.1(4) 5 3_565 ?

Ir2 O1 Li4 92.0(6) . 3_565 ?

Li1 O1 Li4 173.8(7) 3_665 3_565 ?

Ir1 O1 Li5 90.3(4) 5 5 ?

Ir2 O1 Li5 175.2(4) . 5 ?

Li1 O1 Li5 88.6(9) 3_665 5 ?

Li4 O1 Li5 87.3(4) 3_565 5 ?

Ir1 O1 Li3 168.6(10) 5 13_656 ?

Ir2 O1 Li3 95.1(7) . 13_656 ?

Li1 O1 Li3 93.3(7) 3_665 13_656 ?

Li4 O1 Li3 81.5(7) 3_565 13_656 ?

Li5 O1 Li3 80.1(7) 5 13_656 ?

Ir2 O2 Ir2 93.8(7) . 3_565 ?

Ir2 O2 Li2 95.2(7) . . ?

Ir2 O2 Li2 88.0(7) 3_565 . ?

Ir2 O2 Li2 88.0(7) . 3_565 ?

Ir2 O2 Li2 95.2(7) 3_565 3_565 ?

Li2 O2 Li2 175.3(9) . 3_565 ?

Ir2 O2 Li1 176.5(9) . 1_655 ?

Ir2 O2 Li1 89.7(6) 3_565 1_655 ?

Li2 O2 Li1 84.9(7) . 1_655 ?

Li2 O2 Li1 91.7(7) 3_565 1_655 ?

Ir2 O2 Li1 89.7(6) . 3_665 ?

Ir2 O2 Li1 176.5(9) 3_565 3_665 ?

Li2 O2 Li1 91.7(7) . 3_665 ?

Li2 O2 Li1 84.9(7) 3_565 3_665 ?

Li1 O2 Li1 86.8(14) 1_655 3_665 ?

Li3 O3 Li3 73.2(16) 1_454 13_556 ?

Li3 O3 Ir1 169.2(9) 1_454 . ?

Li3 O3 Ir1 96.0(8) 13_556 . ?

Li3 O3 Ir1 96.0(8) 1_454 13 ?

Li3 O3 Ir1 169.2(9) 13_556 13 ?

Ir1 O3 Ir1 94.7(5) . 13 ?

Li3 O3 Li5 88.3(5) 1_454 5_455 ?

Li3 O3 Li5 88.3(5) 13_556 5_455 ?

Ir1 O3 Li5 92.5(5) . 5_455 ?

Ir1 O3 Li5 92.5(5) 13 5_455 ?

Li3 O3 Li4 87.1(5) 1_454 7_455 ?

Li3 O3 Li4 87.1(5) 13_556 7_455 ?

Ir1 O3 Li4 91.3(5) . 7_455 ?

Ir1 O3 Li4 91.3(5) 13 7_455 ?

Li5 O3 Li4 174.3(6) 5_455 7_455 ?

Li2 O4 Ir1 87.9(8) 7_455 . ?

Li2 O4 Ir2 91.5(5) 7_455 . ?

Ir1 O4 Ir2 94.1(5) . . ?

Li2 O4 Li1 87.2(8) 7_455 7 ?

Ir1 O4 Li1 89.9(8) . 7 ?

Ir2 O4 Li1 175.8(10) . 7 ?

Li2 O4 Li3 173.3(10) 7_455 13_656 ?

Ir1 O4 Li3 86.6(7) . 13_656 ?

Ir2 O4 Li3 92.6(4) . 13_656 ?

Li1 O4 Li3 89.0(8) 7 13_656 ?

Li2 O4 Li2 87.4(4) 7_455 . ?

Ir1 O4 Li2 174.0(7) . . ?

Ir2 O4 Li2 89.8(5) . . ?

Li1 O4 Li2 86.1(8) 7 . ?

Li3 O4 Li2 97.8(9) 13_656 . ?

_diffrn_measured_fraction_theta_max 0.999

_diffrn_reflns_theta_full 40.41

_diffrn_measured_fraction_theta_full 0.999

_refine_diff_density_max 43.365

_refine_diff_density_min -12.135

_refine_diff_density_rms 1.912

#===END

Appendix A3. Consent Policies

6/25/2015 Rightslink® by Copyright Clearance Center
https://s100.copyright.com/AppDispatchServlet 1/1
Title: Strategic Crystal Growth and
Physical Properties of SingleCrystalline
LnCo2Al8 (Ln = La–
Nd, Sm, Yb)
Author: Pilanda WatkinsCurry,
Joseph
Vade Burnett, Tapas Samanta, et
al
Publication: Crystal Growth and Design
Publisher: American Chemical Society
Date: Jun 1, 2015
Copyright © 2015, American Chemical Society
If you're a copyright.com
user, you can login to
RightsLink using your
copyright.com credentials.
Already a RightsLink user or
want to learn more?
PERMISSION/LICENSE IS GRANTED FOR YOUR ORDER AT NO CHARGE
This type of permission/license, instead of the standard Terms & Conditions, is sent to you because no
fee is being charged for your order. Please note the following:
Permission is granted for your request in both print and electronic formats, and translations.
If figures and/or tables were requested, they may be adapted or used in part.
Please print this page for your records and send a copy of it to your publisher/graduate school.
Appropriate credit for the requested material should be given as follows: "Reprinted (adapted) with permission from (COMPLETE REFERENCE CITATION). Copyright (YEAR) American Chemical Society." Insert appropriate information in place of the capitalized words.
Onetime
permission is granted only for the use specified in your request. No additional
uses are granted (such as derivative works or other editions). For any other uses, please submit a new request.

Comments? We would like to hear from you. Email
us at customercare@copyright.com
6/25/2015 Rightslink® by Copyright Clearance Center
https://s100.copyright.com/AppDispatchServlet 1/1

Title: Investigation of Mn, Fe, and Ni Incorporation in CeCo2Al8
Author: LaRico J. Treadwell, Pilanda WatkinsCurry, Jacob D. McAlpin, et al
Publication: Inorganic Chemistry
Publisher: American Chemical Society
Date: Feb 1, 2015

Title: Targeting Calcium Magnesium Silicates for Polycaprolactone/Ceramic Composite Scaffolds
Author: Cong Chen, Pilanda WatkinsCurry, Mollie Smoak, et al

Appendix A4. Statement for Reproduced In Part Material

From: Chan, Julia
Sent: Thursday, July 16, 2015 11:01 AM
To: gradetd@lsu.edu
Cc: Watkins-Curry, Pilanda
Subject: FW: Important notice regarding your ETD

To Whom This May Concern:
Please see below.

Julia Chan, Professor
Department of Chemistry
The University of Texas at Dallas
Email: Julia.Chan@utdallas.edu

Associate Editor | *Science Advances* (AAAS)

From: Pilanda Watkins-Curry [mailto:pwatkinscurry@gmail.com]
Sent: Thursday, July 16, 2015 10:50 AM
To: Chan, Julia
Subject: Re: Important notice regarding your ETD

Hi Dr. Chan,

You can send the statement from you UT Dallas account. Please see below.

Reproduced in part material for Chapter 2: Pilanda Watkins-Curry is a co-author of "Investigation of Mn, Fe, and Ni in $CeCo_2Al_8$." She grew single crystals of $CeCo_{2-x}Mn_xAl_8$ and $CeCo_2Al_8$ via the self-flux method. She collected X-ray diffraction data and reported the physical properties of $CeCo_{2-x}Mn_xAl_8$ and $CeCo_2Al_8$. The figures, tables, and pertinent sections have been referenced.
Reproduced in part material for Chapter 4: Pilanda Watkins-Curry is an equal contributing author of "Targeting Calcium Magnesium Silicates for Polycaprolactone/Ceramic Composite Scaffolds.". She synthesized and characterized high purity phases of diopside ($CaMgSi_2O_6$), akermanite ($Ca_2MgSi_2O_7$), monticellite ($CaMgSiO_4$), and merwinite ($Ca_3Mg(SiO_4)_2$). She also characterized each compound by powder X-ray diffraction. The figures, tables, and pertinent sections have been referenced.

Thank you,
Pilanda

Vita

Pilanda Watkins-Curry is a native of Hampton, Virgina. She graduated with highest honors at Bethel High School in Hampton, VA in 2007. She began her undergraduate studies in the fall of 2007 at Spelman College in Atlanta, GA, and during her time there conducted research under the mentorship of Professor Leyte Winfield. In the spring of 2011, she received her Bachelors of Science degree. The following fall semester, she started her graduate studies in the Department of Chemistry at Louisanna State Univeristy in Baton Rouge, Louisiana. While there, she joined Prof. Julia Chan's research group who nurtured her development in the area of solid state chemistry. She is currently a candidate for a doctoral degree in chemistry, where she is set to graduate in august 2015.